Mechanisms of vacuolar protein transport in plants

Dissertation

der Mathematisch-Naturwissenschaftlichen Fakultät

der Eberhard Karls Universität Tübingen

zur Erlangung des Grades eines

Doktors der Naturwissenschaften

(Dr. rer. nat.)

vorgelegt von

Fabian Künzl

aus Kassel

Tübingen

2015

Gedruckt mit Genehmigung der Mathematisch-Naturwissenschaftlichen Fakultät der Eberhard Karls Universität Tübingen

Tag der mündlichen Qualifikation: 20.11.2015

Dekan:	Prof. Dr. Wolfgang Rosenstiel
1. Berichterstatter:	Dr. Peter Pimpl
2. Berichterstatter:	Prof. Dr. Gerd Jürgens

Danksagung

Mit dem Abschluss der Dissertation neigt sich auch meine Zeit in Tübingen dem Ende entgegen und neue persönliche wie berufliche Erfahrungen stehen bevor. Ehe ich jedoch das Ländle verlasse, möchte ich mich bei all denen bedanken, die mir die Eingewöhnung und den Arbeitsalltag am Zentrum für Molekularbiologie der Pflanzen (ZMBP) so leicht bzw. angenehm gemacht haben.

Mein Dank gilt an erster Stelle Herrn Dr. Peter Pimpl. Dir, Peter, danke ich dafür, dass Du mich damals in Deine neue Arbeitsgruppe am ZMBP aufgenommen hast, für die fortwährende Unterstützung sowie für die Freiräume, die Du mir stets gelassen hast, um eigene Ideen zu verwirklichen. Vor allem Deine Liebe zum Detail in experimentellen Belangen hat mich gelehrt, was es heißt, „sauber“ im Labor zu arbeiten. Außerdem danke ich Dir für die Möglichkeit zur Teilnahme an mehreren internationalen Konferenzen, für den Forschungsaufenthalt in Hongkong und die damit verbundenen spannenden Reisen.

Bei Herrn Prof. Dr. Gerd Jürgens bedanke ich mich für die bereitwillige Übernahme des Korreferates dieser Dissertation, aber auch für seine Ratschläge und die Hilfestellungen bei meinen wissenschaftlichen Projekten.

Meinen lieben Kollegen in der AG Pimpl möchte ich für die unkomplizierte Zusammenarbeit und die freundschaftliche Arbeitsatmosphäre danken: Simone Früholz, Florian Fäßler, Natalie Gerling und Diana Vranjkovic. Danke auch den ehemaligen Labormitgliedern Beibei Li, Richard Gavidia und Carola Nill für die gute Zusammenarbeit und die erstklassige technische Unterstützung.

All den anderen Kollegen der Abteilung Entwicklungsgenetik (AGs Jürgens, Müller, Grefen und Ragni) bin ich für die nette Arbeitsatmosphäre im Großraumlabor und die allzeit gebotene Hilfsbereitschaft bei Problemlösungen dankbar. An die abendlichen Ausflüge nach Downtown Tübingen auf das ein oder andere Bierchen werde ich ebenfalls gerne zurückdenken.

Zu guter Letzt möchte ich meiner Familie dafür danken, dass sie mich immer unterstützt hat, vor allem dann, wenn die Zweifel an dem, was man da tut, überhand zu nehmen drohten.

Table of Contents

Danksagung 3
1. Summary 5
2. Zusammenfassung 6
3. List of publications 7
4. Personal contribution 8
5. Introduction 9
5.1 The plant endomembrane system 9
5.1.1 Biosynthetic transport 9
5.1.2 Endocytic transport 11
5.2 Plant vacuolar protein sorting 13
5.2.1 ESCRT-mediated sorting of membrane proteins 14
5.2.2 Receptor-mediated sorting of soluble vacuolar proteins 15
5.2.3 Open questions 18
6. Objectives 19
7. Results and Discussion 20
7.1 Multivesicular bodies mature from the *trans*-Golgi network/early endosome in *Arabidopsis* (Scheuring et al., 2011) 20
7.2 Ubiquitin initiates sorting of Golgi and plasma membrane proteins into the vacuolar degradation pathway (Scheuring et al., 2012) 24
7.3 Vacuolar sorting receptors transport ligands from the ER and the Golgi to the TGN/EE (Künzl et al., submitted manuscript) 28
7.4 Closing remarks 36
8. References 40
9. Appendix 50
9.1 Scheuring et al., 2011
9.2 Scheuring et al., 2012
9.3 Künzl et al., submitted manuscript

1. Summary

Protein transport to plant vacuoles can occur by the biosynthetic pathway, leading from the endoplasmic reticulum (ER) via the Golgi apparatus, or by the endocytic pathway from the plasma membrane (PM). Both routes converge in the *trans*-Golgi network/ early endosome (TGN/EE), from where cargo passes a multivesicular late endosome (MVB/LE) before reaching the vacuole. PM proteins destined for vacuolar degradation are internalized into the intraluminal vesicles of MVBs/LEs in a process involving recognition and sorting by the ESCRT machinery. Soluble vacuolar proteins from the biosynthetic pathway have to interact with vacuolar sorting receptors (VSRs) to be diverted from the secretory pathway and sent into the vacuolar route. Regarding these transport events, several aspects have remained unclear: how are proteins transported from the TGN/EE to the MVB/LE, and how do they arrive in the vacuole? Where does ESCRT recognize its cargo, and when does it initiate intraluminal sorting? What is the sorting signal for entry into the ESCRT-mediated vacuolar pathway? Where in the endomembrane system do VSRs bind soluble cargo ligands and where do they release them?

In this thesis, results from two publications and a currently submitted manuscript are presented. We established that **"multivesicular bodies mature from the *trans*-Golgi network/early endosome in *Arabidopsis*"** (Scheuring et al., 2011) by capturing the moment in which nascent MVBs/LEs bud off from the TGN/EE. Mature MVBs/LEs were found to be non-persistent transport carriers that are steadily consumed by fusion with the vacuole. We showed that ESCRT acts at the TGN/EE and that maturation of MVBs/ LEs and vacuolar transport fail if ESCRT functionality is blocked. ESCRT was also found to localize to the Golgi apparatus, indicating vacuolar sorting in the stack. Translational ubiquitin fusions of a Golgi marker indeed revealed that **"ubiquitin initiates sorting of Golgi and plasma membrane proteins into the vacuolar degradation pathway"** (Scheuring et al., 2012). We then addressed the question as to where in the endomembrane system soluble vacuolar proteins are sorted. In an *in vivo* analysis, all compartments of the vacuolar route were tested individually for the ability to promote VSR-ligand interactions. We showed that VSRs bind ligands in the ER and the Golgi, but neither in the TGN/EE nor in the MVB/LE, indicating that **"vacuolar sorting receptors transport ligands from the ER and the Golgi to the TGN/EE"** (Künzl et al., submitted manuscript). Accordingly, post-TGN/EE trafficking of ligands is VSR-independent, being supported by the observation that non-VSR-ligands are delivered from the TGN/EE to the vacuole by default.

2. Zusammenfassung

Der Proteintransport zu pflanzlichen Vakuolen kann durch den biosynthetischen Weg ausgehend vom Endoplasmatischen Retikulum (ER) über den Golgi-Apparat erfolgen, oder durch den endozytischen Weg von der Plasmamembran (PM). Beide Wege laufen im *trans*-Golgi-Netzwerk/frühen Endosom (TGN/EE) zusammen, von wo aus die Fracht ein multivesikuläres spätes Endosom (MVB/LE) durchläuft, bevor sie die Vakuole erreicht. PM-Proteine, die für den vakuolären Abbau bestimmt sind, werden in die intraluminalen Vesikel der MVBs/LEs aufgenommen, wobei ihre Erkennung und Sortierung durch die ESCRT-Maschinerie erfolgt. Lösliche vakuoläre Proteine des biosynthetischen Wegs müssen mit vakuolären Sortierungsrezeptoren (VSRs) interagieren, um vom sekretorischen in den vakuolären Weg umgeleitet zu werden. Bezüglich dieser Transportereignisse sind einige Aspekte noch unklar: Wie werden Proteine vom TGN/EE zum MVB/LE transportiert, und wie erreichen sie die Vakuole? Wo erkennt ESCRT seine Fracht, und wann initiiert er das intraluminale Sortieren? Was ist das Sortierungssignal für den Eintritt in den ESCRT-vermittelten vakuolären Weg? Wo im Endomembransystem binden VSRs lösliche Fracht und wo geben sie sie wieder frei?

In dieser Dissertation werden die Befunde zweier Publikationen und eines zur Publikation eingereichten Manuskripts vorgestellt. Wir haben nachgewiesen, dass MVBs/LEs aus dem TGN/EE reifen, indem wir den Moment des Knospens neu entstehender MVBs/LEs am TGN/EE festhalten konnten. Die reifen MVBs/LEs identifizierten wir als nicht-persistente Carrier, die durch Fusion mit der Vakuole stetig verbraucht werden. Wir konnten zeigen, dass ESCRT am TGN/EE tätig ist und dass die Reifung von MVBs/LEs sowie der vakuoläre Transport fehlschlagen, wenn ESCRT gestört ist. Darüber hinaus lokalisierten wir ESCRT am Golgi-Apparat, was auf ein dortiges vakuoläres Sortieren hindeutete. Durch Ubiquitinfusionen eines Golgi-Markers konnten wir nachweisen, dass Proteine im Golgi tatsächlich dem vakuolären Abbau zugeführt werden. Ubiquitin identifizierten wir zudem als Sortierungssignal für den vakuolären Transport von PM-Proteinen. Des Weiteren untersuchten wir, wo im Endomembransystem lösliche vakuoläre Proteine sortiert werden. *In vivo* testeten wir alle Kompartimente des vakuolären Wegs individuell daraufhin, ob sie VSR-Liganden-Interaktionen zulassen. Es zeigte sich, dass VSRs Liganden im ER und im Golgi binden, jedoch nicht im TGN/EE und im MVB/LE, was für einen VSR-vermittelten Transport zum TGN/EE spricht. Dass der weiterführende Transport vom TGN/EE zur Vakuole VSR-unabhängig ist, zeigten Nicht-Liganden, die vom TGN/EE passiv die Vakuole erreichten.

3. List of publications

Published articles

3.1 Multivesicular bodies mature from the *trans*-Golgi network/early endosome in *Arabidopsis*

David Scheuring, Corrado Viotti, Falco Krüger, **Fabian Künzl**, Silke Sturm, Julia Bubeck, Stefan Hillmer, Lorenzo Frigerio, David G. Robinson, Peter Pimpl, and Karin Schumacher

The Plant Cell, Sept. 2011, Vol. 23(9): 3463-81, DOI: 10.1105/tpc.111.086918

3.2 Ubiquitin initiates sorting of Golgi and plasma membrane proteins into the vacuolar degradation pathway

David Scheuring*, **Fabian Künzl***, Corrado Viotti, Melody San Wan Yan, Liwen Jiang, Swen Schellmann, David G. Robinson, and Peter Pimpl

(*Equally contributing first authors)

BMC Plant Biology, Sept. 2012, Vol. 12:164, DOI: 10.1186/1471-2229-12-164

Submitted manuscript

3.3 Vacuolar sorting receptors transport ligands from the ER and the Golgi to the TGN/EE

Fabian Künzl, Simone Früholz, Florian Fäßler, Beibei Li, and Peter Pimpl

4. Personal contribution

4.1 Multivesicular bodies mature from the *trans*-Golgi network/early endosome in *Arabidopsis* (Scheuring et al., 2011)

Analysis of the newly generated polyclonal antiserum against *Arabidopsis thaliana* VPS28 by immunoblot analysis performed on total extracts of *Arabidopsis* plants and on suspension-cultured *Arabidopsis* cells expressing VPS28-GFP fusions. Analysis of the RNAi-mediated gene knockdown of *Nicotiana tabacum* annexin 3 by expression of an RNAi-ANNAT3 construct against the *Arabidopsis ANNAT3*. Tobacco mesophyll protoplasts expressing cytGFP ± RNAi-ANNAT3 were subjected to fluorescence-assisted cell sorting and total RNA of positively sorted cells was extracted. RT-PCR was performed to evaluate and verify gene silencing.

4.2 Ubiquitin initiates sorting of Golgi and plasma membrane proteins into the vacuolar degradation pathway (Scheuring et al., 2012)

The aspect of employing compartmental membrane markers with minimal sorting information for either the PM or the Golgi to study ubiquitin-dependent sorting was planned and conducted by me, including: cloning/mutagenesis of all TMD-based reporter constructs, localization studies of the reporters in both tobacco mesophyll protoplasts and leaf epidermal cells by CLSM, biochemical confirmation of expression and vacuolar delivery of all reporters in this study by immunoblot analysis. Furthermore, the experiments were designed and analyzed in collaboration with D.S., C.V., D.G.R. and P.P., and the article was written together with D.S., D.G.R. and P.P.

4.3 Vacuolar sorting receptors transport ligands from the ER and the Golgi to the TGN/EE (Künzl et al., submitted manuscript)

I co-developed the strategy to compartment-specifically analyze VSR-ligand interactions and performed all experimental work (except for Fig. 6), including: localization studies by CLSM, analysis of receptor-ligand interactions by FRET-FLIM incl. statistical evaluation, biochemical analysis of protein transport and molecular interactions (co-IP) by immunoblotting. Furthermore, the experiments were designed and analyzed in collaboration with S.F., F.F. and P.P., and the article was written together with P.P.

5. Introduction

5.1 The plant endomembrane system

The plant endomembrane system is composed of several different membranes, which are distributed throughout the cytosol to subdivide the cell into functionally distinct compartments, also called organelles. Each of these compartments is characterized by an individual composition of enzymes, lipids, and metabolites that render each of them a specialized subcellular reaction chamber. Still, the compartments are in steady contact and exchange material through vesicular carriers, thus constituting a dynamic membranous continuum. Plant cellular compartments include the endoplasmic reticulum (ER), the Golgi apparatus, endosomes, different types of vacuoles, and the plasma membrane (PM). The transport processes within the endomembrane system can be subdivided into two categories: biosynthetic (secretory) transport events provide the proteins and lipids for the individual compartments to ensure their functional integrity, while endocytic transport enables the internalization of plasma membrane proteins, being important to regulate cell growth, for communication with the environment, and to turnover proteins and lipids. As will be presented in the following sections, biosynthetic and endocytic transport comprise multiple trafficking steps mediated by different molecular machineries that have to be tightly coordinated to allow for precise targeting. It will also become evident that important details about several of these steps are still unclear and await further investigation.

5.1.1 Biosynthetic transport

Biosynthetic transport within the endomembrane system is initiated at the ER, where proteins, lipids, and polysaccharides are synthesized. Upon entering the ER, proteins are processed, which includes conformational folding and modifications such as *N*-linked glycosylation (Liu and Howell, 2010). Only proteins that pass the ER quality control mechanisms will be incorporated into vesicles for ER export (Brandizzi and Barlowe, 2013). The vesicles deliver their cargo to the *cis*-cisternae of a Golgi stack, through which secretion progresses in a polar fashion via functionally distinct *medial*- and *trans*-cisternae (Dupree and Sherrier, 1998). While in transit through the Golgi, proteins undergo further post-translational modifications (Strasser, 2014) and become sorted for ongoing transport towards their final destinations. Crucial for post-Golgi sorting steps is the *trans*-Golgi network (TGN), a tubulovesicular structure that is often found closely associated with the *trans*-side of the Golgi stack but can also exist as an

independent, spatially separate entity (Foresti and Denecke, 2008; Viotti et al., 2010; Kang et al., 2011; Uemura et al., 2014). From the TGN, biosynthetic transport may be directed towards the PM or to the vacuolar compartments. Selectivity in all these individual transport steps is achieved by distinct vesicular carriers, which differ in the molecular composition of the coat proteins that mediate cargo sorting and vesicle budding (Hwang and Robinson, 2009). The plant endomembrane system with its different transport routes is schematically depicted in Figure 1.

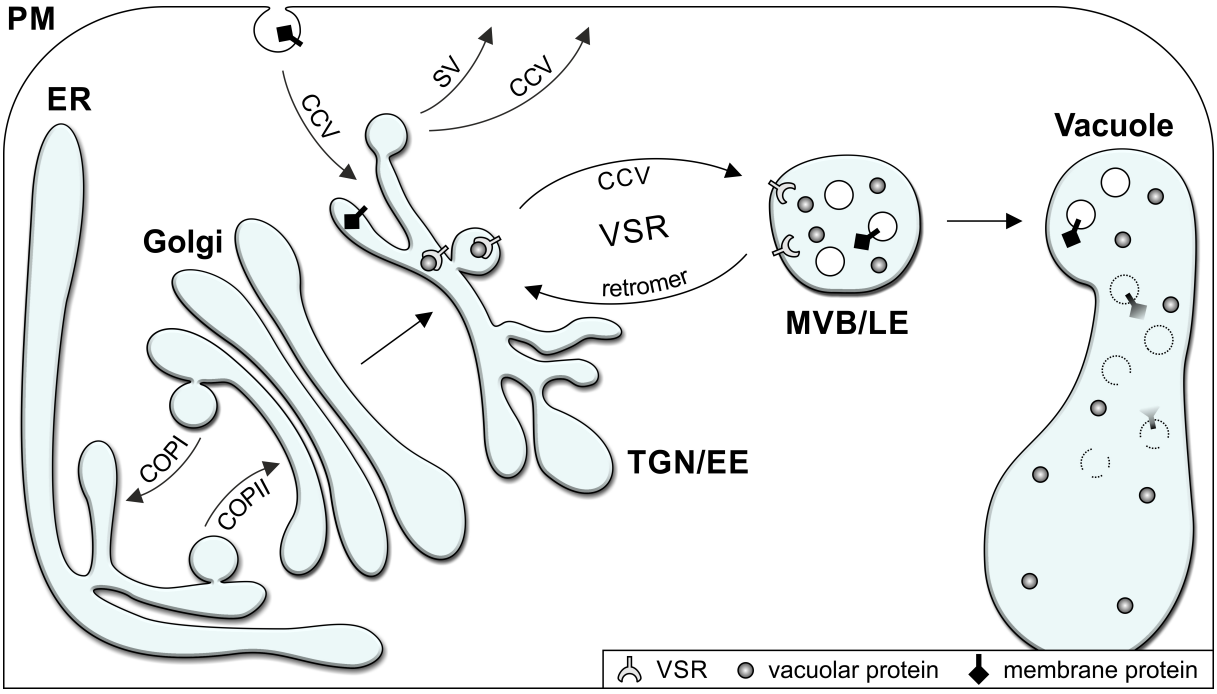

Figure 1. Schematic representation of the transport processes within the plant endomembrane system. The biosynthetic pathway starts at the endoplasmic reticulum (ER) where proteins are synthesized and packaged into COPII-coated vesicles for transport to the Golgi apparatus. Retrograde transport in COPI-coated vesicles ensures the retrieval of escaped ER-resident proteins. After passage through the Golgi, secretory proteins arrive at the *trans*-Golgi network/early endosome (TGN/EE) and are delivered in secretory vesicles (SVs) to the plasma membrane (PM). Vacuolar proteins are bound in the TGN/EE by vacuolar sorting receptors (VSRs) and transported in clathrin-coated vesicles (CCVs) to a multivesicular body/late endosome (MVB/LE). In the MVB/LE, vacuolar proteins are released and the VSRs recycle to the TGN/EE in retromer-coated carriers. Vacuolar delivery finally occurs by fusion of the MVB/LE with the vacuolar membrane. By the endocytic pathway, membrane proteins are internalized from the PM via CCVs and transported to the TGN/EE. There, they either recycle to the PM (putatively in CCVs) or follow the endocytic route towards the lytic vacuole. For degradation, the membrane proteins are sorted into intraluminal vesicles of MVBs/LEs prior to vacuolar delivery. (Adapted and modified from Künzl et al., submitted manuscript)

Transport processes between the ER and the Golgi are collectively referred to as the early secretory pathway, which is operating in a bidirectional manner (Robinson et al., 2007). Forward (anterograde) transport is mediated by coat protein (COP)-II vesicles, which form at discrete ER-export sites (daSilva et al., 2004; Yang et al., 2005) to deliver cargo to the *cis*-Golgi (Takeuchi et al., 2000). For soluble proteins, ER export is thought to occur by default in a step that does not require any sorting signals. The

proteins passively enter COPII vesicles and become part of the secretory bulk flow, which leads via the Golgi and the PM into the extracellular space (Phillipson et al., 2001). Secretory membrane proteins, on the contrary, leave the ER due to specific export signals that interact with COPII coat components to facilitate vesicle formation (Matheson et al., 2006). Soluble ER-resident proteins may nonspecifically enter the secretory default pathway and then have to be returned from the *cis*-Golgi in a reverse (retrograde) sorting step mediated by COPI-coated vesicles (Pimpl et al., 2000). In this process, the C-terminal tetrapeptide H/KDEL functions as ER retrieval signal (Denecke et al., 1992), which is bound by the H/KDEL receptor ERD2 (ER-RETENTION DEFECTIVE2) in the Golgi (Boevink et al., 1998). Retrieval of ERD2, but also of several ER-resident membrane proteins, requires dilysine motifs in their C-terminal cytosolic domains (Gao et al., 2014a), which interact with the COPI coat components. Beyond ER retrieval, COPI vesicles also mediate retrograde intra-Golgi transport, which is necessary to maintain cisternal integrity (Gao et al., 2014a).

Starting from the Golgi stack, the late secretory pathway comprises all the transport events that branch out into two main trafficking routes, leading towards the PM and to the vacuolar compartments (see Figure 1). It is believed that *de novo*-synthesized proteins pass the TGN while in transit to the PM, as was suggested for fluorescently-tagged BRI1 (BRASSINOSTEROID INSENSITIVE1) receptors and for secretory GFP (Viotti et al., 2010). By contrast, newly assembled cellulose synthase complexes were proposed to circumvent the TGN, being delivered directly from the Golgi stack or otherwise being partitioned into an undefined domain of the TGN (Crowell et al., 2009). Two different types of vesicles have been described to form at the TGN: secretory vesicles, whose coat components remain to be identified, and clathrin-coated vesicles (CCVs), which are supposed to mediate vacuolar transport by targeting the multivesicular late endosomes (Kang et al., 2011). However, it can also not be ruled out that the CCVs formed at the TGN recycle endocytosed PM proteins rather than contributing to vacuolar transport (discussed by Robinson and Pimpl, 2014a).

5.1.2 Endocytic transport

The internalization (endocytosis) of proteins from the PM is necessary for the cell to establish and maintain polarity, to allow for cell-to-cell communication, and to respond to environmental stimuli (Fan et al., 2015). In recent years, numerous PM proteins have been identified as endocytic cargos, including PIN (PIN-FORMED) auxin efflux carriers (Dhonukshe et al., 2007) and receptor-like kinases such as the brassinosteroid recep-

tor BRI1 (Russinova et al., 2004) and the flagellin receptor FLS2 (FLAGELLIN SENSING2; Robatzek et al., 2006). Others include transporters like BOR1 (BORON TRANSPORTER1; Takano et al., 2010) or IRT1 (IRON-REGULATED TRANSPORTER1; Barberon et al., 2011) and the aquaporin PIP2;1 (PLASMA MEMBRANE INTRINSIC PROTEIN2;1; Li et al., 2011), to name but a few.

The primary endocytic route into plant cells is apparently by clathrin-mediated endocytosis (CME), although evidence for the existence of clathrin-independent endocytic routes exists (Bandmann and Homann, 2012; Bandmann et al., 2012; Li et al., 2012). CME initiates at the inner leaflet of the PM by assembly of clathrin-coated pits, in which tetrameric adaptor protein (AP)-2 complexes capture and accumulate endocytic cargo (Fan et al., 2015). Successive recruitment of coat components promotes invagination of the PM and leads to the formation of CCVs, which are finally released by dynamin-related protein (DRP)-driven membrane scission (Fujimoto et al., 2010). While the core machinery of CME is evolutionary conserved, plants lack several accessory clathrin adaptors known in animals (Chen et al., 2011), but they do also possess unique ones such as the adaptin-like protein TPLATE, which was recently identified to be involved in cytokinesis (Van Damme et al., 2011). Meanwhile, TPLATE is considered part of an essential adaptor complex in plant CME (Gadeyne et al., 2014). Adaptors confer cargo-sorting specificity by recognizing endocytic sorting signals in the cytosolic domains of PM proteins, which in animals can be linear sequence motifs, structural determinants, or post-translational modifications (Traub and Bonifacino, 2013). In plants, the sorting signals are still poorly defined, but tyrosine-based motifs (YXXΦ, with Φ representing a bulky hydrophobic amino acid), as known from animals, have been identified in plant proteins and were shown to act in endocytosis (Bar and Avni, 2009). Tyrosine-based motifs are however also involved in other transport events such as polar localization of BOR1, which does not depend on YXXΦ-mediated endocytosis but on tyrosine-based endosomal recycling (Takano et al., 2010). Furthermore, phosphorylation was shown to be important for the polar PM localization of PIN auxin efflux carriers (Kleine-Vehn et al., 2009), but still a clear link to the endocytic machinery needs to be established.

Upon internalization, endocytic vesicles fuse with a compartment that is classically defined as the early endosome (EE; Robinson et al., 2008). A tubulovesicular structure, called partially-coated reticulum (PCR), was identified already decades ago to receive endocytic material from the PM (Robinson and Hillmer, 1990). However, it was not until recently that studies combining newly identified TGN markers with endocytic tracers

revealed that the EE and the TGN are in fact one and the same compartment (Dettmer et al., 2006; Lam et al., 2007). Consequently, the TGN/EE is the point of intersection of the biosynthetic and the endocytic pathway. It must be considered an independent compartment that, although derived from the Golgi, becomes finally detached from the stack but can also reassociate temporarily and homotypically interact with other TGNs/ EEs (Viotti et al., 2010; Kang et al., 2011; Uemura et al., 2014).

Within the TGN/EE, endocytosed PM proteins can be sorted in different directions: they may be recycled back to the PM or otherwise passed on to late endosomes (LEs) for delivery to the vacuole. Circles of constitutive internalization and recycling have been described for several PM proteins, including the PINs, BRI1, and BOR1 (Geldner et al., 2003; Geldner et al., 2007; Takano et al., 2010). There is evidence that different recycling pathways exist to return proteins to the PM, one of which leading via distinct recycling endosomes. Although not identified structurally, the existence of a recycling endosome was deduced from functional studies on the ARF-GEF (ADP-ribosylation factor-guanine nucleotide exchange factor) GNOM, which acts to mediate the recycling of PIN1 (Geldner et al., 2003) but does not colocalize with markers for the TGN/EE and the LE (Chow et al., 2008). Other PM proteins were shown to recycle independently of GNOM, indicating that more than one endosomal recycling pathway exists (Kleine-Vehn et al., 2006). PM proteins destined for degradation are delivered to the vacuole, but first they have to be sorted from the TGN/EE to a LE. Structurally, LEs clearly differ from a tubulovesicular TGN/EE. They are spherical bodies characterized by unique intraluminal vesicles and are thus also called multivesicular bodies (MVBs; Tse et al., 2004). Endocytic cargo has been shown to successively pass the TGN/EE and the MVB/LE while in transit to the vacuole (Tse et al., 2004; Dettmer et al., 2006; Viotti et al., 2010), however, a transport mechanism connecting the two compartments has remained elusive.

5.2 Plant vacuolar protein sorting

The proteins of the endomembrane system are in a dynamic equilibrium of synthesis and degradation, which is important not only to turnover aberrant molecules, but also to respond to changing developmental and environmental conditions. In this regard, many of the PM-localized transporters and receptors are tightly regulated in terms of numbers to act on nutrient availability or to finetune signaling processes (Fan et al., 2015). For degradation, proteins are delivered via the endosomal pathway to the lytic vacuole, where acid hydrolases confer digestion. However, the mechanisms, by which

the proteins are transported towards the vacuole differ depending on whether they are integral membrane proteins or soluble.

5.2.1 ESCRT-mediated sorting of membrane proteins

Several PM proteins in plants have been found to localize to the intraluminal vesicles (ILVs) of MVBs/LEs before being degraded in the lytic vacuole, including PIN1, BRI1, BOR1, and the cytokinesis-specific syntaxin KNOLLE (Reichardt et al., 2007; Spitzer et al., 2009; Viotti et al., 2010). Sorting into the ILVs ensures clearance of the proteins from the limiting endosomal membrane prior to fusion of the MVB/LE with the tonoplast, which is necessary to make them accessible for vacuolar digestion (Schellmann and Pimpl, 2009; Reyes et al., 2011). Signals are required to label membrane proteins for intraluminal sorting, as well as the machinery that internalizes the labeled proteins into the endosomal lumen by pinching off ILVs.

In animals and yeast, ubiquitin is the major sorting signal for the entry of membrane proteins into the MVB/LE-mediated vacuolar degradation pathway (Hicke and Dunn, 2003). In a reaction called ubiquitination, ubiquitin is covalently linked to lysine residues of the target proteins (Pickart and Eddins, 2004). Depending on the number of added ubiquitin moieties and the mode of their linkage, ubiquitination can modulate a variety of cellular processes other than MVB-mediated vacuolar sorting (Hurley et al., 2006). In this context, the attachment of poly-ubiquitin chains to cytosolic proteins was early identified as a signal for degradation in the 26S proteasome, while mono-ubiquitination has been associated with the sorting of membrane proteins into the ILVs of MVBs/LEs (Raiborg and Stenmark, 2009). Ubiquitin was also shown to function as an endocytosis signal, acting upstream of endosomal sorting, but the exact type of ubiquitination that triggers internalization from the PM is still under debate (Madshus, 2006). In plants, ubiquitination of membrane proteins and its implications for intracellular sorting have only recently gained attention. Both PIN2 and FLS2 were found to be ubiquitinated and an involvement of ubiquitin in their turnover was suggested (Abas et al., 2006; Gohre et al., 2008), however, a link to the MVB/LE-mediated vacuolar pathway was neither investigated nor mentioned. During the revision and resubmission of our manuscript *“ubiquitin initiates sorting of Golgi and plasma membrane proteins into the vacuolar degradation pathway”* (Scheuring et al., 2012), first studies on that topic appeared, which will be discussed in the context of our findings (see chapter 7.2).

At endosomal membranes, ubiquitinated proteins are recognized by soluble sorting complexes, which are sequentially recruited from the cytosol onto the endosomal

membrane to drive the formation of ILVs. In animals and yeast, these complexes have been extensively studied and collectively termed ESCRT (endosomal sorting complex required for transport) machinery, which consists of four multimeric complexes, numbered ESCRT-0 to ESCRT-III (Raiborg and Stenmark, 2009). First, ESCRT-0 binds and concentrates ubiquitinated cargo before it recruits ESCRT-I and -II, which together induce membrane curvature and confine the cargo within forming buds. Then, ESCRT-III is recruited to cleave the buds, giving rise to ILVs, and finally ESCRT-III-associated proteins trigger the release of the ESCRT complexes from the membrane (Wollert and Hurley, 2010). Plants possess almost all components of the evolutionary conserved ESCRT machinery, but apparently they lack orthologs of the ESCRT-I subunit MVB12 and of the two subunits constituting ESCRT-0 (Winter and Hauser, 2006; Leung et al., 2008). Of the few plant ESCRT components that have been functionally characterized, almost all belong to the ESCRT-III-associated proteins, being the AAA-ATPase SKD1 (SUPPRESSOR OF K^+ TRANSPORT GROWTH DEFECT1) and its positive regulator LIP5 (LYST-INTERACTING PROTEIN5), the SKD1/LIP5 interacting proteins CHMP1A (CHARGED MULTIVESICULAR BODY PROTEIN/CHROMATIN MODIFYING PROTEIN1A) and CHMP1B, and also the deubiquitinating enzyme AMSH3 (ASSOCIATED MOLECULE WITH THE SH3 DOMAIN OF STAM3), which were all shown to be involved in ILV formation and/or vacuolar sorting (Haas et al., 2007; Spitzer et al., 2009; Isono et al., 2010; Shahriari et al., 2010; Katsiarimpa et al., 2011). The ESCRT-I subunit VPS23 (VACUOLAR PROTEIN SORTING23) has been found to localize to endosomal compartments and it was assigned a role in cytokinesis, however a function in vacuolar sorting has not been investigated (Spitzer et al., 2006). Only recently, a plant-specific ESCRT-I subunit, called FREE1 (FYVE DOMAIN PROTEIN REQUIRED FOR ENDOSOMAL SORTING1), was discovered that interacts with VPS23 and was shown to be necessary for ILV formation (Gao et al., 2014b).

5.2.2 Receptor-mediated sorting of soluble vacuolar proteins

In all eukaryotic cells, receptor-mediated sorting mechanisms exist to deliver soluble proteins to a lytic compartment, being either the lysosome in animal cells or vacuoles in both yeast and plant cells. Yet, sorting receptors evolved independently in the three eukaryotic kingdoms, with the animal mannosyl 6-phosphate receptor (MPR; Braulke and Bonifacino, 2009), the yeast receptor VPS10 (Bowers and Stevens, 2005), and the plant vacuolar sorting receptors (VSRs; Robinson and Pimpl, 2014b) being the best known. Among these receptors, the animal MPR was the first to be characterized (iden-

tified by Sahagian et al., 1981) and has become a paradigm for the receptor-mediated protein sorting in the endomembrane system.

Acid hydrolases destined for the lysosome are recognized by MPRs via specific glycosylation patterns, which are introduced in a complex series of events: after initial *N*-linked glycosylation in the ER, the oligosaccharide side chains are further modified in the *cis*-Golgi, but still the lysosomal sorting signal remains cryptic. Only upon arrival in the TGN, the so-called uncovering enzyme exposes mannose 6-phospahte residues as the sorting signal, which is then immediately bound by the MPR. Consequently, the hydrolases become ligands only in the TGN; a situation that does not exist in plants. Still in the TGN, MPR-ligand complexes are packaged into CCVs and transported to an EE, where the ligands are released due to the lower endosomal pH, and the MPRs are returned to the TGN in tubular carriers formed by the coat proteins of the retromer complex (McGough and Cullen, 2011). Once the ligands have entered the EE, onward transport to the lysosome is receptor-independent, with the EE gradually maturing into a LE that finally fuses with the lysosomal membrane to release its contents (Huotari and Helenius, 2011).

In comparison to lysosomal proteins, sorting of soluble proteins to the plant vacuole does not depend on post-translational modifications, but is instead determined by short motifs within the amino acid sequence. These so-called vacuolar sorting determinants (VSDs) are often located at the N- or C-termini of acid hydrolases and storage proteins (Robinson et al., 2005). By the time the first VSDs were characterized (Chrispeels, 1991; Bednarek and Raikhel, 1992; Nakamura and Matsuoka, 1993), a corresponding sorting receptor was not identified, but several vacuolar proteins were found to localize in coated vesicles (Harley and Beevers, 1989; Robinson et al., 1989). Only then, a type I integral membrane protein was purified from CCVs and Golgi membranes of pea (*Pisum sativum*) cotyledons, as it bound at neutral pH to an affinity column prepared with the VSD of barley (*Hordeum vulgare*) proaleurain, from which it was eluted at an acidic pH (Kirsch et al., 1994). Identification of this binding protein of about 80 kDa, called BP80, was actually the first indication that vacuolar transport of soluble proteins is receptor-mediated also in plants.

Molecular cloning and sequence alignments eventually revealed that BP80 defines a conserved family of vacuolar sorting receptors (VSRs) unique to plants (Paris et al., 1997), with seven VSRs (AtVSR1-7) encoded in the genome of *Arabidopsis thaliana* (Shimada et al., 2003). Localization studies in pea, tobacco (*Nicotiana tabacum*) and

Arabidopsis cells demonstrated that VSRs are situated at the *trans*-Golgi/TGN and a hitherto unspecified prevacuolar compartment (PVC; Paris et al., 1997; Sanderfoot et al., 1998; Li et al., 2002). This, together with the pH dependency of BP80 to bind its ligands *in vitro*, led to the postulation of a model for VSR-mediated vacuolar transport that was back then consistent with the concept of MPR-mediated lysosomal transport in animal cells. Accordingly, VSRs were predicted to bind their ligands in the TGN, from where CCVs would bud off to deliver the receptor-ligand complexes to a PVC. A lower pH in the PVC would then cause dissociation of the receptor-ligand complexes, whereupon the discharged receptors would recycle to the TGN in retromer-coated carriers, while the ligands would reach the vacuole by fusion of the PVC with the tonoplast (Paris et al., 1997).

In the meantime, it was shown that the tyrosine-based sorting motif YXXΦ, which is conserved in the cytosolic tails of all BP80-type VSRs, can be bound *in vitro* by the medium (μA) subunit of a clathrin AP complex that localizes to the *trans*-Golgi/TGN in *Arabidopsis* root cells (Happel et al., 2004). Moreover, mutation of the same tyrosine motif caused the retention of AtVSR4 in the *trans*-Golgi/TGN and its partial mislocalization to the PM in tobacco (daSilva et al., 2006). Ultrastructural studies furthermore confirmed that AtVSR1 localizes to the *trans*-Golgi/TGN in developing *Arabidopsis* embryos, where it was found in budding vesicles with clathrin coats (Hinz et al., 2007), being indicative of the fact that VSR sorting probably depends on CCV-mediated transport.

Two important discoveries eventually contributed to a better understanding of how the compartments involved in VSR trafficking are functionally implemented in the plant endomembrane system: the TGN, which was hitherto regarded as the cargo-sorting terminal part of the Golgi, turned out to also receive incoming material from the PM via endocytic CCVs, thus defining it as an EE (Dettmer et al., 2006; Dhonukshe et al., 2007; Lam et al., 2007). Unlike the situation in animal cells, the plant TGN is considered an independent compartment, where biosynthetic and endocytic transport pathways intersect (Viotti et al., 2010) and should hence correctly be termed TGN/EE. Aside from that, the PVC could be identified as a MVB, which receives endocytic cargo downstream of the TGN/EE and is thus the functional equivalent of a LE (Tse et al., 2004). These findings have major implications for the interpretation of the original VSR trafficking model as they necessitate that vesicular sorting of the soluble cargo occurs between an EE and a LE, and thus on the endocytic route.

5.2.3 Open questions

Transport of both endocytosed PM proteins and biosynthetic soluble cargo converge in the TGN/EE while in transit towards the vacuole. However, how they are transported further downstream to a MVB/LE is still unclear. If, as is presumed, transport of VSR-ligand complexes from the TGN/EE to the MVB/LE is CCV-mediated, do endocytosed PM proteins cosegregate into the same vesicles or do they arrive at MVBs/LEs by other mechanisms? Once in the MVB/LE, how is the final transport step to the lytic vacuole executed? A commonly accepted model predicts fusion of MVBs/LEs with the vacuolar tonoplast by analogy to lysosomal delivery in animals (Luzio et al., 2007), but evidence in favor of that assumption is still lacking.

PM proteins are found in the ILVs of MVBs/LEs prior to vacuolar delivery, being the result of intraluminal sorting by the ESCRT machinery. Still, it is largely unknown where and how ESCRT recognizes and sorts cargo, and when ILV budding is initiated, since functional studies have almost exclusively focused on ESCRT-III-associated proteins that act late in the process of ILV formation. Signals for entry into the MVB-mediated vacuolar pathway have not yet been addressed in plants, and while ubiquitination may certainly be the best candidate, a functional link between ESCRT and ubiquitinated membrane proteins still awaits experimental confirmation. Also, it remains to be shown whether ubiquitin can act already at the PM as a signal for internalization of proteins into the endocytic route.

Recent work in our laboratory suggested that VSRs are recycled from the TGN/EE rather than from the MVB/LE (Niemes et al., 2010b), which necessitates that the TGN/EE is already the location of ligand release. Furthermore, it was shown that chimeric VSRs, if localized to the ER, cause coaccumulation of soluble vacuolar cargo (Niemes et al., 2010a), supporting the idea that ligand binding may occur in the early secretory pathway. However, molecular interactions between VSRs and their ligands have not been investigated *in vivo* yet, hence it is still not possible to pinpoint the compartments between which VSR-mediated sorting occurs.

6. Objectives

A prerequisite for unraveling the mechanisms of TGN/EE-to-MVB/LE transport is to understand how MVBs/LEs are formed and how they receive cargo from upstream TGNs/EEs for onward transmission to the vacuole. Hence, we planned on performing ultrastructural analysis to gain insight into the biogenesis of MVBs/LEs, which could give information on how they functionally interact with the TGN/EE. For these studies, we intended to employ the V-ATPase inhibitor concanamycin A (ConcA) as a tool, since it was recently shown that this drug affects the identity and independence of the TGN/EE (Viotti et al., 2010). As a result, both secretory traffic to the PM and transport of endocytosed FM4-64 from the TGN/EE to the vacuole are blocked (Dettmer et al., 2006; Viotti et al., 2010), indicating that ConcA might be instrumental to study the membrane dynamics between the TGN/EE and the MVB/LE.

The intraluminal vesicles (ILVs) are the key morphological feature of MVBs/LEs, which makes the ESCRT machinery the prime candidate for functional studies on MVB/LE biogenesis and the transport processes connecting it to the TGN/EE. Still, where ESCRT recognizes its cargo and initiates ILV budding is unknown, hence we wanted to identify the location of ESCRT assembly by tracking representative subunits of the three ESCRT complexes. By employing dominant-negative ESCRT mutants, we also wanted to examine how ESCRT function influences the biogenesis of the MVB/LE and the delivery of cargo to the vacuole. As cargo-sorting signals for the MVB-mediated vacuolar pathway have not been explored yet, we intended to investigate whether ubiquitination participates in this process. Accordingly, we designed translational ubiquitin fusions based on fluorescent reporters with minimal sorting information for the PM to solely focus on the contribution of the ubiquitin signal to vacuolar delivery.

Receptor-mediated transport of soluble vacuolar cargo is considered to occur between the TGN/EE and the MVB/LE, based mainly on localization data of the VSRs rather than on cargo-binding studies. Molecular interactions between VSRs and soluble cargo could not be assigned to a specific compartment yet. Accordingly, we aimed at developing a strategy that would enable us to test the compartments of the vacuolar transport route individually for their ability to promote VSR-ligand binding *in vivo*. For this, we intended to employ state-of-the-art live cell imaging techniques (FRET-FLIM) that would allow the identification of molecular interactions between the VSRs and their ligands. This way, an intracellular roadmap of ligand binding and release could be prepared that should help settle the controversy about VSR-mediated vacuolar sorting.

7. Results and Discussion

7.1 Multivesicular bodies mature from the *trans*-Golgi network/early endosome in *Arabidopsis* (Scheuring et al., 2011)

Transport of endocytic cargo towards the lytic vacuole was shown to involve both the TGN/EE and the MVB/LE (Viotti et al., 2010), however, a mechanism that enables the transition of proteins from a TGN/EE to a MVB/LE has remained elusive. We thus wanted to investigate which influence TGN/EE functionality has on vacuolar transport and performed drug treatments with the V-ATPase inhibitor concanamycin A (ConcA). Recently, V-ATPase activity had been demonstrated to be essential for the formation of the TGN/EE, as ConcA treatment led to the retention of TGN/EE-intrinsic proteins in morphologically enlarged Golgi stacks (Viotti et al., 2010). When we applied ConcA, a significant reduction in the number of MVBs/LEs was revealed on the ultrastructural level. We found that endogenous BP80-type VSRs, which localize to both the TGN/EE and the MVB/LE (Niemes et al., 2010b; Stierhof and El Kasmi, 2010; Viotti et al., 2010), were likewise retained in Golgi stacks under ConcA treatment, as was the case for the Rab GTPase ARA7 that otherwise localizes mainly to MVBs/LEs (Haas et al., 2007; Robinson et al., 2008). We speculated that once the membrane supply from the TGN/EE ceases, existing MVBs/LEs would gradually disappear through fusion with the lytic vacuole. Transmission electron microscopy in fact revealed that the limiting membrane of the MVB/LE ultimately fuses with the tonoplast to release contents into the vacuolar lumen. Reversal of V-ATPase inhibition by ConcA washout enabled us to capture the moment when nascent MVBs/LEs formed at tubular structures of the TGN/EE. These MVB/LE budding events were frequently seen during recovery from ConcA treatment, which served to synchronize the biosynthesis of MVBs/LEs, however, they also occur under physiological conditions demonstrating that the TGN/EE is the natural source for the formation of MVBs/LEs.

The newly emerging MVBs/LEs already featured the characteristic ILVs and were positively labeled by the Rab GTPase ARA7. This is in agreement with recent live cell imaging studies suggesting that MVB/LE maturation initiates in those subdomains of a TGN/EE where ARA7 is specifically recruited (Singh et al., 2014). Transition from early to late endosomes in yeast and animal cells was shown to be triggered by a Rab-conversion mechanism that replaces EE-localized Rab5-type GTPases for the LE-characteristic Rab7-type GTPases (Rink et al., 2005). A key role in this process has

been assigned to the Mon1/SAND–CCZ1 heterodimeric complex, which acts as a GEF on Rab7 and simultaneously inactivates Rab5 (Nordmann et al., 2010; Poteryaev et al., 2010; Huotari and Helenius, 2011). Recent evidence suggests that a homologous SAND–CCZ1 complex catalyzes the same Rab5-to-Rab7 conversion in plant cells. However, the Rab distribution on plant endosomes is notably shifted, with Rab5-type GTPases like ARA7 mainly localizing to the MVB/LE (Haas et al., 2007; Robinson et al., 2008), while the Rab7-type GTPases are found on MVBs/LEs and the tonoplast (Rutherford and Moore, 2002; Geldner et al., 2009). Hence, SAND activity in plants is required for the fusion of MVBs/LEs with the vacuole, but non-essential for early-to-late endosome maturation, as was revealed by *SAND* knockouts that did not prevent MVB/LE biogenesis (Cui et al., 2014; Singh et al., 2014). Whether a plant-specific GTPase-conversion mechanism aids in the transition from the TGN/EE to the MVB/LE still remains to be shown.

The occurrence of ILVs within the nascent MVBs/LEs furthermore suggested that ESCRT-mediated luminal sorting should have been initiated already at the TGN/EE. We thus investigated the subcellular distribution of the three known ESCRT complexes in plants by focusing on one representative subunit each for ESCRT-I to -III. Immunogold electron microscopy of endogenous ESCRT-I VPS28 revealed its localization at the TGN/EE but not at MVBs/LEs, indicating that ILV budding and MVB formation do indeed coincide at the TGN/EE. To our surprise, VPS28 was also found at Golgi stacks, which is different from the situation described in animals and yeast where ESCRT is restricted to endosomes (Hurley, 2010). Sorting of ubiquitinated membrane proteins at the Golgi apparatus has been assigned to GGA (Golgi-localized, γ-ear-containing, Arf-binding) adapter proteins, which promote the formation of CCVs and the delivery of cargo to EEs where ESCRT takes over (Pelham, 2004; Scott et al., 2004). However, given the fact that discernible GGA orthologs as well as an initiating ESCRT-0 complex do not exist in plants (Hwang, 2008; Leung et al., 2008), ubiquitin-mediated sorting at plant Golgi stacks might have evolved differently. Evidence for the existence of a Golgi-localized vacuolar sorting mechanism in plants was revealed by translational fusions of ubiquitin to a Golgi marker, which caused vacuolar delivery of the protein depending on ESCRT functionality (published by Scheuring et al., 2012; see section 7.2).

We further analyzed the compartmental distribution of the ESCRT machinery by live cell imaging of the ESCRT-II and -III subunits VPS22 and VPS2, respectively. In co-expression with fluorescent markers for the Golgi, the TGN/EE, and the MVB/LE, we

were able to demonstrate that ESCRT-II VPS22 is almost exclusively localized to the TGN/EE, but virtually absent from the Golgi and the MVB/LE. As opposed to this, ESCRT-III VPS2 was found mostly at MVBs/LEs but to a lesser extent also at the TGN/EE, which was further supported by immunofluorescence labeling of endogenous VPS2. The direct comparison of ESCRT-II VPS22 and ESCRT-III VPS2 reflected this differential distribution in that they just partially colocalized, with only VPS2 labeling wortmannin-sensitive MVBs/LEs. These findings indicate that the ESCRT machinery successively assembles along the endocytic pathway, starting already at the TGN/EE to sort cargo into the ILVs of emerging MVBs/LEs. The partial Golgi localization of the ESCRT-I subunit VPS28 furthermore suggests that ESCRT might also sort proteins of the Golgi stack for turnover in the lytic vacuole.

MVB/LE formation and ESCRT assembly coincided spatially at the TGN/EE, hence we wondered if ESCRT functionality could be a prerequisite for MVB/LE maturation. To answer that question, we generated a dominant-negative mutant of the ESCRT-III subunit VPS2, called VPS2-DN, which is incapable of recruiting the ESCRT-associated AAA-ATPase SKD1 that disassembles ESCRT after ILV formation. The importance of this energy-dependent step became apparent when the constitutive overexpression of a dominant-negative SKD1 mutant, lacking ATPase activity, turned out to be lethal in the long term (Haas et al., 2007). In transient expression, the mutant leads to unusually enlarged endosomes with fewer ILVs (Haas et al., 2007; Katsiarimpa et al., 2011), which are considered to be the equivalent to what has been described as a class E compartment in yeast ESCRT mutants (Raymond et al., 1992).

ESCRT-III VPS2 had been partially found at the TGN/EE as subdomains matured into MVBs/LEs, thus we examined what influence the VPS2-DN mutant would have on the progression from an early to a late endosome. In transient expression, we analyzed fluorescent markers for the TGN/EE and the MVB/LE with respect to their relative location in a VPS2-DN overproduction background. It became apparent that TGN/EE and MVB/LE markers clustered together in enlarged endosomal structures reminiscent of class E compartments. We could show that these aberrant endosomes originate from the TGN/EE, in which the MVB/LE markers accumulate over time as endosomal maturation fails. These observations are in agreement with findings from animal cells where class E compartments were shown to be of early endosomal origin (Yoshimori et al., 2000; Doyotte et al., 2005). Spatial separation of the TGN/EE and MVB/LE markers could be affected in a similar way if ConcA was applied, which corresponds

to our ultrastructural data showing the ConcA-induced inhibition of MVB/LE formation. Furthermore, colocalization of the TGN/EE and MVB/LE markers was also revealed if a member of the annexin protein family, *Arabidopsis* ANNAT3, was transcriptionally downregulated by RNAi. The closely related mammalian annexin A2 has been shown to be required for the final budding of multivesicular LEs from EEs, in a process that involves annexin A2-dependent actin nucleation (Mayran et al., 2003; Morel et al., 2009). Although an equivalent role for plant annexins in MVB/LE maturation remains to be established, our data support the idea that ANNAT3 is actively involved in this specific transport event.

Interference with TGN/EE function either by ConcA treatment, ESCRT inhibition, or annexin knockdown had always resulted in maturation defects and consequently in a decrease of MVBs/LEs that would have otherwise functioned as carriers for vacuolar transport. We thus speculated that the delivery of vacuolar proteins should be affected in these cases. Transport analysis in protoplasts using the vacuole-targeted reporters α-amylase-sporamin (amy-spo; Pimpl et al., 2003) and GFP-sporamin (daSilva et al., 2005) indeed revealed a dosage-dependent misrouting into the cell culture medium if treated with ConcA or upon VPS2-DN overproduction. Similarly, induced secretion of amy-spo was shown in a dominant-negative SKD1 mutant background (SKD1(AQ); Shahriari et al., 2010). The extracellular accumulation of the vacuolar proteins likewise implied that secretion is apparently unaffected under conditions that otherwise perturb endosomal maturation. In cases of ESCRT inhibition, this is conceivable assuming that only those TGN/EE subdomains destined to mature into MVBs/LEs will be affected, whereas other sorting steps at the TGN/EE may still be functioning. Transport analysis with the secretory reporter α-amylase (amy; Pimpl et al., 2003) indeed revealed that none of the ESCRT mutants, i.e. SKD1(AQ) and VPS2-DN, had any significant effect on default secretion (Shahriari et al., 2010; D. Scheuring, personal communication). ConcA treatment, we reasoned, has a more severe impact on TGN/EE functionality and might thus influence sorting events other than vacuolar transport. Accordingly, we analyzed the transport of secretory amy in the same ConcA background that otherwise induces secretion of vacuolar amy-spo, but here again no changes in amy secretion were measured (unpublished data). By contrast, secretory GFP and BRI1-YFP accumulated intracellularly along the way to the PM if expressed under ConcA conditions, and the same was true for cell wall xyloglucans that were found enriched in Golgi-derived aggregates (Viotti et al., 2010). These contradictory results are indeed difficult

to reconcile and may be due to the existence of different secretory routes, one of which bypassing the TGN/EE as an intermediate way station towards the PM. Here, further investigations will certainly be necessary to explain this discrepancy.

In summary, we provided evidence that plant MVBs/LEs originate from the TGN/EE in a process equivalent to the endosomal maturation model described in animal cells and yeast (Huotari and Helenius, 2011). This process requires the concerted action of key regulatory factors including the V-ATPase (pH regulation), ESCRT (intraluminal sorting), annexins (MVB/LE budding), and certainly many more to be identified.

7.2 Ubiquitin initiates sorting of Golgi and plasma membrane proteins into the vacuolar degradation pathway (Scheuring et al., 2012)

In animals and yeast, ubiquitination causes sorting of membrane proteins into the ILVs of MVBs/LEs, but it can also induce the internalization of proteins from the PM (Raiborg and Stenmark, 2009). In plants, this issue still needs to be addressed, so we started to investigate whether ubiquitin is sufficient as an endocytic sorting signal for proteins at the PM. For that purpose, we designed fluorescent reporter constructs that are post-translationally inserted into the PM and thus not delivered by the secretory pathway. This would have the advantage that the first possible transport step could only be the internalization from the PM, eliminating any misinterpretation of intracellular signals. PM-anchorage of our GFP-based reporters was ensured by addition of a short amino acid sequence, which contains the 'GC-CG box' motif of a type II ROP GTPase that undergoes *S*-acylation (Lavy and Yalovsky, 2006). The resulting construct, called Box-GFP, efficiently labeled the PM in tobacco protoplasts and leaf epidermal cells but was not found in intracellular compartments. By contrast, translational fusion to ubiquitin (Ub) specifically caused internalization of a Box-GFP-Ub reporter, which was shown to depend on clathrin-mediated endocytosis. The internal signals of Box-GFP-Ub could be tracked along the endocytic pathway labeling both the TGN/EE and the MVB/LE, but they were absent from the Golgi. We could thus unequivocally demonstrate that ubiquitin is sufficient to trigger endocytosis of a PM-localized protein by recruiting the clathrin machinery for vesicle formation.

To our surprise, internalized Box-GFP-Ub passed through the endocytic route only until reaching the MVB/LE where transport apparently came to a halt. We have shown previously that MVBs/LEs ultimately fuse with the vacuole (Scheuring et al., 2011; see

section 7.1), so we actually expected Box-GFP-Ub to arrive either in the tonoplast or, if sorted by the ESCRT machinery, within the vacuolar lumen. We could rule out that the lack of vacuolar fluorescence results from vacuolar degradation but speculated instead that the mode of membrane insertion might possibly not persist beyond the MVB/LE. In this context, reversible *S*-acylation is a common mechanism by which small GTPases are regulated in a temporospatial manner (Linder and Deschenes, 2007), which is known to also include ROP GTPases (Yalovsky, 2015). Whether the specific cysteine residues within the GC-CG box undergo deacylation is unclear, but it could explain a release of Box-GFP-Ub from the membrane. Another important feature of the sequence containing the GC-CG box is a proximal polybasic region, which is supposed to confer membrane specificity by interacting with certain phospholipids (Lavy and Yalovsky, 2006; Sorek et al., 2009). As the lipid composition of the compartments along the endocytic pathway evidently changes, membrane anchorage of the Box-GFP-Ub reporter might gradually be weakened to the point where it is finally lost into the cytosol.

To address this question, we prepared a second set of reporters which by no means would lose membrane association as they were based on a true type I transmembrane domain (TMD). For this, we employed the PM marker RFP-TMD23 (Brandizzi et al., 2002), which is delivered to the PM via the secretory pathway. Once ubiquitin was translationally fused to its cytosolic C-terminus, the resulting construct RFP-TMD23-Ub efficiently labeled the lumen of the lytic vacuole. In order to reach the vacuole, RFP-TMD23-Ub was transported along the endocytic pathway, passing through both the TGN/EE and the MVB/LE. These findings provided evidence that ubiquitin is sufficient to target a PM-localized transmembrane protein for vacuolar degradation. At the same time, we could conclude that the absence of vacuolar delivery we had noticed in case of the reporter Box-GFP-Ub (see above) was indeed most likely due to the reversibility of its membrane anchorage.

Whenever ubiquitin is covalently bound to a target protein, it can be a substrate itself for further ubiquitination reactions that result in specifically linked poly-ubiquitin chains (Pickart and Eddins, 2004). Poly-ubiquitination has been originally associated with the proteasomal degradation of cytosolic or nuclear proteins, whereas mono-ubiquitination was assumed to be a signal for the internalization of PM proteins and their sorting to vacuoles/lysosomes. In the meantime, however, studies of several PM proteins in both animals and yeast could reveal that short poly-ubiquitin chains and/or multiple mono-ubiquitinations do highly increase the efficiency of internalization (Dupre et al., 2004;

Madshus, 2006). We addressed this issue trying to figure out whether the transport of our recombinant ubiquitin fusion proteins is likewise influenced by subsequent post-translational ubiquitination. Inspired by a recent publication, in which a reporter similar to Box-GFP-Ub was used to investigate ubiquitin-dependent internalization events in mammalian cells, we deleted two C-terminal glycine residues of ubiquitin, generating the modified reporters Box-GFP-UbΔGG and RFP-TMD23-UbΔGG. In the mammalian study mentioned, a lack of these two glycine residues evidently prevented any further ubiquitination of a PM-anchored recombinant ubiquitin fusion protein (Chen and De Camilli, 2005).

Expression of the Box-GFP-UbΔGG construct revealed an exclusive PM localization that was indistinguishable from the PM reporter Box-GFP. Internal endosomal signals, as seen for the non-mutagenized Box-GFP-Ub, were missing and thus indicated that endocytosis of the reporter strictly depends on the accessibility of the two C-terminal glycine residues. Interestingly, the same mutation in the reporter of the mammalian study mentioned above did not prevent its internalization in HeLa and CHO cells (Chen and De Camilli, 2005), demonstrating that in these experimental systems, mono-ubiquitination is sufficient to mediate sorting into the endocytic pathway. Our data, on the contrary, suggest that effective endocytosis of PM proteins in plant cells requires more than a single ubiquitin moiety. This is supported by recent findings showing that translational ubiquitin fusions of an *Arabidopsis* PM ATPase (PMA-EGFP-Ub) are less efficiently internalized when mutagenized to prevent poly-ubiquitination, even though vacuolar delivery is not completely inhibited (Herberth et al., 2012). Likewise, endocytic uptake of the auxin efflux carrier PIN2 was shown to depend on poly-ubiquitination (Leitner et al., 2012), whereas endocytosis of the iron transporter IRT1 apparently requires multiple mono-ubiquitinations (Barberon et al., 2011). All these observations point to the fact that only PM proteins labeled by multiple ubiquitin signals are efficiently recognized by the transport machinery for internalization.

Transport analysis of the other mutagenized reporter RFP-TMD23-UbΔGG revealed contradictory results at first glance. This reporter was unaffected by the deletion of the C-terminal glycine residues, being normally delivered to the vacuole as was seen for the non-mutagenized RFP-TMD23-Ub. We speculated that the differential behavior of Box-GFP-UbΔGG and RFP-TMD23-UbΔGG could just be the result of their differential targeting towards the PM: while the post-translationally anchored Box-GFP-UbΔGG displays its UbΔGG signal exclusively at the PM, secretory RFP-TMD23-UbΔGG might

already be recognized prior to reaching the PM and redirected into the biosynthetic vacuolar route. To clarify whether ubiquitin can indeed serve as a vacuolar sorting signal upstream of the PM, we employed the Golgi marker RFP-TMD20, which derives from the PM marker RFP-TMD23 by truncation of its TMD to only 20 amino acids. Due to the shortened TMD, RFP-TMD20 does not progress to the PM but stays in the Golgi stack instead (Brandizzi et al., 2002). By translational fusion to ubiquitin, we generated the reporter RFP-TMD20-Ub, which was efficiently transported to the vacuole via the endosomal route, just as seen before for RFP-TMD23-Ub. Deletion of the C-terminal glycine residues revealed that RFP-TMD20-UbΔGG was equally well delivered to the vacuole, identical to the mutagenized TMD23-based reporter. These findings for one thing indicate that ubiquitin does not only initiate endocytosis and vacuolar delivery of PM proteins, but also mediates vacuolar turnover of proteins from the Golgi. On the other hand, they suggest that depending on the reporters' location within the pathway (PM vs. Golgi), there are differential requirements for the accessibility of the ubiquitin C-terminus, pointing to the fact that endocytic and biosynthetic vacuolar sorting depend on different ubiquitination states. This interpretation is also in agreement with the mentioned findings for the ubiquitin-tagged PM ATPase that still weakly labeled the vacuole if prevented from being poly-ubiquitinated (Herberth et al., 2012). In this case, smaller amounts of the mono-ubiquitinated molecules might have been diverted from the Golgi while in transit to the PM and sent into the vacuolar route.

Vacuolar transport of integral membrane proteins is closely linked to the activity of the ESCRT machinery, which sorts ubiquitinated cargo into the lumen of MVBs/LEs prior to degradation in the lytic vacuole. Since all of our TMD-based ubiquitin reporters exclusively labeled the vacuolar lumen but not the tonoplast, we expected ESCRT to be involved in their sorting. To test for that, we expressed both RFP-TMD20-Ub and RFP-TMD23-Ub in a dominant-negative mutant background of the ESCRT-associated AAA-ATPase SKD1, which is known to cause the formation of class E compartments (Haas et al., 2007; Shahriari et al., 2010; see also section 7.1). Indeed, both ubiquitinated reporters did accumulate in enlarged class E-like endosomes that were also positively labeled by soluble vacuolar cargo. Vacuolar fluorescence was no longer observed, demonstrating that functionality of the ESCRT machinery is essential for endosomal sorting and vacuolar delivery of the reporters.

7.3 Vacuolar sorting receptors transport ligands from the ER and the Golgi to the TGN/EE (Künzl et al., submitted manuscript)

A crucial aspect in deciphering the molecular details of VSR-mediated transport is to understand where in the endomembrane system the receptors recognize and bind their ligands to divert them from default secretion. Ligand-binding studies, however, have been performed almost exclusively *in vitro*, so it is still controversial how these data are to be integrated into the existing model concept of VSR trafficking.

In the manuscript at hand, we developed a strategy that enabled us to test specific compartments for VSR-ligand interactions *in vivo* and thus to pinpoint the location of ligand binding and release. For this, we positioned the luminal ligand-binding domain (LBD) of a VSR within the individual compartments along the vacuolar route by taking advantage of marker proteins with well-defined intracellular localization. The use of full-length VSRs seemed not promising for this purpose, as they do not reliably target only one specific compartment. In this context, several VSR trafficking mutants have been published that bear substitutions of key amino acid motifs within the cytosolic domain, supposed to have sorting information for either the anterograde or retrograde transport machinery (daSilva et al., 2006; Foresti et al., 2010; Saint-Jean et al., 2010). These mutant VSRs reveal localization patterns that are shifted to some degree to either the TGN/EE or the MVB/LE, but they do also partially localize to the PM or to the vacuole. Moreover, in most of these trafficking mutants, the LBD was replaced by fluorophores, hence they might behave differently than binding-competent full-length receptors with the same mutations.

To overcome the problem of specifically targeting a VSR, we uncoupled the ligand-binding properties of the receptor from its intracellular transport by only employing the N-terminal LBD. This LBD fragment enters the secretory pathway as a soluble protein and as such has been shown to interact with vacuolar ligands (Watanabe et al., 2004; daSilva et al., 2005) and to cause their co-secretion (Shen et al., 2013b). In order to position the LBD in specific compartments along the vacuolar route, we intended to attach it to established fluorescent membrane markers. For this, translational fusions were no option as the N-terminal LBD of the type I VSR can only be fused to type I membrane markers (Niemes et al., 2010a), which are however not available for the Golgi and the TGN/EE. To circumvent these topology restrictions, we took advantage of the special properties of a llama heavy-chain antibody that was raised against the green fluorescent protein (GFP). Heavy-chain antibodies from *Camelidae* species are

unusual in that they are devoid of light chains and hence contain only a single variable domain, referred to as V_HH or nanobody, which is the smallest possible antigen-binding fragment (Muyldermans, 2001). A GFP-specific nanobody proved to be a powerful tool that can be recombinantly expressed in living cells to target and/or isolate GFP-tagged proteins (Rothbauer et al., 2006; Rothbauer et al., 2008). Inspired by that, we generated a translational fusion protein consisting of the soluble LBD fragment and the anti-GFP nanobody (abbreviated as Nb), which was named LBD-Nb.

Exploiting the high specificity and affinity of the anti-GFP nanobody, we planned on expressing the soluble LBD-Nb with GFP-tagged membrane proteins that would serve the dual function of being both a compartment-specific marker and a membrane anchor for the LBD. As a key prerequisite, all the markers had to display the GFP in the lumen of their target compartment to enable immune complex formation with the LBD-Nb. These interactions would result in membrane-bound LBDs with well-defined intracellular locations, making them ideal tools to explore the ligand-binding potential of a VSR within a selected compartment. The following compartmental markers were chosen for membrane anchorage of the LBD-Nb: GFP-CNX (ER), Man1-GFP (Golgi), SYP61-GFP (TGN/EE) and GFP-BP80 (MVB/LE). These are all single-spanning transmembrane proteins of either the type I (GFP-CNX and GFP-BP80) or type II (Man1-GFP and SYP61-GFP) and accordingly carry the GFP at their N- and C-termini, respectively. In any case, though, post-translational binding of the LBD-Nb to an anchor exposes an N-terminally accessible LBD, irrespective of the topology of the membrane-anchoring marker.

We first had to establish that the GFP nanobody is able to bind the different GFP-tagged markers, as a prerequisite for the compartment-specific positioning of the LBD. Therefore, we expressed the LBD-Nb with each of the markers in tobacco protoplasts and performed immunoprecipitation experiments. Pull-down of all markers resulted in coimmunoprecipitation of the LBD-Nb, indicating that the nanobody confers membrane anchorage. Furthermore, we ensured that interactions with the LBD-Nb do not alter the intracellular localization of the GFP-tagged markers, as these still colocalized with their corresponding RFP-tagged marker versions in CLSM analysis. To directly visualize the compartmental targeting of the LBD, we generated a fluorescent version of the LBD-Nb construct by insertion of monomeric RFP, yielding LBD-RFP-Nb. In coexpression with either of the markers, LBD-RFP-Nb was efficiently retained from being secreted but colocalized instead in each of the GFP-positive compartments. In summary, these

findings confirmed that the GFP nanobody is in fact a powerful tool that enables the precise compartment-specific positioning of the LBD within the secretory pathway.

Having established a strategy for the compartmental targeting of the LBD, we next aimed at investigating its ligand-binding capability in each of the addressed compartments. We reasoned, if a given compartment meets the environmental requirements for receptor-ligand interactions, then a membrane-anchored LBD-Nb should be able to retain those ligands. To test for this, we employed the fluorescent model ligand Aleu-RFP, which contains the N-terminal vacuolar sorting signal from barley proaleurain (Holwerda et al., 1992). We first ensured that either of the four LBD-Nb:GFP marker complexes is capable of binding Aleu-RFP *in vitro* to rule out that conformational issues might prevent LBD-ligand interactions in an otherwise favoring compartmental environment. For this, the LBD-Nb was coexpressed and coimmunoprecipitated in complex with each of the compartmental markers, and then the preassembled complexes were incubated with Aleu-RFP under binding conditions (Kirsch et al., 1994; Watanabe et al., 2004; Shen et al., 2014). In all cases, coprecipitation of Aleu-RFP occurred, thus confirming that the LBD possess binding competence if in complex with the anchors.

We then successively explored the compartments along the vacuolar route by live cell imaging, starting with the point of origin; the ER. Expression of the marker GFP-CNX normally had no influence on the vacuolar delivery of the ligand Aleu-RFP. Upon coexpression of the LBD-Nb to assemble ER-anchored LBDs, however, Aleu-RFP was effectively retained in the ER and colocalized with GFP-CNX. We tested whether this colocalization results from interactions between Aleu-RFP and the anchored LBD by making use of the physical principle of Förster resonance energy transfer (FRET). FRET describes a non-radiative transfer of energy from an excited donor chromophore to a nearby acceptor chromophore, which may occur if the emission spectrum of the donor overlaps with the absorption spectrum of the acceptor (Clegg, 2009; Ishikawa-Ankerhold et al., 2012). FRET strongly depends on the distance between donor and acceptor and is consequently limited to chromophores that are in close proximity, being separated by no more than 10 nm. These distances are comparable to the dimensions of multimeric protein complexes, rendering FRET measurements a powerful technique to investigate protein-protein interactions in living cells.

We utilized the GFP of the ER marker GFP-CNX as a FRET donor, while RFP in the ligand Aleu-RFP served the function of the FRET acceptor. As these two proteins do not interact, their fluorophores normally do not come close enough to cause FRET.

However, by assembly of LBD-Nb:GFP-CNX complexes within the ER, we were able to detect binding of Aleu-RFP to the LBD since this caused the two fluorophores to get close enough for energy transfer. We took advantage of the fact that FRET decreases the fluorescence lifetime of the donor fluorophore (here the GFP) and thus performed fluorescence lifetime imaging microscopy (FLIM) to detect FRET (Bucherl et al., 2014). The FRET-FLIM analysis of the LBD-Nb:GFP-CNX complexes revealed a significant reduction of the GFP lifetime in the presence of Aleu-RFP, which did not occur in the presence of a non-ligand (Sec-RFP) or in the absence of the LBD. This demonstrated that Aleu-RFP indeed interacts with the anchored LBD and consequently identified the ER as a compartment that favors VSR-ligand binding.

It has been previously suggested that receptor-mediated sorting of vacuolar proteins is already initiated in the early secretory pathway. In this respect, soluble LBDs when fused to the ER-retrieval signal HDEL were shown to cause ER accumulation of soluble vacuolar proteins (Watanabe et al., 2004; daSilva et al., 2005). Although this approach could not resolve whether ligand binding occurs already in the ER or upon arrival in the Golgi, it became apparent that interaction should have happened at the latest in the Golgi. More direct evidence for ligand binding within the ER was provided by LBD fusions to ER-resident membrane proteins that likewise caused vacuolar proteins to accumulate in the ER (Niemes et al., 2010a). Beside these localization data, however, molecular interactions between ER-localizing receptors and ligands have never been proven. Our FRET-FLIM data now provide clear evidence that the ligand Aleu-RFP is bound by VSRs as early as in the ER lumen. We could further confirm these data by immunoprecipitation experiments showing that the ER-assembled LBD-Nb:GFP-CNX complexes coprecipitate the coexpressed Aleu-RFP. Given the fact that plant vacuolar sorting signals do not originate from post-translational modifications (as do lysosomal sorting signals of MPR ligands in animals; see section 5.2.2) but are encoded in the amino acid sequence, it is reasonable to assume that vacuolar proteins are premade ligands once they have been synthesized in the ER and can thus immediately interact with VSRs. In this regard, AtVSR1 was recently shown to be *N*-glycosylated in its LBD, which stabilizes binding of cargo ligands (Shen et al., 2014). As *N*-linked glycosylation occurs in the ER lumen (Liu and Howell, 2010), VSRs putatively adopt their final ligand-binding conformation already upon entering the ER, although it is currently unknown whether the *N*-glycans undergo further modifications in the Golgi.

Having identified the ER as the initial compartment of the secretory pathway to favor ligand binding, we next tested the MVB/LE being the last morphologically characterized compartment *en route* to the vacuole. We decided to proceed with the MVB/LE since here, ligands should have been released at the latest, which makes the compartment the ideal negative control to proof the concept of our FRET-FLIM analysis. The recent postulation of a 'late PVC' being situated in-between the MVB/LE (or PVC) and the vacuole (Foresti et al., 2010) was not taken into consideration here. The only evidence in favor of its existence derives from a fluorescent VSR trafficking mutant defective in recycling, which beside accumulating in the vacuole labels endosomal structures that do not colocalize with markers for the TGN/EE and MVB/LE but apparently with soluble vacuolar cargo (Foresti et al., 2010). Hence, a model was proposed in which a 'late PVC' matures from a MVB/LE via retromer-mediated retrieval of the discharged VSRs, which leaves the released ligands in a 'late PVC' for fusion with the vacuole (Foresti et al., 2010). In every respect, the lack of functional VSRs in the putative 'late PVC' would still render the MVB/LE the last compartment to check for ligand interactions.

Accordingly, we expressed the LBD-Nb fusion with the marker GFP-BP80 to anchor the LBD within the MVB/LE. If coexpressed, Aleu-RFP did indeed colocalize with the LBD-Nb:GFP-BP80 complexes in the MVB/LE, however, this colocalization was also observed in the absence of the LBD-Nb. At steady-state conditions, Aleu-RFP is commonly found in the MVB/LE while in transit towards the vacuole, so colocalization in this compartment cannot necessarily be interpreted as interaction. To get further insights, we applied the drug wortmannin, which induces homotypic fusion of MVBs/LEs and thus dramatically enlarges the compartment (Tse et al., 2004). These bloated MVBs/LEs revealed a differential distribution, with the LBD-Nb:GFP-BP80 complexes labeling the ring-shaped limiting membrane, while Aleu-RFP localized to the lumen of the compartment. This luminal location indicated that the ligand is in fact not bound to the LBD in the MVB/LE. FRET-FLIM analysis finally confirmed these observations as Aleu-RFP did not reduce the fluorescence lifetime of the LBD-Nb:GFP-BP80 complex. FRET could only be triggered in control experiments by assembly of a dual-fluorophore complex consisting of GFP-BP80 and the red fluorescent LBD-RFP-Nb, which proved that FRET-FLIM can be applied to this compartment. In conclusion, our findings for the MVB/LE revealed that only the combination of localization analysis and FRET-FLIM allows for a reliable assessment of whether a given compartment supports or restricts ligand binding.

It has recently been speculated that soluble vacuolar proteins interact with VSRs in the *cis*-Golgi (Gershlick et al., 2014), however that still awaits experimental confirmation. To test this hypothesis, we coexpressed the LBD-Nb fusion with the *cis*-Golgi marker Man1-GFP to anchor LBDs in the Golgi for ligand-interaction analysis. Live cell imaging revealed that the ligand Aleu-RFP indeed colocalizes with the LBD-Nb:Man1-GFP complexes, which was never observed in the absence of the LBD. We confirmed that this results from binding of Aleu-RFP to the anchored LBD by measuring significant reductions in the fluorescence lifetime of the LBD-Nb:Man1-GFP complexes, which did not occur in the absence of the LBD. Accordingly, our data show that VSRs are already associated with their ligands upon arrival at the Golgi apparatus and that these VSR-ligand complexes persist while entering the Golgi and putatively also throughout the stack.

The next compartment *en route* to the vacuole, the TGN/EE, still has the reputation of being the location where ligands are bound by VSRs for vacuolar delivery, based on the original localization data and *in vitro* binding studies mentioned earlier. However, in the light of recent findings identifying the TGN/EE to be Golgi-independent and of endosomal nature at the same time, the situation has to be carefully reassessed. With this in mind, we continued analyzing compartmental VSR-ligand interactions and next assembled LBD-Nb:SYP61-GFP complexes in the TGN/EE. Life cell imaging revealed that vacuolar transport of the ligand Aleu-RFP was unaffected by the anchored LBDs, indicating that the TGN/EE does not support VSR-ligand binding. FRET-FLIM analysis confirmed these findings by showing no reductions in the fluorescence lifetime of the LBD-Nb:SYP61-GFP complex when coexpressed with Aleu-RFP. To demonstrate that positive interactions would have given perceptible readouts, we assembled SYP61-GFP-based complexes with the red fluorescent LBD-RFP-Nb fusion. Assembly of this dual-fluorophore complex proofed that the FRET-FLIM-based analysis is suitable to identify protein-protein interactions in the TGN/EE. This strengthens the notion that the absence of Aleu-RFP-triggered FRET reveals the TGN/EE as being a compartment unfavorable for ligand binding.

Our findings with the TGN/EE-anchored LBDs suggested that ligands are released from their receptors once the VSR-ligand complexes have arrived at the TGN/EE. To demonstrate that ligand binding to the LBD-Nb:SYP61-GFP complex could have happened if the compartmental environment would have favored interactions, we blocked arrival of the proteins at the TGN/EE by applying the drug brefeldin A (BFA). BFA

caused inhibition of the ER export and consequently led to coaccumulation of the LBD-Nb:SYP61-GFP complexes and the ligand Aleu-RFP within the ER. There, Aleu-RFP indeed interacted with the SYP61-GFP-anchored LBDs as was confirmed by FRET-FLIM analysis and coimmunoprecipitation experiments. Altogether, these data indicate that VSRs bind their ligands already in the early secretory pathway and release them upon arrival in the TGN/EE. This is in agreement with the observation that retromer, the coat complex facilitating VSR recycling, localizes to the TGN/EE (Niemes et al., 2010b; Stierhof et al., 2013). Furthermore, our findings showing that MVBs/LEs mature from the TGN/EE and finally fuse with the vacuole (Scheuring et al., 2011, see section 7.1) would render a VSR-mediated vesicular sorting step at the TGN/EE redundant.

Release of ligands has been proposed to depend on acidification of the compartments along the vacuolar pathway (Kirsch et al., 1994), by analogy to the concept of receptor-mediated lysosomal sorting in animal cells. The first VSR (pea BP80) was identified through *in vitro* binding to immobilized ligands at a pH of 7.1, from which it was released when the pH was lowered to 4 (Kirsch et al., 1994). By this time, however, pH values for the individual compartments of plant cells were still unknown. Only very recently, experimental data have become available that provide a roadmap of the compartmental pH values in plants (Martiniere et al., 2013; Shen et al., 2013a; Luo et al., 2015). These data show that the pH within the ER is the highest (pH 7.1 to 7.5), which comes close to the value that was adjusted for binding of BP80 to its ligands *in vitro*. Also the more recent ligand-binding analyses have all been performed at neutral pH (Watanabe et al., 2004; Shen et al., 2014), which is in accordance with our findings suggesting that the environmental conditions within the ER lumen are in favor of ligand binding. The compartmental pH measurements furthermore revealed that starting from the ER, pH values progressively decrease in the following compartments until reaching the TGN/EE being the most acidic compartment (pH 5.6 to 6.3) *en route* to the vacuole. Values for the downstream-situated MVB/LE were shown to be either similar (Shen et al., 2013a) or again more alkaline (Martiniere et al., 2013) than in the TGN/EE. Hence, if acidification is indeed the trigger for ligand release, VSR-mediated sorting is unlikely to occur between the TGN/EE and the MVB/LE, but would rather be expected to take place one step earlier, namely between the Golgi stack (pH 6.8 to 6.9) and the TGN/EE where the greatest pH difference of two neighboring compartments exists.

An alternative idea was lately proposed trying to explain the discrepancy between the acidification-driven sorting model and the concept of VSR-mediated TGN/EE-to-

MVB/LE transport in the light of recent pH measurements (Reguera et al., 2015). The authors refer to former *in vitro* data showing a ligand-binding optimum for pea BP80 to be at pH 6, with a reduction to 50% at pH 5 and 7.5 (Kirsch et al., 1994). Accordingly, they claim that the acidic conditions in the TGN/EE are close to this optimum and thus should favor ligand binding, while the more alkaline pH in the MVB/LE is above the optimum and would consequently trigger ligand release (Reguera et al., 2015). This model view does however not explain how VSR-ligand interactions could be identified in all the previous *in vitro* binding analyses applying neutral (pH 7.0 or 7.1) conditions (Kirsch et al., 1994; Watanabe et al., 2004; Shen et al., 2014), and also why ER-localized LBDs should influence the transport of vacuolar proteins (Watanabe et al., 2004; daSilva et al., 2005; Niemes et al., 2010a) if the neutral pH in the ER would not allow for ligand binding. Lastly, how could we measure interactions between Aleu-RFP and an ER-anchored LBD via FRET-FLIM in a non-invasive approach that does not influence the *in situ* pH of the ER?

Another important factor that influences VSR-ligand interactions was shown to be the concentration of free calcium ions (Ca^{2+}; Stael et al., 2012). It has been suggested that binding of Ca^{2+} to an epidermal growth factor (EGF) repeat induces conformational changes within the LBD of the VSR, thereby modulating receptor-ligand interactions (Cao et al., 2000; Watanabe et al., 2002). Depending on Ca^{2+}, ligand binding was shown to occur and persist even at a pH of 4 (Watanabe et al., 2002), indicating that Ca^{2+} supports ligand binding under otherwise unfavorable conditions. Our knowledge of the Ca^{2+} concentrations within the plant endomembrane system is still limited, but it is generally assumed that the vacuole is the main storage compartment followed by the ER with an estimate of 50 to 500 µM of free Ca^{2+} (Stael et al., 2012). The following transit compartments *en route* to the vacuole apparently lack comparable Ca^{2+} concentrations, as was suggested by measurements of the Golgi apparatus showing Ca^{2+} values in the nanomolar range (Ordenes et al., 2012). Together, these data indicate that VSR-ligand interactions are regulated by an intricate interplay between pH, free Ca^{2+}, and maybe other unknown factors that collectively render a given compartment either favorable or unfavorable for ligand binding. However, since all these biochemical properties are currently not fully understood, interpretation of data concerning single aspects such as pH must be considered with deliberation.

Our compartment-specific ligand-binding analysis identified the ER and the Golgi as compartments that favor VSR-ligand interactions, while the TGN/EE and the MVB/LE

were found to restrict interactions. This implies that *post*-TGN/EE transport of soluble proteins towards the vacuole does not depend on VSRs and consequently also does not require vacuolar sorting signals from the TGN/EE onwards. In order to proof this hypothesis, we sent soluble fluorescent reporters that lack a vacuolar sorting signal to the TGN/EE and analyzed their transport. As these sorting signals are however necessary for the VSR-mediated delivery to the TGN/EE, we took advantage of the early endosomal properties of the TGN/EE and targeted the soluble reporters by endocytic uptake to the TGN/EE. For this, we supplemented suspension-cultured protoplasts with triple RFP (3xRFP)-containing culture medium and then followed endocytosis of the reporter. Live cell imaging revealed that endocytosed 3xRFP is indeed delivered to the vacuole where it accumulates over time. To trace its vacuolar pathway, we modified the reporter to contain the anti-GFP nanobody, generating 3xRFP-Nb, and applied it to cells expressing GFP anchors for either the TGN/EE (SYP61-GFP) or the MVB/LE (GFP-BP80). Nanobody-mediated assembly in these compartments proofed that the reporter transits through the endosomal pathway *en route* to the vacuole, in a process that does not involve sorting by VSRs. Consequently, the vacuole must be considered the default location for soluble proteins upon arrival in the TGN/EE, irrespective of whether these proteins were delivered by the biosynthetic or the endocytic pathway.

7.4 Closing remarks

In the course of my research, different aspects of vacuolar trafficking in plant cells were addressed, including the receptor-mediated transport of soluble proteins and ESCRT-mediated endocytic transport for degradation of membrane proteins. We gained insight into how these routes collectively lead from the TGN/EE to the lytic vacuole and also identified machinery crucial for this endosomal pathway. In the following paragraphs, our findings will be incorporated into a revised model for plant vacuolar trafficking that is schematically depicted in Figure 2.

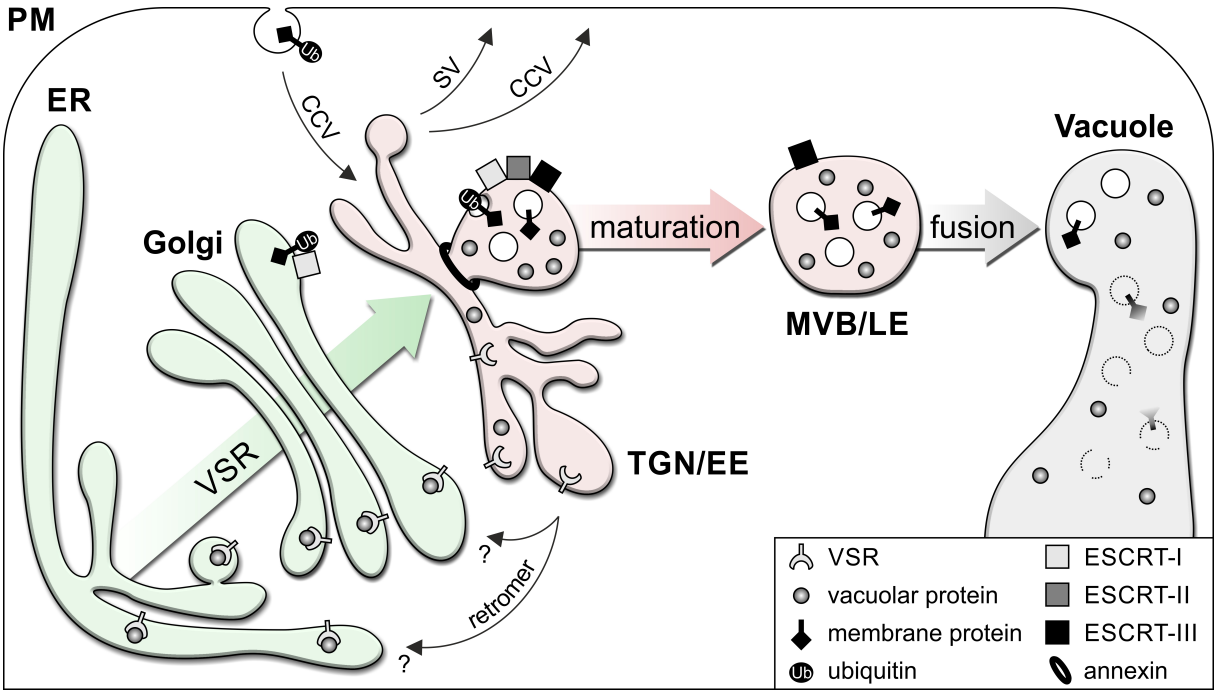

Figure 2. Revised model of the vacuolar transport processes in the plant endomembrane system. Vacuolar sorting of PM proteins is triggered by ubiquitination, which causes endocytosis in CCVs and delivery to the TGN/EE. There, the ESCRT complexes I-III bind the ubiquitinated cargo and initiate sorting into intraluminal vesicles. ESCRT-I also localizes to the Golgi, where it may sort membrane proteins of the biosynthetic pathway for degradation. At the TGN/EE, ESCRT activity is necessary for the maturation of MVBs/LEs from a TGN/EE subdomain. The budding MVBs/LEs are finally pinched off by annexin-driven membrane fission. Mature MVBs/LEs are non-persistent transport carriers that fuse with the vacuole to deliver their cargo. Part of this cargo consists of soluble vacuolar proteins from the biosynthetic pathway. These are bound by VSRs in the ER, as the conditions (neutral pH, high Ca^{2+} conc.) favor interactions. The VSR-ligand complexes are exported (putatively in COPII vesicles) and delivered to the Golgi. While in transit through the Golgi, VSRs and ligands remain in complex until arriving at the TGN/EE where conditions (acidic pH, low Ca^{2+} conc.) trigger ligand release. The discharged VSRs are packaged in retromer-coated carriers for recycling to the Golgi or the ER. The released vacuolar proteins passively enter nascent MVBs/LEs and reach the vacuole by default. Further (non-vacuolar) transport events at the TGN/EE include secretion and recycling of PM proteins via SVs and CCVs, respectively. (Adapted and modified from Künzl et al., submitted manuscript)

Upon being synthesized in the ER, soluble vacuolar cargo is recognized by VSRs, as the present conditions (i.e. high Ca^{2+} conc., neutral pH) favor interactions. The VSR-ligand complexes leave the ER in COPII-coated vesicles together with secretory cargo and are delivered to the *cis*-cisterna of a Golgi stack. While in transit through the stack, the VSRs remain in complex with the ligands until they arrive at the TGN/EE, putatively by maturation of the *trans*-most Golgi cisterna (Kang et al., 2011). In the TGN/EE, the lower Ca^{2+} concentrations and an acidifying V-ATPase provide the conditions for ligand release, whereupon the discharged VSRs are sequestered and packaged in retromer-coated carriers for recycling. The target compartment for VSR recycling is still unknown and could be the Golgi, the ER, or also both. Remarkably, inhibition of retromer function either by expression of mutant sorting nexins or gene knockdown was shown to inhibit the ER export of newly synthesized VSRs together with cargo ligands, while the COPII-mediated export of secretory cargo was unaffected (Niemes et al., 2010a). Retromer-

mediated recycling apparently exhibits a specific feedback control on the ER export of VSR-ligand complexes comparable to that observed for the COPI-/COPII-mediated pathways in bidirectional ER-Golgi trafficking (Stefano et al., 2006). Thus, it is plausible to assume that VSRs are finally recycled back to the ER, with the Golgi stack possibly being a way station on the route. Moreover, the VSR-specific ER export block caused by retromer inhibition has been considered an indication of a COPII-independent ER-export mechanism for VSR-ligand complexes (Niemes et al., 2010a), albeit underlying mechanisms remain unclear.

Vacuolar sorting of proteins from the PM is triggered by ubiquitination, which causes internalization via clathrin-coated vesicles and delivery of the ubiquitin-tagged proteins to the TGN/EE. Here, the complexes of the ESCRT machinery bind and sequester the ubiquitinated cargo and initiate sorting into intraluminal vesicles. Notably, the ESCRT-I complex is also localizing to the Golgi, where it may bind to membrane proteins of the biosynthetic pathway that are destined for vacuolar degradation. This is supported by the observation that a ubiquitin-tagged Golgi marker is sorted in the endosomal route, with ESCRT functionality being a prerequisite for its vacuolar delivery. At the TGN/EE, the joint activity of the three ESCRT complexes is necessary for the formation of the MVB/LE, which matures from a TGN/EE subdomain via budding. The nascent MVB/LE is finally pinched off from the TGN/EE by annexin-driven membrane fission, giving rise to an independent compartment. Mature MVBs/LEs act as vacuolar transport carriers that are consumed by fusion with the tonoplast to deliver their cargo. Part of this cargo consists of the soluble proteins that have been transported by VSRs from the early secretory pathway. Once released from the receptors in the TGN/EE, the soluble cargo becomes passively incorporated into the nascent MVBs/LEs and reaches the vacuole by default. This notion is supported by our findings showing that endocytosed soluble proteins lacking any sorting information whatsoever arrive at the vacuole after being internalized into the TGN/EE.

The suggested model may explain how vacuolar transport of both biosynthetic and endocytic cargo converge in the TGN/EE before jointly proceeding to the vacuole. Still, transport steps other than MVB/LE maturation and retromer-mediated VSR recycling occur at the TGN/EE which need to be included. Recycling of internalized PM proteins can be explained by the existence of TGN/EE-derived CCVs, which probably sort the constitutively cycling PM receptors and transporters, rather than delivering VSR-ligand complexes to a prevacuolar MVB/LE as suggested originally. Yet, it is possible that

more than one type of CCVs is formed at the TGN/EE: beside the AP1 complex that evidently localizes to the TGN/EE (Teh et al., 2013) and is the prime candidate to assemble CCVs for recycling membrane proteins to the PM (discussed by Robinson and Pimpl, 2014a), AP3 complexes have been speculated to localize at least partially to the TGN/EE (Lee et al., 2007). More recent findings however argue for an AP3-mediated sorting step at the Golgi, as the tonoplast sucrose transporter SUC4 specifically accumulated in the *cis*-Golgi if the AP3 β-subunit was knocked out (Wolfenstetter et al., 2012). The same β-subunit was shown to localize to the periphery of FM4-64-labeled BFA compartments, which also suggests a localization at the Golgi rather than at the TGN/EE (Feraru et al., 2010). Hence, AP3 might facilitate vacuolar transport of certain tonoplast-localized proteins in a pathway that bypasses endosomal compartments, being delivered directly from the Golgi as by analogy to AP3-mediated trafficking in yeast (Dell'Angelica, 2009).

Moreover, secretory cargo is thought to pass the TGN/EE before reaching the PM (Viotti et al., 2010). A point in favor of this idea is the occurrence of secretory vesicles at the TGN/EE that contain complex polysaccharides of the cell wall (Kang et al., 2011). If the suggested secretory bulk flow of soluble proteins (Phillipson et al., 2001) includes the TGN/EE, then it is difficult to reconcile how soluble vacuolar cargo is prevented from being secreted once it was released from the VSRs in the TGN/EE. An explanation for this apparent discrepancy may be given by the observation that the TGN/EE exists in two different types: a Golgi-associated or ‘early’ TGN/EE, and a Golgi-independent or ‘late’ TGN/EE (Kang et al., 2011; Uemura et al., 2014). It has been noticed that the Golgi-associated ‘early’ TGNs/EEs are rich in budding secretory vesicles but not in clathrin-coated vesicles, which often arise only on more mature (‘late’) TGNs/EEs (Kang et al., 2011). These ‘late’ TGNs/EEs are however predominantly labeled by the a1-subunit of the endosomal V-ATPase (VHA-a1-GFP), which is less frequently found at the ‘early’ TGN/EE (Kang et al., 2011). It is thus tempting to speculate that ‘early’ TGNs/EEs mainly fulfill secretory functions and still maintain VSR-ligand interactions, until they mature into ‘late’ TGNs/EEs that mainly receive endocytic cargo and become increasingly acidified by the V-ATPase, which finally triggers the release of the vacuolar cargo ligands. Certainly, further experimental work will be necessary to fully unravel the complex sorting events that take place at the TGN/EE, but with the current knowledge and the molecular tools and markers at hand, we will probably soon gain a better understanding of the post-Golgi trafficking in plants.

8. References

Abas, L., Benjamins, R., Malenica, N., Paciorek, T., Wisniewska, J., Moulinier-Anzola, J.C., Sieberer, T., Friml, J., and Luschnig, C. (2006). Intracellular trafficking and proteolysis of the Arabidopsis auxin-efflux facilitator PIN2 are involved in root gravitropism. Nature cell biology **8,** 249-256.

Bandmann, V., and Homann, U. (2012). Clathrin-independent endocytosis contributes to uptake of glucose into BY-2 protoplasts. The Plant journal : for cell and molecular biology **70,** 578-584.

Bandmann, V., Muller, J.D., Kohler, T., and Homann, U. (2012). Uptake of fluorescent nano beads into BY2-cells involves clathrin-dependent and clathrin-independent endocytosis. FEBS Lett **586,** 3626-3632.

Bar, M., and Avni, A. (2009). EHD2 inhibits ligand-induced endocytosis and signaling of the leucine-rich repeat receptor-like protein LeEix2. The Plant journal : for cell and molecular biology **59,** 600-611.

Barberon, M., Zelazny, E., Robert, S., Conejero, G., Curie, C., Friml, J., and Vert, G. (2011). Monoubiquitin-dependent endocytosis of the iron-regulated transporter 1 (IRT1) transporter controls iron uptake in plants. Proceedings of the National Academy of Sciences of the United States of America **108,** E450-458.

Bednarek, S.Y., and Raikhel, N.V. (1992). Intracellular trafficking of secretory proteins. Plant Mol Biol **20,** 133-150.

Boevink, P., Oparka, K., Santa Cruz, S., Martin, B., Betteridge, A., and Hawes, C. (1998). Stacks on tracks: the plant Golgi apparatus traffics on an actin/ER network. The Plant journal : for cell and molecular biology **15,** 441-447.

Bowers, K., and Stevens, T.H. (2005). Protein transport from the late Golgi to the vacuole in the yeast Saccharomyces cerevisiae. Biochimica et biophysica acta **1744,** 438-454.

Brandizzi, F., and Barlowe, C. (2013). Organization of the ER-Golgi interface for membrane traffic control. Nature reviews. Molecular cell biology **14,** 382-392.

Brandizzi, F., Frangne, N., Marc-Martin, S., Hawes, C., Neuhaus, J.M., and Paris, N. (2002). The destination for single-pass membrane proteins is influenced markedly by the length of the hydrophobic domain. The Plant cell **14,** 1077-1092.

Braulke, T., and Bonifacino, J.S. (2009). Sorting of lysosomal proteins. Biochimica et biophysica acta **1793,** 605-614.

Bucherl, C.A., Bader, A., Westphal, A.H., Laptenok, S.P., and Borst, J.W. (2014). FRET-FLIM applications in plant systems. Protoplasma **251,** 383-394.

Cao, X., Rogers, S.W., Butler, J., Beevers, L., and Rogers, J.C. (2000). Structural requirements for ligand binding by a probable plant vacuolar sorting receptor. The Plant cell **12,** 493-506.

Chen, H., and De Camilli, P. (2005). The association of epsin with ubiquitinated cargo along the endocytic pathway is negatively regulated by its interaction with clathrin. Proceedings of the National Academy of Sciences of the United States of America **102,** 2766-2771.

Chen, X., Irani, N.G., and Friml, J. (2011). Clathrin-mediated endocytosis: the gateway into plant cells. Current opinion in plant biology **14,** 674-682.

Chow, C.M., Neto, H., Foucart, C., and Moore, I. (2008). Rab-A2 and Rab-A3 GTPases define a trans-golgi endosomal membrane domain in Arabidopsis that contributes substantially to the cell plate. The Plant cell **20,** 101-123.

Chrispeels, M.J. (1991). Sorting of Proteins in the Secretory System. Annu Rev Plant Phys **42,** 21-53.

Clegg, R.M. (2009). Forster resonance energy transfer-FRET what is it, why do it, and how it's done. Lab Tech Biochem Mol **33,** 1-57.

Crowell, E.F., Bischoff, V., Desprez, T., Rolland, A., Stierhof, Y.D., Schumacher, K., Gonneau, M., Hofte, H., and Vernhettes, S. (2009). Pausing of Golgi bodies on microtubules regulates secretion of cellulose synthase complexes in Arabidopsis. The Plant cell **21,** 1141-1154.

Cui, Y., Zhao, Q., Gao, C., Ding, Y., Zeng, Y., Ueda, T., Nakano, A., and Jiang, L. (2014). Activation of the Rab7 GTPase by the MON1-CCZ1 Complex Is Essential for PVC-to-Vacuole Trafficking and Plant Growth in Arabidopsis. The Plant cell **26,** 2080-2097.

daSilva, L.L., Foresti, O., and Denecke, J. (2006). Targeting of the plant vacuolar sorting receptor BP80 is dependent on multiple sorting signals in the cytosolic tail. The Plant cell **18,** 1477-1497.

daSilva, L.L., Snapp, E.L., Denecke, J., Lippincott-Schwartz, J., Hawes, C., and Brandizzi, F. (2004). Endoplasmic reticulum export sites and Golgi bodies behave as single mobile secretory units in plant cells. The Plant cell **16,** 1753-1771.

daSilva, L.L., Taylor, J.P., Hadlington, J.L., Hanton, S.L., Snowden, C.J., Fox, S.J., Foresti, O., Brandizzi, F., and Denecke, J. (2005). Receptor salvage from the prevacuolar compartment is essential for efficient vacuolar protein targeting. The Plant cell **17,** 132-148.

Dell'Angelica, E.C. (2009). AP-3-dependent trafficking and disease: the first decade. Current opinion in cell biology **21,** 552-559.

Denecke, J., De Rycke, R., and Botterman, J. (1992). Plant and mammalian sorting signals for protein retention in the endoplasmic reticulum contain a conserved epitope. The EMBO journal **11,** 2345-2355.

Dettmer, J., Hong-Hermesdorf, A., Stierhof, Y.D., and Schumacher, K. (2006). Vacuolar H+-ATPase activity is required for endocytic and secretory trafficking in Arabidopsis. The Plant cell **18,** 715-730.

Dhonukshe, P., Aniento, F., Hwang, I., Robinson, D.G., Mravec, J., Stierhof, Y.D., and Friml, J. (2007). Clathrin-mediated constitutive endocytosis of PIN auxin efflux carriers in Arabidopsis. Current biology : CB **17,** 520-527.

Doyotte, A., Russell, M.R., Hopkins, C.R., and Woodman, P.G. (2005). Depletion of TSG101 forms a mammalian "Class E" compartment: a multicisternal early endosome with multiple sorting defects. Journal of cell science **118,** 3003-3017.

Dupre, S., Urban-Grimal, D., and Haguenauer-Tsapis, R. (2004). Ubiquitin and endocytic internalization in yeast and animal cells. Biochimica et biophysica acta **1695,** 89-111.

Dupree, P., and Sherrier, D.J. (1998). The plant Golgi apparatus. Biochimica et biophysica acta **1404,** 259-270.

Fan, L., Li, R., Pan, J., Ding, Z., and Lin, J. (2015). Endocytosis and its regulation in plants. Trends in plant science **20,** 388-397.

Feraru, E., Paciorek, T., Feraru, M.I., Zwiewka, M., De Groodt, R., De Rycke, R., Kleine-Vehn, J., and Friml, J. (2010). The AP-3 beta adaptin mediates the biogenesis and function of lytic vacuoles in Arabidopsis. The Plant cell **22,** 2812-2824.

Foresti, O., and Denecke, J. (2008). Intermediate organelles of the plant secretory pathway: identity and function. Traffic **9,** 1599-1612.

Foresti, O., Gershlick, D.C., Bottanelli, F., Hummel, E., Hawes, C., and Denecke, J. (2010). A recycling-defective vacuolar sorting receptor reveals an intermediate compartment situated between prevacuoles and vacuoles in tobacco. The Plant cell **22,** 3992-4008.

Fujimoto, M., Arimura, S., Ueda, T., Takanashi, H., Hayashi, Y., Nakano, A., and Tsutsumi, N. (2010). Arabidopsis dynamin-related proteins DRP2B and DRP1A participate together in clathrin-coated vesicle formation during endocytosis. Proceedings of the National Academy of Sciences of the United States of America **107,** 6094-6099.

Gadeyne, A., Sanchez-Rodriguez, C., Vanneste, S., Di Rubbo, S., Zauber, H., Vanneste, K., Van Leene, J., De Winne, N., Eeckhout, D., Persiau, G., Van De Slijke, E., Cannoot, B., Vercruysse, L., Mayers, J.R., Adamowski, M., Kania, U., Ehrlich, M., Schweighofer, A., Ketelaar, T., Maere, S., Bednarek, S.Y., Friml, J., Gevaert, K., Witters, E., Russinova, E., Persson, S., De Jaeger, G., and Van Damme, D. (2014). The TPLATE adaptor complex drives clathrin-mediated endocytosis in plants. Cell **156,** 691-704.

Gao, C., Cai, Y., Wang, Y., Kang, B.H., Aniento, F., Robinson, D.G., and Jiang, L. (2014a). Retention mechanisms for ER and Golgi membrane proteins. Trends in plant science **19,** 508-515.

Gao, C., Luo, M., Zhao, Q., Yang, R., Cui, Y., Zeng, Y., Xia, J., and Jiang, L. (2014b). A unique plant ESCRT component, FREE1, regulates multivesicular body protein sorting and plant growth. Current biology : CB **24,** 2556-2563.

Geldner, N., Hyman, D.L., Wang, X., Schumacher, K., and Chory, J. (2007). Endosomal signaling of plant steroid receptor kinase BRI1. Genes Dev **21,** 1598-1602.

Geldner, N., Denervaud-Tendon, V., Hyman, D.L., Mayer, U., Stierhof, Y.D., and Chory, J. (2009). Rapid, combinatorial analysis of membrane compartments in intact plants with a multicolor marker set. The Plant journal : for cell and molecular biology **59,** 169-178.

Geldner, N., Anders, N., Wolters, H., Keicher, J., Kornberger, W., Muller, P., Delbarre, A., Ueda, T., Nakano, A., and Jurgens, G. (2003). The Arabidopsis GNOM ARF-GEF mediates endosomal recycling, auxin transport, and auxin-dependent plant growth. Cell **112,** 219-230.

Gershlick, D.C., Lousa Cde, M., Foresti, O., Lee, A.J., Pereira, E.A., daSilva, L.L., Bottanelli, F., and Denecke, J. (2014). Golgi-dependent transport of vacuolar sorting receptors is regulated by COPII, AP1, and AP4 protein complexes in tobacco. The Plant cell **26,** 1308-1329.

Gohre, V., Spallek, T., Haweker, H., Mersmann, S., Mentzel, T., Boller, T., de Torres, M., Mansfield, J.W., and Robatzek, S. (2008). Plant pattern-recognition receptor FLS2 is directed for degradation by the bacterial ubiquitin ligase AvrPtoB. Current biology : CB **18,** 1824-1832.

Haas, T.J., Sliwinski, M.K., Martinez, D.E., Preuss, M., Ebine, K., Ueda, T., Nielsen, E., Odorizzi, G., and Otegui, M.S. (2007). The Arabidopsis AAA ATPase SKD1 is involved in multivesicular endosome function and interacts with its positive regulator LYST-INTERACTING PROTEIN5. The Plant cell **19,** 1295-1312.

Happel, N., Honing, S., Neuhaus, J.M., Paris, N., Robinson, D.G., and Holstein, S.E. (2004). Arabidopsis mu A-adaptin interacts with the tyrosine motif of the vacuolar sorting receptor VSR-PS1. The Plant journal : for cell and molecular biology **37,** 678-693.

Harley, S.M., and Beevers, L. (1989). Coated Vesicles Are Involved in the Transport of Storage Proteins during Seed Development in Pisum-Sativum-L. Plant physiology **91,** 674-678.

Herberth, S., Shahriari, M., Bruderek, M., Hessner, F., Muller, B., Hulskamp, M., and Schellmann, S. (2012). Artificial ubiquitylation is sufficient for sorting of a plasma membrane ATPase to the vacuolar lumen of Arabidopsis cells. Planta **236,** 63-77.

Hicke, L., and Dunn, R. (2003). Regulation of membrane protein transport by ubiquitin and ubiquitin-binding proteins. Annual review of cell and developmental biology **19,** 141-172.

Hinz, G., Colanesi, S., Hillmer, S., Rogers, J.C., and Robinson, D.G. (2007). Localization of vacuolar transport receptors and cargo proteins in the Golgi apparatus of developing Arabidopsis embryos. Traffic **8,** 1452-1464.

Holwerda, B.C., Padgett, H.S., and Rogers, J.C. (1992). Proaleurain vacuolar targeting is mediated by short contiguous peptide interactions. The Plant cell **4,** 307-318.

Huotari, J., and Helenius, A. (2011). Endosome maturation. The EMBO journal **30,** 3481-3500.

Hurley, J.H. (2010). The ESCRT complexes. Critical reviews in biochemistry and molecular biology **45,** 463-487.

Hurley, J.H., Lee, S., and Prag, G. (2006). Ubiquitin-binding domains. Biochem J **399,** 361-372.

Hwang, I. (2008). Sorting and anterograde trafficking at the Golgi apparatus. Plant physiology **148,** 673-683.

Hwang, I., and Robinson, D.G. (2009). Transport vesicle formation in plant cells. Current opinion in plant biology **12,** 660-669.

Ishikawa-Ankerhold, H.C., Ankerhold, R., and Drummen, G.P. (2012). Advanced fluorescence microscopy techniques--FRAP, FLIP, FLAP, FRET and FLIM. Molecules **17,** 4047-4132.

Isono, E., Katsiarimpa, A., Muller, I.K., Anzenberger, F., Stierhof, Y.D., Geldner, N., Chory, J., and Schwechheimer, C. (2010). The deubiquitinating enzyme AMSH3 is required for intracellular trafficking and vacuole biogenesis in Arabidopsis thaliana. The Plant cell **22,** 1826-1837.

Kang, B.H., Nielsen, E., Preuss, M.L., Mastronarde, D., and Staehelin, L.A. (2011). Electron tomography of RabA4b- and PI-4Kbeta1-labeled trans Golgi network compartments in Arabidopsis. Traffic **12,** 313-329.

Katsiarimpa, A., Anzenberger, F., Schlager, N., Neubert, S., Hauser, M.T., Schwechheimer, C., and Isono, E. (2011). The Arabidopsis deubiquitinating enzyme AMSH3 interacts with ESCRT-III subunits and regulates their localization. The Plant cell **23,** 3026-3040.

Kirsch, T., Paris, N., Butler, J.M., Beevers, L., and Rogers, J.C. (1994). Purification and initial characterization of a potential plant vacuolar targeting receptor. Proceedings of the National Academy of Sciences of the United States of America **91,** 3403-3407.

Kleine-Vehn, J., Dhonukshe, P., Swarup, R., Bennett, M., and Friml, J. (2006). Subcellular trafficking of the Arabidopsis auxin influx carrier AUX1 uses a novel pathway distinct from PIN1. The Plant cell **18,** 3171-3181.

Kleine-Vehn, J., Huang, F., Naramoto, S., Zhang, J., Michniewicz, M., Offringa, R., and Friml, J. (2009). PIN auxin efflux carrier polarity is regulated by PINOID kinase-mediated recruitment into GNOM-independent trafficking in Arabidopsis. The Plant cell **21,** 3839-3849.

Künzl, F., Früholz, S., Fäßler, F., Li, B., and Pimpl, P. (submitted manuscript). Vacuolar sorting receptors transport ligands from the ER and the Golgi to the TGN/EE. Submitted manuscript.

Lam, S.K., Siu, C.L., Hillmer, S., Jang, S., An, G., Robinson, D.G., and Jiang, L. (2007). Rice SCAMP1 defines clathrin-coated, trans-golgi-located tubular-vesicular structures as an early endosome in tobacco BY-2 cells. The Plant cell **19,** 296-319.

Lavy, M., and Yalovsky, S. (2006). Association of Arabidopsis type-II ROPs with the plasma membrane requires a conserved C-terminal sequence motif and a proximal polybasic domain. Plant Journal **46,** 934-947.

Lee, G.J., Kim, H., Kang, H., Jang, M., Lee, D.W., Lee, S., and Hwang, I. (2007). EpsinR2 interacts with clathrin, adaptor protein-3, AtVTI12, and phosphatidylinositol-3-phosphate. Implications for EpsinR2 function in protein trafficking in plant cells. Plant physiology **143,** 1561-1575.

Leitner, J., Petrasek, J., Tomanov, K., Retzer, K., Parezova, M., Korbei, B., Bachmair, A., Zazimalova, E., and Luschnig, C. (2012). Lysine63-linked ubiquitylation of PIN2 auxin carrier protein governs hormonally controlled adaptation of Arabidopsis root growth. Proceedings of the National Academy of Sciences of the United States of America **109,** 8322-8327.

Leung, K.F., Dacks, J.B., and Field, M.C. (2008). Evolution of the multivesicular body ESCRT machinery; retention across the eukaryotic lineage. Traffic **9,** 1698-1716.

Li, R., Liu, P., Wan, Y., Chen, T., Wang, Q., Mettbach, U., Baluska, F., Samaj, J., Fang, X., Lucas, W.J., and Lin, J. (2012). A membrane microdomain-associated protein, Arabidopsis Flot1, is involved in a clathrin-independent endocytic pathway and is required for seedling development. The Plant cell **24,** 2105-2122.

Li, X., Wang, X., Yang, Y., Li, R., He, Q., Fang, X., Luu, D.T., Maurel, C., and Lin, J. (2011). Single-molecule analysis of PIP2;1 dynamics and partitioning reveals multiple modes of Arabidopsis plasma membrane aquaporin regulation. The Plant cell **23,** 3780-3797.

Li, Y.B., Rogers, S.W., Tse, Y.C., Lo, S.W., Sun, S.S., Jauh, G.Y., and Jiang, L. (2002). BP-80 and homologs are concentrated on post-Golgi, probable lytic prevacuolar compartments. Plant & cell physiology **43,** 726-742.

Linder, M.E., and Deschenes, R.J. (2007). Palmitoylation: policing protein stability and traffic. Nature reviews. Molecular cell biology **8,** 74-84.

Liu, J.X., and Howell, S.H. (2010). Endoplasmic reticulum protein quality control and its relationship to environmental stress responses in plants. The Plant cell **22,** 2930-2942.

Luo, Y., Scholl, S., Doering, A., Zhang, Y., Irani, N.G., Di Rubbo, S., Neumetzler, L., Krishnamoorthy, P., Van Houtte, I., Mylle, E., Bischoff, V., Vernhettes, S., Winne, J., Friml, J., Stierhof, Y.D., Schumacher, K., Persson, S., and Russinova, E. (2015). V-ATPase activity in the TGN/EE is required for exocytosis and recycling in Arabidopsis. Nature Plants **1,** article number 15094

Luzio, J.P., Pryor, P.R., and Bright, N.A. (2007). Lysosomes: fusion and function. Nature reviews. Molecular cell biology **8,** 622-632.

Madshus, I.H. (2006). Ubiquitin binding in endocytosis--how tight should it be and where does it happen? Traffic **7,** 258-261.

Martiniere, A., Bassil, E., Jublanc, E., Alcon, C., Reguera, M., Sentenac, H., Blumwald, E., and Paris, N. (2013). In vivo intracellular pH measurements in

tobacco and Arabidopsis reveal an unexpected pH gradient in the endomembrane system. The Plant cell **25,** 4028-4043.

Matheson, L.A., Hanton, S.L., and Brandizzi, F. (2006). Traffic between the plant endoplasmic reticulum and Golgi apparatus: to the Golgi and beyond. Current opinion in plant biology **9,** 601-609.

Mayran, N., Parton, R.G., and Gruenberg, J. (2003). Annexin II regulates multivesicular endosome biogenesis in the degradation pathway of animal cells. The EMBO journal **22,** 3242-3253.

McGough, I.J., and Cullen, P.J. (2011). Recent advances in retromer biology. Traffic **12,** 963-971.

Morel, E., Parton, R.G., and Gruenberg, J. (2009). Annexin A2-dependent polymerization of actin mediates endosome biogenesis. Developmental cell **16,** 445-457.

Muyldermans, S. (2001). Single domain camel antibodies: current status. J Biotechnol **74,** 277-302.

Nakamura, K., and Matsuoka, K. (1993). Protein targeting to the vacuole in plant cells. Plant physiology **101,** 1-5.

Niemes, S., Labs, M., Scheuring, D., Krueger, F., Langhans, M., Jesenofsky, B., Robinson, D.G., and Pimpl, P. (2010a). Sorting of plant vacuolar proteins is initiated in the ER. The Plant journal : for cell and molecular biology **62,** 601-614.

Niemes, S., Langhans, M., Viotti, C., Scheuring, D., San Wan Yan, M., Jiang, L., Hillmer, S., Robinson, D.G., and Pimpl, P. (2010b). Retromer recycles vacuolar sorting receptors from the trans-Golgi network. The Plant journal : for cell and molecular biology **61,** 107-121.

Nordmann, M., Cabrera, M., Perz, A., Brocker, C., Ostrowicz, C., Engelbrecht-Vandre, S., and Ungermann, C. (2010). The Mon1-Ccz1 complex is the GEF of the late endosomal Rab7 homolog Ypt7. Current biology : CB **20,** 1654-1659.

Ordenes, V.R., Moreno, I., Maturana, D., Norambuena, L., Trewavas, A.J., and Orellana, A. (2012). In vivo analysis of the calcium signature in the plant Golgi apparatus reveals unique dynamics. Cell Calcium **52,** 397-404.

Paris, N., Rogers, S.W., Jiang, L.W., Kirsch, T., Beevers, L., Phillips, T.E., and Rogers, J.C. (1997). Molecular cloning and further characterization of a probable plant vacuolar sorting receptor. Plant physiology **115,** 29-39.

Pelham, H.R. (2004). Membrane traffic: GGAs sort ubiquitin. Current biology : CB **14,** R357-359.

Phillipson, B.A., Pimpl, P., daSilva, L.L., Crofts, A.J., Taylor, J.P., Movafeghi, A., Robinson, D.G., and Denecke, J. (2001). Secretory bulk flow of soluble proteins is efficient and COPII dependent. The Plant cell **13,** 2005-2020.

Pickart, C.M., and Eddins, M.J. (2004). Ubiquitin: structures, functions, mechanisms. Biochimica et biophysica acta **1695,** 55-72.

Pimpl, P., Hanton, S.L., Taylor, J.P., Pinto-daSilva, L.L., and Denecke, J. (2003). The GTPase ARF1p controls the sequence-specific vacuolar sorting route to the lytic vacuole. The Plant cell **15,** 1242-1256.

Pimpl, P., Movafeghi, A., Coughlan, S., Denecke, J., Hillmer, S., and Robinson, D.G. (2000). In situ localization and in vitro induction of plant COPI-coated vesicles. The Plant cell **12,** 2219-2236.

Poteryaev, D., Datta, S., Ackema, K., Zerial, M., and Spang, A. (2010). Identification of the switch in early-to-late endosome transition. Cell **141,** 497-508.

Raiborg, C., and Stenmark, H. (2009). The ESCRT machinery in endosomal sorting of ubiquitylated membrane proteins. Nature **458,** 445-452.

Raymond, C.K., Howald-Stevenson, I., Vater, C.A., and Stevens, T.H. (1992). Morphological classification of the yeast vacuolar protein sorting mutants: evidence for a prevacuolar compartment in class E vps mutants. Molecular biology of the cell **3,** 1389-1402.

Reguera, M., Bassil, E., Tajima, H., Wimmer, M., Chanoca, A., Otegui, M.S., Paris, N., and Blumwald, E. (2015). pH Regulation by NHX-Type Antiporters Is Required for Receptor-Mediated Protein Trafficking to the Vacuole in Arabidopsis. The Plant cell **27,** 1200-1217.

Reichardt, I., Stierhof, Y.D., Mayer, U., Richter, S., Schwarz, H., Schumacher, K., and Jurgens, G. (2007). Plant cytokinesis requires de novo secretory trafficking but not endocytosis. Current biology : CB **17,** 2047-2053.

Reyes, F.C., Buono, R., and Otegui, M.S. (2011). Plant endosomal trafficking pathways. Current opinion in plant biology **14,** 666-673.

Rink, J., Ghigo, E., Kalaidzidis, Y., and Zerial, M. (2005). Rab conversion as a mechanism of progression from early to late endosomes. Cell **122,** 735-749.

Robatzek, S., Chinchilla, D., and Boller, T. (2006). Ligand-induced endocytosis of the pattern recognition receptor FLS2 in Arabidopsis. Genes Dev **20,** 537-542.

Robinson, D.G., and Hillmer, S. (1990). Endocytosis in Plants. Physiol Plantarum **79,** 96-104.

Robinson, D.G., and Pimpl, P. (2014a). Clathrin and post-Golgi trafficking: a very complicated issue. Trends in plant science **19,** 134-139.

Robinson, D.G., and Pimpl, P. (2014b). Receptor-mediated transport of vacuolar proteins: a critical analysis and a new model. Protoplasma **251,** 247-264.

Robinson, D.G., Balusek, K., and Freundt, H. (1989). Legumin Antibodies Recognize Polypeptides in Coated Vesicles Isolated from Developing Pea Cotyledons. Protoplasma **150,** 79-82.

Robinson, D.G., Oliviusson, P., and Hinz, G. (2005). Protein sorting to the storage vacuoles of plants: a critical appraisal. Traffic **6,** 615-625.

Robinson, D.G., Jiang, L., and Schumacher, K. (2008). The endosomal system of plants: charting new and familiar territories. Plant physiology **147,** 1482-1492.

Robinson, D.G., Herranz, M.C., Bubeck, J., Pepperkok, R., and Ritzenthaler, C. (2007). Membrane dynamics in the early secretory pathway. Crit Rev Plant Sci **26,** 199-225.

Rothbauer, U., Zolghadr, K., Muyldermans, S., Schepers, A., Cardoso, M.C., and Leonhardt, H. (2008). A versatile nanotrap for biochemical and functional studies with fluorescent fusion proteins. Mol Cell Proteomics **7,** 282-289.

Rothbauer, U., Zolghadr, K., Tillib, S., Nowak, D., Schermelleh, L., Gahl, A., Backmann, N., Conrath, K., Muyldermans, S., Cardoso, M.C., and Leonhardt, H. (2006). Targeting and tracing antigens in live cells with fluorescent nanobodies. Nat Methods **3,** 887-889.

Russinova, E., Borst, J.W., Kwaaitaal, M., Cano-Delgado, A., Yin, Y., Chory, J., and de Vries, S.C. (2004). Heterodimerization and endocytosis of Arabidopsis brassinosteroid receptors BRI1 and AtSERK3 (BAK1). The Plant cell **16,** 3216-3229.

Rutherford, S., and Moore, I. (2002). The Arabidopsis Rab GTPase family: another enigma variation. Current opinion in plant biology **5,** 518-528.

Sahagian, G.G., Distler, J., and Jourdian, G.W. (1981). Characterization of a membrane-associated receptor from bovine liver that binds phosphomannosyl residues of bovine testicular beta-galactosidase. Proceedings of the National Academy of Sciences of the United States of America **78,** 4289-4293.

Saint-Jean, B., Seveno-Carpentier, E., Alcon, C., Neuhaus, J.M., and Paris, N. (2010). The cytosolic tail dipeptide Ile-Met of the pea receptor BP80 is required for recycling from the prevacuole and for endocytosis. The Plant cell **22,** 2825-2837.

Sanderfoot, A.A., Ahmed, S.U., Marty-Mazars, D., Rapoport, I., Kirchhausen, T., Marty, F., and Raikhel, N.V. (1998). A putative vacuolar cargo receptor partially colocalizes with AtPEP12p on a prevacuolar compartment in Arabidopsis roots. Proceedings of the National Academy of Sciences of the United States of America **95,** 9920-9925.

Schellmann, S., and Pimpl, P. (2009). Coats of endosomal protein sorting: retromer and ESCRT. Current opinion in plant biology **12,** 670-676.

Scheuring, D., Kunzl, F., Viotti, C., Yan, M.S., Jiang, L., Schellmann, S., Robinson, D.G., and Pimpl, P. (2012). Ubiquitin initiates sorting of Golgi and plasma membrane proteins into the vacuolar degradation pathway. BMC plant biology **12,** 164.

Scheuring, D., Viotti, C., Kruger, F., Kunzl, F., Sturm, S., Bubeck, J., Hillmer, S., Frigerio, L., Robinson, D.G., Pimpl, P., and Schumacher, K. (2011). Multivesicular bodies mature from the trans-Golgi network/early endosome in Arabidopsis. The Plant cell **23,** 3463-3481.

Scott, P.M., Bilodeau, P.S., Zhdankina, O., Winistorfer, S.C., Hauglund, M.J., Allaman, M.M., Kearney, W.R., Robertson, A.D., Boman, A.L., and Piper, R.C. (2004). GGA proteins bind ubiquitin to facilitate sorting at the trans-Golgi network. Nature cell biology **6,** 252-259.

Shahriari, M., Keshavaiah, C., Scheuring, D., Sabovljevic, A., Pimpl, P., Hausler, R.E., Hulskamp, M., and Schellmann, S. (2010). The AAA-type ATPase AtSKD1 contributes to vacuolar maintenance of Arabidopsis thaliana. The Plant journal : for cell and molecular biology **64,** 71-85.

Shen, J., Ding, Y., Gao, C., Rojo, E., and Jiang, L. (2014). N-linked glycosylation of AtVSR1 is important for vacuolar protein sorting in Arabidopsis. The Plant journal : for cell and molecular biology **80,** 977-992.

Shen, J., Zeng, Y., Zhuang, X., Sun, L., Yao, X., Pimpl, P., and Jiang, L. (2013a). Organelle pH in the Arabidopsis endomembrane system. Mol Plant **6,** 1419-1437.

Shen, J., Suen, P.K., Wang, X., Lin, Y., Lo, S.W., Rojo, E., and Jiang, L. (2013b). An in vivo expression system for the identification of cargo proteins of vacuolar sorting receptors in Arabidopsis culture cells. The Plant journal : for cell and molecular biology **75,** 1003-1017.

Shimada, T., Fuji, K., Tamura, K., Kondo, M., Nishimura, M., and Hara-Nishimura, I. (2003). Vacuolar sorting receptor for seed storage proteins in Arabidopsis thaliana. Proceedings of the National Academy of Sciences of the United States of America **100,** 16095-16100.

Singh, M.K., Kruger, F., Beckmann, H., Brumm, S., Vermeer, J.E., Munnik, T., Mayer, U., Stierhof, Y.D., Grefen, C., Schumacher, K., and Jurgens, G. (2014). Protein delivery to vacuole requires SAND protein-dependent Rab GTPase conversion for MVB-vacuole fusion. Current biology : CB **24,** 1383-1389.

Sorek, N., Bloch, D., and Yalovsky, S. (2009). Protein lipid modifications in signaling and subcellular targeting. Current opinion in plant biology **12,** 714-720.

Spitzer, C., Reyes, F.C., Buono, R., Sliwinski, M.K., Haas, T.J., and Otegui, M.S. (2009). The ESCRT-related CHMP1A and B proteins mediate multivesicular

body sorting of auxin carriers in Arabidopsis and are required for plant development. The Plant cell **21,** 749-766.

Spitzer, C., Schellmann, S., Sabovljevic, A., Shahriari, M., Keshavaiah, C., Bechtold, N., Herzog, M., Muller, S., Hanisch, F.G., and Hulskamp, M. (2006). The Arabidopsis elch mutant reveals functions of an ESCRT component in cytokinesis. Development **133,** 4679-4689.

Stael, S., Wurzinger, B., Mair, A., Mehlmer, N., Vothknecht, U.C., and Teige, M. (2012). Plant organellar calcium signalling: an emerging field. J Exp Bot **63,** 1525-1542.

Stefano, G., Renna, L., Chatre, L., Hanton, S.L., Moreau, P., Hawes, C., and Brandizzi, F. (2006). In tobacco leaf epidermal cells, the integrity of protein export from the endoplasmic reticulum and of ER export sites depends on active COPI machinery. The Plant journal : for cell and molecular biology **46,** 95-110.

Stierhof, Y.D., and El Kasmi, F. (2010). Strategies to improve the antigenicity, ultrastructure preservation and visibility of trafficking compartments in Arabidopsis tissue. European journal of cell biology **89,** 285-297.

Stierhof, Y.D., Viotti, C., Scheuring, D., Sturm, S., and Robinson, D.G. (2013). Sorting nexins 1 and 2a locate mainly to the TGN. Protoplasma **250,** 235-240.

Strasser, R. (2014). Biological significance of complex N-glycans in plants and their impact on plant physiology. Front Plant Sci **5,** 363.

Takano, J., Tanaka, M., Toyoda, A., Miwa, K., Kasai, K., Fuji, K., Onouchi, H., Naito, S., and Fujiwara, T. (2010). Polar localization and degradation of Arabidopsis boron transporters through distinct trafficking pathways. Proceedings of the National Academy of Sciences of the United States of America **107,** 5220-5225.

Takeuchi, M., Ueda, T., Sato, K., Abe, H., Nagata, T., and Nakano, A. (2000). A dominant negative mutant of sar1 GTPase inhibits protein transport from the endoplasmic reticulum to the Golgi apparatus in tobacco and Arabidopsis cultured cells. The Plant journal : for cell and molecular biology **23,** 517-525.

Teh, O.K., Shimono, Y., Shirakawa, M., Fukao, Y., Tamura, K., Shimada, T., and Hara-Nishimura, I. (2013). The AP-1 mu adaptin is required for KNOLLE localization at the cell plate to mediate cytokinesis in Arabidopsis. Plant & cell physiology **54,** 838-847.

Traub, L.M., and Bonifacino, J.S. (2013). Cargo recognition in clathrin-mediated endocytosis. Cold Spring Harb Perspect Biol **5,** a016790.

Tse, Y.C., Mo, B., Hillmer, S., Zhao, M., Lo, S.W., Robinson, D.G., and Jiang, L. (2004). Identification of multivesicular bodies as prevacuolar compartments in Nicotiana tabacum BY-2 cells. The Plant cell **16,** 672-693.

Uemura, T., Suda, Y., Ueda, T., and Nakano, A. (2014). Dynamic behavior of the trans-golgi network in root tissues of Arabidopsis revealed by super-resolution live imaging. Plant & cell physiology **55,** 694-703.

Van Damme, D., Gadeyne, A., Vanstraelen, M., Inze, D., Van Montagu, M.C., De Jaeger, G., Russinova, E., and Geelen, D. (2011). Adaptin-like protein TPLATE and clathrin recruitment during plant somatic cytokinesis occurs via two distinct pathways. Proceedings of the National Academy of Sciences of the United States of America **108,** 615-620.

Viotti, C., Bubeck, J., Stierhof, Y.D., Krebs, M., Langhans, M., van den Berg, W., van Dongen, W., Richter, S., Geldner, N., Takano, J., Jurgens, G., de Vries, S.C., Robinson, D.G., and Schumacher, K. (2010). Endocytic and secretory traffic in Arabidopsis merge in the trans-Golgi network/early endosome, an independent and highly dynamic organelle. The Plant cell **22,** 1344-1357.

Watanabe, E., Shimada, T., Kuroyanagi, M., Nishimura, M., and Hara-Nishimura, I. (2002). Calcium-mediated association of a putative vacuolar sorting receptor PV72 with a propeptide of 2S albumin. J Biol Chem **277,** 8708-8715.

Watanabe, E., Shimada, T., Tamura, K., Matsushima, R., Koumoto, Y., Nishimura, M., and Hara-Nishimura, I. (2004). An ER-localized form of PV72, a seed-specific vacuolar sorting receptor, interferes the transport of an NPIR-containing proteinase in Arabidopsis leaves. Plant & cell physiology **45,** 9-17.

Winter, V., and Hauser, M.T. (2006). Exploring the ESCRTing machinery in eukaryotes. Trends in plant science **11,** 115-123.

Wolfenstetter, S., Wirsching, P., Dotzauer, D., Schneider, S., and Sauer, N. (2012). Routes to the tonoplast: the sorting of tonoplast transporters in Arabidopsis mesophyll protoplasts. The Plant cell **24,** 215-232.

Wollert, T., and Hurley, J.H. (2010). Molecular mechanism of multivesicular body biogenesis by ESCRT complexes. Nature **464,** 864-869.

Yalovsky, S. (2015). Protein lipid modifications and the regulation of ROP GTPase function. J Exp Bot **66,** 1617-1624.

Yang, Y.D., Elamawi, R., Bubeck, J., Pepperkok, R., Ritzenthaler, C., and Robinson, D.G. (2005). Dynamics of COPII vesicles and the Golgi apparatus in cultured Nicotiana tabacum BY-2 cells provides evidence for transient association of Golgi stacks with endoplasmic reticulum exit sites. The Plant cell **17,** 1513-1531.

Yoshimori, T., Yamagata, F., Yamamoto, A., Mizushima, N., Kabeya, Y., Nara, A., Miwako, I., Ohashi, M., Ohsumi, M., and Ohsumi, Y. (2000). The mouse SKD1, a homologue of yeast Vps4p, is required for normal endosomal trafficking and morphology in mammalian cells. Molecular biology of the cell **11,** 747-763.

9. Appendix

9.1 Scheuring et al., 2011

9.2 Scheuring et al., 2012

9.3 Künzl et al., submitted manuscript

9.1 Multivesicular bodies mature from the *trans*-Golgi network/early endosome in *Arabidopsis*

David Scheuring, Corrado Viotti, Falco Krüger, **Fabian Künzl**, Silke Sturm, Julia Bubeck, Stefan Hillmer, Lorenzo Frigerio, David G. Robinson, Peter Pimpl, and Karin Schumacher

The Plant Cell, Sept. 2011, Vol. 23(9): 3463-81 (http://www.plantcell.org/cgi/content/short/tpc.111.086918?keytype=ref&ijkey=x1F4bvTISFBLQKd)

Title: Multivesicular Bodies mature from the *trans*-Golgi-Network/Early Endosome in *Arabidopsis*

Authors and affiliations:

David Scheuring[a,1], Corrado Viotti[b,1], Falco Krüger[a], Fabian Künzl[c], Silke Sturm[a], Julia Bubeck[b], Stefan Hillmer[a], Lorenzo Frigerio[d], David G. Robinson[a], Peter Pimpl[a,c,2] and Karin Schumacher [b]

[a] Plant Cell Biology, Centre for Organismal Studies, University of Heidelberg, 69120 Heidelberg, Germany

[b] Developmental Biology of Plants, Centre for Organismal Studies, University of Heidelberg, 69120 Heidelberg, Germany

[c] Developmental Genetics, Centre for Plant Molecular Biology, University of Tübingen, 72076 Tübingen, Germany

[d] Department of Biological Sciences, University of Warwick, Coventry CV4 7AL, UK

[1] These authors contributed equally to this work.

[2]Corresponding author:

Address correspondence to peter.pimpl@zmbp.uni-tuebingen.de

The author responsible for distribution of materials integral to the findings presented in this article in accordance with the policy described in the Instructions for Authors (www.plantcell.org) is: Peter Pimpl (peter.pimpl@zmbp.uni-tuebingen.de)

Running title: MVB maturation

Estimated length of the article from the page calculator: 17.4

SYNOPSIS

We have examined the origin and fate of multivesicular bodies/late endosomes (MVB/LE). We have traced their formation back to the *trans*-Golgi network/early endosome (TGN/EE) and show that their maturation into MVBs requires V-ATPase activity and ESCRT for the formation of the intraluminal vesicles, and annexins for the release of MVBs from the TGN as transport carriers that fuse with the vacuole.

ABSTRACT

The plant *trans*-Golgi network/early endosome (TGN/EE) is a major hub for secretory and endocytic trafficking with complex molecular mechanisms controlling sorting and transport of cargo. Vacuolar transport from the TGN/EE to multivesicular bodies/late endosomes (MVBs/LEs) is assumed to occur via clathrin-coated vesicles (CCVs); here, we present evidence that *post*-TGN transport towards lytic vacuoles occurs independently of clathrin and that MVBs/LEs are derived from the TGN/EE through maturation. We show that the V-ATPase-inhibitor concanamycin A significantly reduces the number of MVBs and causes TGN- and MVB-markers to colocalize in *Arabidopsis* roots. Ultrastructural analysis reveals the formation of MVBs from the TGN/EE and their fusion with the vacuole. The localization of the ESCRT-components VPS28, VPS22 and VPS2 at the TGN/EE and MVBs/LEs indicates that the formation of intraluminal vesicles starts already at the TGN/EE. Accordingly, a dominant-negative mutant of VPS2 causes TGN- and MVB-markers to colocalize and blocks vacuolar transport. RNAi-mediated knock-down of the annexin ANNAT3 also yields the same phenotype. Together, these data indicate that MVBs originate from the TGN/EE via maturation that requires the action of ESCRT for the formation of intraluminal vesicles and annexins for the final step of releasing MVBs as a transport carrier to the vacuole.

INTRODUCTION

The endomembrane system of eukaryotic cells provides the spatial and temporal separation required for the sequence of steps involved in protein trafficking. The flux of membranes and cargo through the *post*-Golgi compartments is enormous and, although substantial progress has been made in the identification of the different endosomal compartments in plants, we know very little about their biogenesis and their highly dynamic spatio-temporal relationships. In mammalian cells endocytic cargo proteins are first delivered to early endosomes (EE) (van Meel and Klumperman, 2008; Jovic et al., 2010), compartments that typically have two structurally distinct domains: a central more-or-less spherical structure with a few 50 nm diameter intraluminal vesicles (ILV), and an extensive network of tubules projecting outwardly into the cytoplasm (Griffiths and Gruenberg, 1991; Tooze and Hollinshead, 1991). The tubular extensions of the EE bear clathrin-coated buds (Stoorvogel et al., 1996), which are positive for the two adaptor complexes AP-1 and AP-3 (Peden et al., 2004). The small (sorting nexins 1 and 2) and large subunits of retromer are also present on these tubules (Carlton et al., 2005; Mari et al., 2008). According to Mari et al. (2008), EE in mammalian cells are defined as compartments accessible to internalized transferrin, and have 1-8 ILV. By contrast, the LE is more or less spherical, contains at least 9 ILV and is devoid of transferrin.

Endocytosed cargo destined for degradation becomes ubiquitinated at the PM, and this signal causes them to be sorted into the ILV (Polo et al., 2002). This step, which effectively segregates ligand-receptor complexes from the cytoplasm, is critical for

the cessation of signaling cascades which continue even after internalization of the receptor-ligand complex (Taub et al., 2007). Sorting into the ILV involves recognition of the ubiquitin tag by the first of four ESCRT complexes which associate with the surface of the endosomal membrane. ESCRT-0 associates with the membrane of the endosome through an interaction of the FYVE (named after the four cysteine-rich proteins: Fab1, YOTB, Vac1 and EEA1) domain of HRS (hepatocyte growth factor regulated Tyr-kinase substrate) with PI_3P (phosphatidylinositol 3-phosphate). It sequesters ubiquitinated cargo molecules into double-layered clathrin microdomains (Clague, 2002). These domains are visible at the surface of both EE and LE (Sachse et al., 2002; Murk et al., 2003). ESCRT-I and –II complexes then deform the limiting membrane into inwardly directed buds, and recruit the ESCRT-0 + attached ubiquitinated cargo into the necks of the buds. ESCRT-III, in collaboration with a deubiquitinating enzyme (Doa4) then releases the ubiquitin and causes a scission of the buds (Wollert and Hurley, 2010). Finally, the activity of an AAA-ATPase (Vps4) leads to dissociation of the ESCRT-complexes. Delivery of the ILV to the lysosome interior then occurs by fusion of the LE with the lysosome (Luzio et al., 2009).

In mammalian cells it is generally regarded that the movement of molecules along the biosynthetic-endocytic pathways to the lysosome is accompanied by a maturation of endosomal organelles. Many of the key factors in this process have now been identified. In addition to the ESCRT complexes, both COPI (Aniento et al., 1996; Gabriely et al., 2007; Razi et al., 2009) and annexin A2 are specifically required (Mayran et al., 2003; Futter and White, 2007; Morel and Gruenberg, 2009). Also critical for the transition EE to LE are the proteins SAND-1/Mon1, which appear to be responsible for the exchange of Rab GTPases, from Rab5 (EE) to Rab 7 (LE) (Poteryaev et al., 2010).

The organelles of the plant endocytic pathway have both similarities and differences to those present in mammalian cells. Perhaps the greatest similarity lies in the morphology of the LE, occasionally termed the pre-vacuolar compartment in the plant literature (Lam et al., 2007; Miao et al., 2008). This is spherical, contains ILV, and also bears a plaque on its surface and is often named a multivesicular body (MVB) (Tse et al., 2004; Otegui and Spitzer, 2008; Viotti et al., 2010). However, unlike the situation in animal cells, several studies have shown that higher plants do not have separate TGN and EE compartments (Dettmer et al., 2006; Lam et al., 2007; Reichardt et al., 2007; Otegui and Spitzer, 2008; Robinson et al., 2008; Toyooka et al., 2009; Viotti et al., 2010). The TGN in plants appears to be synonymous with the “partially coated reticulum” (Pesacreta and Lucas, 1984; Hillmer et al., 1988; Tanchak et al., 1988), and is a tubular/vesicular structure bearing CCVs (Kang and Staehelin, 2008; Toyooka et al., 2009). The recent demonstration that plant retromer is present at the TGN rather than the MVB (Niemes et al., 2010b), is therefore in agreement with the location of this recycling coat complex to the tubular extensions of the EE in mammalian cells. Thus, at the morphological level, the higher plant TGN shares many features with the mammalian EE.

Based on studies with the brassinosteroid receptor BRI1, it has been established that plants also show endosomal-based signaling which appears to cease when the receptor reaches the LE (Geldner et al., 2007). Plants also possess ESCRT proteins (Winter and Hauser, 2006; Schellmann and Pimpl, 2009, Shahriari et al., 2011), but there are no clear homologs to the ESCRT-0 complex (Leung et al., 2008), and the exact location of the other complexes is unclear. Nevertheless, several studies with mutated ESCRT proteins point to their presence at least at the LE. Expression of a

mutant form of Vps4 (SKD1) leads to the missorting of vacuolar proteins (Shahriari et al., 2010), as well as to an enlargement of MVBs with fewer ILV (Haas et al., 2007). A reduction in number of ILV and a displacement of cargo molecules destined for vacuolar degradation to the boundary membrane of the MVB was also observed after expression of mutated forms of the ESCRT-related CHMP1A /B proteins (Spitzer et al., 2009).

In this paper we present evidence that in plants the MVB/LE is derived from the TGN/EE through a process of maturation and finally mediates vacuolar delivery by fusing with the tonoplast. Proceeding from our previous observation that vacuolar sorting receptors (VSRs) recycle from the TGN and thus do not contribute to *post*-TGN transport of soluble vacuolar proteins (Niemes et al., 2010a), we now show that inhibition of clathrin-mediated transport does not prevent the arrival of soluble cargo molecules, carrying vacuolar sorting determinants, in the vacuole. This raises questions about the mechanism of TGN to MVB/LE transport. Based on the observation that the V-ATPase inhibitor concanamycin A (ConcA) causes the incorporation of TGN proteins into the Golgi stack in *Arabidopsis* root cells (Viotti et al., 2010), we now show that this treatment also leads to a drastic reduction in MVBs. We have been able to capture the moment of MVB formation at the TGN, an event that can also be observed during the recovery of the Golgi apparatus upon ConcA washout. This data is supported by a series of experiments in which the separation of signals for fluorescent TGN and MVB marker proteins was prevented by ConcA and a dominant-negative mutant of ESCRT-III as well as the knockdown of an *Arabidopsis* annexin ANNAT3. Moreover, we show that ESCRT-I, -II and –III show a differential distribution between TGN and MVB and that ESCRT-III is required for vacuolar transport.

RESULTS

GFP-Hub1 inhibits endocytosis but not transport to the lytic vacuole

We wanted to investigate whether CCVs contribute to the delivery of soluble cargo molecules to the vacuole. The expression of the C-terminal third of the clathrin heavy chain – also known as the clathrin hub – inhibits CCV formation and thus clathrin-mediated transport events (Liu et al., 1995; Liu et al., 1998; Dhonukshe et al., 2007). It was recently shown that expression of a fluorescently tagged clathrin Hub (GFP-Hub1) in *Arabidopsis* protoplasts inhibits the endocytic uptake of the amphiphilic styryl dye FM4-64 (Dhonukshe et al., 2007). We have now utilized this inhibitory effect on FM4-64 uptake as a positive control for the inhibition of clathrin-mediated trafficking. In control protoplasts, the dye stained the PM instantly after addition (Figure 1A) and internalized signals were detectable 30 min later (Figure 1B). When GFP-Hub1 was expressed, an inhibition of FM4-64 uptake was observed (Figure 1C). To quantify this effect we have counted and compared the number of internal FM4-64 signals in protoplasts in the presence and absence of GFP-Hub1. For this, 20 protoplasts showing an observable amount of cytoplasm were considered. In control protoplasts the number of internal FM4-64 signals was 37±12, but the number of signals in protoplasts expressing GFP-Hub1 dropped to 7±3 (Figure 1D). To test whether clathrin is required for transport to the lytic vacuole, we carried out coexpression experiments of GFP-Hub1 with the soluble, vacuolar reporter spRFP-AFVY (Hunter et al., 2007). This reporter is efficiently transported to the vacuole,

even if coexpressed with fluorescent cytosolic proteins (cytGFP, Figure 1E). The expression of GFP-Hub1 does not change the intensity of the vacuolar signal pattern of spRFP-AFVY (Figure 1F), indicating that the reporter still reaches the lumen of the vacuole under these conditions.

V-ATPase activity is required for MVB biogenesis

To examine the function of the TGN for vacuolar transport, we have analyzed the effect of the V-ATPase inhibitor ConcA. Transmission electron microscopy (TEM) analysis revealed that the number of MVBs decreased significantly upon ConcA treatment. In one hundred sectioned cells, the number of MVBs is 220±30, whereas it is ca. 5 fold lower (40±15) after ConcA treatment (Figure 2A). We have shown previously that ConcA leads to morphological changes of both the Golgi apparatus and the TGN and causes intrinsic TGN-membrane proteins to locate to the Golgi stack (Viotti et al., 2010). We thus decided to investigate the behavior of MVB-markers upon ConcA treatment using immunogold electron microscopy. In *Arabidopsis* roots the endogenous VSR BP80 localizes to both the TGN and the MVB (Figure 2C), (Niemes et al., 2010b; Stierhof and El Kasmi, 2010; Viotti et al., 2010), while upon ConcA treatment BP80 locates mainly to the Golgi stack (Figures 2B, 2D and 2E). The same result was obtained with the Rab GTPase ARA7 which in untreated cells is localized on the limiting membrane of MVBs (Figure 2F) (Haas et al., 2007; Robinson et al., 2008), while it locates to the Golgi stack in ConcA treated cells (Figures 2B and 2G). Interestingly, both BP80 and ARA7 are still detectable to the limiting membrane of the remaining MVBs after ConcA treatment (Figures 2E and 2G). These data have been confirmed by confocal laser scanning microscopy (CLSM) analysis of transgenic *Arabidopsis* seedlings expressing the TGN-marker VHA-a1-GFP and the MVB-marker mRFP-ARA7. In order to quantify colocalization results, we have calculated the linear Pearson (r_p) and the non-linear Spearman´s rank (r_s) correlation coefficient (PSC) for the pixels representing the fluorescence signals in both channels. Levels of colocalization can range from +1 for positive correlation to -1 for negative correlation (French et al., 2008). The fluorescence values of pixels across the two channels were additionally depicted in an intensity scatter plot. In untreated cells the VHA-a1-GFP and mRFP-ARA7 signals were mostly separate (Supplemental Figure 1A and 1B online; r_p=0.22 and r_s=0.19), but colocalization increased upon 30 min ConcA treatment (Supplemental Figure 1C and 1D online, r_p=0.45 and r_s=0.43).

Together, these findings show that V-ATPase activity is required not only for the functionality of the TGN but also for the occurrence of MVBs.

Inhibition of TGN function by ConcA inhibits protein export from the TGN but also reduces the overall number of MVBs per cell. This suggests that MVBs that once existed can disappear if the vacuolar transport route is perturbed at this step. One explanation for this could be that they are consumed in the process of vacuolar transport by fusion with the vacuole. The analysis of untreated high pressure frozen *Arabidopsis* root cells confirmed that MVBs indeed fuse with the tonoplast to deliver their content into the vacuolar lumen (Figure 3A to 3D).

We then used TEM to investigate the origin of MVBs. Mature MVBs have an almost spherical shape (Figures 4A and 4B). TEM analysis of high pressure frozen *Arabidopsis* root cells revealed nascent MVBs still being connected to tubular structures, indicating their TGN-based biogenesis (Figures 4C and 4D). However, after ConcA-treatment followed by a short recovery period in the absence of the

inhibitor, we detected multiple examples of MVBs of unusual size and form, often with bottleneck terminations indicating that they are still connected to tubular structures of the TGN (Figures 4E to 4H). A clear connection between nascent MVBs and TGN-like structures is shown in Figures 4I and 4K. Finally, we tested the identity of these multivesiculated compartments with IEM of mRFP-ARA7 in ConcA-treated cells. Indeed, we were able to detect ARA7 to the limiting membrane of MVBs displaying bottleneck terminations (Figure 4K).

The ESCRT-components VPS28, VPS22 and VPS2 are differentially distributed between the TGN/EE and the MVB/LE

If MVBs are indeed derived from the TGN/EE via maturation, it has to be assumed that the ESCRT-mediated formation of ILVs starts already at the TGN/EE. Therefore, we examined the subcellular distribution of the ESCRT machinery.
We generated antibodies against VPS28-1 (one of the two *Arabidopsis* VPS28 isoforms, hereafter referred to as VPS28), a subunit of ESCRT-I, the potentially initiating complex in plants. To determine the specificity of the antiserum we performed immunoblot analysis on total extracts from 7 day old *Arabidopsis* plants and expressed a fluorescent fusion of VPS28 (VPS28-GFP) in protoplasts derived from suspension cultivated *Arabidopsis* cells. The antibody recognizes an endogenous protein in the total extracts, which correlates well with the calculated MW of 23.5 kDa for VPS28, and an about 50 kDa protein, representing VPS28-GFP (Figure 5A). Immunogold electron microscopy of the endogenous VPS28 using high-pressure frozen and freeze-substituted roots from *Arabidopsis* revealed a specific labeling of the TGN and the Golgi, but not the MVB (Figure 5B, 5C and 5D for quantitative analysis). The unexpected TGN localization of VPS28 was confirmed by immuno colocalization in an *Arabidopsis* line, expressing a TGN marker (SYP61-CFP) under the control of the endogenous promoter (Figure 5E) and the detection of VPS28 in the core of the BFA compartment in root cells of wild-type *Arabidopsis* plants (Figure 5F).
To determine the localization of other putative ESCRT complexes, we analyzed VPS22, representing ESCRT-II and VPS2.1 (one of the three *Arabidopsis* VPS2 isoforms, hereafter referred to as VPS2), representing ESCRT-III, in coexpression studies with marker proteins for different compartments in tobacco protoplasts.
Coexpression of VPS22-GFP with the TGN/EE marker YFP-SYP61 reveals significantly higher values of the PSC coefficients than for VPS22-GFP coexpressed with the MVB/LE marker mRFP-VSR2 (Figures 6A to 6C and Supplemental Figures 2A to 2D online), indicating that the ESCRT-II component mainly localizes to the TGN/EE. In contrast, the values of the PSC coefficients of VPS2-GFP and YFP-SYP61 are lower than for VPS2-GFP coexpressed with the MVB/LE marker mRFP-VSR2 (Figures 6D to 6F and Supplemental Figures 2E to 2H online).
Both VPS22-GFP and VPS2-GFP, when coexpressed with the Golgi marker Man1-RFP, have very low or even negative r_p and r_s values (Supplemental Figures 3A to 3F online). Immunolabeling using VPS2 antibodies also confirmed that endogenous VPS2 is not present at the Golgi stack but partially localizes to the MVB/LE (Supplemental Figures 3J to 3L online). In agreement with the differential distribution of VPS22-GFP and VPS2-GFP, coexpression of these two ESCRT-components resulted in PSC coefficients of r_p=0.61 and r_s=0.20 (Figures 6G and 6I, Supplemental Figures 2I and 2J online). Treatment with wortmannin (WM) showed that only VPS2-RFP signals, but not VPS22-GFP signals were sensitive to WM, judged by the

appearance of typical ring-like structures (magnified insert, Figure 6G). The number of VPS2-RFP signals exceeded that of VPS22-GFP (21.5±5.5 for VPS2-RFP and 12.2±3.4 for VPS22-GFP, Figure 6H). It is therefore likely that VPS22-GFP and VPS2-RFP colocalize at the TGN/EE but not at the MVB/LE. However, due to the cytosolic nature and the resulting background of the analyzed fluorescent ESCRT proteins, all of the r_p and r_s values are relatively low. Even if fusions of VPS2 with different fluorescent proteins are coexpressed, the values for the PSC coefficients do not exceed r_p=0.66 and r_s=0.44 (VPS2-GFP and VPS2-RFP, Supplemental Figure 3G and 3I online). These combined findings indicate that the ESCRT-II component VPS22 and the ESCRT-III component VPS2 are gradually distributed along the vacuolar route.

VPS2-DN and treatment with Concanamycin A prevents the arrival of soluble reporter molecules in the vacuole

We next asked whether ESCRT function is required for vacuolar transport. To answer this, we used a dominant-negative VPS2-mutant (VPS2-DN) which was generated by deleting the C-Terminal MIT-interacting motif (MIM) responsible for the interaction with SKD1 (Obita et al., 2007; Hurley and Yang, 2008). Vacuolar transport of the reporter α–amylase-sporamin (amy-spo) was measured as the secretion index (SI) given by the ratio of amy-spo detected in the culture medium and within the cells (Pimpl et al., 2003). Coexpression of VPS2-DN caused dosage-dependent induced secretion of amy-spo indicating that vacuolar transport was blocked (Figure 7A). A comparable dosage-dependent misrouting of vacuolar cargo was also caused by ConcA treatment (Figure 7B). In order to biochemically compare the effects of VPS2-DN and ConcA we used protein gel blots and analyzed the processing of the soluble cargo GFP-sporamin in the vacuole. Only a faint GFP-sporamin signal was detected in the medium whereas two strong bands corresponding to GFP-sporamin and the processed form of GFP (vacuolar form) were detectable in the cell fraction (Figure 7C). Treatment with 0.3 µM ConcA showed an increase of the signal detected in the medium, and increasing concentrations of VPS2-DN also showed increasing signal strength in the medium together with a loss of the vacuolar form of GFP in the cells (Figure 7C).

VPS2-DN induces increased colocalization of TGN/EE and MVB/LE markers

Since VPS2-DN affects vacuolar transport, we analyzed its effects on the localization of YFP-SYP61 and mRFP-VSR2 as markers for the TGN/EE and the MVB/LE. During transient expression in protoplasts, fluorescent signals of both markers first became detectable 6h after transfection. At this early time point, both markers mainly colocalized but the signals of the markers separate steadily over time (Supplemental Figure 4A to 4C online), until they reach their typical distribution (Figure 8A, Supplemental Figures 5A and 5B online).
To observe the spatio-temporal effect of VPS2-DN on the distribution of the MVB/LE marker mRFP-VSR2 and the TGN/EE marker YFP-SYP61, we have analyzed different time points post transfection. After 14 h coexpression, VPS2-DN causes enlargement of the YFP-SYP61 signals but TGN/EE and MVB/LE markers were still found to be separate (Figure 8B). However, 18 h after transfection, mRFP-VSR2 was mainly found to localize to the enlarged structures of the TGN (Figures 8C and 8D,

Supplemental Figures 5C and 5D online). Comparable effects were observed when VPS2-DN was coexpressed with YFP-SYP61 and the MVB/LE markers mRFP-ARA7 (Figures 8E to 8H, Supplemental Figures 5E to 5H) or ARA6-mRFP (Figures 8I to 8L, Supplemental Figures 5I to 5L online). The effect of VPS2-DN expression on YFP-SYP61 and ARA6-mRFP distribution resulted in the highest observed r_p and r_s values, leaving almost no signals uncorrelated (Figure 8L and Supplemental Figure 5L online; for comparison of all values see Supplemental Figure 5M online). This temporal progression shows that VPS2-DN affects the TGN/EE first and suggests that the accumulation of the MVB/LE marker in the enlarged TGN/EE is due to perturbed MVB/LE maturation.
To demonstrate that the observed effects are specific for an inhibition of MVB maturation, we used an RNAi-based knock-down of the retromer-component sorting nexin 2a (RNAi-SNX2a). It was recently shown that RNAi-based SNX knock-down results in a change of VSR2 localization but does not affect vacuolar transport (Niemes et al., 2010a). In accordance with this, we could detect changes in the distribution of YFP-SYP61 and mRFP-VSR2 resulting in a four-fold increase of the r_p and r_s values (Supplemental Figures 6A to 6D online). Moreover, no VPS2-DN-like effect was observed when RNAi-SNX2a was coexpressed with other markers for the MVB/LE. The distribution of YFP-SYP61 and mRFP-ARA7 (Supplemental Figures 6E to 6H online) and YFP-SYP61 and ARA6-mRFP (Supplemental Figures 6I to 6L online) remain unaltered when coexpressed with RNAi-SNX2a (for comparison the values for all PSC coefficients are shown in Supplemental Figure 6M).

ConcA treatment and RNAi-mediated knockdown of the annexin ANNAT3 both causes increased colocalization of TGN/EE and MVB/LE markers

In mammals it has been shown that Annexin A2, a calcium-dependent phospholipid-binding protein, is involved in the last step of endosomal maturation in which the MVB is pinched off and released from the early endosome (Mayran et al., 2003). Therefore we investigated if members of the plant annexin family might serve a similar function. The *Arabidopsis* genome encodes eight annexins (ANNAT1-8) and based on phylogenetic analysis ANNAT3, 4, 5 and 8 are more closely related to human annexins. However, ANNAT5 and 8 are only expressed during pollen and embryo development and were thus excluded from further analysis (Supplemental Figures 7A and 7B online). The potential function of ANNAT3 in MVB maturation was analyzed by RNA interference in protoplasts expressing YFP-SYP61 as TGN/EE and mRFP-VSR2 as MVB/LE markers. Coexpression of both markers with RNAi-ANNAT3 increases the values of the PSC coefficients from r_p=0.14 and r_s=-0.09 to r_p=0.51 and r_s=0.28 (compare Figures 9A to 9C with 9G to 9I), as a result of the reduced transcript level of the endogenous annexin (Supplemental Figure 7C) online). ConcA treatment also results in increased values of the PSC coefficients (Figures 9D to 9F) which is in agreement with the observed effect of ConcA on the TGN/MVB marker distribution in stably transformed plants (Supplemental Figure 1 online).

DISCUSSION

V-ATPase activity and TGN integrity are required for vacuolar transport and MVB formation

Binding of the vacuolar-sorting receptor BP80 to an affinity column using the vacuolar sorting motif NPIR from barley (*Hordeum vulgare*) proaleurain as bait occurred at neutral pH and was abolished at acidic pH (Kirsch et al., 1994). Based on this finding and the progressive acidification in the secretory and endocytic pathway of mammalian cells (Mellman et al., 1986), it has been postulated that binding of vacuolar cargo to VSRs takes place in the TGN whereas dissociation would take place in the more acidic MVBs (Paris et al., 1997). However, it is important to note that – at least to our knowledge – pH has neither been measured directly for the TGN/EE nor the MVB/LE of plant cells. The finding that a high density of V-ATPase complexes is found in the TGN/EE rather than at the MVB/LE (Dettmer et al., 2006) suggests that the TGN is an acidic compartment making it unfavorable for the binding of vacuolar cargo to VSRs. A more appropriate upstream location for receptor-ligand interaction could be the ER, since vacuolar cargo is retained in the ER when the luminal domain of VSRs is anchored to an ER membrane protein (Niemes et al., 2010a). On the other hand, the relative lack of V-ATPase complexes in MVB/LEs (Dettmer et al., 2006) does not necessarily mean that the pH in MVBs is any less acidic than the TGN. If, as we postulate, the TGN/EE matures into the MVB/LE the pH in the TGN, once established would not change during the maturation process.

Although a role for the V-PPase or a P-type H^+-ATPase in the MVBs can at the present not be excluded; several lines of evidence indicate that V-ATPase dependent acidification is required for the structure and function of the TGN/EE. ConcA inhibits the V-ATPase and blocks vacuolar transport (Matsuoka et al., 1997; Dettmer et al., 2006). This treatment prevents the formation of the TGN/EE and causes the retention of TGN/EE proteins into an enlarged Golgi stack (Dettmer et al., 2006; Viotti et al., 2010). In contrast, V-ATPase proteins are not detectable in MVBs by immuno staining either in the CLSM or the electron microscope, and the structure of MVBs remains unchanged after ConcA treatment. However, the number of MVBs was found to be drastically reduced after short-term inhibition of the V-ATPase. The decreased number suggests that MVB/LEs are non-persistent transport carriers which are continuously formed at the TGN/EE, and as the ultrastructural analysis shows, are ultimately consumed through fusion with the vacuole. It also means that V-ATPase activity at the TGN/EE is required for MVB/LE biogenesis.

As suggested by our ultrastructural analysis of TGN regeneration after ConcA wash-out, MVB formation and separation from the TGN appears to be a rapid event, and therefore difficult to capture under normal conditions. However, budding of MVBs from tubular, putative TGN structures is not restricted to recovery from drug treatment situations, but can also be seen under physiological conditions. This is in agreement with earlier observations, that dilations of the partially coated reticulum (Pesacreta and Lucas, 1984; Hillmer et al., 1988), contain intralumenal vesicles (Tanchak et al., 1988). A recent electron tomographic analysis of the TGN (Kang et al., 2011) failed to provide evidence for the formation of MVBs, although it was speculated that the membrane fragments that arise as a result of TGN fragmentation “may become precursors of MVBs”. According to Kang et al. (2011), the TGN dissociates from the stack and disintegrates into 3 parts: smooth vesicles (SV), CCV and tubules, which connected both putative carriers prior to fragmentation. The SV are considered to carry secretory cargo but also recycle receptors to the PM; in contrast the CCV would

transport endocytosed PM receptors destined for degradation first to MVBs and then to the vacuole. However, there are several problems with this model. First, it excludes entirely a role for the TGN in the transport of anterograde cargo proteins to the vacuole. Second, it goes against the well-established fact that in mammalian cells PM receptors are recycled from the EE by CCV and not SV (Stoorvogel et al., 1996; van Dam and Stoorvogel, 2002). Third, it does not take into account the dynamics of the relationship between the TGN and the Golgi as previously observed by Viotti et al. (2010) in a live cell imaging analysis.

MVB/LE maturation: An alternative model for transport towards the lytic vacuole

According to current concepts, lytic enzymes are recognized by VSRs at the TGN and become packaged into CCVs for anterograde transport to the MVB (Foresti et al., 2010; Kim et al., 2010; Saint-Jean et al., 2010; Zouhar et al., 2010). This model is based on analogy to mammalian cells, in which lysosomal acid hydrolases are recognized in the TGN by mannosyl 6-phosphate receptors (MPRs), then sequestered into CCVs and transported to the EE (Braulke and Bonifacino, 2009). After ligand dissociation the MPRs are returned to the TGN with the help of sorting nexins (SNXs) and retromer (Bonifacino and Hurley, 2008; Mari et al., 2008). However, the EE of mammalian cells characteristically has extensive tubular protrusions, many of which end in CCVs in which internalized PM receptors collect to be recycled to the PM (van Meel and Klumperman, 2008). Thus, in mammalian cells, CCVs are formed at both the TGN and the EE with different functions at each compartment. Does the TGN/EE hybrid in plants have two different classes of CCVs? A final decision on this cannot be taken at the present: not only do we lack evidence for CCV-mediated transport to the PM from so-called recycling endosomes, but even more importantly in this context, there is no unequivocal proof that TGN-derived CCVs in plants carry VSRs. Indeed, the recent reports of VSRs at the PM (Saint-Jean et al., 2010; Wang et al., 2011) suggests that the VSRs originally isolated from fractions enriched in CCVs (Kirsch et al., 1994) may actually have been present in endocytic CCVs. Our experiments with clathrin hub expression strengthen the notion that anterograde traffic to the vacuole does not require the participation of CCVs, and as a consequence occurs without the recycling of receptors from a *post*-TGN compartment as recently proposed by Niemes et al. (2010a).

A widely-accepted feature of the mammalian endocytic pathway is that transport of lysosomal acid hydrolases after entry into the EE is receptor-independent and occurs by gradual maturation of the EE into the LE followed by fusion with the lysosome (Piper and Katzmann, 2007; van Weering et al., 2010). The notion that a similar maturation-based sorting process may take place in the plant endocytic pathway has only recently been considered by plant scientists (Niemes et al., 2010b), and the data presented here indicates that the mechanism and the molecular machinery involved in endosomal maturation might be conserved between animals and plants.

Molecules involved in MVB-maturation: Rabs, ESCRT and Annexins

In mammalian cells, maturation of LE from EE is triggered by a Rab-conversion mechanism in which the EE-localized Rab5 is replaced by SAND-1/Mon1, which in turn recruits Rab7, resulting in a Rab7 positive LE (Rink et al., 2005; Poteryaev et al., 2010). Whether a comparable mechanism also functions in plants is a matter for speculation. Plant MVB/LE posses the Rab5 type GTPases ARA6/7 (Haas et al., 2007), while Rab11 type class A/B Rabs are found at the TGN/EE (Chow et al.,

2008). However, a protein with similarity to the Rab exchange protein SAND-1/Mon1 is encoded in the *Arabidopsis* genome and its functional analysis will hopefully reveal if a similar mechanism is indeed operational in plants. Nevertheless, when MVB maturation is blocked, an MVB/LE marker should become detectable at the TGN/EE, and this does indeed occur. We have shown that the ConcA-induced inhibition of protein transport at the TGN (Dettmer et al., 2006; Viotti et al., 2010) markedly shifts the steady-state distribution of the predominantly MVB/LE-localized proteins mRFP-ARA7 and ARA6-mRFP towards the TGN/EE.

The characteristic internal vesicles of MVBs originate as a result of ESCRT-mediated vesicle budding from the limiting membrane into the lumen of endosomes (Hurley and Hanson, 2010). In this process, ESCRT-0 clusters cargo, ESCRT-I and -II induce the formation of buds and sequester cargo into them, and ESCRT-III finally mediates vesicle fission (Hurley and Hanson, 2010; Wollert and Hurley, 2010). Our EM data, showing the formation of MVB/LE at the TGN/EE, suggests that the ESCRT machinery might already act at this early developmental stage. To test for this, we have ultrastructurally analyzed the localization of VPS28 in high pressure frozen *Arabidopsis* root cells This ESCRT-I component localizes to the Golgi and the TGN/EE but not to the MVB/LE, demonstrating that ESCRT-mediated sorting and thus the formation of ILVs is not restricted to the MVB/LE.

We have furthermore analyzed tobacco protoplasts, transiently coexpressing the fluorescently-tagged ESCRT-II or -III subunits VPS22-GFP or VPS2-GFP with fluorescent markers for the TGN/EE and MVB/LE. The majority of fluorescent signals of VPS22-GFP colocalized with the TGN/EE marker, while colocalization with the MVB/LE marker was low. In contrast, VPS2-GFP signals were found to colocalize mainly with the MVB/LE marker, but occasionally also with the TGN marker. However, almost all ESCRT-II VPS22 signals colocalized with the ESCRT-III VPS2, supporting the participation of ESCRT in the early development of MVB/LE. The reason for this differential distribution of ESCRT subunits could be explained by different requirements for their release from membranes. This has indeed been shown for yeast ESCRTs, where the disassembly of ESCRT-III, but not of earlier ESCRTs, is strictly dependent on the AAA ATPase Vps4 (Nickerson et al., 2010). SKD1, the *Arabidopsis* homolog of Vps4, localizes to MVB/LE (Haas et al., 2007) and interacts with ESCR-III and ESCRT-associated proteins, but not with ESCRT-I or -II subunits (Spitzer et al., 2009; Shahriari et al., 2010). Therefore, the localization of the ESCRT-III subunit VPS2 at the MVB/LE is in agreement with the localization of the ESCRT-associated AAA ATPase.

To understand better the role of the ESCRT machinery for the transport of vacuolar cargo between the TGN/EE and the MVB/LE, we have generated a VPS2-mutant (VPS2-DN). Expression of this mutant in tobacco protoplasts blocks transport of the soluble vacuolar reporter molecules amy-spo or GFP-spo in a dose-dependent manner. This effect is comparable to that of an ATP hydrolysis-deficient mutant of SKD1 (Shahriari et al., 2010). Coexpression of the mutant with the TGN/EE marker YFP-SYP61 and the MVB/LE cargo mRFP-VSR2 yielded their colocalization in large structures, indicating that protein transport from the TGN/EE to the MVB/LE is blocked. Interestingly, the loss of Class E vps (vacuolar protein sorting) genes (Raymond et al., 1992), all of which encode for ESCRT and ESCRT-related proteins (Katzmann et al., 2001; Babst et al., 2002a; Babst et al., 2002b; Bilodeau et al., 2002), results in the formation of exaggerated prevacuolar organelles, termed class E compartment (Raymond et al., 1992). In mammalian cells, these compartments are of early endosomal origin, accumulate EE marker, endocytosed receptors and lysosomal proteins (Yoshimori et al., 2000; Doyotte et al., 2005) and have therefore

been referred to as multicisternal early endosomes (Doyotte et al., 2005).
VSR-based MVB/LE cargo molecules accumulate at the TGN/EE, when retromer-mediated recycling is perturbed after RNAi knockdown of the sorting nexin SNX2a (Niemes et al., 2010b). However, in this situation vacuolar transport via the MVB/LE is not blocked. Therefore, we considered it necessary to determine whether the VPS2-DN induced transport inhibition between TGN and MVB/LE was indeed due to a block in the transport route, rather than to an interaction between mRFP-VSR2 and the ESCRT machinery. Coexpression of VPS2-DN with the MVB/LE markers ARA6-mRFP or mRFP-ARA7, which are recruited from the cytosol onto their target membranes, also resulted in their colocalization with the TGN/EE marker in enlarged structures, suggesting inhibited maturation of the MVB/LE. Similar effects were seen during RNAi-induced knockdown of the annexins ANNAT3. In mammalian cells, annexin II has been shown to be required for the fission of MVBs from the EE in a process downstream of the ESCRT-mediated budding of intralumenal vesicles (Mayran et al., 2003). This process requires the Annexin A2-dependent polymerization of actin (Morel and Gruenberg, 2009). On the basis of our EM data, showing MVB/LE containing bottleneck structures after ConcA washout, it is tempting to speculate that such structures might be a target for annexin action. However, the function of plant annexins with respect to the modulation of membrane dynamics remains to be established (Laohavisit and Davies, 2011).
In the past, *post*-Golgi protein trafficking to the vacuole in plants has been considered to occur through vesicles moving between stable compartments: the TGN/EE and the MVB/LE. Although a fusion of the MVB/LE with the vacuole has been previously discussed, the consequence of this event, i.e. the replenishment of the MVB/LE population has not been addressed. Here, we have provided evidence pointing to a continual non-vesicular flux of membrane from the TGN to the MVB. Thus, when the structure and integrity of the TGN is perturbed, MVB formation is inhibited. As in mammals, the endosomal system of plants is not a static set of clearly separable structures but characterized by the dynamic generation and consumption of membrane compartments that are derived from each other by maturation (Figure 10).

METHODS

Plant Materials and Growth Conditions

Tobacco plants (*Nicotiana tabacum* var. SR1) were grown as previously described (Pimpl et al., 2006). Suspension cultures of *Arabidopsis thaliana* var. Landsberg *erecta* PSB-D and tobacco Bright Yellow 2 (BY-2) (*Nicotiana tabacum*) stably expressing GONST1-YFP or GFP-BP80 (Tse et al., 2004) were cultivated as described (Miao et al., 2006; Miao and Jiang, 2007); and utilized 3 d after sub-culturing. *Arabidopsis thaliana* ecotype Columbia-0 was used for IEM and CLSM analysis. *Arabidopsis* seedlings were grown on Murashige and Skoog (MS) medium supplemented with 1% sucrose at 22°C, with cycles of 16 h light for 4 to 5 d. For ConcA treatments, seedlings were incubated in 1 mL of liquid medium (half-strength MS medium with 0.5% sucrose, pH 5.8) containing 1 µM ConcA for 45 min, at room temperature. For the wash-out, seedlings were immerged in fresh liquid medium for 15 minutes. The ConcA stock solution was 1 mM in DMSO. Wortmannin was added 1h prior to CLSM analysis in 30 µM concentration. The stock solution was 20 mM in DMSO.

Plasmid Constructs and Plant Transformation

Established plasmids were used encoding for markers/reporters as indicated: mRFP-VSR2 (Miao et al., 2008), YFP–SYP61 (Uemura et al., 2004), Man1–RFP (Nebenführ et al., 1999), GFP–sporamin (daSilva et al., 2005), mRFP-ARA7 and ARA6-mRFP (Ueda et al., 2004) and α-amylase-sporamin (Pimpl et al., 2003). For new recombinant plasmids, all DNA manipulations were performed according to established procedures. Coding sequences were amplified by PCR from either first-strand cDNA prepared from 3-d-old seedlings (Pimpl et al., 2003) or existing plasmid DNA. Recipient vectors were cut according to the restriction sites of the fragments and dephosphorylated prior to ligation. The *Escherichia coli* strain MC1061 (Casadaban and Cohen, 1980) was used for the amplification of all plasmids. The coding sequences of VPS2 and VPS22 were amplified from cDNA with *Nhe*I and *Not*I restriction sites using the VPS2-GFP.FOR and the VPS2-GFP.REV primers for *VPS2* and the VPS22-GFP.FOR and the VPS22-GFP.REV primers for *VPS22* and then ligated in the accordingly cut vector pSN9 (encoding for SNX2a-GFP) (Niemes et al., 2010b) to produce GFP fusions. For an RFP fusion of VPS2 the coding sequence was amplified from VPS2-GFP with *Bgl*II and *Xba*I restriction sites using the VPS2-RFP.FOR and the VPS2-RFP.REV primers and then ligated in the plasmid pBP30 (Nebenführ et al., 1999) cut the same way. The truncated VPS2 (VPS2-DN) was constructed using the VPS2-DN.FOR and VPS2-DN.REV primers for amplification from VPS2-GFP resulting in a 41 bp shorter coding region and then ligated with *Cla*I and *Xba*I restriction sites into pSar1 (Phillipson et al., 2001). To generate the RNAi construct of *ANNAT3* the wild type gene was amplified from *Arabidopsis thaliana* cDNA, using the primers ANNAT3-WT.FOR and ANNAT3-WT.REV. The primers created an N-terminal *Nhe*I and a C-terminal *Sal*I restriction site for insertion into the pSN13 donor vector (Niemes et al., 2010b). The RNAi construct was then generated by cloning a C-terminal 178bp fragment (from C754 to C932) of the *ANNEXIN* wild type construct in sense and antisense orientations, linked by the PDK intron of pHannibal, into pGD5 (Niemes et al., 2010b). All constructs were verified by sequencing.

For the generation of a stably transformed *Arabidopsis* line expressing mRFP-ARA7, the coding sequence of ARA7 was amplified using primers mRFP-ARA7.FOR and mRFP-ARA7.REV. This fragment was then cloned into the BglII/BamHI sites of pURTkan, a derivative of pJHA212 (Yoo et al., 2005), containing the Ubiquitin 10 promoter and the mRFP coding sequence. The resulting binary plasmid was introduced into *Agrobacterium tumefaciens* strain GV3101:pMP90 and selected on 5 mg/mL rifampicin, 10 mg/mL gentamycin and 100 mg/mL spectinomycin. Col-0 plants were transformed according to Clough and Bent, 1998, and transgenic plants were selected on MS medium with 1% sucrose and 50 mg/mL kanamycin. All primers used for cloning are shown in Supplemental Table 1 online. The stably transformed Arabidopsis line expressing SYP61-CFP under the endogenous promoter (Robert et al., 2008) was kindly provided by Natasha Raikhel.

Generation of Antibodies

The coding sequence of *Arabidopsis* VPS28 and VPS2 were amplified from cDNA using the primer pairs VPS28.FOR / VPS28.REV and VPS2.FOR / VPS2.REV, respectively and then ligated into the GST expression vector pGEX-4T3 (accession U13855) previously cut with *Eco*RI/*Sal*I. The GST fusion proteins were expressed for 3 h in *E. coli* BL21 after induction with 1 mM IPTG. Inclusion bodies containing GST–VPS28 or GST-VPS2 were solubilized using an established protocol with *N*-

laurylsarcosine (Frangioni and Neel, 1993). The recombinant proteins were then affinity purified with GST–sepharose. For further purification, SDS-PAGE was performed and the protein bands of interest were excised and electroeluted from the gel using an Elutrap Electroelution System (www.whatman.com) at 4°C with 50 mA for 16h. Eluted proteins were dialysed 3 times for 2 h against TBS (50 mM Tris, 152 mM NaCl, pH 7.4) prior to lyophilization. Three hundred milligrams of each lyophilized GST–fusion protein was used for commercial immunization of rabbits (Eurogentec, Belgium). All primers used for cloning are shown in Supplemental Table 1 online.

Protein extraction and Gel Blot Analysis

7 day old Arabidopsis plants were frozen in liquid N_2 and homogenized with glass beads in a TissueLyser II (Qiagen, www.qiagen.com) in extraction buffer containing 100 mM Tris pH 7.8, 200 mM NaCl, 1 mM EDTA, 2 % (v/v) β-Mercaptoethanol and 0.2 % (v/v) Triton X-100. Protein gel blots and immunodetection were performed on total cell extracts processed as described previously (Pimpl et al., 2006). The polyclonal antiserum raised against VPS28 was used in a 1:10.000 dilution, the VPS2 antiserum was diluted 1:2500. Monoclonal antibodies against GFP (Roche, www.roche-applied-science.com) were diluted 1:1000.

Isolation of Protoplasts and Transient Gene Expression

Tobacco mesophyll protoplasts were isolated from leaves of 6–8 week-old plants and subsequently transfected via electroporation as described previously (Bubeck et al., 2008). Unless otherwise stated, 10 µg of plasmid DNA were use for transfection and protoplasts were incubated for 16-24 h. *Arabidopsis* protoplasts were generated from cell suspension cultures 3 days after sub-cultivation and subsequently transformed either via PEG mediated transformation as described before (Negrutiu, 1987) or via electroporation as previously described (Niemes et al. 2010a). 20 µg of plasmid DNA were used for each transformation. Afterwards, the protoplasts were incubated in the dark at 26 °C for a minimum of 20 hours.

Fluorescence assisted cell sorting (FACS) and RT-PCR

Tobacco protoplasts expressing cytosolic GFP alone or coexpressing the RNAi-ANNAT3 plasmid for 24 h were subjected to fluorescence assisted cell sorting (FACS) using a MoFlo flow cytometer (Beckman-Coulter). 70,000 fluorescent Protoplasts were sorted for each condition using a 100 µM nozzle. The sheath solution was PBS at pH 7.0 and the core/sheath was operated at 30.7 psi / 30.0 psi, respectively. GFP fluorescence was excited with a standard 488 nm Argon laser powered to 50 mW. Emission was detected in FL1 (504-522nm) and plotted against FL2 (565-605nm) to spread signals derived from GFP and autofluorescence. Autofluorescence signals were gated out by analyzing a mock transfected protoplast population. Data acquisition and analysis were performed using the MOFLO Summit 4.3 software. For each condition, total RNA from 70,000 sorted protoplasts was extracted using the RNeasy Plant Mini Kit (Qiagen, www.qiagen.com) according to the instructions of the manufacturer and 250 ng of the total RNA was used for the synthesis of first-strand cDNA (RevertAid™ H Minus First Strand cDNA Synthesis Kit, Fermentas, www.fermentas.com). RT-PCR for ANNEXIN1 or ANNEXIN3 from *Nicotiana tabacum* was performed with the primer pairs NtAnx1.FOR / NtAnx1.REV or NtAnx3.FOR / NtAnx3.REV. Actin was amplified as a control using the primer pair Actin.FOR / Actin.REV.

Confocal Microscopy and Immunofluorescence Labeling

Imaging was performed using a Zeiss Axiovert LSM 510 meta confocal laser scanning microscope (http://www.zeiss.com/) and C-Apochromat 63 x/1.2 W corr water immersion objective. At the Metadetector, main beam splitters (HFT) 405/514, 458/514 and 488/543 were used. The following fluorophores (excited and emitted by frame switching in the multitracking mode) were used: GFP, 488 nm/496–518 nm; YFP, 514 nm/529–550 nm; RFP, 543 nm/593–636 nm. Pinholes were adjusted to 1 Airy unit for each wavelength. Post-acquisition image processing was performed using the Zeiss LSM 510 image browser (4.2.0.121) and Corel-DrawX4 (14.0.0.567) (Corel, http://www.corel.com).

For immunofluorescence analysis, BY-2 cells were fixed and processed as previously described (Ritzenthaler et al., 2002). Samples were incubated overnight at 4°C with the VPS2 antibodies diluted at 1:200. The Alexa-Fluor® 546 conjugate (Invitrogen, http://www.invitrogen.com) was used as secondary antibody.

Statistical Analysis of CLSM localization data

For statistical analysis the Pearson and Spearman correlation (PSC) colocalization plug-in (French et al., 2008) for ImageJ (Abramoff, 2004) was used to calculate the linear Pearson correlation coefficient (r_p) and the non-linear Spearman´s rank correlation coefficient (r_s) of red and green fluorescent signals. Values between -1 (negative correlation) and +1 (positive correlation). The fluorescence values of all pixels across the two channels of all analyzed signals were depicted in a scatter plot. Masking of areas of was carried out with the ImageJ brush tool as described in French et al., 2008. For every analyzed image punctuate signals were selected and the threshold level, under which pixels were treated as background noise, was set to 10. At least 10 individual cells and a minimum of 200 signals were considered for every experiment.

Quantification of intrinsic FM4-64 signals in *Arabidopsis* protoplasts

FM4-64 uptake assays in *Arabidopsis* protoplasts were carried out in double blind experiments. For every condition 20 individual pictures were captured 30 minutes after the addition of FM4-64. All intracellular FM4-64 signals were considered as intrinsic signals. Standard errors were calculated using Excel (Microsoft).

High Pressure Freezing and Immunogold Electron Microscopy

Four- to five-day-old *Arabidopsis* root tips were cut from the seedling, submerged in 140 mM sucrose, 7 mM trehalose and 7 mM Tris buffer (pH 6.6), transferred into planchettes (Wohlwend GmbH, Sennwald, Switzerland; type 241 and 242) and frozen in a high-pressure freezer (HPM010; Bal-Tec). Freeze substitution was performed in a Leica EM AFS2 freeze substitution unit (Leica; Germany) in dry acetone supplemented with 0.4% uranyl acetate at −85°C for 16 h before gradually warming up to −50°C over an 5 -h period. After washing with 100% ethanol for 60 min, the roots were infiltrated and embedded in Lowicryl HM20 at −50°C (intermediate steps of 30, 50, 75 % HM20 in ethanol, 1 h each), and polymerized for 3 days with ultraviolet (UV) light in the freeze substitution apparatus. Ultrathin sections were cut on a Leica Ultracut S (Leica) and incubated with antibodies against BP80 (1: 50, Niemes et al., 2010b) or RFP (1: 20; Clontech, Living Colors DsRed polyclonal rabbit antibodies), followed by incubation with 10-nm gold-coupled secondary antibodies (BioCell GAR10; BioCell) at a dilution of 1:50 in PBS supplemented with 1% BSA. Double immunogold labeling on the *Arabidopsis* SYP61-CFP line was performed using monoclonal mouse GFP antibodies (Roche,

www.roche-applied-science.com) diluted 1:25, followed by incubation with 5-nm gold-coupled secondary antibodies (BioCell GAR10; BioCell). Subsequently immunogold labeling using the polyclonal rabbit VPS28 antibody (1:600) was carried out on the same sections, followed by incubation with 15-nm gold-coupled secondary antibodies (BioCell GAR10; BioCell). For structural analysis, root tips were freeze substituted (72 h, –90°C; 8 h, –60°C; 8 h, –35°C and 4 h, 0°C) in acetone containing 2% osmium tetroxide, washed at 0°C and embedded in Spurr. Sections were examined in a JEM1400 transmission electron microscope (JEOL, Japan) operating at 80 kV. Micrographs were recorded with a FastScan F214 digital camera (TVIPS, Germany).

Chemical Fixation for Electron Microscopy

Arabidopsis seedlings were fixed immersed in 25 mM cacodylate (Caco) buffer pH 7.2 containing 2% (v/v) glutaraldehyde and 10% (v/v) saturated picric acid at 4°C for 16 h. After four washes of 15 min each in 25 mM Caco buffer pH 7.2, seedlings were transferred in a secondary fixative containing 2% (w/v) osmium tetroxide and 0.5% (w/v) potassium ferrocyanid in 25 mM Caco buffer pH 7.2 for 2 h at room temperature (RT). Seedlings were washed twice in 25 mM Caco pH 7.2, and twice in distilled water before transferring to 2% (w/v) aqueous uranyl acetate for 16 hr at 4°C. After four washes in water, seedlings were dehydrated in acetone 30, 50, 70, 90% in water and twice in acetone 100% for 15 min each at RT. Root-tips were cut from the seedlings and submerged in 25, 50, 75% Spurr in acetone and than in 100% Spurr for 45 min each at RT and finally transferred in fresh Spurr 100% at 4°C for 16 h. Samples were transferred in fresh Spurr 100% for 4 h, and then placed in the oven at 60°C for polymerization.

Quantification of MVBs in root cells

The quantification was conducted on ultrathin sections of 5-day-old *Arabidopsis* root-tips using a JEM 1400 transmission electron microscope (JEOL) operating at 80 kV. The root-tips were sectioned longitudinally, close to the central axis. Multivesicular bodies were counted in all the cell types of the meristematic zone. Standard deviations were calculated using Excel (Microsoft).

Quantitative Analysis of IEM

The quantitative analysis was conducted on ultrathin sections previously immunolabeled at the optimal dilution of the respective antibodies for BP80, mRFP-ARA7 and VPS28. The sections were analyzed and every Golgi apparatus and/or every endosomal compartment encountered during the screening of cells that did not present folding, scratches, or any source of unspecific labeling was taken into consideration. For the labeling density parameter the area of the single compartments was calculated using the image processing program ImageJ (http://rsbweb.nih.gov/ij). Standard deviations were calculated using Excel (Microsoft).

Supplemental Data
The following materials are available in the online version of this article.
Supplemental Figure 1. ConcA affects the distribution of marker proteins for TGN/EE and MVB/LE.
Supplemental Figure 2. Differential localization of the ESCRT-components VPS22-GFP and VPS2-GFP.
Supplemental Figure 3. VPS22-GFP and VPS2-GFP do not colocalize with Golgi markers but VPS2 is found at the MVB/LE.
Supplemental Figure 4. Time course to study the temporal distribution of YFP-SYP61 and mRFP-VSR2 as TGN/EE and MVB/LE makers.
Supplemental Figure 5. Expression of VPS2-DN affects the distribution of markers for the TGN/EE and MVB/LE.
Supplemental Figure 6. RNAi-SNX2a prevents arrival of mRFP-VSR2 at the MVB/LE but does not affect vacuolar transport.
Supplemental Figure 7. Relationship, expression and knockdown of plant annexins.
Supplemental Table 1. Primers used for cloning.

Accession Numbers
Sequence data from this article can be found in the *Arabidopsis* Genome Initiative or GenBank/EMBL databases under the following accession numbers: VPS28, AT4G21560; VPS22, At4g27040; VPS2, At2g06530; VHA-a1, At2g28520; ARA6, At3g54840; ARA7, At4g19640; SYP61, At1g28490; VSR2, At2g30290; ANNAT3, At2g38760; NtAnx1, GI:3219615; NtAnx3, GI:4580919

ACKNOWLEDGEMENTS
The authors wish to thank Liwen Jiang (CHUK, Hong Kong) for kindly providing mRFP-VSR2 encoding plasmids and BP80 antisera and Natasha Raikhel (UC Riverside, USA) for kindly providing the SYP61-CFP *Arabidopsis* line. We are gratefull to York-Dieter Stierhof (ZMBP Tübingen) for helpful discussions on EM. We thank Joachim Kilian and Kenneth W. Berendzen (ZMBP Tübingen) for Fluorescence Assisted Cell Sorting of protoplasts and Barbara Jesenofsky, Beate Schöfer and Steffi Gold (COS Heidelberg) for technical help. The financial support of the Deutsche Forschungsgemeinschaft (PI 769/1-1 and RO 440/14-1) is gratefully acknowledged.

AUTHOR CONTRIBUTIONS
D.S., C.V., D.G.R., P.P. and K.S. designed and analyzed the experiments; D.S., C.V., F.Kr., F.Kü., S.S., J.B., and S.H. performed the experiments; L.F. contributed unpublished material; D.S., C.V., D.G.R., P.P. and K.S. wrote the article.

FIGURE LEGENDS
Figure 1. Clathrin-Hub1 expression inhibits endocytosis but not vacuolar transport in *Arabidopsis* protoplasts.
(A) and **(B)** Staining of the PM directly after FM4-64 addition (A) and endocytic uptake of the dye after 30 min incubation (B).
(C) Protoplasts expressing the GFP tagged clathrin-Hub1 (GFP-Hub1) were stained with FM4-64 and incubated for 30 min. The dye is not internalized and remains at the PM.
(D) Comparative quantification of intrinsic FM4-64 signals from 20 protoplasts either in the presence or absence of GFP-Hub1. Error bars indicate the standard deviation of signal numbers.

(E) Coexpression of the soluble vacuolar marker spRFP-AFVY and cytosolic GFP (cytGFP) in protoplasts. spRFP is efficiently transported into the lumen of the vacuole, even if fluorescent cytosolic proteins (cytGFP) are coexpressed.
(F) Coexpression of GFP-Hub1 and the soluble vacuolar marker spRFP-AFVY in protoplasts. The presence of GFP-Hub1 in the cytosol does not perturb vacuolar transport of spRFP-AFVY (compare to (E)).
Scale bars = 5 µm.

Figure 2. EM analysis of the effects of ConcA on MVBs.
(A) ConcA treatment reduces the number of MVBs in the cell. Roots of four independent plants were analyzed either in the absence or presence of ConcA by counting the number of MVBs in 100 sectioned cells per root. Per 100 control cells, 220±30 MVBs were identified, whereas after ConcA treatment, the number of MVBs was five-fold lower (40±15). Error bars indicate the standard deviation.
(B) Quantitative analysis of ConcA effects on the endogenous VSR BP80 and the Rab GTPase ARA7 in an mRFP-ARA7 expressing *Arabidopsis* line. The Golgi localization of BP80 and mRFP-ARA7 was analyzed in Roots of four independent plants ether in the absence or presence of ConcA by counting the labeling on 50 randomly chosen Golgi stacks per root. Under standard conditions, BP80 and mRFP-ARA7 do not localize to the Golgi (11±4 % and 15±2 % of Golgi labeling, respectively), whereas in the presence of ConcA, both proteins also significantly localize to the Golgi stacks (59±5 % and 58±4 % of Golgi labeling, respectively). Error bars indicate the standard deviation.
(C) IEM localization of the endogenous BP80 in *Arabidopsis* roots after high pressure freezing, freeze-substitution and Lowicryl HM20 resin-embedding. The VSR BP80 localizes to both the TGN (arrowheads) and MVBs (empty arrowheads).
(D) and **(E)** Upon ConcA treatment, BP80 is detected at the Golgi stack (arrows), and at enlarged vesicles in the surrounding area (D; arrowheads). Although ConcA reduces the number of MVBs, those MVBs that are still present, show unaltered BP80 labeling (E, empty arrowheads).
(F) The Rab GTPase mRFP-ARA7 localizes to the limiting membrane of MVBs (arrowheads).
(G) After ConcA treatment, mRFP-ARA7 localizes to both, swollen vesicles (arrowheads) and Golgi stack (arrows).
(H) In the presence of ConcA, mRFP-ARA7 is detected at the limiting membrane of the remaining MVBs (empty arrowheads).
Scale bars = 200 nm

Figure 3. Multivesicular bodies fuse with the vacuole.
Fusion of MVBs with the vacuole in sections of cells from high pressure frozen *Arabidopsis* roots.
(A) and **(B)** The limiting membrane of an MVB (arrow) has fused with the Tonoplast, resulting in the merge of the lumen of both compartments. In (B) additionally, internal vesicles are recognizable in the lumen of the vacuole (arrowheads), sharing shape and size with ILVs, typically seen in MVBs (courtesy of York-Dieter Stierhof).
(C) An MVB (arrow) almost entirely fused with a small vacuole.
(D) An MVB (arrow), entirely fused with a small vacuole, shows a polarized distribution of the inner vesicles, suggesting that the fusion occurred shortly before freezing of the cells. Note that there is another MVB in the vicinity (arrowhead).
V = vacuole; Scale bars = 200 nm

Figure 4. MVBs mature from tubular-vesicular structures.
(A) and **(B)** Mature MVBs in sections from high pressure frozen untreated (untr) root cells typically have an almost perfect circular profile. Depending upon the plane of section, a plaque (arrow in B) is occasionally visible.
(C) An MVB (arrow) attached to a tubular-vesicular structure (arrowhead) in untreated *Arabidopsis* root-tip cells.
(D) An MVB showing a tubular connection (arrow) and bottleneck terminations (arrowheads) in untreated *Arabidopsis* root-tip cells.
(E) to **(H)** MVBs seen in *Arabidopsis* root-tip cells during recovery from ConcA-treatment (45 min ConcA; followed by 15 min wash-out) are pleiomorphic, often with bottle-neck terminations. In (E) and (F), MVBs (arrows) are attached to tubular structures (arrowheads) in the area of the TGN; in (G) and (H), pleiomorphic MVBs display bottle-neck terminations (arrowheads), indicating a possible connection to tubular structures above or beneath the plane of section.
(I) and **(J)** MVBs (arrows) directly connected to TGN-like structures (arrowheads). In (J), root-tip cells were chemically fixed.
(K) mRFP-ARA7 localization to the limiting membrane of these unusually shaped (compared to (A) and (B)) multivesiculated structures, confirms their identity as MVBs.
G = Golgi; Scale bars = 200 nm.

Figure 5. The ESCRT-I component VPS28 localizes to the Golgi and the TGN
(A) Immunodetection of VPS28 in total protein extracts from 7 day old *Arabidopsis* plants (left) using antibodies against VPS28 (αVPS28) and VPS28-GFP transiently expressed in protoplasts isolated from Arabidopsis suspension cultures (middle and right). Protoplasts were transfected with 3, 10, 30 or 100 µg plasmid DNA encoding for VPS28-GFP or mock-transfected (-). Total protein extracts from protoplasts were probed with antibodies against VPS28 (αVPS28) and antibodies against GFP (αGFP).
(B) Immunogold electron microscopy (IEM) analysis using the αVPS28 antibody on high pressure frozen *Arabidopsis* WT root cells shows that the endogenous VPS28 localizes to the Golgi stacks and the TGN (arrows).
(C) IEM of the endogenous VPS28 shows that VPS28 localizes to the Golgi stack and the TGN (arrows) but is not detected on the multivesicular body
(D) Quantitative analysis of VPS28 IEM. The labeling density, expressed as the number of gold particles per micrometer^2 (gold/µm^2), is significantly higher for the TGN and the Golgi apparatus (18.8 and 11.1 gold/µm^2, respectively) respect to the MVBs (3.1 gold/µm^2) or plastids/mitocondria (1.4 gold/µm^2). N°= number of compartments encountered; N° lab.= number of compartments labeled; µm^2= total area considered; gold= total number of gold particles detected; gold/µm^2= labeling density.
(E) Double immunolocalization of VPS28 in an *Arabidopsis* line expressing the TGN marker SYP61-CFP under the control of the endogenous promoter, using the polyclonal αVPS28 antibodies from rabbit in combination with 15-nm (arrowheads) gold-coupled secondary antibodies and monoclonal αGFP antibodies from mouse in combination with 5-nm (arrows) gold-coupled secondary antibodies. Both, the TGN-marker and VPS28 localize to the same tubular-vesicular structure, immediately adjacent to the Golgi stacks.
(F) In BFA treated *Arabidopsis* plants, VPS28 labels the core of the BFA-compartment, confirming TGN localization of this ESCRT-I subunit.
G = Golgi; T = TGN; M = MVB/LE; B = BFA compartment; Scale bars = 200 nm.

Figure 6. Gradual distribution of the ESCRT-II component VPS22 and the ESCRT-III component VPS2.
Tobacco mesophyll protoplasts were transfected with plasmids encoding fluorescent markers/reporters as indicated below. Proteins were expressed for 18-24 h prior to CLSM analysis. White arrows indicate colocalization. For quantification, the Pearson and Spearman correlation (PSC) coefficients (r_p and r_s) were calculated after analysis of at least 10 individual protoplasts and a minimum of 200 signals. The level of colocalization ranges from +1 for perfect correlation to -1 for negative correlation. For the corresponding scatter plots of the fluorescence values of pixels across the two channels see Supplemental Figure 2 online.
(A) Coexpression of VPS22-GFP and the TGN/EE marker YFP-SYP61.
(B) VPS22-GFP was coexpressed with the MVB/LE marker mRFP-VSR2.
(C) Quantification of VPS22-GFP colocalization with TGN/EE (YFP-SYP61) and MVB/LE (mRFP-VSR2) marker.
(D) Coexpression of VPS2-GFP and YFP-SYP61.
(E) VPS2-GFP and mRFP-VSR2 were coexpressed.
(F) Quantification of VPS2-GFP colocalization with TGN/EE and MVB/LE marker.
(G) Coexpression of VPS22-GFP and VPS2-RFP. Some VPS2-RFP signals do not colocalize (white arrowheads). Only VPS2-RFP signals localize to wortmannin (WM)-sensitive compartments as indicated by the magnified ring-like structure.
(H) Quantitative comparison of the number of VPS2-RFP and VPS22-GFP signals. Error bars indicate the standard deviation of numbers of signals.
(I) Quantification of VPS22-GFP and VPS2-RFP colocalization.
Scale bars = 5 µm.

Figure 7. Effects of ConcA and the ESCRT-III mutant VPS2-DN on vacuolar transport.
Tobacco mesophyll protoplasts were transfected with plasmids encoding for reporters/effectors as indicated below. Proteins were expressed for 18-24 h prior to analysis.
For analyzing vacuolar transport the α-amylase derivative amylase-sporamin (amy-spo) was used. The secretion index (SI) is calculated as the ratio of the activity of amy-spo secreted to the culture medium and the activity of amy-spo within the cells.
(A) VPS2-DN causes a dosage-dependent missorting of the vacuolar reporter amy-spo and subsequent secretion into the culture medium. Error bars indicate standard deviation of 5 individual experiments.
(B) Treatment with increasing concentrations of ConcA leads to the same effect than described in (C) but stronger (ten-fold increase of the SI). Error bars indicate standard deviation of 5 individual experiments.
(C) Immunoblot analysis of protein transport after transient expression of the soluble vacuolar reporter GFP-sporamin in the presence of ConcA (left panel) or coexpression with VPS2-DN (right panel), using GFP-antibodies for immuno-detection of the reporter. (-) mock-transfection, (+) positive control of GFP-sporamin expression without effector.

Figure 8. VPS2-DN causes marker proteins for TGN/EE and MVB/LE to colocalize.
Tobacco mesophyll protoplasts were transfected with plasmids encoding for fluorescent markers/reporters as indicated below. Proteins were expressed for 18 h prior to CLSM analysis. For quantification, the Pearson and Spearman correlation (PSC) coefficients (r_p and r_s) were calculated after analysis of at least 10 individual

protoplasts and a minimum of 200 signals. The level of colocalization ranges from +1 for perfect correlation to -1 for negative correlation. For the corresponding scatter plots of the fluorescence values of pixels across the two channels see supplemental figure 5.
(A) Coexpression of TGN/EE and MVB/LE markers YFP-SYP61 and mRFP-VSR2 18 h after transfection.
(B) Effect of VPS2-DN on the distribution of TGN/EE and MVB/LE marker 14 h after transfection.
(C) Analysis 18 h after transfection: VPS2-DN causes a change in the signal pattern of the marker proteins. The signals accumulate in bigger but fewer structures.
(D) Quantification of the marker colocalization. The r_p and r_s values increase when VPS2-DN is expressed.
(E) Coexpression of TGN/EE and MVB/LE markers YFP-SYP61 and mRFP-ARA7 18 h after transfection.
(F) Effect of the VPS2-DN coexpression with YFP-SYP61 and mRFP-ARA7 14 h post transfection.
(G) When expressed for 18 h, VPS2-DN increases colocalization of YFP-SYP61 and mRFP-ARA7. As observed in (C) the signals change structurally.
(H) Quantification revealed higher r_p and r_s values for the marker proteins when VPS2-DN was expressed.
(I) to **(L)** An experiment as described in (E) to (H) was carried out, except ARA6-mRFP was used as MVB/LE marker. Here, the highest increase of r_p and r_s values was found (L).
Scale bars = 5 µm.

Figure 9. RNAi knockdown of the annexin ANNAT3 increases colocalization of TGN/EE and MVB/LE marker proteins.
Tobacco mesophyll protoplasts were transfected with plasmids encoding for fluorescent markers/reporters as indicated below. Proteins were expressed for 18-24 h prior to CLSM analysis. For quantification, the Pearson and Spearman correlation (PSC) coefficients (r_p and r_s) were calculated after analysis of at least 10 individual protoplasts and a minimum of 200 signals. The level of colocalization ranges from +1 for positive correlation to -1 for negative correlation,and the fluorescence values of pixels across the two channels are depicted in an intensity scatter plot.
(A) Tobacco protoplast expressing YFP-SYP61 as TGN/EE marker and mRFP-VSR2 as MVB/LE marker.
(B) Intensities of fluorescent signals from (A), representing YFP-SYP61 (green) and mRFP-VSR2 (red), are depicted in a scatter plot. The calculated PSC values are given in the upper right corner.
(C) Bar chart to illustrate the PSC coefficients from (B).
(D) Protoplasts from (A) were incubated for 1 h in the presence of 1 µM ConcA **(E)** Intensities of fluorescent signals from (D), representing YFP-SYP61 (green) and mRFP-VSR2 (red), are depicted in a scatter plot. The calculated PSC values are given in the upper right corner.
(F) Bar chart to illustrate the PSC coefficients from (E).
(G) RNAi-based knockdown of ANNAT3 by cotransfection of plasmid DNA encoding for RNAi-ANNAT3 and the markers YFP-SYP61 and mRFP-VSR2.
(H) Intensities of fluorescent signals from (G), representing YFP-SYP61 (green) and mRFP-VSR2 (red), are depicted in a scatter plot. The calculated PSC values are given in the upper right corner. The r_p and r_s values are considerably higher

compared to the control (B).
(I) Bar chart to illustrate the PSC coefficients from (H)
Scale bars = 5 µm.

Figure 10. Model illustrating TGN to MVB maturation.
According to this model, the TGN is continually formed and released from the Golgi stack. It also functions as an EE and receives incoming cargo from the plasma membrane (PM) via clathrin coated vesicles (CCVs). As it differentiates, the TGN probably subdivides into domains where secretory vesicles (SV) are released to the PM, into domains releasing CCVs for recycling to the PM (recycling endosomes) and into a domain which matures into a multivesicular body (MVB). Participating in the latter process, as indicated, are the ESCRT complexes I, II and III, as well as annexin. As in mammalian cells, we postulate that *post*-TGN trafficking of soluble proteins to the lytic compartment (vacuole) occurs receptor-independently and is accompanied by a gradual transformation of part of the EE (TGN) into the LE (MVB), which ultimately fuses with the vacuole membrane.

REFERENCES

Abramoff, M.D., Magelhaes, P.J., and Ram, S.J. (2004). Image processing with ImageJ. Biophotonics International **11,** 36-42.

Aniento, F., Papavassiliou, A.G., Knecht, E., and Roche, E. (1996). Selective uptake and degradation of c-Fos and v-Fos by rat liver lysosomes. FEBS Lett **390,** 47-52.

Babst, M., Katzmann, D.J., Estepa-Sabal, E.J., Meerloo, T., and Emr, S.D. (2002a). Escrt-III: an endosome-associated heterooligomeric protein complex required for mvb sorting. Dev Cell **3,** 271-282.

Babst, M., Katzmann, D.J., Snyder, W.B., Wendland, B., and Emr, S.D. (2002b). Endosome-associated complex, ESCRT-II, recruits transport machinery for protein sorting at the multivesicular body. Dev Cell **3,** 283-289.

Bilodeau, P.S., Urbanowski, J.L., Winistorfer, S.C., and Piper, R.C. (2002). The Vps27p Hse1p complex binds ubiquitin and mediates endosomal protein sorting. Nat Cell Biol **4,** 534-539.

Bonifacino, J.S., and Hurley, J.H. (2008). Retromer. Curr Opin Cell Biol **20,** 427-436.

Braulke, T., and Bonifacino, J.S. (2009). Sorting of lysosomal proteins. Biochim Biophys Acta **1793,** 605-614.

Bubeck, J., Scheuring, D., Hummel, E., Langhans, M., Viotti, C., Foresti, O., Denecke, J., Banfield, D.K., and Robinson, D.G. (2008). The syntaxins SYP31 and SYP81 control ER-Golgi trafficking in the plant secretory pathway. Traffic **9,** 1629-1652.

Carlton, J.G., Bujny, M.V., Peter, B.J., Oorschot, V.M., Rutherford, A., Arkell, R.S., Klumperman, J., McMahon, H.T., and Cullen, P.J. (2005). Sorting nexin-2 is associated with tubular elements of the early endosome, but is not essential for retromer-mediated endosome-to-TGN transport. J Cell Sci **118,** 4527-4539.

Casadaban, M.J., and Cohen, S.N. (1980). Analysis of gene control signals by DNA fusion and cloning in Escherichia coli. J Mol Biol **138,** 179-207.

Clough, S.J and Bent, A.F. (1998). Floral dip: a simplified method for Agrobacterium-mediated transformation of Arabidopsis thaliana. Plant J **16,** 735-743.

Chow, C.M., Neto, H., Foucart, C., and Moore, I. (2008). Rab-A2 and Rab-A3 GTPases define a trans-golgi endosomal membrane domain in Arabidopsis that contributes substantially to the cell plate. Plant Cell **20,** 101-123.

Clague, M.J. (2002). Membrane transport: a coat for ubiquitin. Curr Biol **12,** R529-531.

daSilva, L.L., Taylor, J.P., Hadlington, J.L., Hanton, S.L., Snowden, C.J., Fox, S.J., Foresti, O., Brandizzi, F., and Denecke, J. (2005). Receptor salvage from the prevacuolar compartment is essential for efficient vacuolar protein targeting. Plant Cell **17,** 132-148.

Dettmer, J., Hong-Hermesdorf, A., Stierhof, Y.D., and Schumacher, K. (2006). Vacuolar H+-ATPase activity is required for endocytic and secretory trafficking in Arabidopsis. Plant Cell **18,** 715-730.

Dhonukshe, P., Aniento, F., Hwang, I., Robinson, D.G., Mravec, J., Stierhof, Y.D., and Friml, J. (2007). Clathrin-mediated constitutive endocytosis of PIN auxin efflux carriers in Arabidopsis. Curr Biol **17,** 520-527.

Doyotte, A., Russell, M.R., Hopkins, C.R., and Woodman, P.G. (2005). Depletion of TSG101 forms a mammalian "Class E" compartment: a multicisternal early endosome with multiple sorting defects. J Cell Sci **118,** 3003-3017.

Foresti, O., Gershlick, D.C., Bottanelli, F., Hummel, E., Hawes, C., and Denecke, J. (2010). A Recycling-Defective Vacuolar Sorting Receptor Reveals an Intermediate Compartment Situated between Prevacuoles and Vacuoles in Tobacco. Plant Cell **22,** 3992-4008.

Frangioni, J.V., and Neel, B.G. (1993). Solubilization and purification of enzymatically active glutathione S-transferase (pGEX) fusion proteins. Anal Biochem **210,** 179-187.

French, A.P., Mills, S., Swarup, R., Bennett, M.J., and Pridmore, T.P. (2008). Colocalization of fluorescent markers in confocal microscope images of plant cells. Nat Protoc **3,** 619-628.

Futter, C.E., and White, I.J. (2007). Annexins and endocytosis. Traffic **8,** 951-958.

Gabriely, G., Kama, R., and Gerst, J.E. (2007). Involvement of specific COPI subunits in protein sorting from the late endosome to the vacuole in yeast. Mol Cell Biol **27,** 526-540.

Geldner, N., Hyman, D.L., Wang, X., Schumacher, K., and Chory, J. (2007). Endosomal signaling of plant steroid receptor kinase BRI1. Genes Dev **21,** 1598-1602.

Griffiths, G., and Gruenberg, J. (1991). The arguments for pre-existing early and late endosomes. Trends Cell Biol **1,** 5-9.

Haas, T.J., Sliwinski, M.K., Martinez, D.E., Preuss, M., Ebine, K., Ueda, T., Nielsen, E., Odorizzi, G., and Otegui, M.S. (2007). The Arabidopsis AAA ATPase SKD1 is involved in multivesicular endosome function and interacts with its positive regulator LYST-INTERACTING PROTEIN5. Plant Cell **19,** 1295-1312.

Hillmer, S., Freundt, H., and Robinson, D.G. (1988). The partially coated reticulum and its relationship to the Golgi apparatus in higher plant cells. Eur J Cell Biol **47,** 206-212.

Hunter, P.R., Craddock, C.P., Di Benedetto, S., Roberts, L.M., and Frigerio, L. (2007). Fluorescent reporter proteins for the tonoplast and the vacuolar lumen identify a single vacuolar compartment in Arabidopsis cells. Plant Physiol **145,** 1371-1382.

Hurley, J.H., and Yang, D. (2008). MIT domainia. Dev Cell **14,** 6-8.

Hurley, J.H., and Hanson, P.I. (2010). Membrane budding and scission by the ESCRT machinery: it's all in the neck. Nat Rev Mol Cell Biol **11,** 556-566.

Jovic, M., Sharma, M., Rahajeng, J., and Caplan, S. (2010). The early endosome: a busy sorting station for proteins at the crossroads. Histol Histopathol **25,** 99-112.

Kang, B.H., and Staehelin, L.A. (2008). ER-to-Golgi transport by COPII vesicles in Arabidopsis involves a ribosome-excluding scaffold that is transferred with the vesicles to the Golgi matrix. Protoplasma **234,** 51-64.

Kang, B.H., Nielsen, E., Preuss, M.L., Mastronarde, D., and Staehelin, L.A. (2011). Electron tomography of RabA4b- and PI-4Kbeta1-labeled trans Golgi network compartments in Arabidopsis. Traffic **12,** 313-329.

Katzmann, D.J., Babst, M., and Emr, S.D. (2001). Ubiquitin-dependent sorting into the multivesicular body pathway requires the function of a conserved endosomal protein sorting complex, ESCRT-I. Cell **106,** 145-155.

Kim, H., Kang, H., Jang, M., Chang, J.H., Miao, Y., Jiang, L., and Hwang, I. (2010). Homomeric interaction of AtVSR1 is essential for its function as a vacuolar sorting receptor. Plant Physiol **154,** 134-148.

Kirsch, T., Paris, N., Butler, J.M., Beevers, L., and Rogers, J.C. (1994). Purification and initial characterization of a potential plant vacuolar targeting receptor. Proc Natl Acad Sci U S A **91,** 3403-3407.

Lam, S.K., Siu, C.L., Hillmer, S., Jang, S., An, G., Robinson, D.G., and Jiang, L. (2007). Rice SCAMP1 defines clathrin-coated, trans-golgi-located tubular-vesicular structures as an early endosome in tobacco BY-2 cells. Plant Cell **19,** 296-319.

Laohavisit, A., and Davies, J.M. (2011). Annexins. New Phytol **189,** 40-53.

Leung, K.F., Dacks, J.B., and Field, M.C. (2008). Evolution of the multivesicular body ESCRT machinery; retention across the eukaryotic lineage. Traffic **9,** 1698-1716.

Liu, S.H., Marks, M.S., and Brodsky, F.M. (1998). A dominant-negative clathrin mutant differentially affects trafficking of molecules with distinct sorting motifs in the class II major histocompatibility complex (MHC) pathway. J Cell Biol **140,** 1023-1037.

Liu, S.H., Wong, M.L., Craik, C.S., and Brodsky, F.M. (1995). Regulation of clathrin assembly and trimerization defined using recombinant triskelion hubs. Cell **83,** 257-267.

Luzio, J.P., Piper, S.C., Bowers, K., Parkinson, M.D., Lehner, P.J., and Bright, N.A. (2009). ESCRT proteins and the regulation of endocytic delivery to lysosomes. Biochem Soc Trans **37,** 178-180.

Mari, M., Bujny, M.V., Zeuschner, D., Geerts, W.J., Griffith, J., Petersen, C.M., Cullen, P.J., Klumperman, J., and Geuze, H.J. (2008). SNX1 defines an early endosomal recycling exit for sortilin and mannose 6-phosphate receptors. Traffic **9,** 380-393.

Matsuoka, K., Higuchi, T., Maeshima, M., and Nakamura, K. (1997). A Vacuolar-Type H+-ATPase in a Nonvacuolar Organelle Is Required for the Sorting of Soluble Vacuolar Protein Precursors in Tobacco Cells. Plant Cell **9,** 533-546.

Mayran, N., Parton, R.G., and Gruenberg, J. (2003). Annexin II regulates multivesicular endosome biogenesis in the degradation pathway of animal cells. Embo J **22,** 3242-3253.

Mellman, I., Fuchs, R., and Helenius, A. (1986). Acidification of the endocytic and exocytic pathways. Annu Rev Biochem **55,** 663-700.

Miao, Y., Yan, P.K., Kim, H., Hwang, I., and Jiang, L. (2006). Localization of green fluorescent protein fusions with the seven Arabidopsis vacuolar sorting receptors to prevacuolar compartments in tobacco BY-2 cells. Plant Physiol **142,** 945-962.

Miao, Y., and Jiang, L. (2007). Transient expression of fluorescent fusion proteins in protoplasts of suspension cultured cells. Nat Protoc **2,** 2348-2353.

Miao, Y., Li, K.Y., Li, H.Y., Yao, X., and Jiang, L. (2008). The vacuolar transport of aleurain-GFP and 2S albumin-GFP fusions is mediated by the same pre-vacuolar compartments in tobacco BY-2 and Arabidopsis suspension cultured cells. Plant J **56,** 824-839.

Morel, E., and Gruenberg, J. (2009). Annexin A2 binding to endosomes and functions in endosomal transport are regulated by tyrosine 23 phosphorylation. J Biol Chem **284,** 1604-1611.

Murk, J.L., Humbel, B.M., Ziese, U., Griffith, J.M., Posthuma, G., Slot, J.W., Koster, A.J., Verkleij, A.J., Geuze, H.J., and Kleijmeer, M.J. (2003). Endosomal compartmentalization in three dimensions: implications for membrane fusion. Proc Natl Acad Sci U S A **100,** 13332-13337.

Nebenführ, A., Gallagher, L.A., Dunahay, T.G., Frohlick, J.A., Mazurkiewicz, A.M., Meehl, J.B., and Staehelin, L.A. (1999). Stop-and-go movements of plant Golgi stacks are mediated by the acto-myosin system. Plant Physiol **121,** 1127-1142.

Negrutiu, I., Shillito, R., Potrykus, I., Biasini, G. and Sala, F. (1987). Hybrid genes in the analysis of transformation conditions. Plant Mol. Biol **8,** 363-373.

Nickerson, D.P., West, M., Henry, R., and Odorizzi, G. (2010). Regulators of Vps4 ATPase activity at endosomes differentially influence the size and rate of formation of intralumenal vesicles. Mol Biol Cell **21,** 1023-1032.

Niemes, S., Labs, M., Scheuring, D., Krueger, F., Langhans, M., Jesenofsky, B., Robinson, D.G., and Pimpl, P. (2010a). Sorting of plant vacuolar proteins is initiated in the ER. Plant J **62,** 601-614.

Niemes, S., Langhans, M., Viotti, C., Scheuring, D., San Wan Yan, M., Jiang, L., Hillmer, S., Robinson, D.G., and Pimpl, P. (2010b). Retromer recycles vacuolar sorting receptors from the trans-Golgi network. Plant J **61,** 107-121.

Obita, T., Saksena, S., Ghazi-Tabatabai, S., Gill, D.J., Perisic, O., Emr, S.D., and Williams, R.L. (2007). Structural basis for selective recognition of ESCRT-III by the AAA ATPase Vps4. Nature **449,** 735-739.

Otegui, M.S., and Spitzer, C. (2008). Endosomal functions in plants. Traffic **9,** 1589-1598.

Paris, N., Rogers, S.W., Jiang, L., Kirsch, T., Beevers, L., Phillips, T.E., and Rogers, J.C. (1997). Molecular cloning and further characterization of a probable plant vacuolar sorting receptor. Plant Physiol **115,** 29-39.

Peden, A.A., Oorschot, V., Hesser, B.A., Austin, C.D., Scheller, R.H., and Klumperman, J. (2004). Localization of the AP-3 adaptor complex defines a novel endosomal exit site for lysosomal membrane proteins. J Cell Biol **164,** 1065-1076.

Pesacreta, T.C., and Lucas, W.J. (1984). Plasma membrane coat and a coated vesicle-associated reticulum of membranes: their structure and possible interrelationship in Chara corallina. J Cell Biol **98,** 1537-1545.

Phillipson, B.A., Pimpl, P., daSilva, L.L., Crofts, A.J., Taylor, J.P., Movafeghi, A., Robinson, D.G., and Denecke, J. (2001). Secretory bulk flow of soluble proteins is efficient and COPII dependent. Plant Cell **13,** 2005-2020.

Pimpl, P., Hanton, S.L., Taylor, J.P., Pinto-daSilva, L.L., and Denecke, J. (2003). The GTPase ARF1p controls the sequence-specific vacuolar sorting route to the lytic vacuole. Plant Cell **15,** 1242-1256.

Pimpl, P., Taylor, J.P., Snowden, C., Hillmer, S., Robinson, D.G., and Denecke, J. (2006). Golgi-mediated vacuolar sorting of the endoplasmic reticulum chaperone BiP may play an active role in quality control within the secretory pathway. Plant Cell **18,** 198-211.

Piper, R.C., and Katzmann, D.J. (2007). Biogenesis and function of multivesicular bodies. Annu Rev Cell Dev Biol **23,** 519-547.

Polo, S., Sigismund, S., Faretta, M., Guidi, M., Capua, M.R., Bossi, G., Chen, H., De Camilli, P., and Di Fiore, P.P. (2002). A single motif responsible for ubiquitin recognition and monoubiquitination in endocytic proteins. Nature **416,** 451-455.

Poteryaev, D., Datta, S., Ackema, K., Zerial, M., and Spang, A. (2010). Identification of the switch in early-to-late endosome transition. Cell **141,** 497-508.

Raymond, C.K., Howald-Stevenson, I., Vater, C.A., and Stevens, T.H. (1992). Morphological classification of the yeast vacuolar protein sorting mutants: evidence for a prevacuolar compartment in class E vps mutants. Mol Biol Cell **3,** 1389-1402.

Razi, M., Chan, E.Y., and Tooze, S.A. (2009). Early endosomes and endosomal coatomer are required for autophagy. J Cell Biol **185,** 305-321.

Reichardt, I., Stierhof, Y.D., Mayer, U., Richter, S., Schwarz, H., Schumacher, K., and Jurgens, G. (2007). Plant cytokinesis requires de novo secretory trafficking but not endocytosis. Curr Biol **17,** 2047-2053.

Rink, J., Ghigo, E., Kalaidzidis, Y., and Zerial, M. (2005). Rab conversion as a mechanism of progression from early to late endosomes. Cell **122,** 735-749.

Ritzenthaler, C., Nebenfuhr, A., Movafeghi, A., Stussi-Garaud, C., Behnia, L., Pimpl, P., Staehelin, L.A., and Robinson, D.G. (2002). Reevaluation of the effects of brefeldin A on plant cells using tobacco Bright Yellow 2 cells expressing Golgi-targeted green fluorescent protein and COPI antisera. Plant Cell **14,** 237-261.

Robert, S., Chary, S.N., Drakakaki, G., Li, S., Yang, Z., Raikhel, N.V., and Hicks, G.R. (2008). Endosidin1 defines a compartment involved in endocytosis of the brassinosteroid receptor BRI1 and the auxin transporters PIN2 and AUX1. Proc Natl Acad Sci U S A **105,** 8464-8469.

Robinson, D.G., Jiang, L., and Schumacher, K. (2008). The endosomal system of plants: charting new and familiar territories. Plant Physiol **147,** 1482-1492.

Sachse, M., Urbe, S., Oorschot, V., Strous, G.J., and Klumperman, J. (2002). Bilayered clathrin coats on endosomal vacuoles are involved in protein sorting toward lysosomes. Mol Biol Cell **13,** 1313-1328.

Saint-Jean, B., Seveno-Carpentier, E., Alcon, C., Neuhaus, J.M., and Paris, N. (2010). The cytosolic tail dipeptide Ile-Met of the pea receptor BP80 is required for recycling from the prevacuole and for endocytosis. Plant Cell **22,** 2825-2837.

Schellmann, S., and Pimpl, P. (2009). Coats of endosomal protein sorting: retromer and ESCRT. Curr Opin Plant Biol **12,** 670-676.

Shahriari, M., Keshavaiah, C., Scheuring, D., Sabovljevic, A., Pimpl, P., Hausler, R.E., Hulskamp, M., and Schellmann, S. (2010). The AAA-type ATPase AtSKD1 contributes to vacuolar maintenance of Arabidopsis thaliana. Plant J **64,** 71-85.

Shahriari, M., Richter, K., Keshavaiah, C., Sabovljevic, A., Huelskamp, M., and Schellmann, S. (2011). The Arabidopsis ESCRT protein-protein interaction network. Plant Mol Biol **76,** 85-96.

Spitzer, C., Reyes, F.C., Buono, R., Sliwinski, M.K., Haas, T.J., and Otegui, M.S. (2009). The ESCRT-related CHMP1A and B proteins mediate multivesicular body sorting of auxin carriers in Arabidopsis and are required for plant development. Plant Cell **21,** 749-766.

Stierhof, Y.D., and El Kasmi, F. (2010). Strategies to improve the antigenicity, ultrastructure preservation and visibility of trafficking compartments in Arabidopsis tissue. Eur J Cell Biol **89,** 285-297.

Stoorvogel, W., Oorschot, V., and Geuze, H.J. (1996). A novel class of clathrin-coated vesicles budding from endosomes. J Cell Biol **132,** 21-33.

Tanchak, M.A., Rennie, P.J., and Fowke, L.C. (1988). Ultrastrucure of the partially coated reticulum and dictyosomes during endocytosis by soybean protoplasts. Planta **175,** 433-441.

Taub, N., Teis, D., Ebner, H.L., Hess, M.W., and Huber, L.A. (2007). Late endosomal traffic of the epidermal growth factor receptor ensures spatial and temporal fidelity of mitogen-activated protein kinase signaling. Mol Biol Cell **18,** 4698-4710.

Tooze, J., and Hollinshead, M. (1991). Tubular early endosomal networks in AtT20 and other cells. J Cell Biol **115,** 635-653.

Toyooka, K., Goto, Y., Asatsuma, S., Koizumi, M., Mitsui, T., and Matsuoka, K. (2009). A mobile secretory vesicle cluster involved in mass transport from the Golgi to the plant cell exterior. Plant Cell **21,** 1212-1229.

Tse, Y.C., Mo, B., Hillmer, S., Zhao, M., Lo, S.W., Robinson, D.G., and Jiang, L. (2004). Identification of multivesicular bodies as prevacuolar compartments in Nicotiana tabacum BY-2 cells. Plant Cell **16,** 672-693.

Ueda, T., Uemura, T., Sato, M.H., and Nakano, A. (2004). Functional differentiation of endosomes in Arabidopsis cells. Plant J **40,** 783-789.

Uemura, T., Ueda, T., Ohniwa, R.L., Nakano, A., Takeyasu, K., and Sato, M.H. (2004). Systematic analysis of SNARE molecules in Arabidopsis: dissection of the post-Golgi network in plant cells. Cell Struct Funct **29,** 49-65.

van Dam, E.M., and Stoorvogel, W. (2002). Dynamin-dependent transferrin receptor recycling by endosome-derived clathrin-coated vesicles. Mol Biol Cell **13,** 169-182.

van Meel, E., and Klumperman, J. (2008). Imaging and imagination: understanding the endo-lysosomal system. Histochem Cell Biol **129,** 253-266.

van Weering, J.R., Verkade, P., and Cullen, P.J. (2010). SNX-BAR proteins in phosphoinositide-mediated, tubular-based endosomal sorting. Semin Cell Dev Biol **21,** 371-380.

Viotti, C., Bubeck, J., Stierhof, Y.D., Krebs, M., Langhans, M., van den Berg, W., van Dongen, W., Richter, S., Geldner, N., Takano, J., Jurgens, G., de Vries, S.C., Robinson, D.G., and Schumacher, K. (2010). Endocytic and secretory traffic in Arabidopsis merge in the trans-Golgi network/early endosome, an independent and highly dynamic organelle. Plant Cell **22,** 1344-1357.

Wang, H., Zhuang, X., Hillmer, S., Robinson, D.G., and Jiang, L. (2011). Vacuolar Sorting Receptor (VSR) Proteins Reach the Plasma Membrane in Germinating Pollen Tubes. Mol Plant **doi:10.1093/mp/ssr011**.

Winter, V., and Hauser, M.T. (2006). Exploring the ESCRTing machinery in eukaryotes. Trends Plant Sci **11,** 115-123.

Wollert, T., and Hurley, J.H. (2010). Molecular mechanism of multivesicular body biogenesis by ESCRT complexes. Nature **464,** 864-869.

Yoo, S.Y., Bomblies, K., Yoo, S.K., Yang, J.W., Choi, M.S., Lee, J.S., Weigel, D., and Ahn, J.H. (2005). The 35S promoter used in a selectable marker gene of a plant transformation vector affects the expression of the transgene. Planta **221,** 523-530.

Yoshimori, T., Yamagata, F., Yamamoto, A., Mizushima, N., Kabeya, Y., Nara, A., Miwako, I., Ohashi, M., Ohsumi, M., and Ohsumi, Y. (2000). The mouse SKD1, a homologue of yeast Vps4p, is required for normal endosomal trafficking and morphology in mammalian cells. Mol Biol Cell **11,** 747-763.

Zouhar, J., Munoz, A., and Rojo, E. (2010). Functional specialization within the vacuolar sorting receptor family: VSR1, VSR3 and VSR4 sort vacuolar storage cargo in seeds and vegetative tissues. Plant J **64,** 577-588.

Figure 1

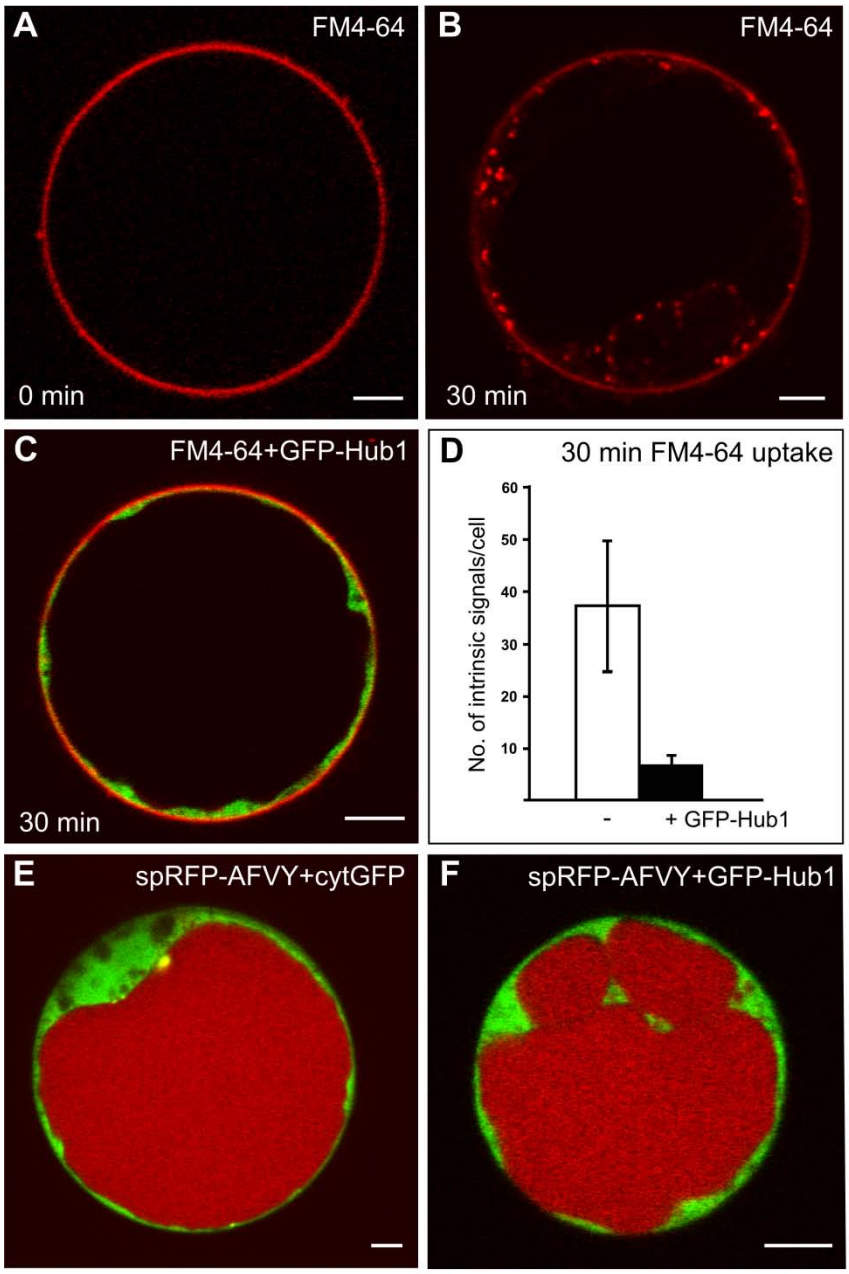

Figure 1. Clathrin-Hub1 expression inhibits endocytosis but not vacuolar transport in *Arabidopsis* protoplasts. (A) and **(B)** Staining of the PM directly after FM4-64 addition (A) and endocytic uptake of the dye after 30 min incubation (B). **(C)** Expression of the GFP tagged clathrin-Hub1 (GFP-Hub1) inhibits endocytic uptake of FM4-64. **(D)** Comparative quantification of intrinsic FM4-64 signals from at least 10 protoplasts either in the presence or absence of GFP-Hub1. **(E)** The soluble vacuolar marker spRFP-AFVY is efficiently transported into the lumen of the vacuole, even if fluorescent cytosolic proteins (cytGFP) are coexpressed. **(F)** Inhibition of clathrin-mediated transport by the expression of GFP-Hub1 does not perturb vacuolar transport of spRFP-AFVY. Scale bars = 5 µm.

Figure 2

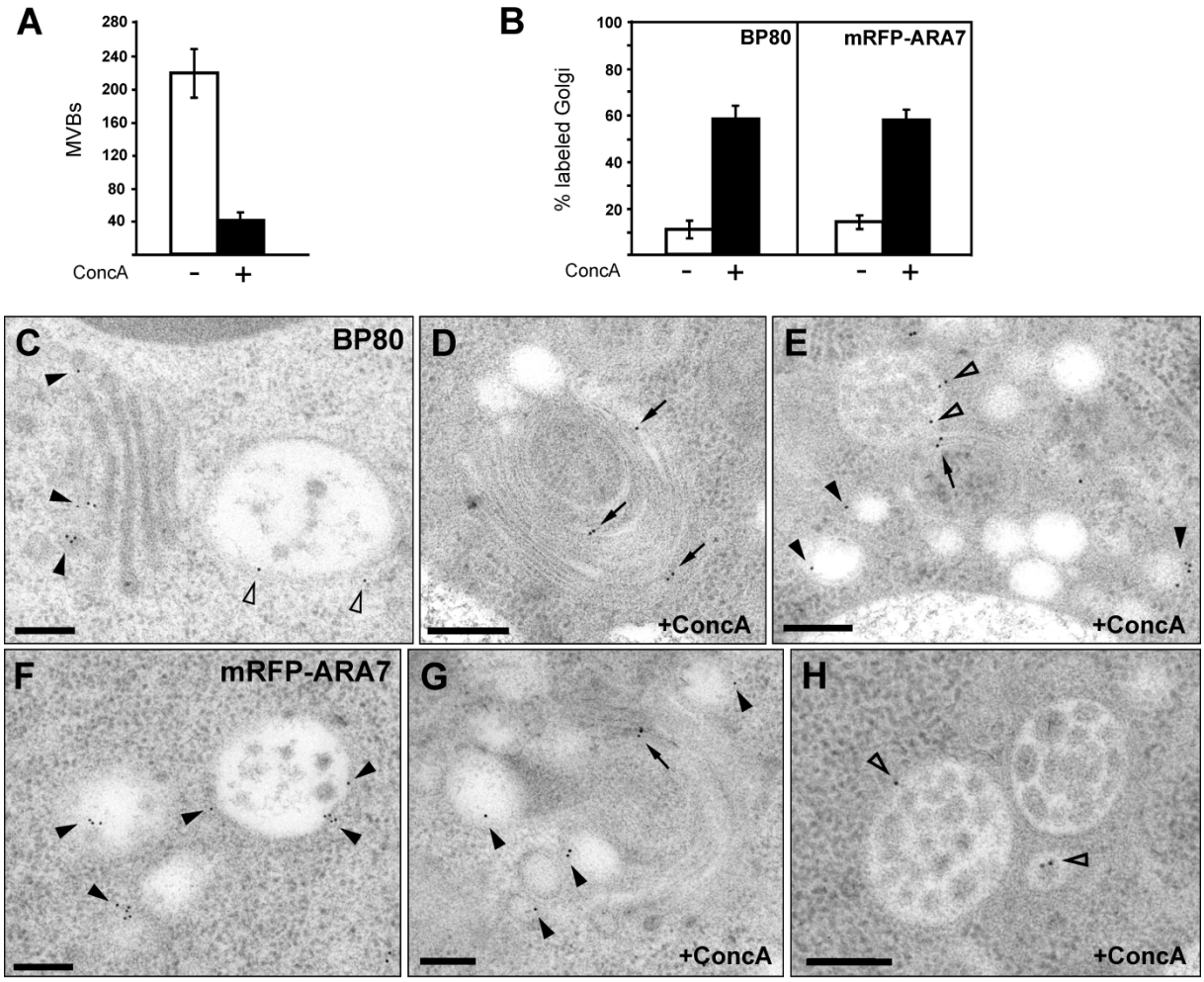

Figure 2. EM analysis of the effects of ConcA on MVBs. (A) ConcA treatment reduces the number of MVBs in the cell. Roots of four independent plants were analyzed either in the absence or presence of ConcA by counting the number of MVBs in 100 sectioned cells per root. Per 100 control cells, 220±30 MVBs were identified, whereas after ConcA treatment, the number of MVBs was five-fold lower (40±15). **(B)** Quantitative analysis of ConcA effects on the endogenous VSR BP80 and the Rab GTPase ARA7 in an mRFP-ARA7 expressing *Arabidopsis* line. The Golgi localization of BP80 and mRFP-ARA7 was analyzed in roots of four independent plants either in the absence or presence of ConcA by counting the labeling on 50 randomly chosen Golgi stacks per root. Under standard conditions, BP80 and mRFP-ARA7 do not localize to the Golgi (11±4 % and 15±2 % of Golgi labeling, respectively), whereas in the presence of ConcA, both proteins also significantly localize to the Golgi stacks (59±5 % and 58±4 % of Golgi labeling, respectively). **(C)** IEM localization of the endogenous BP80 in *Arabidopsis* roots after high pressure freezing, freeze-substitution and Lowicryl HM20 resin-embedding. The VSR BP80 localizes to both the TGN (arrowheads) and MVBs (empty arrowheads), but is rarely detected at the Golgi stacks. **(D)** and **(E)** Upon ConcA treatment, BP80 is detected at the Golgi stack (arrows), and at enlarged vesicles in the surrounding area (D; arrowheads). Although ConcA reduces the number of MVBs, those MVBs that are still present, show unaltered BP80 labeling (E, empty arrowheads). **(F)** The Rab GTPase mRFP-ARA7 localizes to the limiting membrane of MVBs (arrowheads). **(G)** After ConcA treatment, mRFP-ARA7 localizes to both, swollen vesicles (arrowheads) and Golgi stack (arrows). **(H)** In the presence of ConcA, mRFP-ARA7 is detected at the limiting membrane of the remaining MVBs (empty arrowheads). Scale bars = 200 nm.

Figure 3

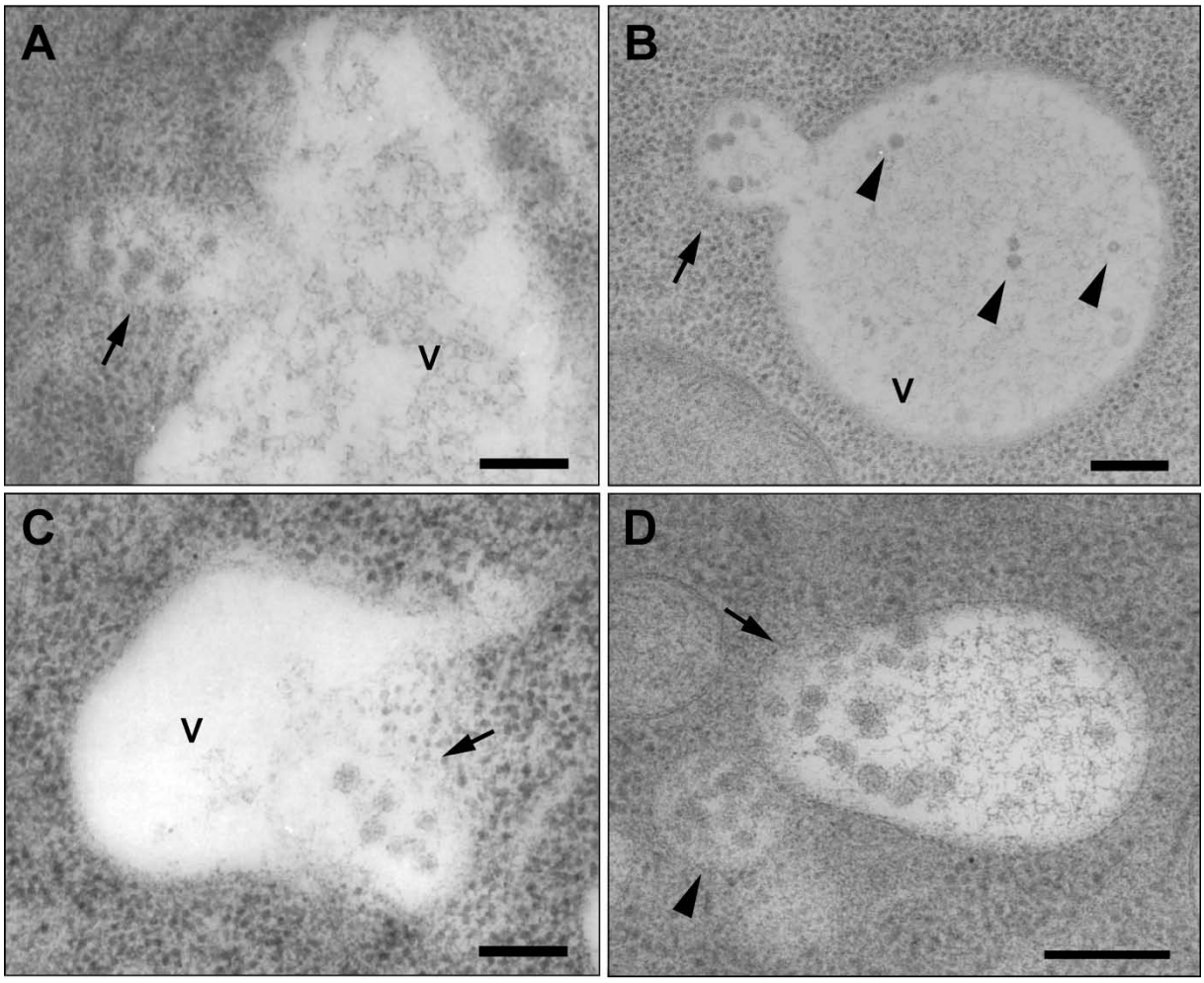

Figure 3. Multivesicular bodies fuse with the vacuole. Fusion of MVBs with the vacuole in sections of cells from high pressure frozen *Arabidopsis* roots. **(A)** and **(B)** The limiting membrane of an MVB (arrow) has fused with the Tonoplast, resulting in the merge of the lumen of both compartments. In (B) additionally, internal vesicles are recognizable in the lumen of the vacuole (arrowheads), sharing shape and size with ILVs, typically seen in MVBs (courtesy of York-Dieter Stierhof). **(C)** An MVB (arrow) almost entirely fused with a small vacuole. **(D)** An MVB (arrow), entirely fused with a small vacuole, shows a polarized distribution of the inner vesicles, suggesting that the fusion occurred shortly before freezing of the cells. Note that there is another MVB in the vicinity (arrowhead). V = vacuole; Scale bars = 200 nm.

Figure 4

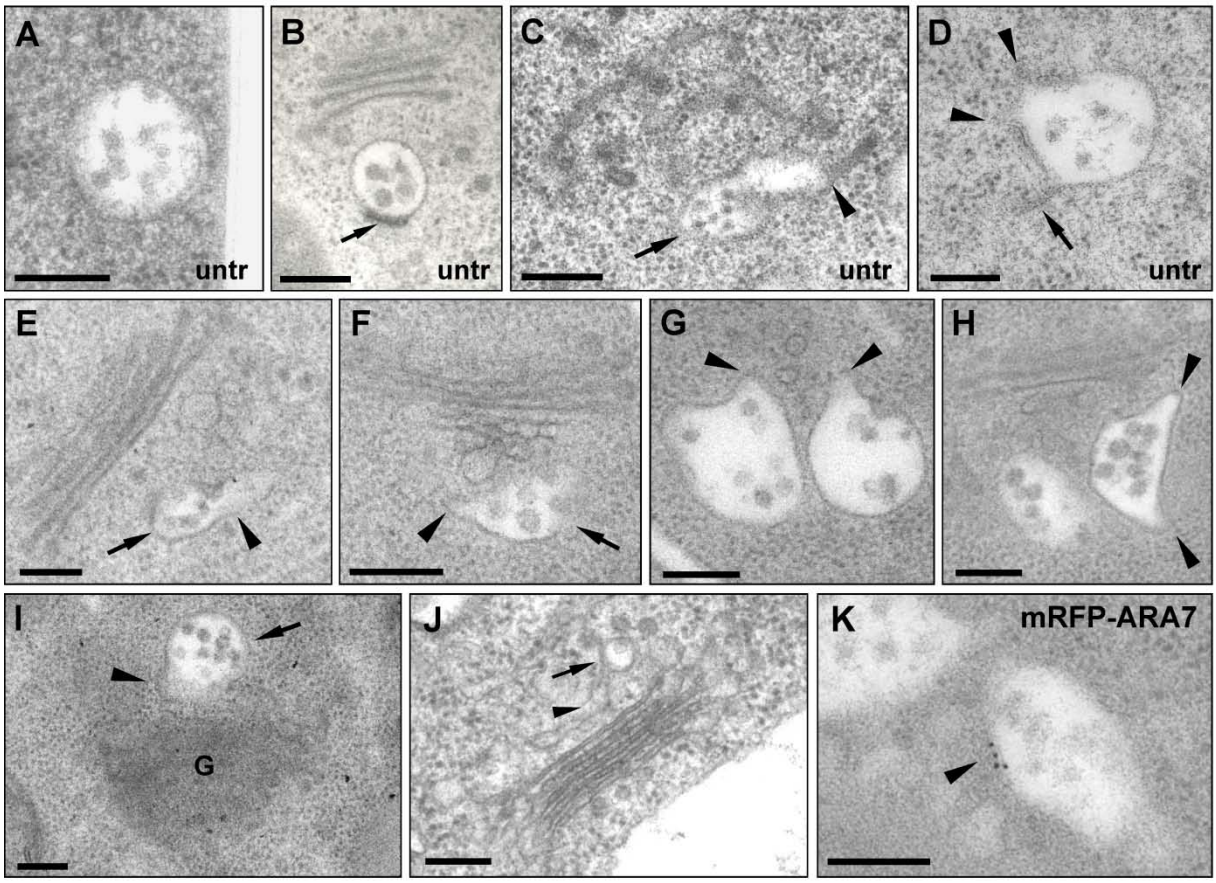

Figure 4. MVBs mature from tubular-vesicular structures.

(A) and **(B)** Mature MVBs in sections from high pressure frozen untreated (untr) root cells typically have an almost perfect circular profile. Depending upon the plane of section, a plaque (arrow in B) is occasionally visible. **(C)** An MVB (arrow) attached to a tubular-vesicular structure (arrowhead) in untreated *Arabidopsis* root-tip cells. **(D)** An MVB showing a tubular connection (arrow) and bottleneck terminations (arrowheads) in untreated *Arabidopsis* root-tip cells. **(E)** to **(H)** MVBs seen in *Arabidopsis* root-tip cells during recovery from ConcA-treatment (45 min ConcA; followed by 15 min wash-out) are pleiomorph, often with bottle-neck terminations. In (E) and (F), MVBs (arrows) are attached to tubular structures (arrowheads) in the area of the TGN; in (G) and (H), pleiomorphic MVBs display bottle-neck terminations (arrowheads), indicating a possible connection to tubular structures above or beneath the plane of section. **(I)** and **(J)** MVBs (arrows) directly connected to TGN-like structures (arrowheads). In (J), root-tip cells were chemically fixed. **(K)** mRFP-ARA7 localization to the limiting membrane of these unusually shaped (compared to (A) and (B)) multivesiculated structures, confirms their identity as MVBs. G = Golgi; Scale bars = 200 nm.

Figure 5

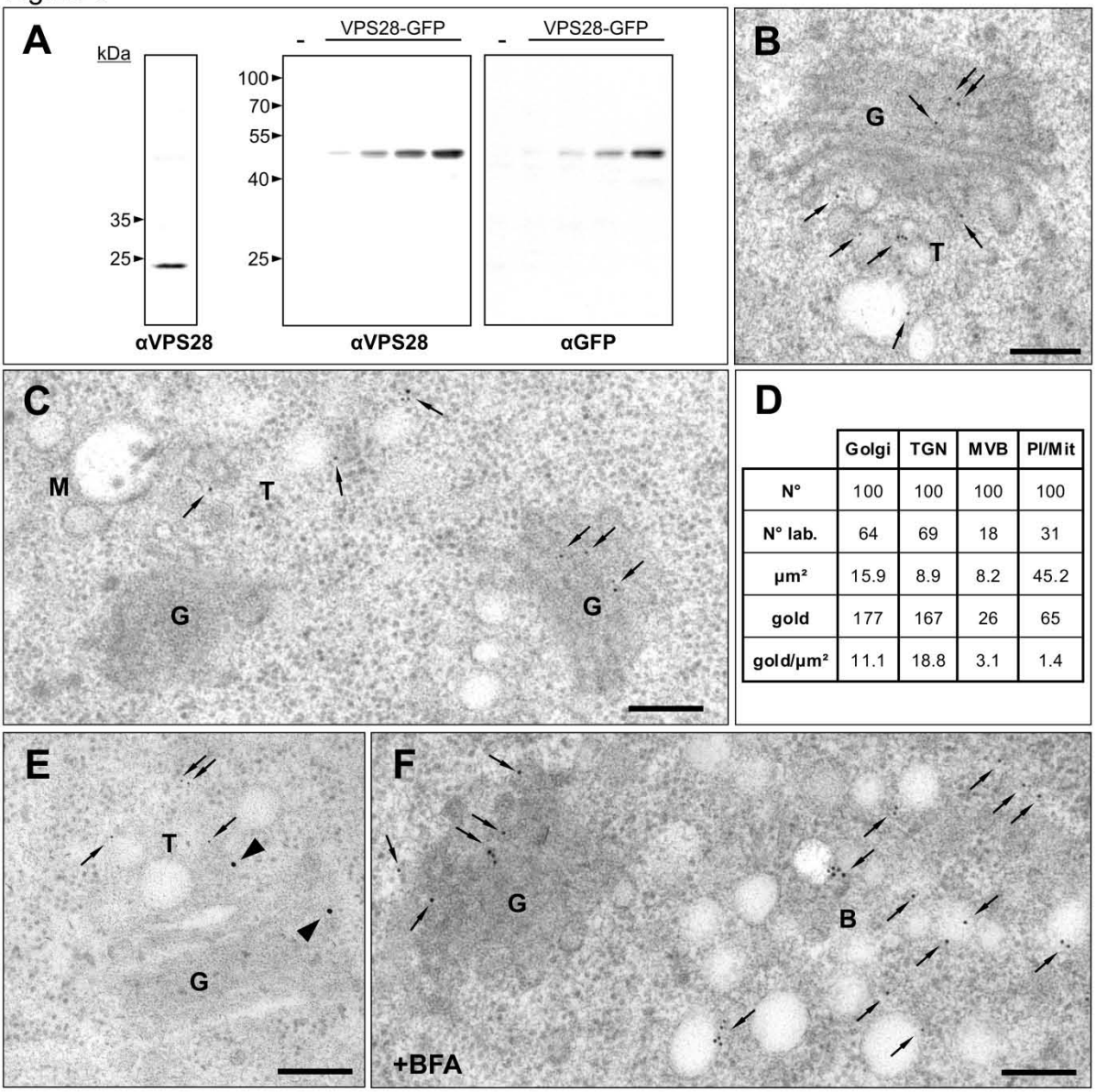

	Golgi	TGN	MVB	Pl/Mit
N°	100	100	100	100
N° lab.	64	69	18	31
µm²	15.9	8.9	8.2	45.2
gold	177	167	26	65
gold/µm²	11.1	18.8	3.1	1.4

The ESCRT-I component VPS28 localizes to the Golgi and the TGN

(A) Immunodetection of VPS28 in total protein extracts from 7 day old Arabidopsis plants (left) using antibodies against VPS28 (αVPS28) and VPS28-GFP transiently expressed in protoplasts isolated from Arabidopsis suspension cultures (middle and right). Protoplasts were transfected with 3, 10, 30 or 100 µg plasmid DNA encoding for VPS28-GFP or mock-transfected (–). Total protein extracts from protoplasts were probed with antibodies against VPS28 (αVPS28) and antibodies against GFP (αGFP).

(B) Immunogold electron microscopy (IEM) analysis using the αVPS28 antibody on high pressure frozen Arabidopsis WT root cells shows that the endogenous VPS28 localizes to the Golgi stacks and the TGN (arrows).

(C) IEM of the endogenous VPS28 shows that VPS28 localizes to the Golgi stack and the TGN (arrows) but is not detected on the multivesicular body.

(D) Quantitative analysis of VPS28 IEM. The labeling density, expressed as the number of gold particles per micrometer^2 (gold/µm^2), is significantly higher for the TGN and the Golgi apparatus (18.8 and 11.1 gold/µm^2, respectively) respect to the MVBs (3.1 gold/µm^2) or plastids/mitocondria (1.4 gold/µm^2). N°= number of compartments encountered; N° lab.= number of compartments labeled; µm^2= total area considered; gold= total number of gold particles detected; gold/µm^2= labeling density.

(E) Double immunolocalization of VPS28 in an Arabidopsis line expressing the TGN marker SYP61-CFP under the control of the endogenous promoter, using the polyclonal αVPS28 antibodies from rabbit in combination with 15-nm (arrowheads) gold-coupled secondary antibodies and monoclonal αGFP antibodies from mouse in combination with 5 nm (arrows) gold-coupled secondary antibodies. Both, the TGN-marker and VPS28 localize to the same tubular-vesicular structure, immediately adjacent to the Golgi stacks.

(F) In BFA treated Arabidopsis plants, VPS28 labels the core of the BFA-compartment, confirming TGN localization of this ESCRT-I subunit. G = Golgi; T = TGN; M = MVB/LE; B = BFA compartment; Scale bars = 200 nm.

Figure 6

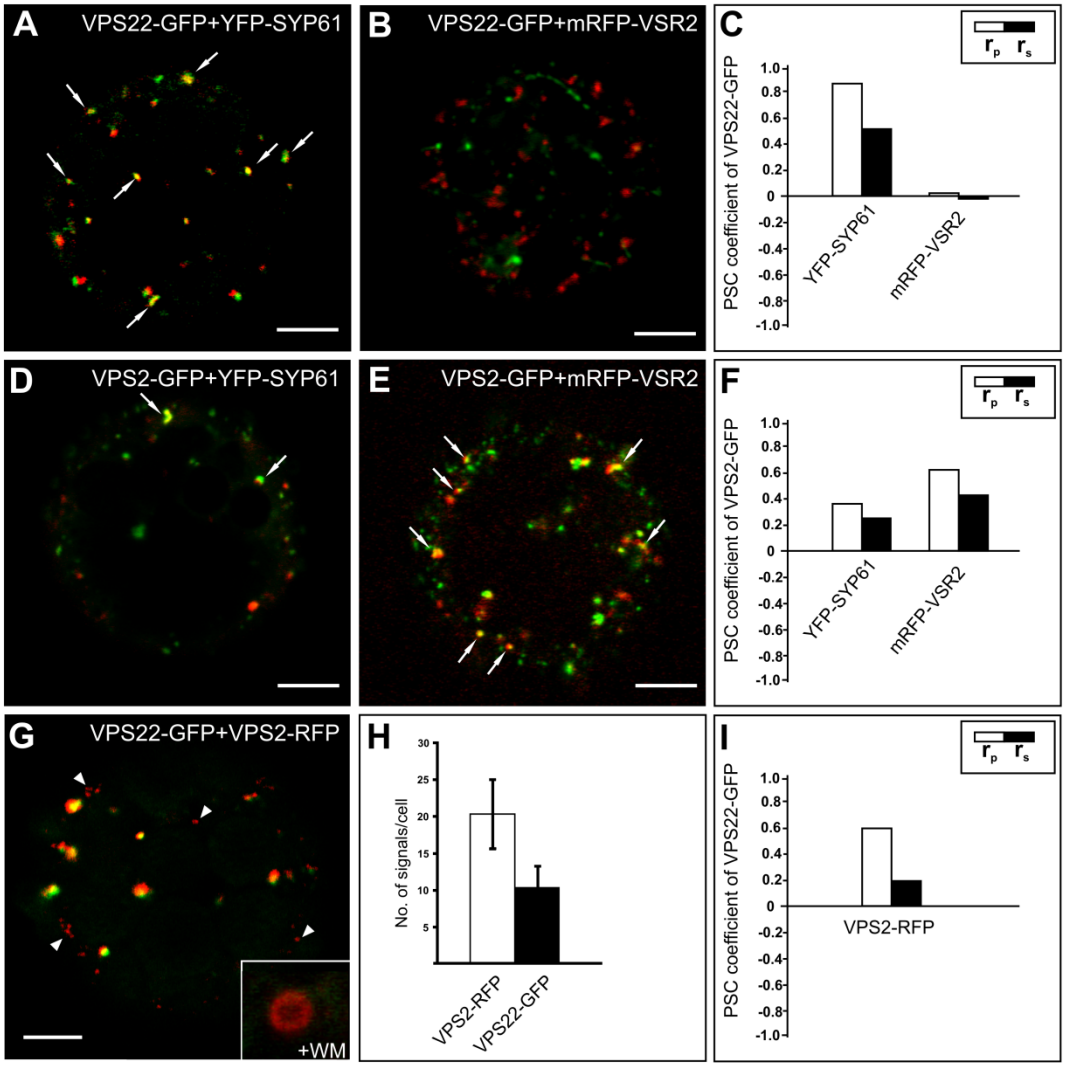

Figure 6. Gradual distribution of the ESCRT-II component VPS22 and the ESCRT-III component VPS2. Tobacco mesophyll protoplasts were transfected with plasmids encoding for fluorescent markers/reporters as indicated below. Proteins were expressed for 18-24 h prior to CLSM analysis. White arrows indicate colocalization. For quantification the Pearson and Spearman correlation (PSC) coefficients (r_p and r_s) were calculated after analysis of at least 10 individual protoplasts and a minimum of 200 signals. The level of colocalization ranges from +1 for perfect correlation to -1 for negative correlation. For the corresponding scatterplots see Supplemental Figure 2 online. **(A)** Coexpression of VPS22-GFP and the TGN/EE marker YFP-SYP61. **(B)** VPS22-GFP was coexpressed with the MVB/LE marker mRFP-VSR2. **(C)** Quantification of VPS22-GFP colocalization with TGN/EE (YFP-SYP61) and MVB/LE (mRFP-VSR2) marker. **(D)** Coexpression of VPS2-GFP and YFP-SYP61. **(E)** VPS2-GFP and mRFP-VSR2 were coexpressed. **(F)** Quantification of VPS2-GFP colocalization with TGN/EE and MVB/LE marker. **(G)** Coexpression of VPS22-GFP and VPS2-RFP. Some VPS2-RFP signals do not colocalize (white arrowheads). Only VPS2-RFP signals localize to wortmannin (WM)-sensitive compartments as indicated by the magnified ring-like structure. **(H)** Quantitative comparison of the number of VPS2-RFP and VPS22-GFP signals. **(I)** Quantification of VPS22-GFP and VPS2-RFP colocalization. Scale bars = 5 µm.

Figure 7

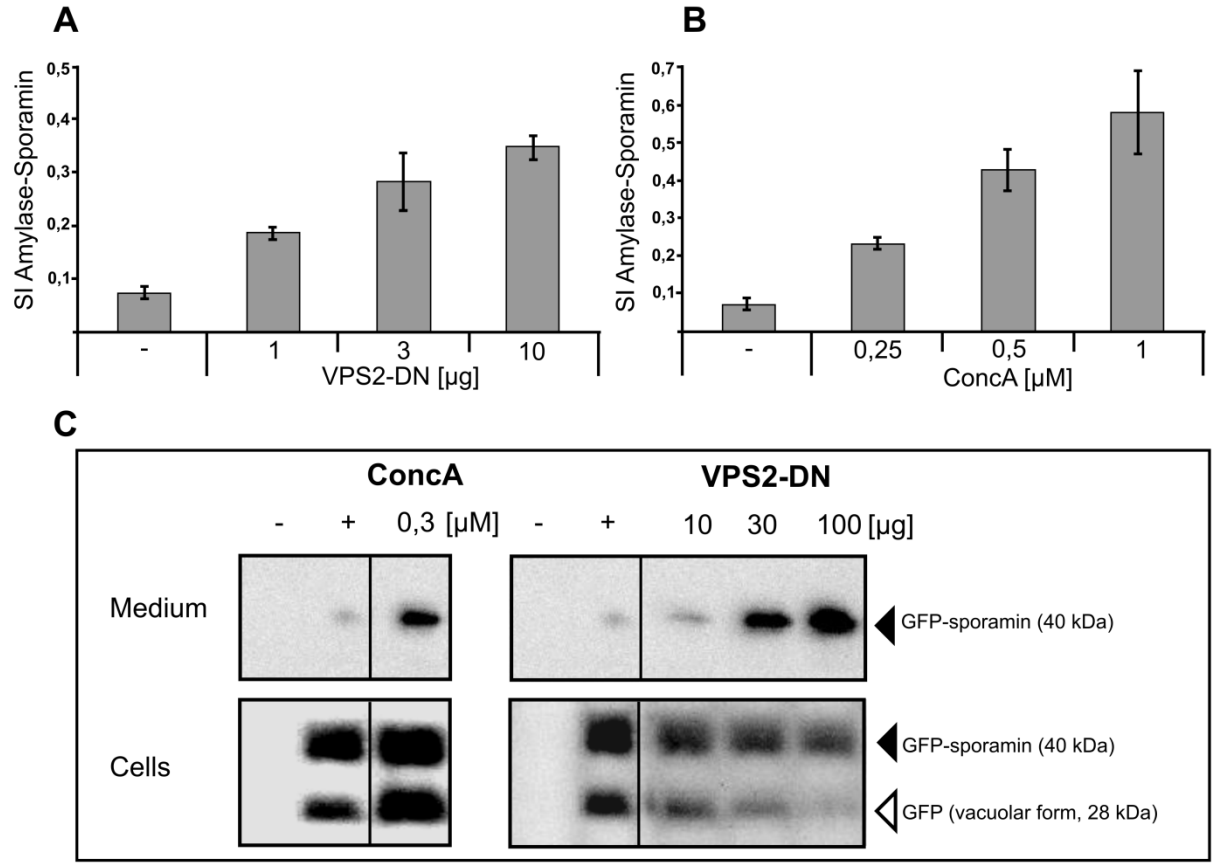

Figure 7. Effects of ConcA and the ESCRT-III mutant VPS2-DN on vacuolar transport. Tobacco mesophyll protoplasts were transfected with plasmids encoding for reporters/effectors as indicated below. Proteins were expressed for 18-24 h prior to analysis. For analyzing vacuolar transport the α-amylase derivative amylase-sporamin (amy-spo) was used. The secretion index (SI) is calculated as the ratio of the activity of amy-spo secreted to the culture medium and the activity of amy-spo within the cells. **(A)** VPS2-DN causes a dosage-dependent missorting of the vacuolar reporter amy-spo and subsequent secretion into the culture medium. **(B)** Treatment with increasing concentrations of ConcA leads to the same effect than described in (C) but stronger (ten-fold increase of the SI). **(C)** Western blot analysis of protein transport after transient expression of the soluble vacuolar reporter GFP-sporamin in the presence of ConcA (left panel) or coexpression with VPS2-DN (right panel), using GFP-antibodies for immuno-detection of the reporter. (-) mock-transfection, (+) positive control of GFP-sporamin expression without effector.

Figure 8

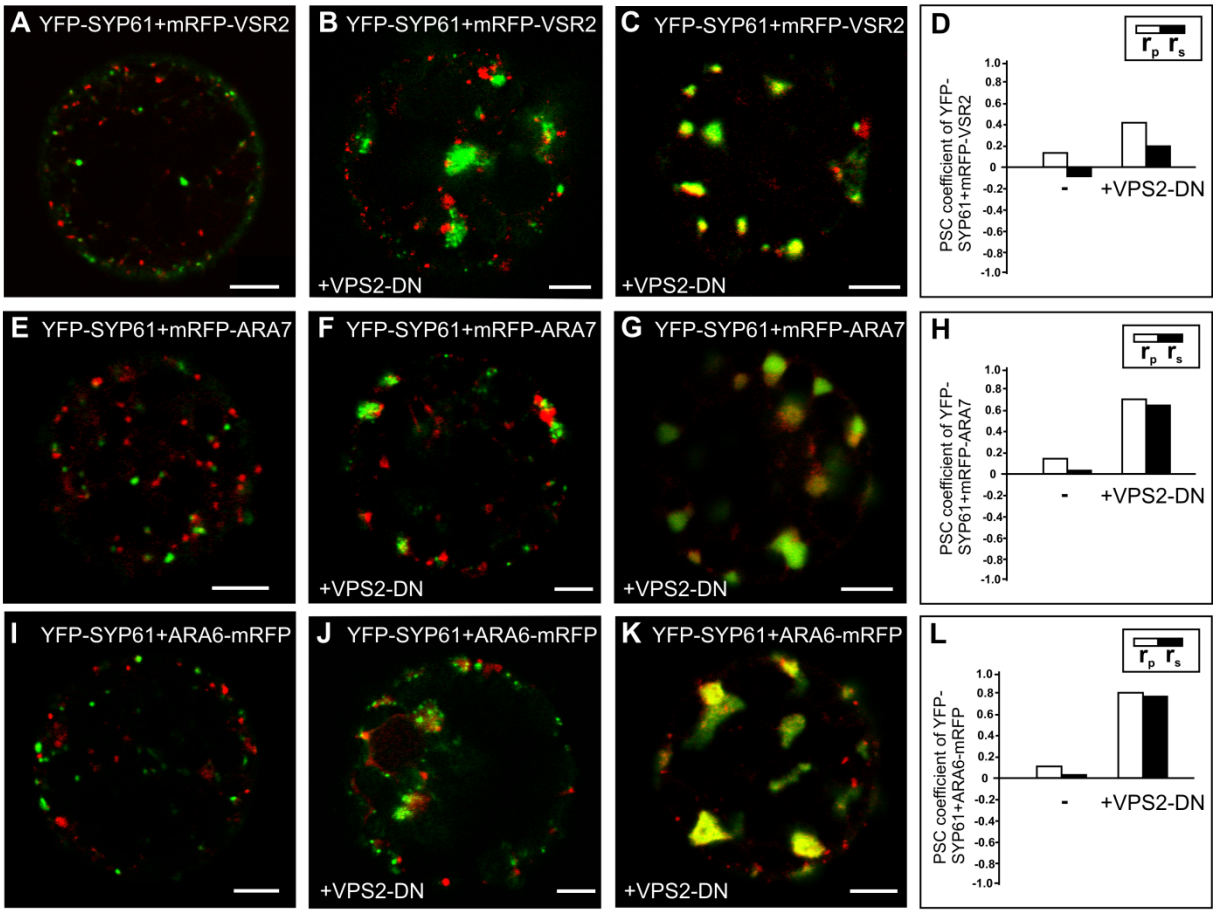

Figure 8. VPS2-DN causes marker proteins for TGN/EE and MVB/LE to colocalize. Tobacco mesophyll protoplasts were transfected with plasmids encoding for fluorescent markers/reporters as indicated below. Proteins were expressed for 18 h prior to CLSM analysis. For quantification, the Pearson and Spearman correlation (PSC) coefficients (r_p and r_s) were calculated after analysis of at least 10 individual protoplasts and a minimum of 200 signals. The level of colocalization ranges from +1 for perfect correlation to -1 for negative correlation. For the corresponding scatterplots see supplemental figure 5. **(A)** Coexpression of TGN/EE and MVB/LE markers YFP-SYP61 and mRFP-VSR2 18 h after transfection. **(B)** Effect of VPS2-DN on the distribution of TGN/EE and MVB/LE marker 14 h after transfection. **(C)** Analysis 18 h after transfection: VPS2-DN causes a change in the signal pattern of the marker proteins. The signals accumulate in bigger but fewer structures. **(D)** Quantification of the marker colocalization. The r_p and r_s values increase when VPS2-DN is expressed. **(E)** Coexpression of TGN/EE and MVB/LE markers YFP-SYP61 and mRFP-ARA7 18 h after transfection. **(F)** Effect of the VPS2-DN coexpression with YFP-SYP61 and mRFP-ARA7 14 h post transfection. **(G)** When expressed for 18 h, VPS2-DN increases colocalization of YFP-SYP61 and mRFP-ARA7. As observed in (C) the signals change structurally. **(H)** Quantification revealed higher r_p and r_s values for the marker proteins when VPS2-DN was expressed. **(I)** to **(L)** An experiment as described in (E) to (H) was carried out, except ARA6-mRFP was used as MVB/LE marker. Here, the highest increase of r_p and r_s values was found (L). Scale bars = 5 µm.

Figure 9

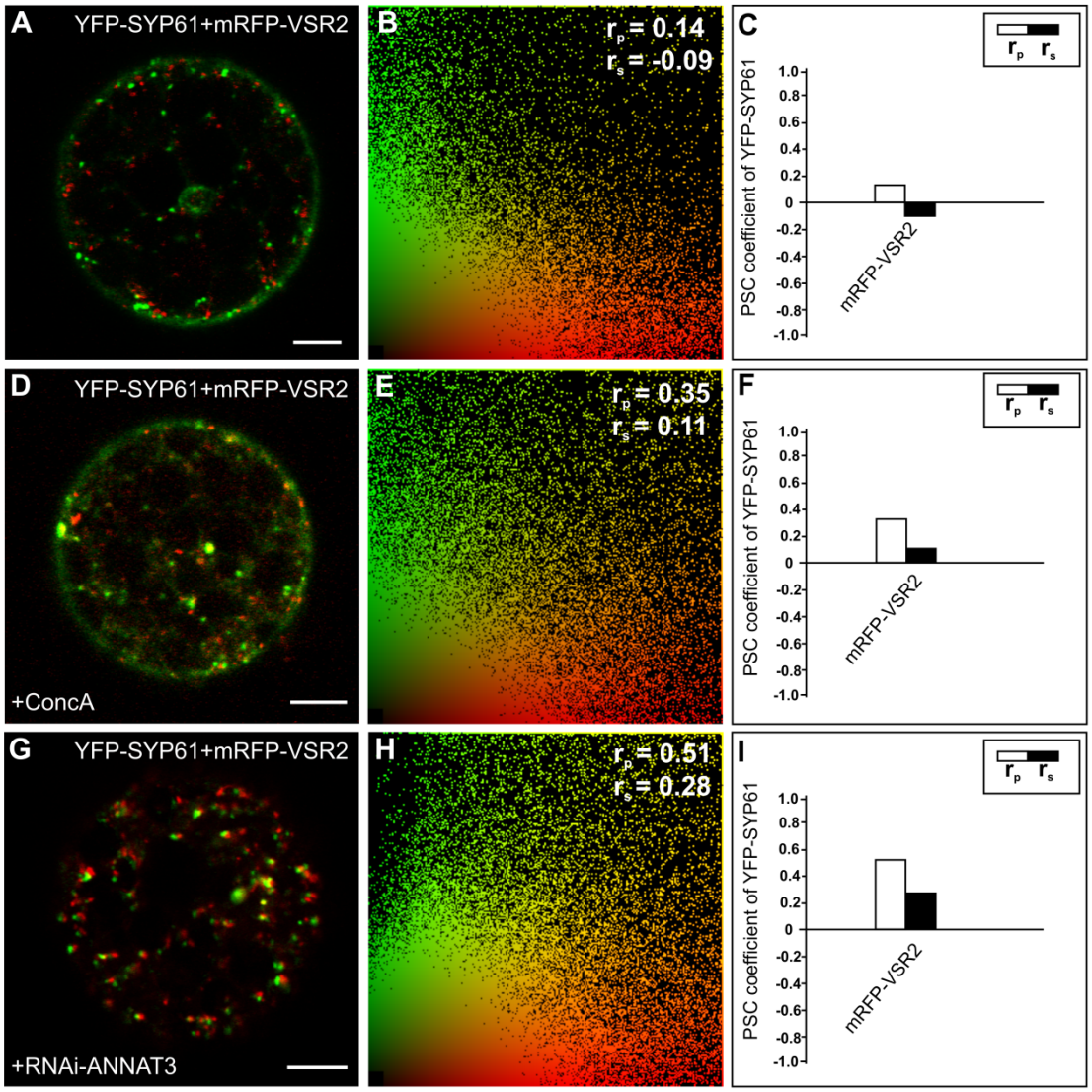

Figure 9. RNAi knockdown of the annexin ANNAT3 increases colocalization of TGN/EE and MVB/LE marker proteins. Tobacco mesophyll protoplasts were transfected with plasmids encoding for fluorescent markers/reporters as indicated below. Proteins were expressed for 18-24 h prior to CLSM analysis. For quantification, the Pearson and Spearman correlation (PSC) coefficients (r_p and r_s) were calculated after analysis of at least 10 individual protoplasts and a minimum of 200 signals. The level of colocalization ranges from +1 for perfect correlation to -1 for negative correlation. **(A)** Tobacco protoplast expressing YFP-SYP61 as TGN/EE marker and mRFP-VSR2 as MVB/LE marker. **(B)** The PSC values for YFP-SYP61 and mRFP-VSR2 were calculated and pictured in a scatterplot. **(C)** Bar chart to illustrate the PSC coefficients from (B). **(D)** Protoplasts from (A) were incubated for 1 h in the presence of 1 µM ConcA **(E)** Calculated r_p and r_s values from (D) are pictured in a scatterplot.**(F)** Bar chart to illustrate the PSC coefficients from (E).**(G)** RNAi-based knockdown of ANNAT3 by cotransfection of plasmid DNA encoding for RNAi-ANNAT3 and the markers YFP-SYP61 and mRFP-VSR2.**(H)** Calculated PSC values from (G) are pictured in a scatterplot. The r_p and r_s values are considerably higher compared to the control (B). (I) Bar chart to illustrate the PSC coefficients from (E). Scale bars = 5 µm.

Figure 10

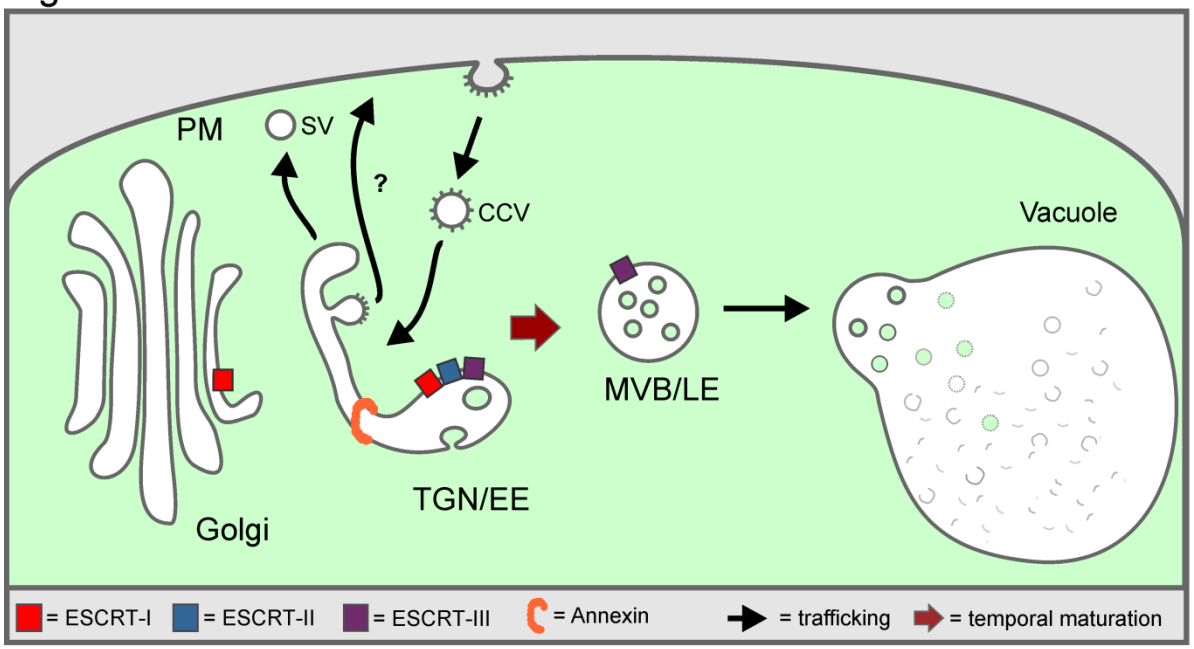

Figure 10. Model illustrating TGN to MVB maturation. According to this model, the TGN is continually formed and released from the Golgi stack. It also functions as an EE and receives incoming cargo from the plasma membrane (PM) via clathrin coated vesicles (CCVs). As it differentiates, the TGN probably subdivides into domains where secretory vesicles (SV) are released to the PM, into domains releasing CCVs for recycling to the PM (recycling endosomes) and into a domain which matures into a multivesicular body (MVB). Participating in the latter process, as indicated, are the ESCRT complexes I, II and III, as well as annexin. As in mammalian cells, we postulate that *post*-TGN trafficking of soluble proteins to the lytic compartment (vacuole) occurs receptor-independent and is accompanied by a gradual transformation of part of the EE (TGN) into the LE (MVB) which ultimately fuses with the vacuole membrane.

Supplemental data. Scheuring et al. (2011). Plant Cell 10.1105/tpc.111.086918

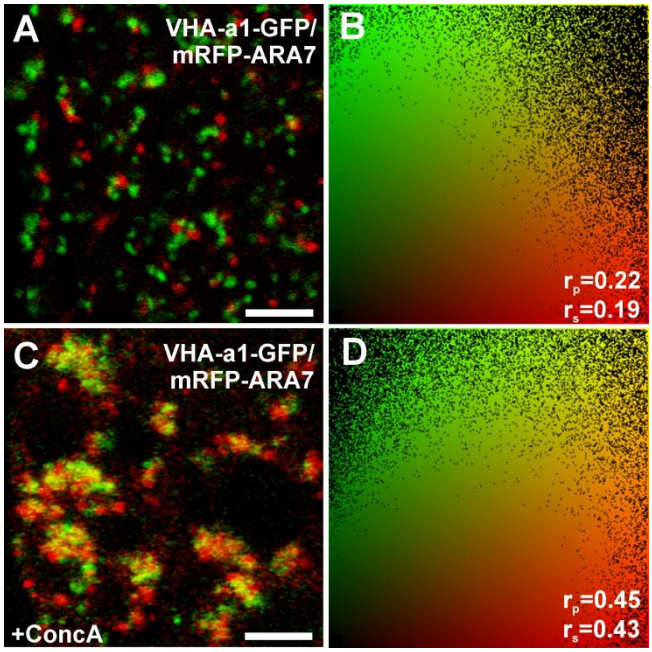

Supplemental Figure 1. ConcA affects the distribution of marker proteins for TGN/EE and MVB/LE. In order to quantify colocalization results, we have calculated the linear Pearson (r_p) and the non-linear Spearman´s rank (r_s) correlation coefficient (PSC) for the pixels representing the fluorescence signals in both channels. Levels of colocalization can range from +1 for positive correlation to -1 for negative correlation (French et al., 2008). The fluorescence values of pixels across the two channels were additionally depicted in an intensity scatter plot. At least 20 cells and a minimum of 400 signals were analyzed. **(A)** *Arabidopsis* seedlings expressing the TGN/EE marker VHA-a1-GFP and the MVB/LE marker mRFP-ARA7. **(B)** Intensities of fluorescent signals from (A), representing VHA-a1-GFP (green) and mRFP-ARA7 (red), are depicted in a scatter plot. The calculated PSC values are given in the lower right corner. The two signals do not colocalize. **(C)** Upon ConcA treatment the TGN/EE marker VHA-a1-GFP and the MVB/LE marker mRFP ARA7 were in closer proximity, showing an increased colocalization. **(D)** The values for the PSC coefficients of panel (C) are the double for both r_p and r_s respect to the untreated cells. Scale bars = 5 µm.

Supplemental data. Scheuring et al. (2011). Plant Cell 10.1105/tpc.111.086918

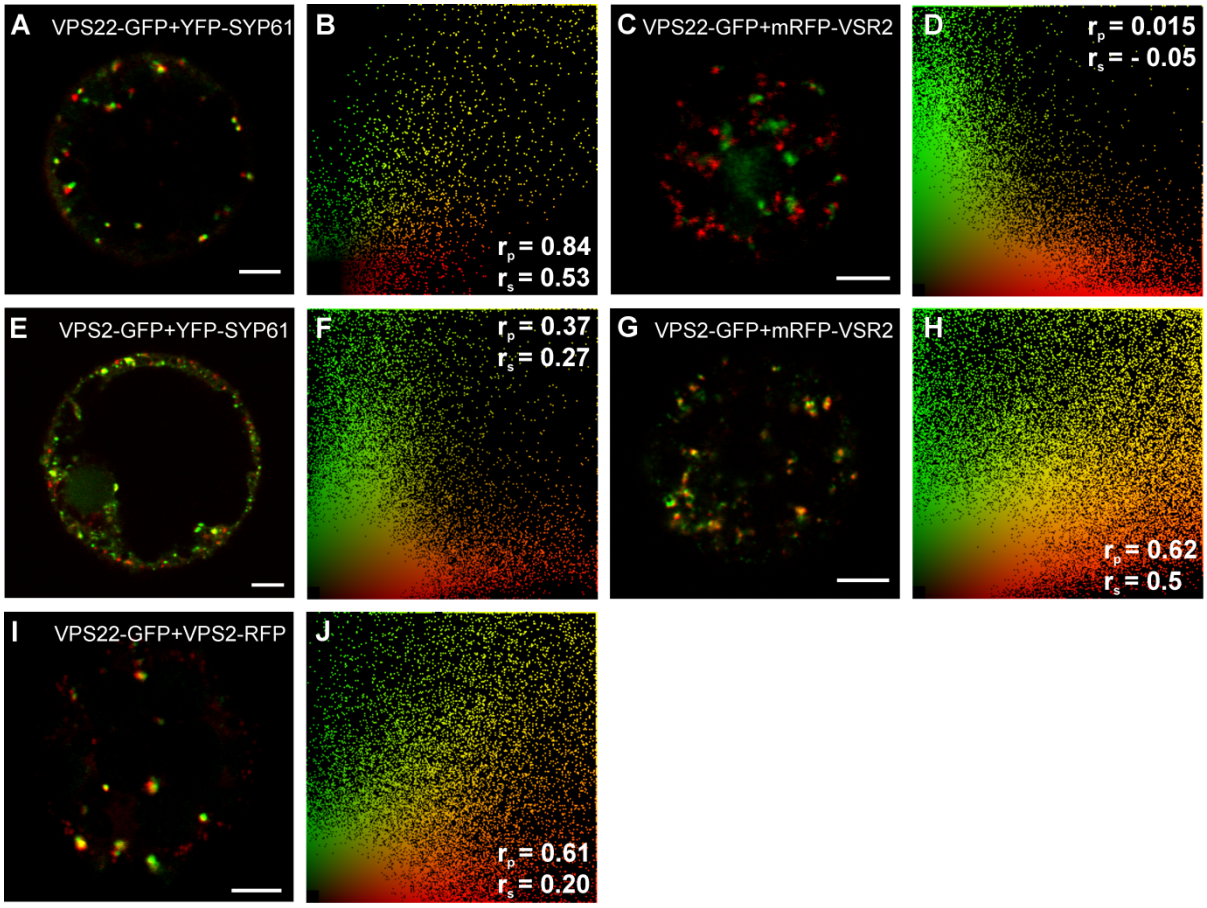

Supplemental Figure 2. Differential localization of the ESCRT-components VPS22-GFP and VPS2-GFP. Tobacco mesophyll protoplasts were transfected with plasmids encoding for fluorescent markers/reporters as indicated below. Fluorescent proteins were expressed for 18 h prior to CLSM analysis. At least 10 protoplasts and a minimum of 200 signals were used for the quantification as described in supplemental figure 1. **(A)** Coexpression of the TGN/EE marker YFP-SYP61 (red) and VPS22-GFP (green). **(B)** PSC coefficients and corresponding scatter plot of (A). **(C)** VPS22-GFP coexpressed with mRFP-VSR2. **(D)** PSC coefficients and corresponding scatter plot of (C). **(E)** Coexpression of the TGN/EE marker YFP-SYP61 (red) and VPS2-GFP (green). **(F)** PSC coefficients and scatter plot of (E). **(G)** VPS2-GFP coexpressed with the MVB/LE marker mRFP-VSR2. **(H)** Scatter plot and PSC coefficients of (G). **(I)** Coexpression of VPS22-GFP and VPS2-RFP. **(J)** Scatter plot and PSC coefficients of (I). Scale bars = 5 µm.

Supplemental data. Scheuring et al. (2011). Plant Cell 10.1105/tpc.111.086918

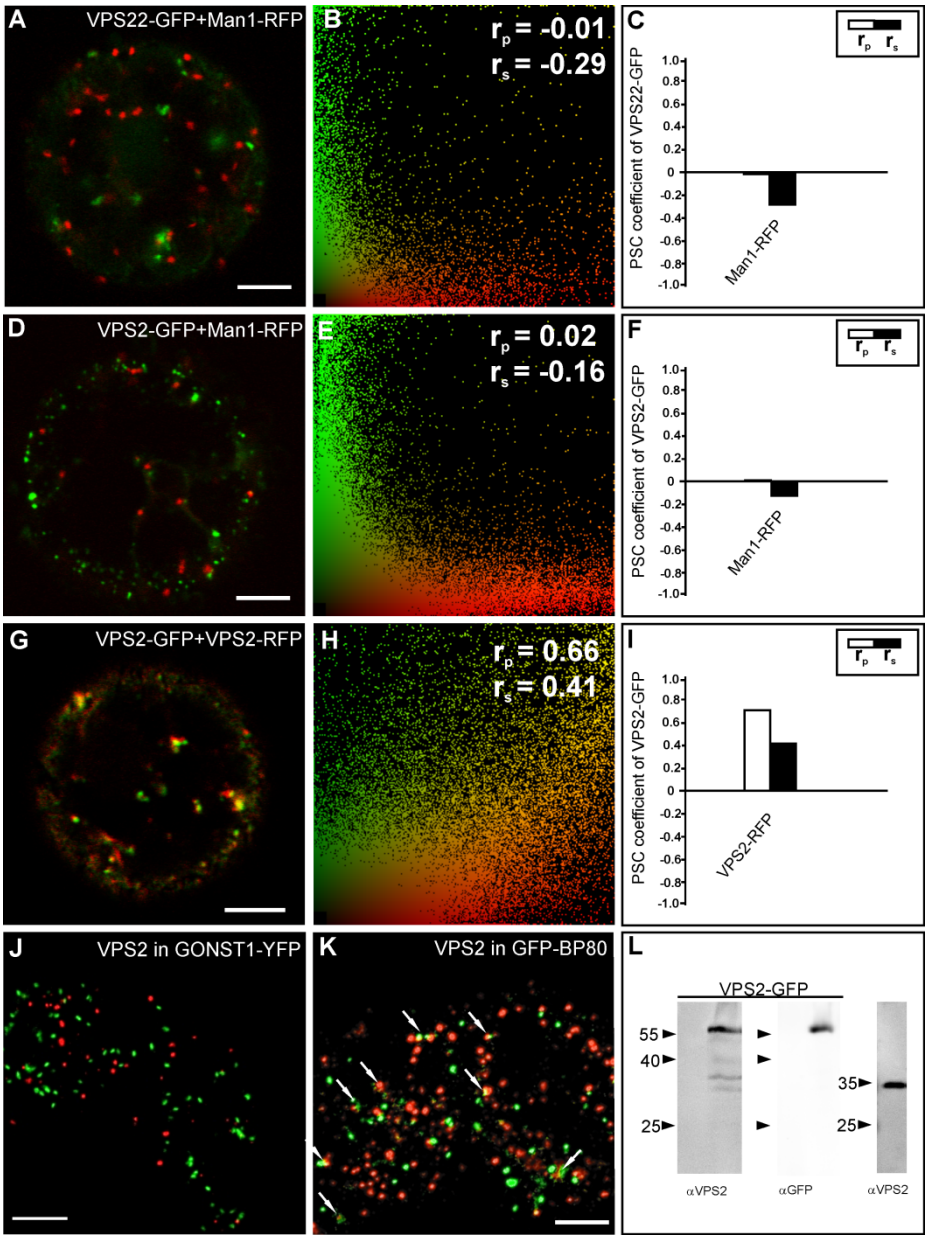

Supplemental Figure 3. VPS22-GFP and VPS2-GFP do not colocalize with Golgi markers but VPS2 is found at the MVB/LE. Tobacco mesophyll protoplasts were transfected with plasmids encoding for fluorescent markers/reporters as indicated below. Fluorescent proteins were expressed for 18 h prior to CLSM analysis. At least 10 protoplasts and a minimum of 200 signals were used for the quantification as described in supplemental figure 1. For immunolabeling the VPS2 antibody was used in a 1:200 dilution. White arrows indicate colocalization. **(A)** Coexpression of the Golgi marker Man1-RFP and VPS22-GFP. **(B)** PSC coefficients and corresponding scatter plot of (A). **(C)** Bar chart of the r_p and r_s values from (B). **(D)** VPS2 coexpressed with Man1-RFP. **(E)** Scatter plot and PSC coefficients of (D). **(F)** Bar chart of the r_p and r_s values from (E). **(G)** To rule out different behavior of fluorescent protein tags VPS2-RFP and VPS22-GFP were coexpressed. **(H)** Quantification of (G) reveals high values of the PSC coefficients. **(I)** Bar chart of (H). **(J)** Immunolabeling of VPS2 (red) in BY2 cells stably expressing the Golgi marker GONST1-YFP (green). **(K)** Immunolabeling of VPS2 (red) in BY2 cells stably expressing the MVB/LE marker GFP-BP80 (green). **(L)** Immunodetection of endogenous VPS2 in total extracts from wild-type BY2 cells (right side). The antibody cross-reacts with a protein of around 30 kDa. VPS2-GFP could also be detected with a GFP antibody in Immunoblot analysis (left side). Scale bars = 5 µm.

Supplemental data. Scheuring et al. (2011). Plant Cell 10.1105/tpc.111.086918

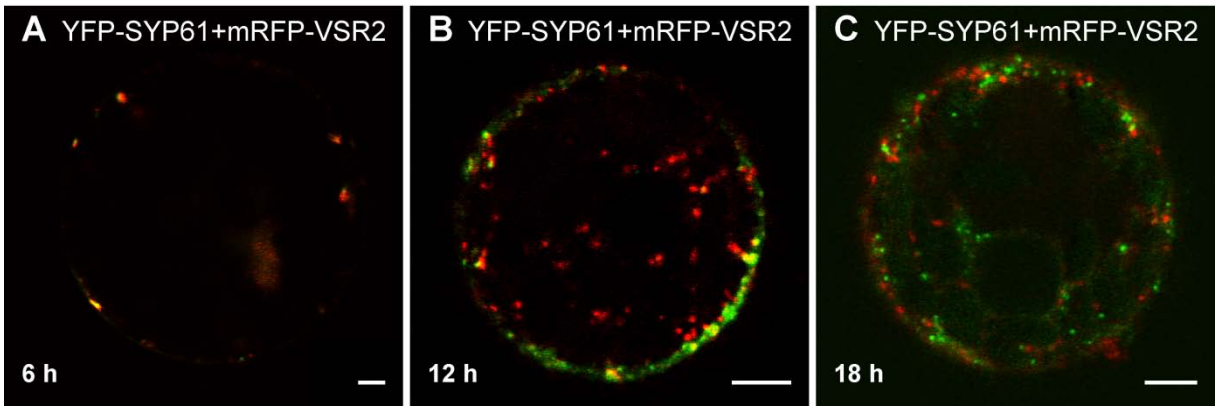

Supplemental Figure 4. Time course to study the temporal distribution of YFP-SYP61 and mRFP-VSR2 as TGN/EE and MVB/LE markers. Tobacco mesophyll protoplasts were transfected with plasmids encoding for fluorescent markers/reporters as indicated below. Fluorescent proteins were expressed for 6 to 18 h prior to CLSM analysis. **(A)** to **(C)** YFP-SYP61 (green) and mRFP-VSR2 (red) are coexpressed as markers for the TGN/EE and MVB/LE and their localization was analyzed in a time dependent manner. **(A)** After 6h signals were detectable. **(B)** The signal strength increases 12 h post transfection. **(C)** Typical distribution of TGN/EE and MVB/LE markers YFP-SYP61 and mRFP-VSR2 18 h after transfection. Scale bars = 5 µm.

Supplemental data. Scheuring et al. (2011). Plant Cell 10.1105/tpc.111.086918

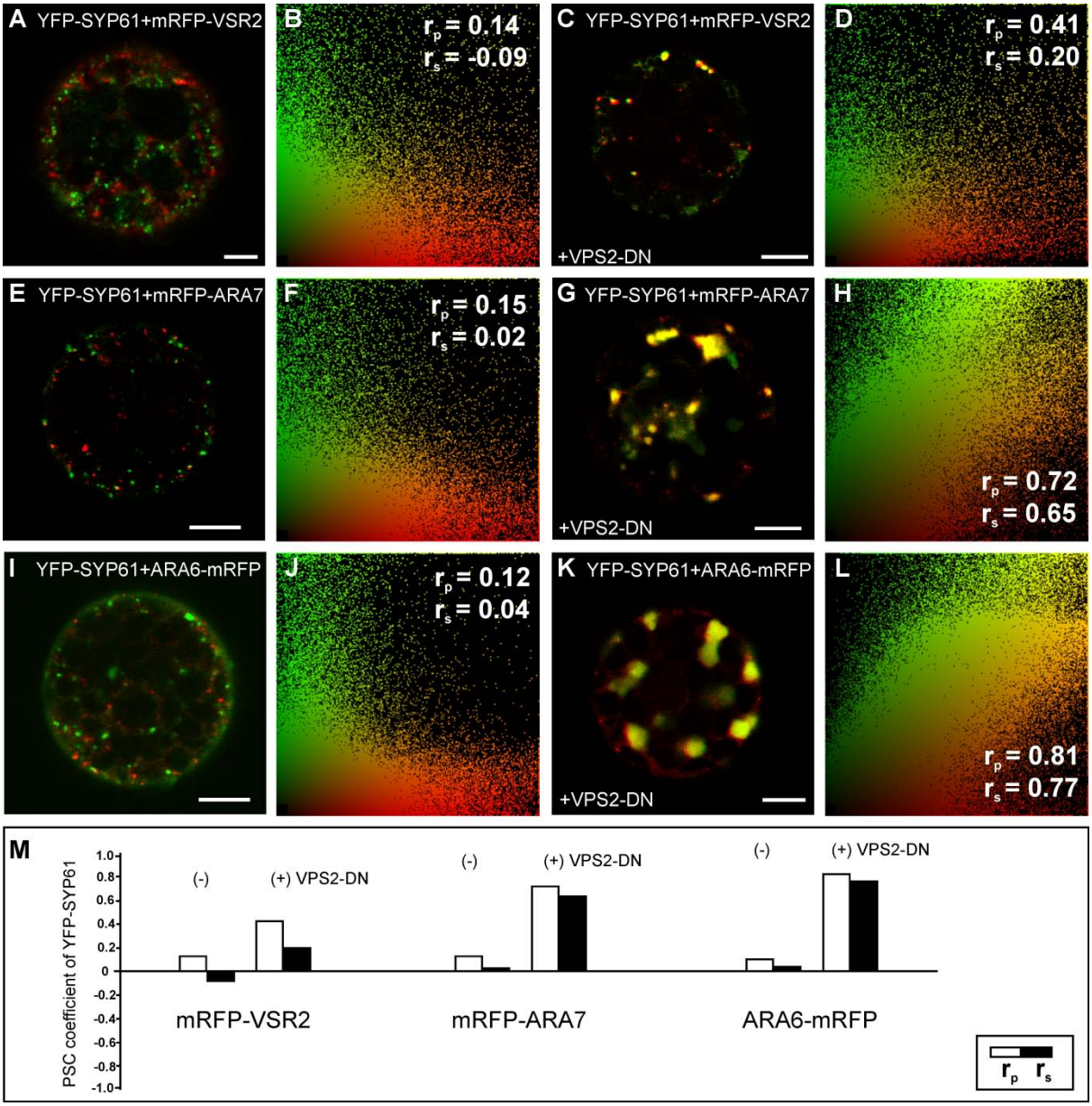

Supplemental Figure 5. Expression of VPS2-DN affects the distribution of markers for the TGN/EE and MVB/LE. Tobacco mesophyll protoplasts were transfected with plasmids encoding for fluorescent markers/reporters as indicated below. Fluorescent proteins were expressed for 18 h prior to CLSM analysis. At least 10 protoplasts and a minimum of 200 signals were used for the quantification as described in supplemental figure 1. **(A)** Coexpression of TGN/EE and MVB/LE markers YFP-SYP61 (green) and mRFP-VSR2 (red). **(B)** Scatter plot and PSC coefficients of (A). **(C)** Changed distribution of TGN/EE marker and MVB/LE marker when VPS2-DN is coexpressed. **(D)** Scatter plot and PSC coefficients of (C). **(E)** Coexpression of the TGN/EE marker YFP-SYP61 (green) and the MVB/LE marker mRFP-ARA7 (red). **(F)** Scatter plot and PSC coefficients of (E). **(G)** Changed distribution of TGN/EE marker and MVB/LE marker when VPS2-DN is coexpressed. **(H)** Scatter plot and PSC coefficients of (G). **(I)** to **(L)** The same experiment as described in (E) to (H) was carried out, except ARA6-mRFP was used as a marker for the MVB/LE. **(M)** Comparison of all obtained PSC coefficients. Scale bars = 5 µm.

Supplemental data. Scheuring et al. (2011). Plant Cell 10.1105/tpc.111.086918

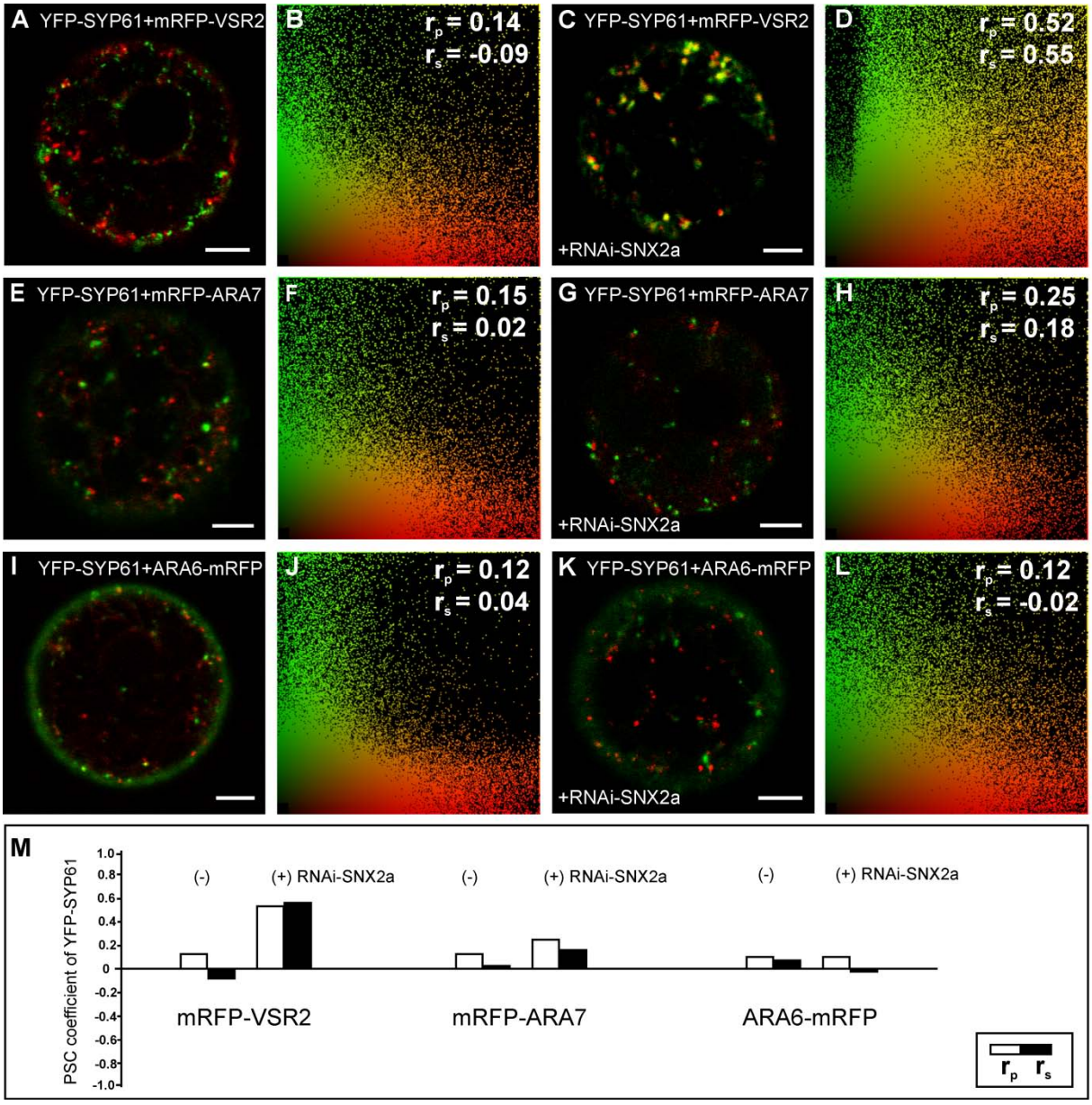

Supplemental Figure 6. RNAi-SNX2a prevents arrival of mRFP-VSR2 at the MVB/LE but does not affect vacuolar transport. Tobacco mesophyll protoplasts were transfected with plasmids encoding for fluorescent markers/reporters as indicated below. Fluorescent proteins were expressed for 18 h prior to CLSM analysis. At least 10 protoplasts and a minimum of 200 signals were used for the quantification as described in supplemental figure 1. **(A)** Coexpression of TGN/EE and MVB/LE markers YFP-SYP61 (green) and mRFP-VSR2 (red). **(B)** Scatter plot and PSC coefficients of (A). **(C)** Changed distribution of TGN/EE marker and MVB/LE marker when RNAi-SNX2a is coexpressed. **(D)** Scatter plot and PSC coefficients of (C). **(E)** Coexpression of the TGN/EE marker YFP-SYP61 (green) and the MVB/LE marker mRFP-ARA7 (red). **(F)** Scatter plot and PSC coefficients of (E). **(G)** Signal distribution of TGN/EE marker and MVB/LE marker when RNAI-SNX2a is coexpressed. **(H)** Scatter plot and PSC coefficients of (G). **(I)** to **(L)** The same experiment as described in (E) to (H) was carried out, except ARA6-mRFP was used as a marker for the MVB/LE. **(M)** Comparison of all obtained PSC coefficients. Scale bars = 5 µm.

Supplemental data. Scheuring et al. (2011). Plant Cell 10.1105/tpc.111.086918

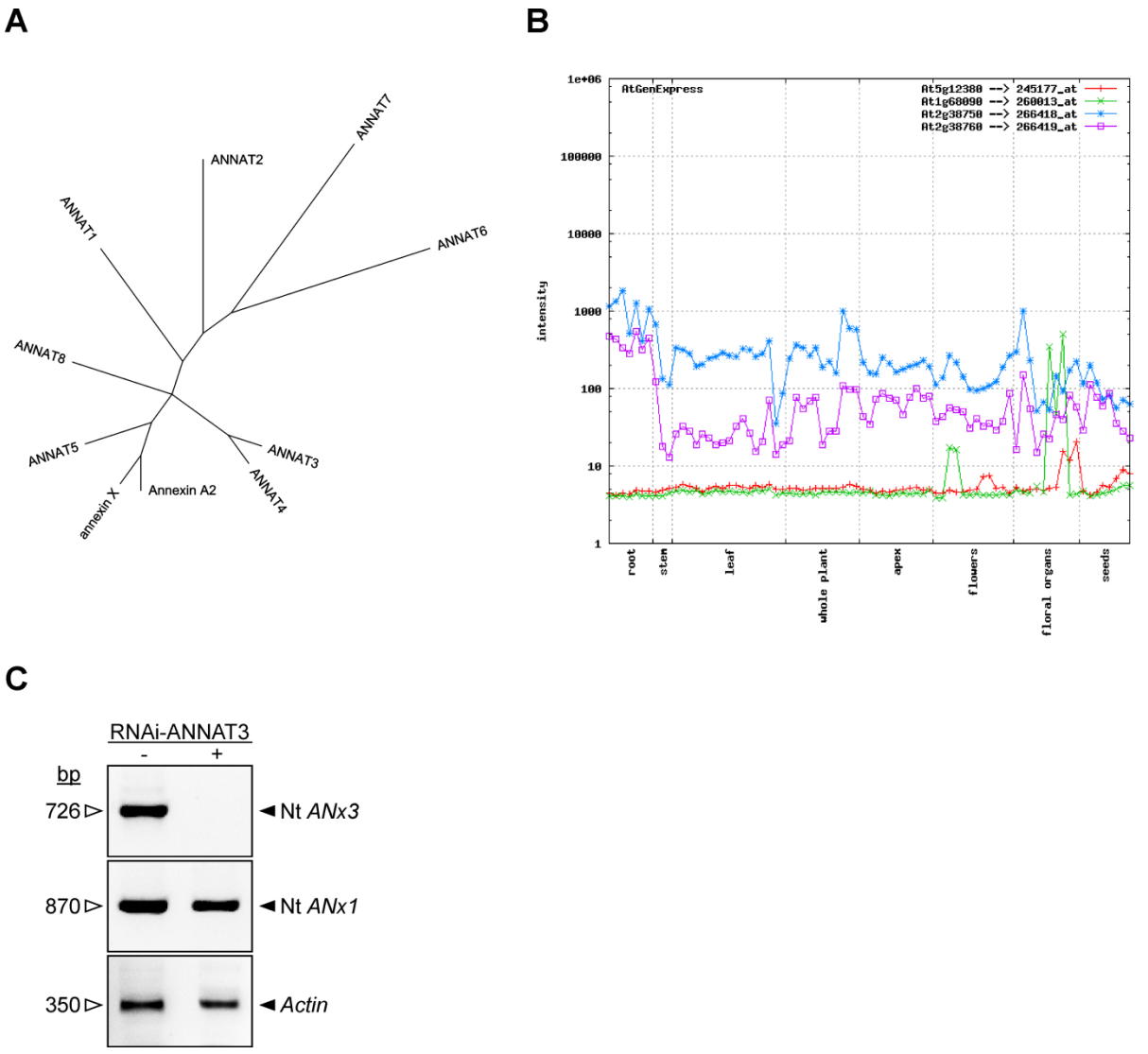

Supplemental Figure 7. Relationship, expression and knockdown of plant annexins.
(A) Neighbour-Joining Tree based on Geneious-Alignment of the *Arabidopsis* Annexins ANNAT1-8 with human Annexin A2 (P07355) and *Drosophila* Annexin X (AAF45380), Cost matrix: Blosum62, Gap open penalty: 12, Gap extension penalty: 3. **(B)** AtGenExpress-Development Data for ANNAT3 (At2g38760), 4 (At2g38750), 5 (At1g68090) and 8 (At5g12380)**. (C)** Analysis of the RNAi-mediated knockdown of *Nicotiana tabacum* Annexin 3 (Nt *ANx3*). Tobacco mesophyll protoplasts were cotransfected with plasmids encoding for RNAi-ANNAT3 and cytosolic GFP (cytGFP), allowing for fluorescence-assisted cell sorting. This way, we took advantage of the high cotransfection efficiency of elektrotransformation (93.6 ± 3.5 % in cotransfection with two plasmids; Niemes et al., 2010a), to monitor for cells expressing the RNAi construct. Positively sorted cells were subjected to RT-PCR using primers specific for endogenous Nt *ANx3*. Non-silenced control cells (-) expressing only cytGFP reveal an amplification product of the expected size, which is absent in the RNAi background (+). The expression of another tobacco annexin, Nt *ANx1*, is not affected by RNAi-ANNAT3 showing specificity of the knockdown. A fragment amplified from the actin coding sequence serves as an internal control.

Supplemental data. Scheuring et al. (2011). Plant Cell 10.1105/tpc.111.086918

Supplemental Table 1: Primers used for cloning

Oligonucleotide	Sequence (5' – 3' direction)	Recipient vector
VPS2-GFP.FOR	ACCACCGCTAGCATGATGAATTCAATC	pSN09
VPS2-GFP.REV	ACCACCGCGGCCGCGCATTTTTCTAAGGTT	pSN09
VPS22-GFP.FOR	TGGAGCTAGCTCATTTAAGTATCAGATC	pSN09
VPS22-GFP.REV	ATAAGCGGCCGCAAGATGCGACGACGA	pSN09
VPS2-RFP.FOR	ACCACCAGATCTATGATGAATTCAATC	pBP30
VPS2-RFP.REV	ACCACCTCTAGAGCGCATTTTTCTAAG	pBP30
VPS2-DN.FOR	ACCACCATCGATGATGAATTCAATC	pSar1
VPS2-DN.REV	ACCACCTCTAGATTATATACCTCCACTGTC	pSar1
ANNAT3-WT.FOR	ATTCTCGCTAGCATGGCCACCATTAGA	pSN13
ANNAT3-WT.REV	TCAATAGTCGACTCAGATCAGCATCTC	pSN13
mRFP-ARA7.FOR	ATAAGATCTATGGCCTCCTCCGAGGAC	pJHA212
mRFP-ARA7.REV	ATAAGATCTGGATCCCTAAGCACAACAAG	pJHA212
VPS28.FOR	CTGAAAGAATTCCGTCAAGTTATGGAAT	pGEX-4T3
VPS28.REV	GTGGCAGTCGACTTAATTACCAGCATT	pGEX-4T3
VPS2.FOR	CATGATGAATTCAATCTTCGG	pGEX-4T3
VPS2.REV	ACAGGAGTCGACTCACATTTTTCTAAG	pGEX-4T3
Nt *ANx1*.FOR	TGTTCCGGCAGAAGTTCCTT	-
Nt *ANx1*.REV	ACCTCCACGAAGTAGTGCTC	-
Nt *ANx3*.FOR	CCAACATCTGTTCCAGAACC	-
Nt *ANx3*.REV	AGCAATTGCACGGTCCAATG	-
Actin.FOR	ATTCAGATGCCCAGAAGTCTT	-
Actin.REV	TCTGTGAACGATTCCTGGACCTG	-

9.2 Ubiquitin initiates sorting of Golgi and plasma membrane proteins into the vacuolar degradation pathway

David Scheuring*, **Fabian Künzl***, Corrado Viotti, Melody San Wan Yan, Liwen Jiang, Swen Schellmann, David G. Robinson, and Peter Pimpl

(*Equally contributing first authors)

BMC Plant Biology, Sept. 2012, Vol. 12:164
(http://www.biomedcentral.com/1471-2229/12/164)

BMC Plant Biology

RESEARCH ARTICLE Open Access

Ubiquitin initiates sorting of Golgi and plasma membrane proteins into the vacuolar degradation pathway

David Scheuring[2†], Fabian Künzl[1†], Corrado Viotti[2,3], Melody San Wan Yan[4], Liwen Jiang[4], Swen Schellmann[5], David G Robinson[2] and Peter Pimpl[1,2*]

Abstract

Background: In yeast and mammals, many plasma membrane (PM) proteins destined for degradation are tagged with ubiquitin. These ubiquitinated proteins are internalized into clathrin-coated vesicles and are transported to early endosomal compartments. There, ubiquitinated proteins are sorted by the endosomal sorting complex required for transport (ESCRT) machinery into the intraluminal vesicles of multivesicular endosomes. Degradation of these proteins occurs after endosomes fuse with lysosomes/lytic vacuoles to release their content into the lumen. In plants, some PM proteins, which cycle between the PM and endosomal compartments, have been found to be ubiquitinated, but it is unclear whether ubiquitin is sufficient to mediate internalization and thus acts as a primary sorting signal for the endocytic pathway. To test whether plants use ubiquitin as a signal for the degradation of membrane proteins, we have translationally fused ubiquitin to different fluorescent reporters for the plasma membrane and analyzed their transport.

Results: Ubiquitin-tagged PM reporters localized to endosomes and to the lumen of the lytic vacuole in tobacco mesophyll protoplasts and in tobacco epidermal cells. The internalization of these reporters was significantly reduced if clathrin-mediated endocytosis was inhibited by the coexpression of a mutant of the clathrin heavy chain, the clathrin hub. Surprisingly, a ubiquitin-tagged reporter for the Golgi was also transported into the lumen of the vacuole. Vacuolar delivery of the reporters was abolished upon inhibition of the ESCRT machinery, indicating that the vacuolar delivery of these reporters occurs via the endocytic transport route.

Conclusions: Ubiquitin acts as a sorting signal at different compartments in the endomembrane system to target membrane proteins into the vacuolar degradation pathway: If displayed at the PM, ubiquitin triggers internalization of PM reporters into the endocytic transport route, but it also mediates vacuolar delivery if displayed at the Golgi. In both cases, ubiquitin-tagged proteins travel via early endosomes and multivesicular bodies to the lytic vacuole. This suggests that vacuolar degradation of ubiquitinated proteins is not restricted to PM proteins but might also facilitate the turnover of membrane proteins in the early secretory pathway.

* Correspondence: peter.pimpl@zmbp.uni-tuebingen.de
†Equal contributors
[1]Department of Developmental Genetics, Center for Plant Molecular Biology (ZMBP), University of Tübingen, Tübingen 72076, Germany
[2]Department of Plant Cell Biology, Centre for Organismal Studies, University of Heidelberg, Heidelberg 69120, Germany
Full list of author information is available at the end of the article

BioMed Central

© 2012 Scheuring et al.; licensee BioMed Central Ltd. This is an Open Access article distributed under the terms of the Creative Commons Attribution License (http://creativecommons.org/licenses/by/2.0), which permits unrestricted use, distribution, and reproduction in any medium, provided the original work is properly cited.

Background

The endocytic uptake of proteins and lipids is the driving force that establishes and maintains cellular polarity, but also allows for intercellular communication and facilitates interactions with the environment [1,2]. Endocytosis involves invagination and fission of vesicles at the plasma membrane (PM) and their transport to endosomes. Endocytosis in walled plant cells has been shown to exist by the use of fluorescent dyes in the early 2000s and has been confirmed by the subsequent identification of endocytic cargo molecules like the auxin efflux facilitator PINFORMED 1 (PIN1) [3] or cell surface receptors like the brassinosteroid receptor BRASSINOSTEROID INSENSITIVE 1 (BRI1) and the flagellin receptor FLAGELLIN-SENSING 2 (FLS2) [4-6].

In yeast and mammals, the uptake of certain membrane proteins from the PM requires ubiquitin as an internalization signal [7-9]. Ubiquitin is a highly conserved protein that is found in all eukaryotes ranging from unicellular organisms to mammals and higher plants [10]. Ubiquitination is one of the most common *post*-translational protein modifications being responsible for proteasomal degradation, membrane transport events, DNA repair and other mechanisms such as signaling and cell cycle control [11]. The C-terminus of ubiquitin is able to form covalent bonds with other proteins and once a single ubiquitin moiety is bound, it can be conjugated with additional ubiquitin molecules in a process called poly-ubiquitination [12,13]. Here, number and spatial orientation of added ubiquitin entities are crucial for a protein's destiny [8,14,15]. In this context, poly-ubiquitination of soluble proteins results in their cytosolic degradation by the 26S proteasome [16,17], while the attachment of a single ubiquitin monomer to membrane-bound proteins facilitates sorting into intralumenal vesicles (ILVs) of late endosomes (LEs/MVBs, multivesicular bodies) followed by lysosomal degradation [18]. However, details about the number of required ubiquitin moieties to trigger internalization at the PM are still controversially discussed [19].

In plants, FLS2 internalization at the PM is triggered by flg22, a 22 amino acid epitope of bacterial flagellin. In the presence of this elicitor, FLS2 was found to be ubiquitinated [20], but it is unclear whether this ubiquitination represents the sorting signal for its endocytic uptake. It has been shown that down-regulation of the PM-localized iron transporter IRON-REGULATED TRANSPORTER 1 (IRT1) involves multiple mono-ubiquitinations [21]. In the case of BORON TRANSPORTER 1 (BOR1), however, down-regulation requires the combined action of ubiquitin and tyrosine-based sorting signals for internalization and for endosomal sorting [22]. Very recently, ubiquitination of PIN2 was shown to be essential for its function in root gravitropism [23] and translational fusion of ubiquitin to PIN2 or to the plasma membrane ATPase PMA, which mimics constitutive ubiquitination, was shown to alter the localization and stability of these proteins [23,24]. These findings suggest that ubiquitin-dependent sorting mechanisms for PM proteins also exist in plants. However, vacuolar degradation of some integral PM proteins does not necessarily depend on ubiquitination as has been reported for the RICE SECRETORY CARRIER MEMBRANE PROTEIN 1 (OsSCAMP1) and the leucine-rich repeat receptor-like kinase AtLRR84A [25].

A common step in the vacuolar degradation pathway of membrane proteins is their sorting into ILVs of endosomes. This process is mediated by four ESCRT (endosomal sorting complex required for transport) complexes, termed ESCRT-0 to ESCRT-III [18]. ESCRT-0 but also ESCRT-I and ESCRT-II recognize and concentrate ubiquitinated cargo and recruit ESCRT-III. This complex recruits in turn ESCRT-associated proteins like the deubiquitinating enzyme Doa4/UBPY and the AAA-ATPase Vps4/SKD1 and drives the formation of the intralumenal vesicles, resulting in the formation of MVBs [18]. ESCRT homologues have been shown to exist in plants [26-31] although molecular interactions between ubiquitinated cargo and ESCRT components have not yet been demonstrated. Nonetheless, the cytokinesis-specific syntaxin KNOLLE as well as PIN1, BRI1 and the vacuolar sorting receptor BP80 all locate to the ILVs of MVBs [32-35]. Moreover, the localization of PIN1, PIN2 and the auxin influx carrier AUX1 was found to be dependent on the function of the ESCRT machinery [34]. Together, this suggests that ESCRT-mediated sorting contributes to the regulation of membrane proteins via vacuolar degradation.

However, degradation does not necessarily have to follow endocytosis, since PIN1 and BRI1 also cycle constitutively between the PM and endosomes [3,36]. The signals that mediate protein sorting into the endocytic, the recycling or the degradation pathways in plants are not yet fully understood. The analysis of sorting determinants for individual transport steps within this complex network of transport routes is further complicated by the fact that PM proteins reach the PM via the secretory pathway which merges with the endocytic route at the *trans*-Golgi network (TGN)/early endosome (EE) [35,37,38]. Hence, it is difficult to judge whether a given protein that localizes to this compartment has just been internalized or is still on its way to its primary destination. To overcome this problem and to analyze specific sorting signals for individual transport routes, we have prepared conceptually different fluorescent PM reporters. The first class of reporters is *post*-translationally inserted into the PM, which determines the internalization at the PM as the first possible transport step. These reporters are based on the observation that the 26 C-terminal residues of the *Arabidopsis* type-II ROP-GTPase AtROP10 are sufficient to cause PM attachment when fused to the C-terminus of cytosolic

GFP [39]. The respective sequence contains a 15 amino acid polybasic domain followed by a highly conserved motif. This motif consists of two glycine/cysteine pairs flanking 5–6 non-specified residues and is known as the [GC-CG] box. The *post*-translational PM recruitment is supposed to occur after S-acylation of the two cysteines [39]. The second class of reporters is based on type-I transmembrane proteins, which are delivered to the PM via the secretory pathway.

Here, we show, that ubiquitin is sufficient to target the *post*-translationally inserted PM reporter Box-GFP-Ub and the transmembrane protein reporter RFP-TMD23-Ub into the endocytic pathway. Interestingly, ubiquitin was also found to be sufficient to target the Golgi-localized transmembrane protein RFP-TMD20 into the lumen of the lytic vacuole. The vacuolar delivery of these reporters can be inhibited when a mutagenized ESCRT-associated component (AtSKD1(AQ)) is expressed. The use of reporters carrying a mutagenized derivative of ubiquitin furthermore reveals different ubiquitin requirements for the internalization at the PM compared to the ubiquitin-mediated sorting at the Golgi. Together, these results show that ubiquitin acts as a signal for vacuolar degradation of membrane proteins and is not restricted to sorting events at the PM.

Results

Ubiquitin causes internalization of a non-secretory reporter at the PM

To analyze sorting signals for the endocytic pathway, we have created GFP-based reporters that are *post*-translationally inserted into the PM but also allow the analysis of internalization signals by fusing the 26 C-terminal residues of AtROP10 (hereafter named Box) to the N-terminus of GFP (Figure 1A). To test whether ubiquitin causes internalization of proteins from the PM, we fused ubiquitin (Ub) to the C-terminus of Box-GFP, resulting in the construct Box-GFP-Ub (Figure 1B). We also generated a control construct lacking the N-terminal Box sequence (GFP-Ub), to assess the requirement for PM insertion (Figure 1C). Expression of these reporters in tobacco mesophyll protoplasts shows that Box-GFP is localized to the PM (Figure 1D), indicating efficient recruitment from the cytosol to the PM. It also demonstrates that the function of the Box is independent of its C- or N-terminal position at the reporter. In sharp contrast, the vast majority of Box-GFP-Ub localized to discrete punctae (Figure 1E, Additional file 1), indicating successful internalization of the reporter. Neither discrete punctae nor PM signals were observed in case of GFP-Ub (Figure 1F). As expected for this cytosolic reporter, fluorescence was distributed throughout the cytoplasm and the nuclear matrix. This suggests that the punctae of the reporter Box-GFP-Ub depend on membrane association and the presence of ubiquitin. To rule out that the observed localization might be due to specific properties of protoplasts, we have expressed the reporters in tobacco leaves via *Agrobacterium*-mediated transfection. The expression of Box-GFP in epidermal cells revealed its localization at the PM (Figure 1G), while Box-GFP-Ub was again found to label numerous punctate structures (Figure 1H and I). This shows that the localization of the reporters in protoplasts and *in planta* is the same. To analyze whether the punctate Box-GFP-Ub structures represent endosomes, we performed co-expression experiments with markers for the TGN/EE (YFP-SYP61; [40,41]), the MVB/LE (Ara6-RFP; [40]) and the Golgi (Man1-RFP; [42]). In these experiments, Box-GFP-Ub partially colocalized with YFP-SYP61 (Figure 2A-C, Additional file 2A) and Ara6-RFP (Figure 2D-F, Additional file 2B). LE/MVB-localization of Box-GFP-Ub is furthermore supported by the appearance of the fluorescent signals in ring-like structures after incubation with the drug wortmannin (WM, inset in Figure 2D), which form as a result of the drug-induced fusion of LEs/MVBs [43]. Box-GFP-Ub signals did not overlap with the signals of the Golgi marker (Additional file 2C), suggesting that the localization of Box-GFP-Ub is restricted to endosomes.

We next analyzed whether Box-GFP-Ub reaches its endosomal localization via the endocytic pathway, a transport that involves the formation of clathrin-coated vesicles at the PM. It was shown that this process is inhibited by the expression of a truncated mutant of the clathrin heavy chain, the clathrin hub [28,44-46]. Therefore we compared the numbers of punctate Box-GFP-Ub signals in control cells, expressing only Box-GFP-Ub (Figure 2G), with signals in cells coexpressing the clathrin hub (RFP-Hub1, Figure 2H). Figure 2I shows that the number of Box-GFP-Ub signals is significantly reduced upon RFP-Hub1 coexpression (Figure 2H-I), confirming that the endosomal localization of Box-GFP-Ub is indeed due to internalization at the PM via clathrin-mediated endocytosis.

Ubiquitin causes a plasma membrane protein to traffic to the vacuole

The previous experiments showed that a PM-associated protein can be efficiently internalized by a C-terminal fusion to ubiquitin. However, the fluorescent reporter was transported along the endocytic route only as far as the MVB/LE but could not be detected in the vacuole, even when expressed for 48 hours (data not shown). Since fluorescent signals of GFP-based reporters can be routinely detected in the lytic vacuole under these experimental conditions (Additional file 3, compare A and B), we conclude that the lack of vacuolar fluorescence of the Box-GFP-Ub is not due to vacuolar degradation, but instead due to a failure of vacuolar delivery. One reason for this could be that the membrane association via

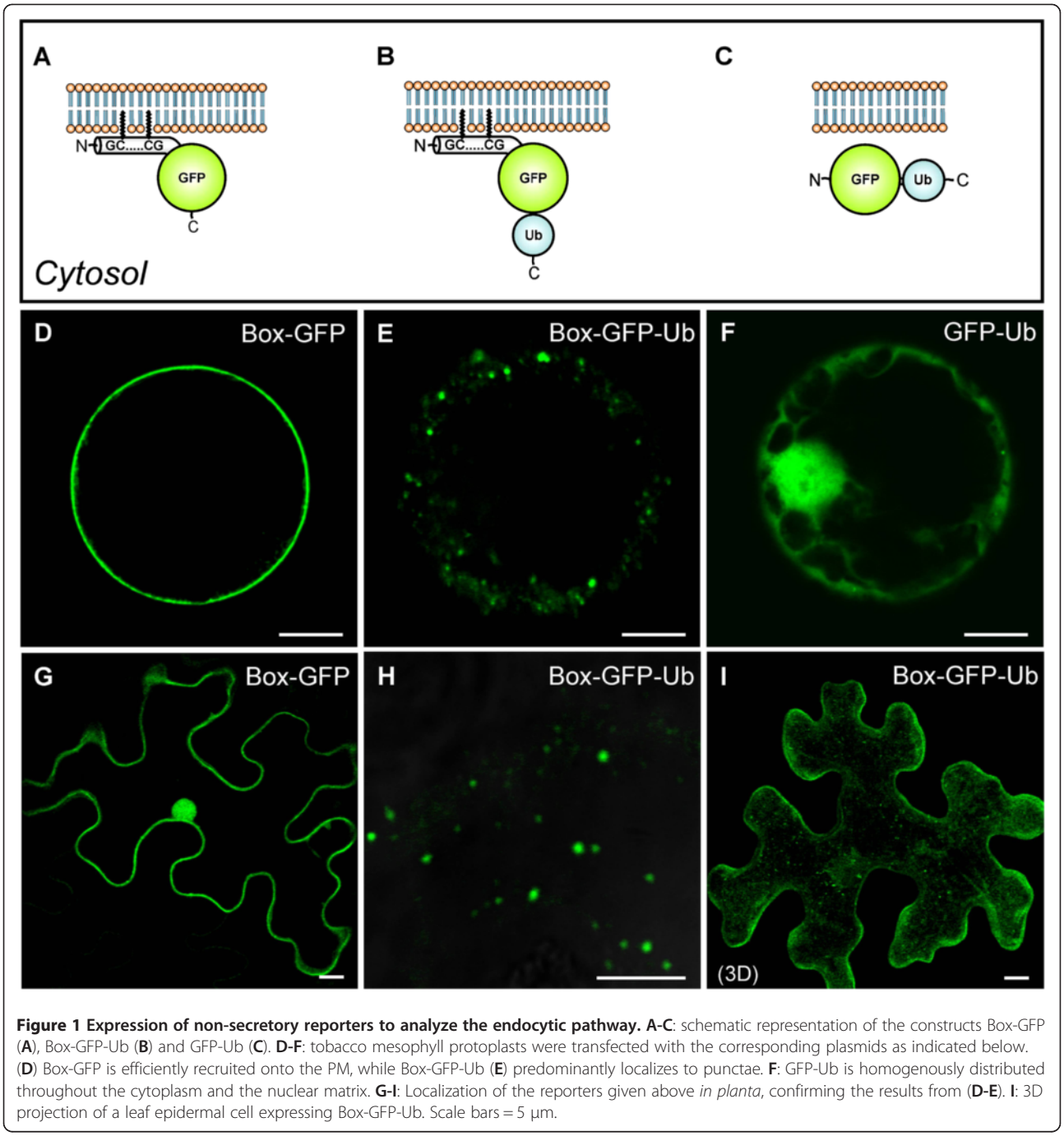

Figure 1 Expression of non-secretory reporters to analyze the endocytic pathway. A-C: schematic representation of the constructs Box-GFP (**A**), Box-GFP-Ub (**B**) and GFP-Ub (**C**). **D-F**: tobacco mesophyll protoplasts were transfected with the corresponding plasmids as indicated below. (**D**) Box-GFP is efficiently recruited onto the PM, while Box-GFP-Ub (**E**) predominantly localizes to punctae. **F**: GFP-Ub is homogenously distributed throughout the cytoplasm and the nuclear matrix. **G-I**: Localization of the reporters given above *in planta*, confirming the results from (**D-E**). **I**: 3D projection of a leaf epidermal cell expressing Box-GFP-Ub. Scale bars = 5 μm.

S-acylation is not stable enough to survive MVB-mediated sorting. Alternatively, the translational fusion of ubiquitin to the reporter prevents deubiquitination, a requirement for vacuolar delivery in yeast [47].

To answer this question, we have prepared a PM-targeted ubiquitin fusion construct based on a type-I transmembrane protein (RFP-TMD23-Ub, Figure 3A) by adding the ubiquitin sequence to the C-terminus of the PM marker RFP-TMD23, (Figure 3B; TM23 in [48]). In contrast to the lipid-anchored Box-GFP-Ub (see Figure 1B, E, H, I), expression of RFP-TMD23-Ub yields a vacuolar pattern in protoplasts and isolated vacuoles (Figure 3C, D), which was never observed for RFP-TMD23, lacking a C-terminal ubiquitin (Figure 3e). Comparison of RFP-TMD23-Ub with the vacuolar reporter spL-RFP [49] furthermore reveals that both molecules are equally well delivered to the vacuole (Additional file 3C, D). The same vacuolar pattern can be seen when RFP-TMD23-Ub is analyzed *in planta* (Figure 3F-H), indicating that sorting and transport mechanisms of these reporters do not differ between both

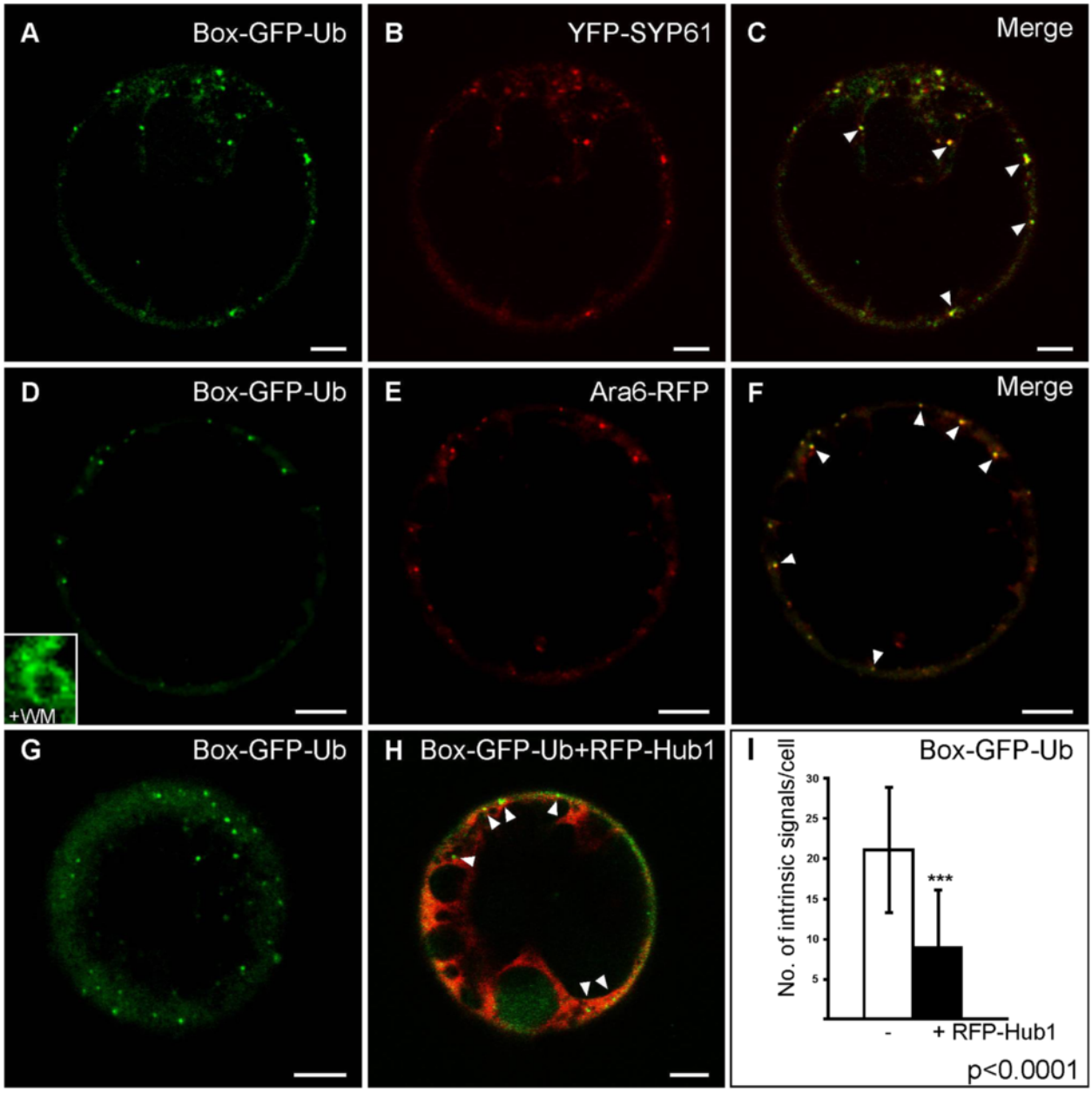

Figure 2 Ubiquitin-dependent internalization of Box-GFP-Ub. Expression of markers/reporters in tobacco mesophyll protoplasts as indicated below. **A-C**: Box-GFP-Ub (green) and the TGN/EE marker YFP-SYP61 (red) partially colocalize (arrowheads). **D-F**: Box-GFP-Ub (green) and MVB/LE marker Ara6-RFP (red) colocalize to a high degree (arrowheads). Box-GFP-Ub localizes to characteristic ring-like MVB structures after wortmannin-treatment (+WM; inset in **D**). For quantitative analysis of colocalization see Additional file 2. Endosomal signals of Box-GFP-Ub (**G**) are significantly reduced in quantity if coexpressed with the clathrin hub (RFP-Hub1; red, **H**). Arrowheads indicate remaining Box-GFP-Ub-positive endosomes. **I**: Statistical analysis reveals that the punctate signals are about 57% less abundant in cells coexpressing the RFP-Hub1 (+) as compared to control cells (–). (***) $p < 0.0001$. Scale bars = 5 μm.

experimental systems. Together, this suggests that it is the type of membrane association rather than the requirement for deubiquitination that prevented the vacuolar delivery of the Box-GFP-Ub reporter.

The RFP-TMD23-Ub signal was not restricted to the vacuolar lumen but was also detected at the PM and was occasionally associated with organelles in the peripheral cytoplasm. We therefore performed coexpression experiments with markers for TGN/EE (YFP-SYP61) and MVB/LE (GFP-BP80; [50]). This analysis was performed with detection parameters that reduced the strong and diffuse vacuolar background of RFP-TMD23-Ub. A large number

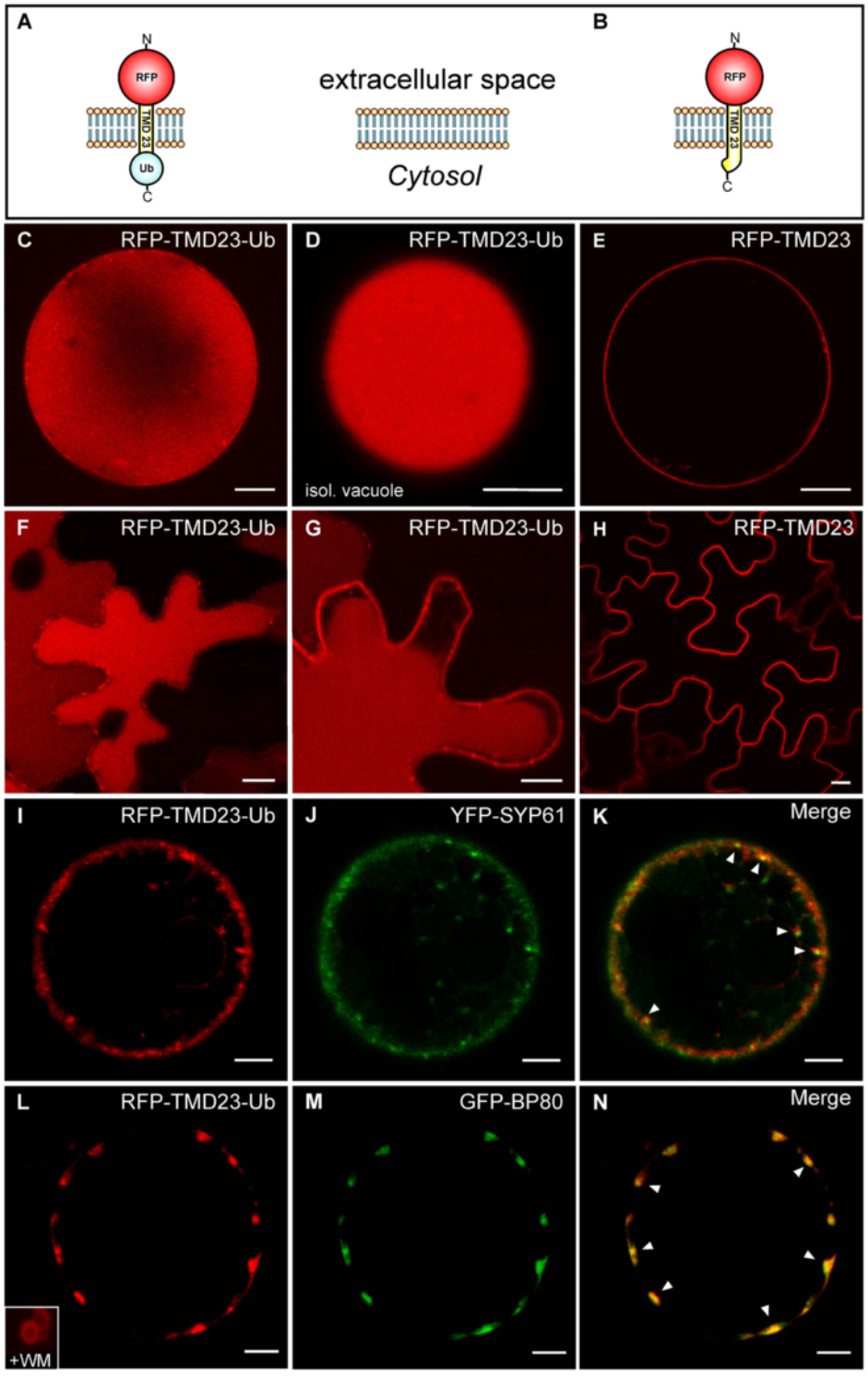

Figure 3 Ubiquitin-dependent transport of an integral PM protein to the vacuole. A-B: Schematic representation of the constructs RFP-TMD23-Ub (**A**) and RFP-TMD23 (**B**). Localization of the constructs in tobacco mesophyll protoplasts after 36 h (C-E, to allow for vacuolar accumulation) or 24 h (**I-N**, for colocalization analysis) and leaf epidermal cells (**F-H**). **C**: RFP-TMD23-Ub is targeted into the vacuolar lumen. (**D**) Isolated vacuole. (**E**) RFP-TMD23 localizes to the PM. F-H: Localization of the reporters given above *in planta*, confirming the results from **C-E. I-K**: RFP-TMD23-Ub (red) and YFP-SYP61 (green) partially colocalize (arrowheads). **L-N**: RFP-TMD23-Ub (red) and MVB/LE marker GFP-BP80 (green) overlap in punctate structures (arrowheads). RFP-TMD23-Ub localizes to ring-like MVB structures after wortmannin-treatment (+WM; inset in **L**). Scale bars = 5 μm. For quantitative analysis of colocalization see Additional file 2.

of the punctate signals overlapped with the markers for the TGN/EE (Figure 3I-K, additional file D) and the MVB/LE (Figure 3L-N, inset in 3 L and additional file E), both of which are transit compartments along the vacuolar route.

It is assumed that mono-ubiquitination mediates internalization of PM proteins, whereas poly-ubiquitination serves as signal for proteasomal degradation [10,51]. However, it has also been reported that PM proteins, with short polyubiquitin chains, are more efficiently internalized [19,52-54]. Moreover, deletion of the two C-terminal glycines of a recombinantly linked ubiquitin has been shown to prevent further ubiquitination, suggesting that these glycines act as an additional site for poly-ubiquitination [55]. Therefore, we have deleted both terminal glycine residues of Box-GFP-Ub (Box-GFP-UbΔGG) and RFP-TMD23-Ub (RFP-TMD23-UbΔGG). Interestingly, the expression of Box-GFP-UbΔGG in both tobacco protoplasts (Figure 4A) and leaves (Figure 4D) revealed a clear PM localization (Figure 4A and 4D) that was indistinguishable from the PM reporter Box-GFP (Figure 4B and 4E). Endosomal signals, as seen with the internalized Box-GFP-Ub construct (compare Figure 4A to 4C and 4D to 4F), were never observed. This suggests that the terminal glycine residues of ubiquitin are required for internalization of this molecule from the PM. The differential transport properties of Box-GFP-Ub and Box-GFP-UbΔGG furthermore demonstrate that ubiquitin acts as a specific sorting signal, rather than merely triggering a degradation response due to the individual properties of the reporter. In sharp contrast, deletion of the terminal glycine residues in RFP-TMD23-UbΔGG did not inhibit the ubiquitin-mediated internalization, as judged by the unperturbed vacuolar delivery of this reporter in protoplasts and *in planta* (Figure 4G and 4J; compare 4G to H and I and compare 4J to K and L).

Ubiquitin directs Golgi-localized proteins to the vacuole

The previous results show that the fusion of ubiquitin to the cytosolic tail of PM reporters is sufficient for internalization, but the transport of the two ΔGG variants differs significantly. Therefore, it seemed plausible to assume that these differences are due to their different transport routes towards the PM. In contrast to the directly targeted Box-GFP-UbΔGG, the RFP-TMD23-UbΔGG transits the secretory pathway. We hypothesized that this reporter might already be sorted into the vacuolar transport route from a compartment *en route* to the PM. Therefore, we have used the Golgi marker RFP-TMD20 (TM20 in [48]) (Figure 5A) to generate the ubiquitin fusion protein RFP-TMD20-Ub (Figure 5B). Expression of RFP-TMD20 in tobacco protoplasts revealed a punctate pattern (Figure 5C), which showed colocalization with the Golgi marker Man1-GFP (Additional file 4). In contrast, expression of the ubiquitin fusion (RFP-TMD20-Ub) yielded a strong vacuolar signal (Figure 5D), but punctae, representing wortmannin-sensitive LEs/MVBs (inset in Figure 5D), could also be observed. Interestingly, the ubiquitin fusion construct lacking both C-terminal glycine residues (RFP-TMD20-UbΔGG) was equally well delivered to the vacuole (Figure 5E). The same localization patterns for RFP-TMD20, RFP-TMD20-Ub and RFP-TMD20-UbΔGG were observed *in planta* (Figure 5F-H), suggesting that ubiquitin-mediated vacuolar sorting exhibits differential demands on the C-terminus of ubiquitin, dependent on the location within the secretory pathway.

To analyze vacuolar delivery biochemically, we have compared the GFP-based reporters with the soluble vacuolar molecule GFP-sporamin (Figure 6A), which yields a characteristic vacuolar degradation product of GFP, termed GFP core [50]. Since vacuolar RFP does not yield a degradation product, we have compared all RFP-based reporters with the soluble vacuolar protein spRFP-AFVY, serving as a size marker for vacuolar RFP (Figure 6B). Protein gel blot analysis with GFP/RFP antibodies reveals specific signals of the calculated molecular weight for each of the reporters (Figure 6A and 6B). As concluded from the CLSM results (Figure 1, 2), neither Box-GFP-Ub, Box-GFP-UbΔGG nor the cytosolic GFP-Ub yields a signal in size of the GFP core, as indication for the lack of vacuolar arrival. All ubiquitin fusions show an additional signal, which is in each case about 8 kDa smaller than the calculated weight of the fusion protein (asterisks), approximating that of monomeric ubiquitin. In contrast to the GFP-fusions, all RFP-ubiquitin constructs show an additional third signal, which is precisely the size of the vacuolar reporter spRFP-AFVY. Together with the CLSM localization, the appearance of this lower molecular weight form indicates vacuolar arrival. This suggests that ubiquitin is capable to target proteins from the PM into the endocytic route but also targets proteins from the Golgi into the vacuolar transport pathway.

Ubiquitin-mediated transport of membrane proteins to the vacuole occurs via the MVB

We wanted to test whether ubiquitin-facilitated transport from the PM and from the Golgi utilizes the ESCRT-dependent vacuolar route. It has been shown that expression of AtSKD1(AQ), a dominant-negative mutant of the ESCRT-III-associated AAA-ATPase, inhibits arrival of soluble vacuolar cargo [56]. In control experiments, co-expression of either of the vacuolar targeted RFP-TMD23-Ub and RFP-TMD20-Ub with the soluble vacuolar reporter aleurain-GFP [57] showed that both the membrane

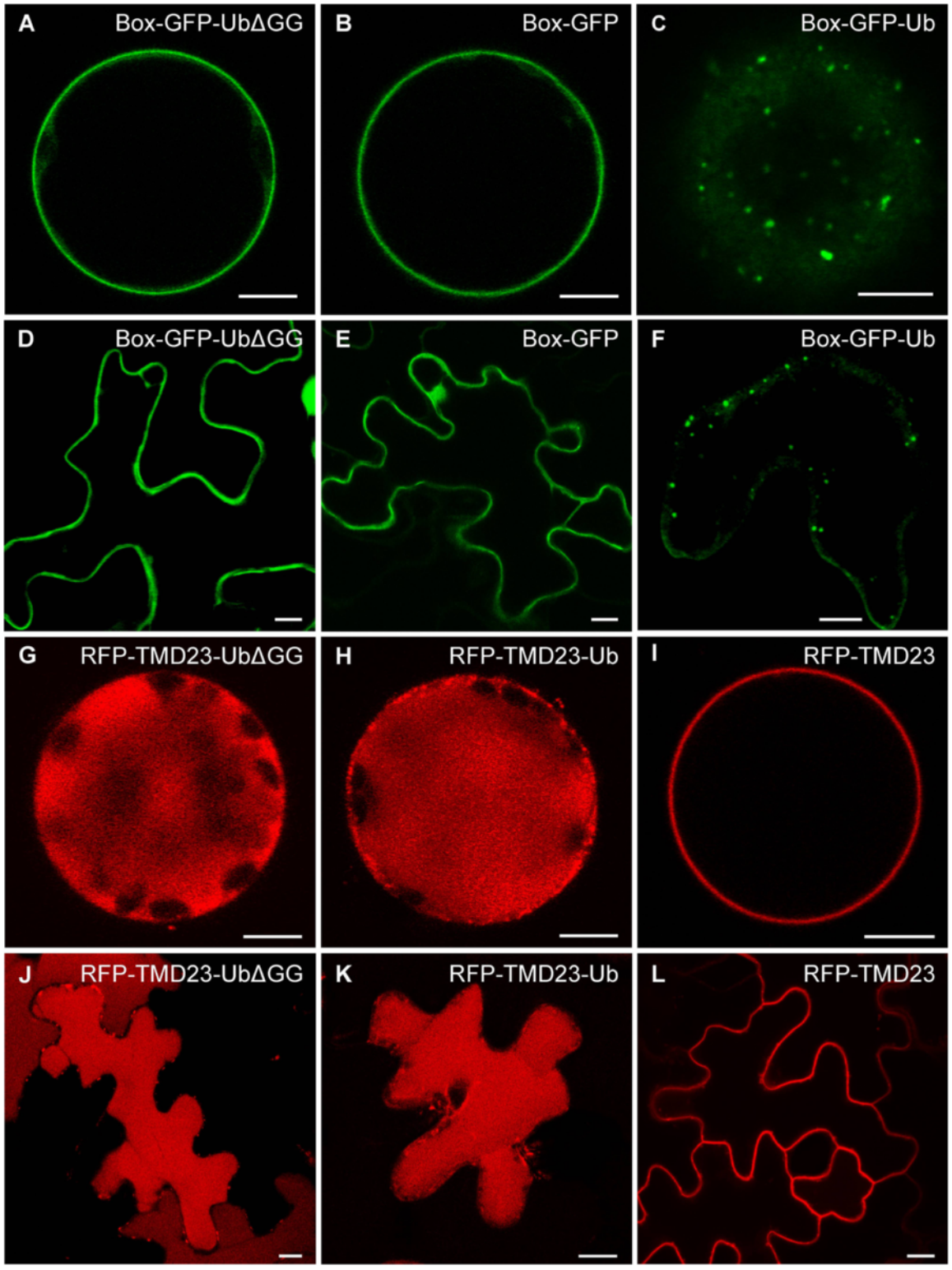

Figure 4 The C-terminus of ubiquitin is important for PM internalization. Tobacco mesophyll protoplasts and leaf epidermal cells expressing the plasmids indicated below. **A**. Box-GFP-UbΔGG is not internalized and localizes to the PM like Box-GFP (**B**) and does not localize to punctate structures like Box-GFP-Ub (**C**). **D-F**: Localization of the reporters given above *in planta*, confirming the results from (**A-C**). Vacuolar transport of RFP-TMD23-UbΔGG is not affected by the ΔGG mutation (**G**), compared to RFP-TMD23-Ub (**H**). Its phenotype thus differs from that of the PM marker RFP-TMD23 (**I**). **J-L**: Confirmation of the localization from **G-I** in leaf epidermal cells. Scale bars = 5 μm.

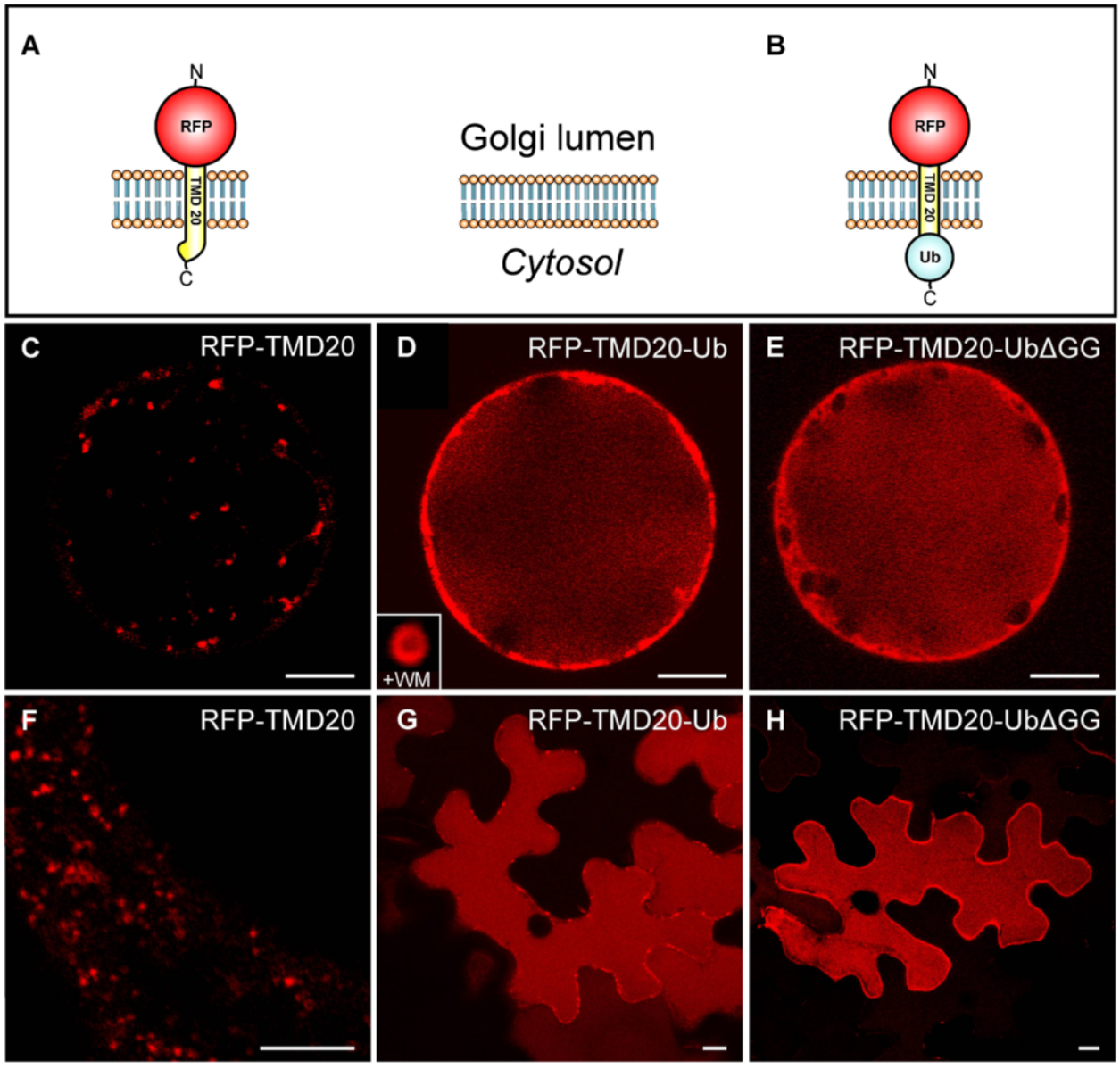

Figure 5 Ubiquitin-dependent transport from the Golgi to the vacuole. A-B: Schematic representation of the constructs RFP-TMD20 (**A**) and RFP-TMD20-Ub (**B**). Tobacco mesophyll protoplasts and leaf epidermal cells expressing the plasmids indicated below. RFP-TMD20 (**C**) exhibits a punctate pattern, while RFP-TMD20-Ub (**D**) is efficiently transported into the vacuolar lumen and also accumulates in ring-like structures after wortmannin-treatment (+WM; inset in **D**). Vacuolar transport of RFP-TMD20-UbΔGG (**E**) and RFP-TMD20-Ub is indistinguishable. **F-H**: Confirmation of the localization from **C-E** in leaf epidermal cells. Scale bars = 5 μm.

reporters and aleurain-GFP are delivered equally well to the vacuole (Figure 7A-C and Figure 7D-F, respectively). In the presence of AtSKD1(AQ), which inhibits vacuolar delivery of the soluble vacuolar protein GFP-sporamin and induces its secretion (Figure 7G), none of these reporters reached the vacuole but instead accumulated in intracellular compartments (Figure 7H and 7I).

Discussion

Targeting of membrane proteins in the secretory pathway

Secretion into the apoplast is regarded as being the "default pathway" for soluble proteins in the secretory pathway [58,59]. For plant membrane proteins, the situation is not that clear. It has been suggested that the tonoplast represents the default destination for this class of

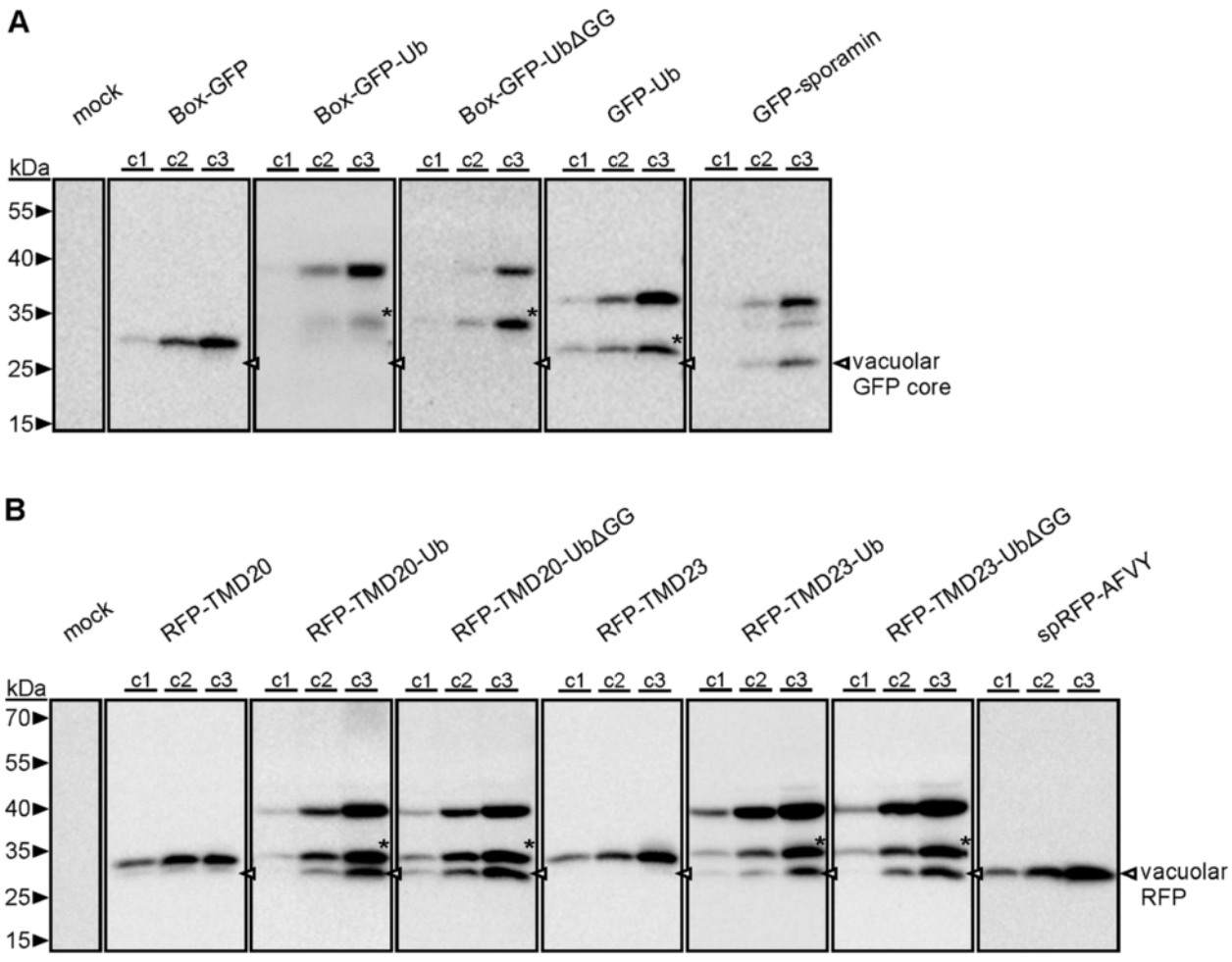

Figure 6 Western-blot analysis to monitor for vacuolar delivery. Tobacco mesophyll protoplasts were transfected with 10, 30 or 100 μg plasmid DNA encoding for each marker/reporter as indicated below or mock-transfected. Gel blot analysis using GFP (**A**) or RFP antibodies (**B**) reveals signals corresponding to the calculated molecular weight of the expressed proteins. Signals which might correspond to reporters with proteolytically cleavaged ubiquitin moiety are indicated by asterisks. Arrowheads indicate the size of the vacuolar GFP core and vacuolar RFP.

proteins [60,61] but this concept has recently been challenged. It was shown that mutants of the ER-resident p24 protein family that lack the di-lysine ER retrieval signal in their cytosolic domain and thus escape their first instance of sorting at the Golgi apparatus are indeed transported to the tonoplast but are also efficiently transported to the PM [62]. This dual localization of membrane proteins at the PM and the tonoplast is not restricted to mutants which have lost a specific sorting signal, since it can also be observed when fluorescent PM proteins like the plasma membrane ATPase (PMA) or the LOW-TEMPERATURE-INDUCIBLE PROTEIN (LTI6a) are analyzed [24]. The reasons for this differential localization are unclear as the sorting signals for these proteins have not yet been deciphered. It has also to be considered that all of these functional proteins are subject to cellular regulation mechanisms like quality control and turnover, which could contribute to vacuolar localization.

Although universal sorting signals for membrane proteins that allow for compartment-specific targeting are largely unknown, it has been demonstrated that the length of the TMD provides sufficient sorting information for targeting type-I proteins either to the ER, the Golgi or the PM [48]. This property has also been applied to the plant vacuolar sorting receptor (VSR) BP80, which localizes to the TGN/EE and the MVB/LE. In this case, various constructs carrying length-modified BP80-TMDs, but lacking the cytosolic tail, never deviated from this “default pathway”, suggesting that sorting into the vacuolar route requires additional information [48]. These examples furthermore show that the final location of a membrane protein is the result of a combination of sorting signals. For these reasons, we have decided to analyze the role of ubiquitin in protein targeting by the use of translational ubiquitin fusions, mimicking constitutive ubiquitination, based on reporters like

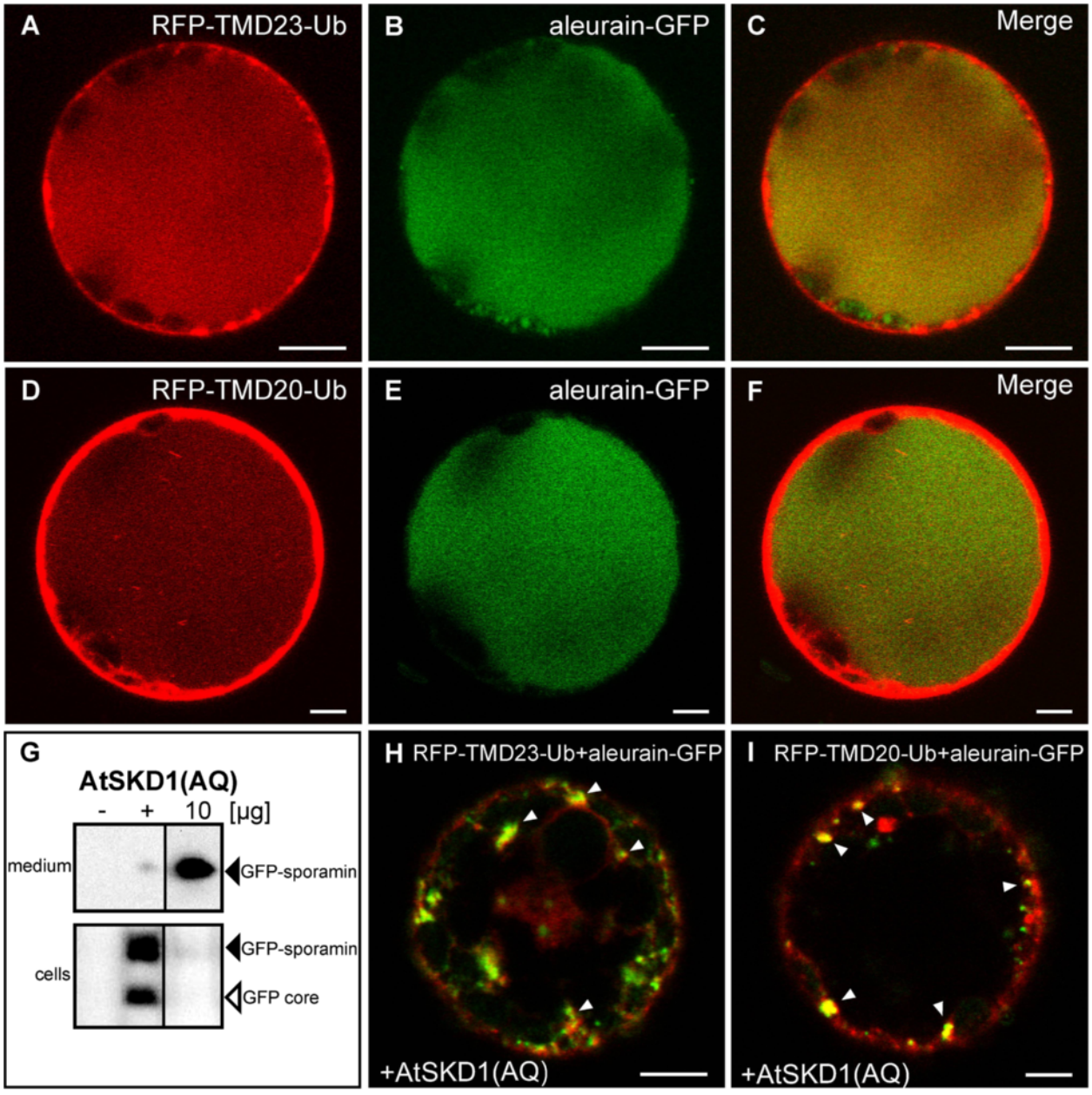

Figure 7 Inhibition of ESCRT function inhibits vacuolar arrival of ubiquitin-modified reporters. CLSM and western-blot analysis of tobacco mesophyll protoplasts expressing the indicated plasmids. **A-F**: RFP-TMD23-Ub (A-C, red) or RFP-TMD20-Ub (D-F, green). and the soluble vacuolar marker aleurain-GFP (green) colocalize in the vacuole. (**G**) The vacuolar GFP core of GFP-sporamin (open arrowhead) and the cellular transit form (closed arrowhead) disappear when coexpressed with 10 µg plasmid DNA encoding for the dominant-negative mutant AtSKD1(AQ). (–) mock-transfected, (+) positive control. **H-I**: AtSKD1(AQ) expression inhibits vacuolar delivery of RFP-TMD23-Ub (red) and aleurain-GFP (green) (H) or RFP-TMD20-Ub (red) and aleurain-GFP (green) (**I**). All reporters accumulate in punctae (arrowheads) under these conditions.

Box-GFP or RFP-TMD20/23, which possess minimal but defined sorting signals for either the PM or the Golgi. The use of reporters that are *post*-translationally inserted into the PM (BOX-GFP) and reporters that are transported via the secretory pathway (RFP-TMD23/20) permits the exposure of identical sorting signals at different intracellular locations and thus allows the analysis of specific sorting signals for individual transport steps within the cell.

Ubiquitin as a sorting signal for the endocytic pathway

We have addressed the question as to whether ubiquitin functions as a sorting signal for the endocytic pathway in plants by generating ubiquitin fusion proteins based on the

PM-localized markers Box-GFP and RFP-TMD23. Despite differences in their transport towards the PM – Box-GFP is inserted *post*-translationally, whereas RFP-TMD23 transits via the secretory pathway – both molecules are internalized when fused to ubiquitin and colocalize with endosomal markers. This demonstrates that both reporters are indeed sorted into the endocytic transport route, which has been suggested to comprise the TGN/EE and the MVB/LE as transit compartments [5,37,63].

Even though both reporters undergo endocytosis, there are differences in their final location: RFP-TMD23-Ub yields fluorescent signals in the vacuolar lumen, while Box-GFP-Ub only reaches the MVB/LE and is never detected in the vacuole. One explanation for the failed vacuolar delivery of Box-GFP-Ub could be that this reporter is released from the MVB/LE membrane into the cytosol. This is possible, since the attachment of proteins to membranes via the Box sequence harbors two weak points: first, the reversibility of the membrane anchorage [64] and second, the specific interaction of the polybasic region with phospholipids of the membrane, which mediates the specificity during the recruitment [39,65]. In this regard, a gradual change in the lipid composition of the compartments along the endocytic route could trigger a release of the reporter from the membrane into the cytosol.

A translational ubiquitin fusion protein, which is *post*-translationally inserted into the PM via a lipid modification, has previously been used as a reporter to analyze internalization events in mammalian cells [55]. After expression, the reporter was found to be poly-ubiquitinated, while a derivative of the reporter that lacked the C-terminal glycine residues was not. However, both reporters appeared to be equally well internalized, indicating that a single ubiquitin moiety is sufficient to act as an endocytic sorting signal [55]. Inspired by this work, we have generated reporter derivatives lacking the C-terminal glycines of the ubiquitin. Box-GFP-UbΔGG localizes exclusively to the PM and is not internalized, compared to the Box-GFP-Ub. Therefore it is tempting to speculate that in plants, a single ubiquitin may not be sufficient to mediate sorting into the endocytic pathway. This view is also in agreement with recent findings based on translational ubiquitin fusions of the *Arabidopsis* plasma membrane ATPase (PMA-EGFP-UB), mutagenized in the ubiquitin moiety to prevent poly-ubiquitination [24]. The mutants, some of which were also lacking both C-terminal glycine residues, localized to the PM in addition to the vacuole in the majority of the cells, while a non-mutagenized ubiquitin fusion was mainly found in vacuoles and punctae but not at the PM. This suggests that the endocytic uptake of putatively mono-ubiquitinated reporters was also less efficient. This interpretation is also supported by the recent demonstration that the endocytic uptake and thus the stability of PIN2 depends on poly-ubiquitin chains [23] and the observation that IRT1 mutants, which lack two putative ubiquitination sides, fail to be internalized and accumulate at the PM instead [21]. This furthermore indicates that both multi-ubiquitination and poly-ubiquitination can act as internalization signals. Surprisingly, the transmembrane reporter RFP-TMD23-UbΔGG is still efficiently transported to the vacuole. At first glance, these observations are contradictory and difficult to reconcile, since both reporters carry identical sorting signals. However, in case of Box-GFP-UbΔGG, the signal is exclusively displayed at the PM, whereas in case of RFP-TMD23-UbΔGG, the signal is displayed throughout its journey towards the PM and might thus be captured and redirected before reaching the PM.

The finding that fusion of ubiquitin to a *post*-translationally inserted PM resident reporter is sufficient to trigger its internalization implies that plants possess an endogenous machinery capable of recognizing and sorting ubiquitin-tagged cargo. This hypothesis is supported by the recent identification of AvrPtoB, an effector of the plant pathogenic bacterium *Pseudomonas syringae* pv *tomato* DC3000, that acts as an E3 ubiquitin ligase [20]. The authors showed that AvrPtoB catalyzes poly-ubiquitination of FLS2. In combination with flg22, the effector induces the internalization of the receptor, leading to the suggestion that the degradation of FLS2 might be a mechanism of the pathogen to overcome plant innate immunity [20]. The demonstration that *Arabidopsis* lines lacking the cytosolic deubiquitinating enzyme AMSH3 are impaired in vacuolar biogenesis and, consequently, fail in vacuolar delivery of PIN2 [66] supports the significance of endogenous ubiquitin-mediated sorting processes.

Ubiquitin as a vacuolar sorting signal

Taking into consideration that the deletion of one sorting signal redirects an ER-resident protein to the PM or an MVB/LE localized VSR to the Golgi, it is plausible to assume that the addition of a sorting signal is capable of overriding an existing one. The fusion of UbΔGG to the cytosolic tail of PM marker RFP-TMD23 represents just such an additional sorting signal, while it is the only existing sorting signal in the context of the *post*-translationally inserted PM reporter Box-GFP. Since the signal UbΔGG fails to drive internalization of Box-GFP-UbΔGG, it is plausible to assume that this also occurs in case of RFP-TMD23-UbΔGG. However, RFP-TMD23-UbΔGG was efficiently transported to the vacuole, which was also observed for the PMA-EGFP-UB mutants before [24], but it did not accumulate at the PM. We therefore speculated that a portion of the RFP-TMD23-UbΔGG molecules could have been sorted into the vacuolar pathway at a transit compartment prior to reaching the PM. It

was recently suggested that direct trafficking from the Golgi to the vacuole does not significantly contribute to the vacuolar transport of ubiquitinated PM proteins, but it was also shown that a ubiquitin fusion of a MVB marker (AtVSR1-EGFP-UB) is also targeted to the vacuole [24]. If ubiquitin-dependent sorting of membrane proteins would be restricted to the PM, one would have to assume that ubiquitin firstly redirects AtVSR1-EGFP-UB from the vacuolar route towards the PM in order to trigger vacuolar delivery via the endocytic route. To test for ubiquitin-mediated sorting from the Golgi, we fused ubiquitin and UbΔGG to the cytosolic domain of the Golgi marker RFP-TMD20 [48]. This marker localizes to this compartment due to its TMD length of 20 amino acids, and does neither progress to the PM or into the vacuolar route. Both of the resulting reporters (RFP-TMD20-Ub and RFP-TMD20-UbΔGG) were efficiently sorted to the lytic vacuole and did not accumulate at the PM. These results show that ubiquitin-dependent vacuolar sorting can occur at the Golgi. We have shown that UbΔGG is insufficient to trigger the internalization at the PM. Since RFP-TMD20-UbΔGG does not accumulate at the PM, these results show that ubiquitin-dependent vacuolar sorting of this reporter does not occur via the PM.

The concept of ubiquitin-mediated sorting at the Golgi is also in agreement with our previous observation that the ESCRT-I subunit VPS28 localizes to the Golgi and the TGN/EE in *Arabidopsis* root cells, but that it is absent from MVBs/LEs, which can act as TGN-derived carriers that connect the TGN/EE in an clathrin-independent transport mode with the vacuole [28]. In yeast and mammals, ubiquitinated membrane proteins can already be recognized at the TGN by GGAs (Golgi-localized, γ-ear-containing ARF-binding proteins). These clathrin adaptors mediate protein sorting into clathrin-coated vesicles, which deliver their cargo to EEs where it is handed over to the ESCRT machinery [67,68]. The *Arabidopsis* genome, however, does not encode for GGA proteins [69]. In combination with a lack of homologous genes for ESCRT-0 and the ESCRT-I subunit Mvb12 [70], it is plausible to assume that the initial steps of ubiquitin-mediated sorting in plants differ from those in mammals and yeast.

The ubiquitin-dependent vacuolar delivery of the Golgi marker raised the question as to whether the transport of this chimera occurs through the biosynthetic vacuolar transport route via the TGN/EE and the MVB/LE. It was recently shown that a dominant-negative mutant of the ESCRT-associated AAA-ATPase SKD1 (AtSKD1(AQ)) is a potent inhibitor of transport of the soluble vacuolar reporter α-amylase-sporamin [56]. This soluble reporter is sorted into the vacuolar route via VSRs [50,71], but not via a direct interaction with the ESCRT machinery. However, this route collapses, if the ESCRT machinery is perturbed [56]. We have therefore applied this tool to analyze the transport route of the ubiquitin fusions RFP-TMD23-Ub and RFP-TMD20-Ub in direct comparison with the transport of the soluble vacuolar cargo aleurain-GFP. AtSKD1 (AQ) prevented the vacuolar arrival of aleurain-GFP and both ubiquitin fusion proteins. This demonstrates that ubiquitin acts also as a sorting signal for the biosynthetic vacuolar route, when displayed at the surface of the Golgi/TGN.

This concept is supported by data obtained from yeast. There, newly synthesized membrane proteins are sorted

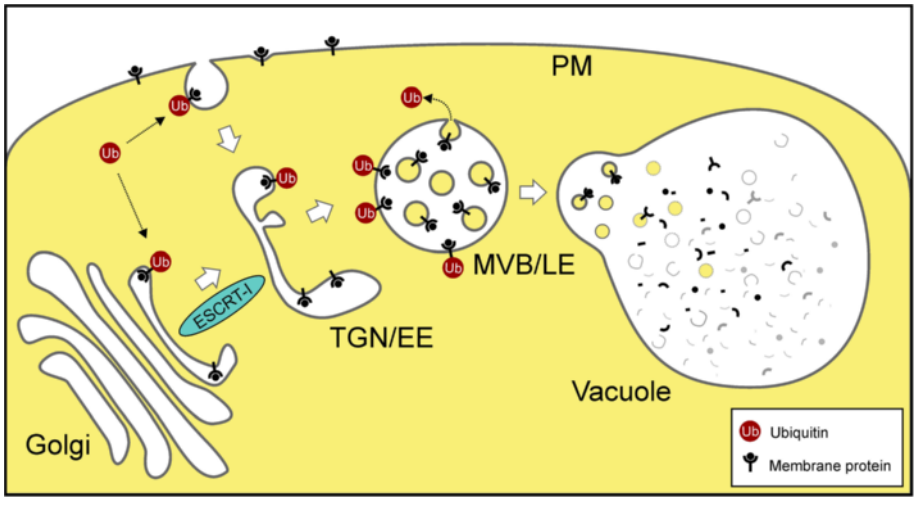

Figure 8 Model illustrating ubiquitin-mediated vacuolar transport of membrane proteins. Ubiquitin acts as an internalization signal at the PM for the endocytic route but also redirects Golgi-localized membrane proteins into the vacuolar degradation pathway. Both pathways merge at the TGN/EE. The ESCRT-I subunit VPS28 localizes to the Golgi and the TGN/EE but not to the MVB/LE [28]. This could suggest that ESCRT-mediated sorting is initiated at these compartments.

in the TGN in a ubiquitin-based manner: proteins which are not ubiquitinated travel to the PM, whereas those which are, move down the endosomal pathway to the vacuole [72,73]. This is furthermore supported by the recent finding that the down-regulation of the PM-localized transporter BOR1 requires the combined action of tyrosine-based sorting signals as well as mono- and di-ubiquitination [22]. In this scenario, it is assumed that the tyrosine-based sorting signals confer internalization, while ubiquitin might be employed during endosomal sorting [22]. A similar role for ubiquitin has also been shown to operate in *Drosophila* [74]. It is therefore quite plausible that ubiquitin acts as a sorting signal already in the Golgi/TGN of plant cells.

Conclusions

Our results show that ubiquitin acts as a sorting signal that mediates internalization at the PM but also redirects proteins from the early secretory pathway into the vacuolar degradation route (Figure 8). This might explain how ubiquitin as the sole sorting signal could lead to vacuolar delivery in a transport route that spans multiple compartments. Ubiquitin-mediated sorting at the Golgi/TGN might also hint to the existence of a ubiquitin-mediated, ESCRT-driven mechanism to enable the turnover of membrane proteins in the early secretory pathway, at a location beyond the ER-associated degradation (ERAD) pathway.

Methods

Plant materials

Nicotiana tabacum var. SR1 was grown under sterile conditions as previously described [75]. For leaf infiltrations, *Nicotiana benthamiana* was grown 5–6 weeks on soil. Wortmannin-treatment (30 μM) occurred for 1 h.

Recombinant plasmid production

The following plasmids were used: Ara6-RFP [40], YFP-SYP61 [41], Man1-RFP and Man1-GFP [42], GFP-BP80 [50], aleurain-GFP [57], spRFP-AFVY and spL-RFP [49] and AtSKD1(AQ) [56].

Coding sequences were amplified by PCR from either first-strand cDNA [71] or plasmid DNA. Recipient vectors were cut according to restriction sites of fragments and dephosphorylated prior to ligation. All primers used are shown in Additional file 5: Table S1. The *Escherichia coli* strain MC1061 [76] was used for all plasmid amplifications. Box-GFP-Ub (pDS10) was assembled by ligating the Box coding sequence of AtROP10 [AT3G480409] - generated by annealed oligonucleotides -, the PCR-amplified GFP from pSN9 [32] and ubiquitin [AT5G03240] amplified from *Arabidopsis* cDNA into pAmy-HDEL [58]. Box-GFP-UbΔGG (pDS21) was amplified from pDS10 and cloned into pDS10 to replace Box-GFP-Ub. Box-GFP (pDS9) and cytosolic GFP-Ub (pFK17) were amplified from pDS10 and cloned into pAmy-HDEL and pPP11 ([71], respectively. RFP-TMD23 [77] and RFP-TMD20 (TM20 in [48]) were first subcloned into pPP11, resulting in pFK12 and pFK23. The coding sequence for ubiquitin and UbΔGG were amplified from pDS10 and ligated into pFK12 and pFK23, resulting in RFP-TMD23-Ub (pFK13), RFP-TMD20-Ub (pFK24), RFP-TMD23-UbΔGG (pFK19) and RFP-TMD20-UbΔGG (pFK25).

For leaf infiltrations, expression cassettes were subcloned into the binary Ti vector pGreenII 0029 [78]. This vector was previously modified to eliminate an intrinsic *Nhe*I site and to introduce MCS-flanking *Eco*RI and *Hind*III sites (pCN1). RFP-Hub1 (pFK26) was generated by PCR amplification of the C-terminal 1860 bps of CHC-1 [AT3G11130] from cDNA and ligation with the amplified RFP sequence from pFK13 into pGD5 [32].

Transient gene expression, isolation of vacuoles, and leaf infiltration

Mesophyll protoplasts were isolated from 6–8 week-old plants and transfected via electroporation as described previously [77]. Unless otherwise stated, 10 μg of plasmid DNA were used for transfection followed by incubation for 24 h. Vacuoles were isolated 36 h after transfection as described previously [71]. Tobacco leafs were infiltrated with *Agrobacterium tumefaciens* (strain GV3101) as described previously [79].

Protein extraction and immunoblot analysis

Cellular proteins were extracted in a final volume of 250 μL in 100 mM Tris pH 7.8, 200 mM NaCl, 1 mM EDTA, 2% (v/v) β-Mercaptoethanol and 0.2% (v/v) Triton X-100 by sonication. SDS-PAGE and immunoblot analysis were performed as described previously [75]. Antibodies were used as follows: anti-GFP (rabbit polyclonal [35]) 1:10,000 and anti-RFP (rat monoclonal, ChromoTek) 1:5,000. Peroxidase-conjugated antibodies against rabbit IgGs (Millipore) or rat (Sigma-Aldrich) were used according to the manufacturer. Signals were detected by the use of AceGlow (PEQLAB) in combination with the Chemocam imager (Intas).

Confocal microscopy and immunofluorescence labeling

Imaging was performed using a Zeiss Axiovert LSM 510 meta CLSM as described previously [28]. *Post*-acquisition image processing was performed using the Zeiss LSM image browser and Corel-DrawX4. For the quantification of Box-GFP-Ub internalization, fluorescent punctate signals present in the cortical cytoplasm of n = 58 protoplasts were considered. Error bars were calculated as the standard deviation of the mean value and the p-value was computed using the *t*-test calculator from http://www.graphpad.com/.

Statistical analysis of CLSM localization data

For statistical analysis, the PSC colocalization plug-in [80] for ImageJ [81] was used to calculate the linear Pearson correlation coefficient (rp) and the nonlinear Spearman's rank correlation coefficient (rs) of red and green fluorescent signals. Values were between −1 (negative correlation) and +1 (positive correlation). The fluorescence values of all pixels across the two channels of all analyzed signals were depicted in a scatterplot. Masking of areas of was performed with the ImageJ brush tool as described by French et al. (2008). For every analyzed image, punctuate signals were selected and the threshold level, under which pixels were treated as background noise, was set to 10. At least 6 individual cells and a minimum of 100 signals were considered for every experiment.

Additional files

Additional file 1: Analysis of the Box-GFP-Ub expression pattern. Tobacco mesophyll protoplasts were transfected with plasmids encoding for Box-GFP-Ub. The reporter was expressed for 24 h prior to CLSM analysis. Scale bars = 5 μm. Fluorescence signals of a tobacco protoplast are shown in a cortical view (A), in an optical section (B) and in a 3D projection (C), revealing localization of Box-GFP-Ub at the plasma membrane and in punctae.

Additional file 2: Quantitative analysis of the localization of Box-GFP-Ub and RFP-TMD23-Ub. Tobacco mesophyll protoplasts were transfected with plasmids encoding for fluorescent markers/reporters as indicated below. Fluorescent proteins were expressed for 24 h prior to CLSM analysis. Scale bars = 5 μm. For quantification, the PSC coefficients (rp and rs) were calculated after analysis of at least 6 representative protoplasts and a minimum of 100 signals. The level of colocalization ranges from +1 for perfect correlation to −1 for negative correlation. The fluorescence values of all pixels across the two channels of all analyzed signals were depicted in a scatterplot. A: Box-GFP-Ub and the TGN-marker YFP-SYP61 show rp and rs values in a range that indicates colocalization. B: While the same is true for coexpression of Box-GFP-Ub and the MVB-marker Ara6-RFP, no positive correlation was observed with the Golgi marker Man1-RFP (C). Coexpression of RFP-TMD23-Ub with the same endosomal markers results in similar rp and rs values compared to A-B as predicted for an endocytic cargo molecule (D-E).

Additional file 3: Comparison of the ubiquitin-modified reporters and soluble vacuolar cargo. Tobacco mesophyll protoplasts were transfected with plasmids encoding for fluorescent markers/reporters as indicated below. Fluorescent proteins were expressed for 24 h prior to CLSM analysis. Scale bars = 5 μm. Aleurain-GFP is delivered to the lumen of the vacuole (A), whereas Box-GFP-Ub reveals punctuate signals in the cortical cytoplasm (B). spL-RFP (the linker peptide from proricin fused to RFP, (C)) and RFP-TMD23-Ub (D) give the same expression pattern being localized to the vacuolar lumen.

Additional file 4: Analysis of Golgi markers and modified derivatives. Tobacco mesophyll protoplasts were transfected with plasmids encoding for fluorescent markers/reporters as indicated below. Fluorescent proteins were expressed for 24 h prior to CLSM analysis. Scale bars = 5 μm. A-C: Coexpression of RFP-TMD20 with the Golgi marker Man1-GFP, demonstrating colocalization of both molecules.

Additional file 5: Table S1. Primers used for cloning.

Competing interests

The authors declare that they have no competing interests.

Authors' contributions

DS, FK, CV, DR and PP designed and analyzed the experiments; DS, FK, CV and MSWY performed the experiments; SS and LJ contributed unpublished material; DS, FK DR, and PP and wrote the article. All authors approved the manuscript.

Acknowledgements

The authors wish to thank M. Langhans and S. Sturm, née Niemes, for CLSM support and B. Jesenofsky and C. Nill for technical help. The authors also wish to thank Lorenzo Frigerio from the University of Warwick, UK, for the markers spL-RFP and spRFP-AFVY. The financial support of the Deutsche Forschungsgemeinschaft (PI 769/1-1, PI 769/1-2 and RO 440/14-1) is gratefully acknowledged.

Author details

[1]Department of Developmental Genetics, Center for Plant Molecular Biology (ZMBP), University of Tübingen, Tübingen 72076, Germany. [2]Department of Plant Cell Biology, Centre for Organismal Studies, University of Heidelberg, Heidelberg 69120, Germany. [3]Plant Developmental Biology, Centre for Organismal Studies, University of Heidelberg, Heidelberg 69120, Germany. [4]School of Life Sciences, Centre for Cell and Developmental Biology, The Chinese University of Hong Kong, Shatin NT, Hong Kong, PR China. [5]Botanical Institute, Biozentrum Köln, University of Cologne, Cologne 50674, Germany.

Received: 4 May 2012 Accepted: 13 July 2012
Published: 12 September 2012

References

1. Doherty GJ, McMahon HT: **Mechanisms of endocytosis.** *Annu Rev Biochem* 2009, **78:**857–902.
2. Shivas JM, Morrison HA, Bilder D, Skop AR: **Polarity and endocytosis: reciprocal regulation.** *Trends Cell Biol* 2010, **20:**445–452.
3. Geldner N, Friml J, Stierhof YD, Jurgens G, Palme K: **Auxin transport inhibitors block PIN1 cycling and vesicle trafficking.** *Nature* 2001, **413:**425–428.
4. Altenbach D, Robatzek S: **Pattern recognition receptors: from the cell surface to intracellular dynamics.** *Mol Plant Microbe Interact* 2007, **20:**1031–1039.
5. Robinson DG, Jiang L, Schumacher K: **The endosomal system of plants: charting new and familiar territories.** *Plant Physiol* 2008, **147:**1482–1492.
6. Russinova E, de Vries S: **Receptor-Mediated Endocytosis in Plants**. In *Plant Endocytosis*, Volume 1. Edited by Samaj J. Heidelberg: Springer; 2006:103115.
7. Hicke L: **A new ticket for entry into budding vesicles-ubiquitin.** *Cell* 2001, **106:**527–530.
8. Hicke L, Dunn R: **Regulation of membrane protein transport by ubiquitin and ubiquitin-binding proteins.** *Annu Rev Cell Dev Biol* 2003, **19:**141–172.
9. Rotin D, Staub O, Haguenauer-Tsapis R: **Ubiquitination and endocytosis of plasma membrane proteins: role of Nedd4/Rsp5p family of ubiquitin-protein ligases.** *J Membr Biol* 2000, **176:**1–17.
10. Pickart CM, Eddins MJ: **Ubiquitin: structures, functions, mechanisms.** *Biochim Biophys Acta* 2004, **1695:**55–72.
11. Hurley JH, Lee S, Prag G: **Ubiquitin-binding domains.** *Biochem J* 2006, **399:**361–372.
12. Peng J, Schwartz D, Elias JE, Thoreen CC, Cheng D, Marsischky G, Roelofs J, Finley D, Gygi SP: **A proteomics approach to understanding protein ubiquitination.** *Nat Biotechnol* 2003, **21:**921–926.
13. Xu P, Peng J: **Characterization of polyubiquitin chain structure by middle-down mass spectrometry.** *Anal Chem* 2008, **80:**3438–3444.
14. Ikeda F, Dikic I: **Atypical ubiquitin chains: new molecular signals. 'Protein Modifications: Beyond the Usual Suspects' review series.** *EMBO Rep* 2008, **9:**536–542.
15. Kim HT, Kim KP, Lledias F, Kisselev AF, Scaglione KM, Skowyra D, Gygi SP, Goldberg AL: **Certain pairs of ubiquitin-conjugating enzymes (E2s) and ubiquitin-protein ligases (E3s) synthesize nondegradable forked ubiquitin chains containing all possible isopeptide linkages.** *J Biol Chem* 2007, **282:**17375–17386.
16. Chau V, Tobias JW, Bachmair A, Marriott D, Ecker DJ, Gonda DK, Varshavsky A: **A multiubiquitin chain is confined to specific lysine in a targeted short-lived protein.** *Science* 1989, **243:**1576–1583.

17. Finley D, Sadis S, Monia BP, Boucher P, Ecker DJ, Crooke ST, Chau V: **Inhibition of proteolysis and cell cycle progression in a multiubiquitination-deficient yeast mutant.** *Mol Cell Biol* 1994, **14:**5501–5509.
18. Raiborg C, Stenmark H: **The ESCRT machinery in endosomal sorting of ubiquitylated membrane proteins.** *Nature* 2009, **458:**445–452.
19. Madshus IH: **Ubiquitin binding in endocytosis–how tight should it be and where does it happen?** *Traffic* 2006, **7:**258–261.
20. Göhre V, Spallek T, Haweker H, Mersmann S, Mentzel T, Boller T, de Torres M, Mansfield JW, Robatzek S: **Plant pattern-recognition receptor FLS2 is directed for degradation by the bacterial ubiquitin ligase AvrPtoB.** *Curr Biol* 2008, **18:**1824–1832.
21. Barberon M, Zelazny E, Robert S, Conejero G, Curie C, Friml J, Vert G: **Monoubiquitin-dependent endocytosis of the iron-regulated transporter 1 (IRT1) transporter controls iron uptake in plants.** *Proc Natl Acad Sci U S A* 2011, **108:**E450–E458.
22. Kasai K, Takano J, Miwa K, Toyoda A, Fujiwara T: **High boron-induced ubiquitination regulates vacuolar sorting of the BOR1 borate transporter in Arabidopsis thaliana.** *J Biol Chem* 2010, **286:**6175–6183.
23. Leitner J, Petrasek J, Tomanov K, Retzer K, Parezova M, Korbei B, Bachmair A, Zazimalova E, Luschnig C: **Lysine63-linked ubiquitylation of PIN2 auxin carrier protein governs hormonally controlled adaptation of Arabidopsis root growth.** *Proc Natl Acad Sci U S A* 2012, **109:**8322–8327.
24. Herberth S, Shahriari M, Bruderek M, Hessner F, Muller B, Hulskamp M, Schellmann S: **Artificial ubiquitylation is sufficient for sorting of a plasma membrane ATPase to the vacuolar lumen of Arabidopsis cells.** *Planta* 2012, **236:**63–77.
25. Cai Y, Zhuang X, Wang J, Wang H, Lam SK, Gao C, Wang X, Jiang L: **Vacuolar Degradation of Two Integral Plasma Membrane Proteins, AtLRR84A and OsSCAMP1, Is Cargo Ubiquitination-Independent and Prevacuolar Compartment-Mediated in Plant Cells.** *Traffic* 2012, **13:**1023–1040.
26. Reyes FC, Buono R, Otegui MS: **Plant endosomal trafficking pathways.** *Curr Opin Plant Biol* 2011, **14:**666–673.
27. Schellmann S, Pimpl P: **Coats of endosomal protein sorting: retromer and ESCRT.** *Curr Opin Plant Biol* 2009, **12:**670–676.
28. Scheuring D, Viotti C, Kruger F, Kunzl F, Sturm S, Bubeck J, Hillmer S, Frigerio L, Robinson DG, Pimpl P, Schumacher K: **Multivesicular bodies mature from the trans-Golgi network/early endosome in Arabidopsis.** *Plant Cell* 2011, **23:**3463–3481.
29. Shahriari M, Richter K, Keshavaiah C, Sabovljevic A, Huelskamp M, Schellmann S: **The Arabidopsis ESCRT protein-protein interaction network.** *Plant Mol Biol* 2011, **76:**85–96.
30. Spitzer C, Schellmann S, Sabovljevic A, Shahriari M, Keshavaiah C, Bechtold N, Herzog M, Muller S, Hanisch FG, Hulskamp M: **The Arabidopsis elch mutant reveals functions of an ESCRT component in cytokinesis.** *Development* 2006, **133:**4679–4689.
31. Winter V, Hauser MT: **Exploring the ESCRTing machinery in eukaryotes.** *Trends Plant Sci* 2006, **11:**115–123.
32. Niemes S, Langhans M, Viotti C, Scheuring D, San Wan Yan M, Jiang L, Hillmer S, Robinson DG, Pimpl P: **Retromer recycles vacuolar sorting receptors from the trans-Golgi network.** *Plant J* 2010, **61:**107–121.
33. Reichardt I, Stierhof YD, Mayer U, Richter S, Schwarz H, Schumacher K, Jurgens G: **Plant cytokinesis requires de novo secretory trafficking but not endocytosis.** *Curr Biol* 2007, **17:**2047–2053.
34. Spitzer C, Reyes FC, Buono R, Sliwinski MK, Haas TJ, Otegui MS: **The ESCRT-related CHMP1A and B proteins mediate multivesicular body sorting of auxin carriers in Arabidopsis and are required for plant development.** *Plant Cell* 2009, **21:**749–766.
35. Viotti C, Bubeck J, Stierhof YD, Krebs M, Langhans M, van den Berg W, van Dongen W, Richter S, Geldner N, Takano J, Jurgens G, de Vries SC, Robinson DG, Schumacher K: **Endocytic and Secretory Traffic in Arabidopsis Merge in the Trans-Golgi Network/Early Endosome, an Independent and Highly Dynamic Organelle.** *Plant Cell* 2010, **22:**1344–1357.
36. Geldner N, Hyman DL, Wang X, Schumacher K, Chory J: **Endosomal signaling of plant steroid receptor kinase BRI1.** *Genes Dev* 2007, **21:**1598–1602.
37. Dettmer J, Hong-Hermesdorf A, Stierhof YD, Schumacher K: **Vacuolar H+−ATPase activity is required for endocytic and secretory trafficking in Arabidopsis.** *Plant Cell* 2006, **18:**715–730.
38. Lam SK, Siu CL, Hillmer S, Jang S, An G, Robinson DG, Jiang L: **Rice SCAMP1 defines clathrin-coated, trans-golgi-located tubular-vesicular structures as an early endosome in tobacco BY-2 cells.** *Plant Cell* 2007, **19:**296–319.
39. Lavy M, Yalovsky S: **Association of Arabidopsis type-II ROPs with the plasma membrane requires a conserved C-terminal sequence motif and a proximal polybasic domain.** *Plant J* 2006, **46:**934–947.
40. Ueda T, Uemura T, Sato MH, Nakano A: **Functional differentiation of endosomes in Arabidopsis cells.** *Plant J* 2004, **40:**783–789.
41. Uemura T, Ueda T, Ohniwa RL, Nakano A, Takeyasu K, Sato MH: **Systematic analysis of SNARE molecules in Arabidopsis: dissection of the post-Golgi network in plant cells.** *Cell Struct Funct* 2004, **29:**49–65.
42. Nebenführ A, Gallagher LA, Dunahay TG, Frohlick JA, Mazurkiewicz AM, Meehl JB, Staehelin LA: **Stop-and-go movements of plant Golgi stacks are mediated by the acto-myosin system.** *Plant Physiol* 1999, **121:**1127–1142.
43. Wang J, Cai Y, Miao Y, Lam SK, Jiang L: **Wortmannin induces homotypic fusion of plant prevacuolar compartments.** *J Exp Bot* 2009, **60:**3075–3083.
44. Dhonukshe P, Aniento F, Hwang I, Robinson DG, Mravec J, Stierhof YD, Friml J: **Clathrin-mediated constitutive endocytosis of PIN auxin efflux carriers in Arabidopsis.** *Curr Biol* 2007, **17:**520–527.
45. Liu SH, Marks MS, Brodsky FM: **A dominant-negative clathrin mutant differentially affects trafficking of molecules with distinct sorting motifs in the class II major histocompatibility complex (MHC) pathway.** *J Cell Biol* 1998, **140:**1023–1037.
46. Liu SH, Wong ML, Craik CS, Brodsky FM: **Regulation of clathrin assembly and trimerization defined using recombinant triskelion hubs.** *Cell* 1995, **83:**257–267.
47. Amerik AY, Li SJ, Hochstrasser M: **Analysis of the deubiquitinating enzymes of the yeast Saccharomyces cerevisiae.** *Biol Chem* 2000, **381:**981–992.
48. Brandizzi F, Frangne N, Marc-Martin S, Hawes C, Neuhaus JM, Paris N: **The destination for single-pass membrane proteins is influenced markedly by the length of the hydrophobic domain.** *Plant Cell* 2002, **14:**1077–1092.
49. Hunter PR, Craddock CP, Di Benedetto S, Roberts LM, Frigerio L: **Fluorescent reporter proteins for the tonoplast and the vacuolar lumen identify a single vacuolar compartment in Arabidopsis cells.** *Plant Physiol* 2007, **145:**1371–1382.
50. da Silva LL, Taylor JP, Hadlington JL, Hanton SL, Snowden CJ, Fox SJ, Foresti O, Brandizzi F, Denecke J: **Receptor salvage from the prevacuolar compartment is essential for efficient vacuolar protein targeting.** *Plant Cell* 2005, **17:**132–148.
51. Dupre S, Urban-Grimal D, Haguenauer-Tsapis R: **Ubiquitin and endocytic internalization in yeast and animal cells.** *Biochim Biophys Acta* 2004, **1695:**89–111.
52. Galan JM, Haguenauer-Tsapis R: **Ubiquitin lys63 is involved in ubiquitination of a yeast plasma membrane protein.** *EMBO J* 1997, **16:**5847–5854.
53. Geetha T, Jiang J, Wooten MW: **Lysine 63 polyubiquitination of the nerve growth factor receptor TrkA directs internalization and signaling.** *Mol Cell* 2005, **20:**301–312.
54. Springael JY, Galan JM, Haguenauer-Tsapis R, Andre B: **NH4+−induced down-regulation of the Saccharomyces cerevisiae Gap1p permease involves its ubiquitination with lysine-63-linked chains.** *J Cell Sci* 1999, **112**(Pt 9):1375–1383.
55. Chen H, De Camilli P: **The association of epsin with ubiquitinated cargo along the endocytic pathway is negatively regulated by its interaction with clathrin.** *Proc Natl Acad Sci U S A* 2005, **102:**2766–2771.
56. Shahriari M, Keshavaiah C, Scheuring D, Sabovljevic A, Pimpl P, Hausler RE, Hulskamp M, Schellmann S: **The AAA-type ATPase AtSKD1 contributes to vacuolar maintenance of Arabidopsis thaliana.** *Plant J* 2010, **64:**71–85.
57. Humair D, Hernandez Felipe D, Neuhaus JM, Paris N: **Demonstration in yeast of the function of BP-80, a putative plant vacuolar sorting receptor.** *Plant Cell* 2001, **13:**781–792.
58. Phillipson BA, Pimpl P, da Silva LL, Crofts AJ, Taylor JP, Movafeghi A, Robinson DG, Denecke J: **Secretory bulk flow of soluble proteins is efficient and COPII dependent.** *Plant Cell* 2001, **13:**2005–2020.
59. Vitale A, Denecke J: **The endoplasmic reticulum-gateway of the secretory pathway.** *Plant Cell* 1999, **11:**615–628.
60. Barrieu F, Chrispeels MJ: **Delivery of a secreted soluble protein to the vacuole via a membrane anchor.** *Plant Physiol* 1999, **120:**961–968.
61. Höfte H, Chrispeels MJ: **Protein sorting to the vacuolar membrane.** *Plant Cell* 1992, **4:**995–1004.
62. Langhans M, Marcote MJ, Pimpl P, Virgili-Lopez G, Robinson DG, Aniento F: **In vivo trafficking and localization of p24 proteins in plant cells.** *Traffic* 2008, **9:**770–785.

63. Lam SK, Tse YC, Robinson DG, Jiang L: **Tracking down the elusive early endosome.** *Trends Plant Sci* 2007, **12:**497–505.
64. Linder ME, Deschenes RJ: **Palmitoylation: policing protein stability and traffic.** *Nat Rev Mol Cell Biol* 2007, **8:**74–84.
65. Sorek N, Bloch D, Yalovsky S: **Protein lipid modifications in signaling and subcellular targeting.** *Curr Opin Plant Biol* 2009, **12:**714–720.
66. Isono E, Katsiarimpa A, Muller IK, Anzenberger F, Stierhof YD, Geldner N, Chory J, Schwechheimer C: **The deubiquitinating enzyme AMSH3 is required for intracellular trafficking and vacuole biogenesis in Arabidopsis thaliana.** *Plant Cell* 2010, **22:**1826–1837.
67. Bonifacino JS: **The GGA proteins: adaptors on the move.** *Nat Rev Mol Cell Biol* 2004, **5:**23–32.
68. Scott PM, Bilodeau PS, Zhdankina O, Winistorfer SC, Hauglund MJ, Allaman MM, Kearney WR, Robertson AD, Boman AL, Piper RC: **GGA proteins bind ubiquitin to facilitate sorting at the trans-Golgi network.** *Nat Cell Biol* 2004, **6:**252–259.
69. Boehm M, Bonifacino JS: **Adaptins: the final recount.** *Mol Biol Cell* 2001, **12:**2907–2920.
70. Leung KF, Dacks JB, Field MC: **Evolution of the multivesicular body ESCRT machinery; retention across the eukaryotic lineage.** *Traffic* 2008, **9:**1698–1716.
71. Pimpl P, Hanton SL, Taylor JP, Pinto-daSilva LL, Denecke J: **The GTPase ARF1p controls the sequence-specific vacuolar sorting route to the lytic vacuole.** *Plant Cell* 2003, **15:**1242–1256.
72. Helliwell SB, Losko S, Kaiser CA: **Components of a ubiquitin ligase complex specify polyubiquitination and intracellular trafficking of the general amino acid permease.** *J Cell Biol* 2001, **153:**649–662.
73. Soetens O, De Craene JO, Andre B: **Ubiquitin is required for sorting to the vacuole of the yeast general amino acid permease, Gap1.** *J Biol Chem* 2001, **276:**43949–43957.
74. Keleman K, Rajagopalan S, Cleppien D, Teis D, Paiha K, Huber LA, Technau GM, Dickson BJ: **Comm sorts robo to control axon guidance at the Drosophila midline.** *Cell* 2002, **110:**415–427.
75. Pimpl P, Taylor JP, Snowden C, Hillmer S, Robinson DG, Denecke J: **Golgi-mediated vacuolar sorting of the endoplasmic reticulum chaperone BiP may play an active role in quality control within the secretory pathway.** *Plant Cell* 2006, **18:**198–211.
76. Casadaban MJ, Cohen SN: **Analysis of gene control signals by DNA fusion and cloning in Escherichia coli.** *J Mol Biol* 1980, **138:**179–207.
77. Bubeck J, Scheuring D, Hummel E, Langhans M, Viotti C, Foresti O, Denecke J, Banfield DK, Robinson DG: **The syntaxins SYP31 and SYP81 control ER-Golgi trafficking in the plant secretory pathway.** *Traffic* 2008, **9:**1629–1652.
78. Hellens RP, Edwards EA, Leyland NR, Bean S, Mullineaux PM: **pGreen: a versatile and flexible binary Ti vector for Agrobacterium-mediated plant transformation.** *Plant Mol Biol* 2000, **42:**819–832.
79. Sparkes IA, Runions J, Kearns A, Hawes C: **Rapid, transient expression of fluorescent fusion proteins in tobacco plants and generation of stably transformed plants.** *Nat Protoc* 2006, **1:**2019–2025.
80. French AP, Mills S, Swarup R, Bennett MJ, Pridmore TP: **Colocalization of fluorescent markers in confocal microscope images of plant cells.** *Nat Protoc* 2008, **3:**619–628.
81. Abramoff MD, Magelhaes PJ, Ram SJ: **Image processing with ImageJ.** *Biophotonics International* 2004, **11:**36–42.

doi:10.1186/1471-2229-12-164
Cite this article as: Scheuring *et al.*: Ubiquitin initiates sorting of Golgi and plasma membrane proteins into the vacuolar degradation pathway. *BMC Plant Biology* 2012 **12**:164.

Submit your next manuscript to BioMed Central and take full advantage of:

- **Convenient online submission**
- **Thorough peer review**
- **No space constraints or color figure charges**
- **Immediate publication on acceptance**
- **Inclusion in PubMed, CAS, Scopus and Google Scholar**
- **Research which is freely available for redistribution**

Submit your manuscript at
www.biomedcentral.com/submit

BioMed Central

Additional file 1

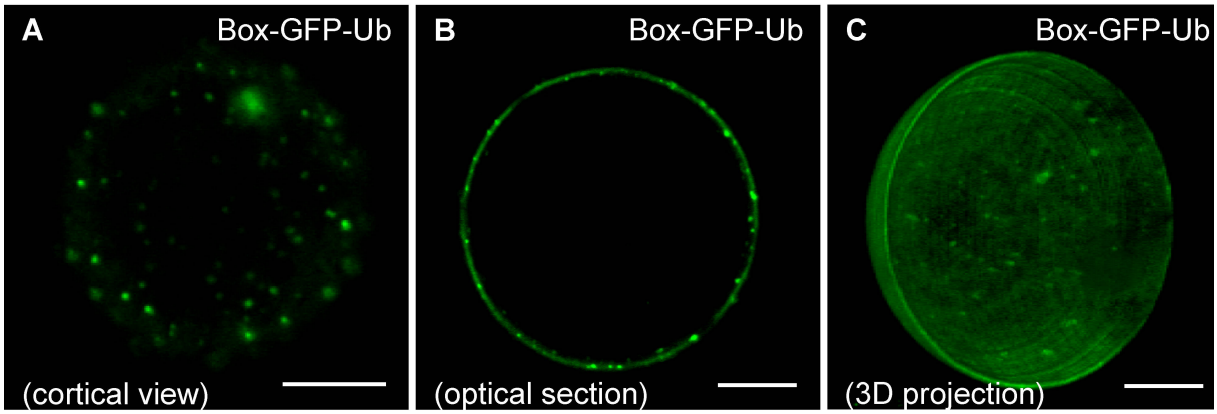

Additional file 1. Analysis of the Box-GFP-Ub expression pattern. Tobacco mesophyll protoplasts were transfected with plasmids encoding for Box-GFP-Ub. The reporter was expressed for 24 h prior to CLSM analysis. Scale bars = 5 µm. Fluorescence signals of a tobacco protoplast are shown in a cortical view (**A**), in an optical section (**B**) and in a 3D projection (**C**), revealing localization of Box-GFP-Ub at the plasma membrane and in punctae.

Additional file 2

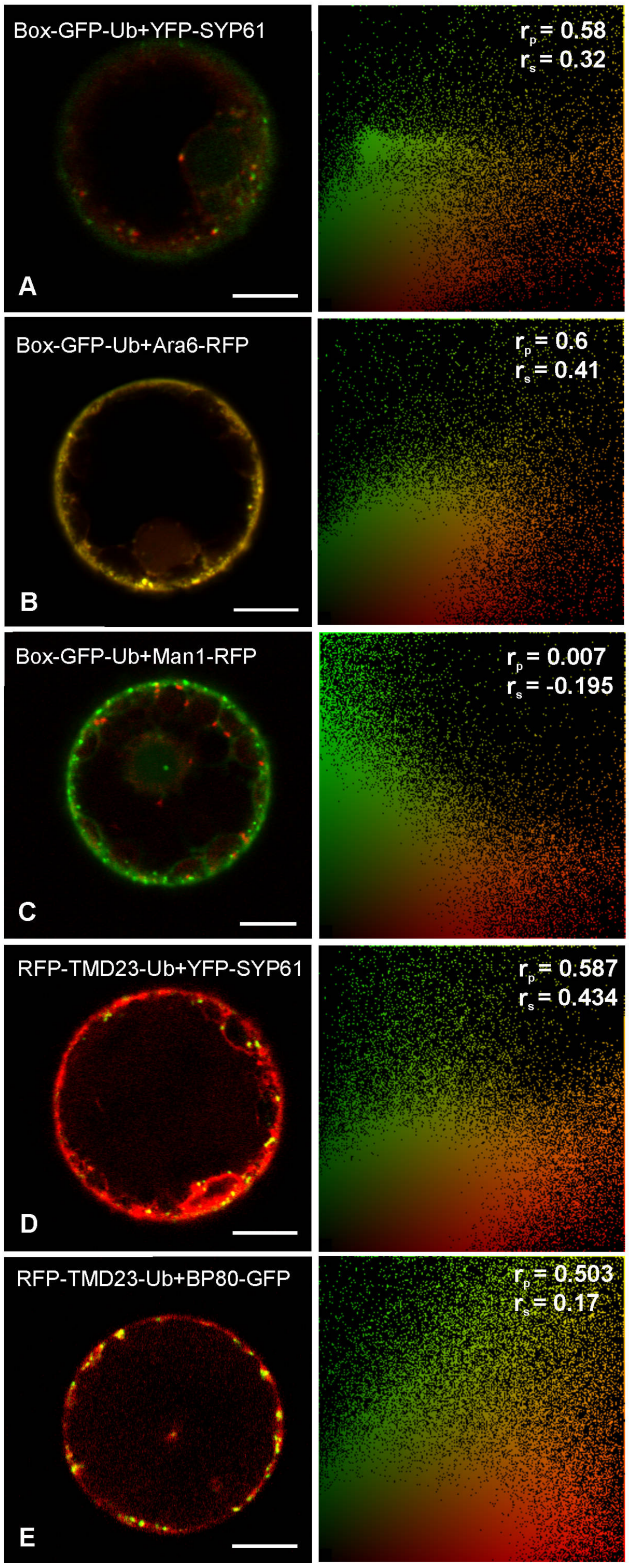

Additional file 2. Quantitative analysis of the localization of Box-GFP-Ub and RFP-TMD23-Ub. Tobacco mesophyll protoplasts were transfected with plasmids encoding for fluorescent markers/ reporters as indicated below. Fluorescent proteins were expressed for 24 h prior to CLSM analysis. Scale bars = 5 µm. For quantification, the PSC coefficients (r_p and r_s) were calculated after analysis of at least 6 representative protoplasts and a minimum of 100 signals. The level of colocalization ranges from +1 for perfect correlation to −1 for negative correlation. The fluorescence values of all pixels across the two channels of all analyzed signals were depicted in a scatterplot. **A**: Box-GFP-Ub and the TGN-marker YFP-SYP61 show r_p and r_s values in a range that indicates colocalization. **B**: While the same is true for coexpression of Box-GFP-Ub and the MVB-marker Ara6-RFP, no positive correlation was observed with the Golgi marker Man1-RFP (**C**). Coexpression of RFP-TMD23-Ub with the same endosomal markers results in similar r_p and r_s values compared to **A-B** as predicted for an endocytic cargo molecule (**D-E**).

Additional file 3

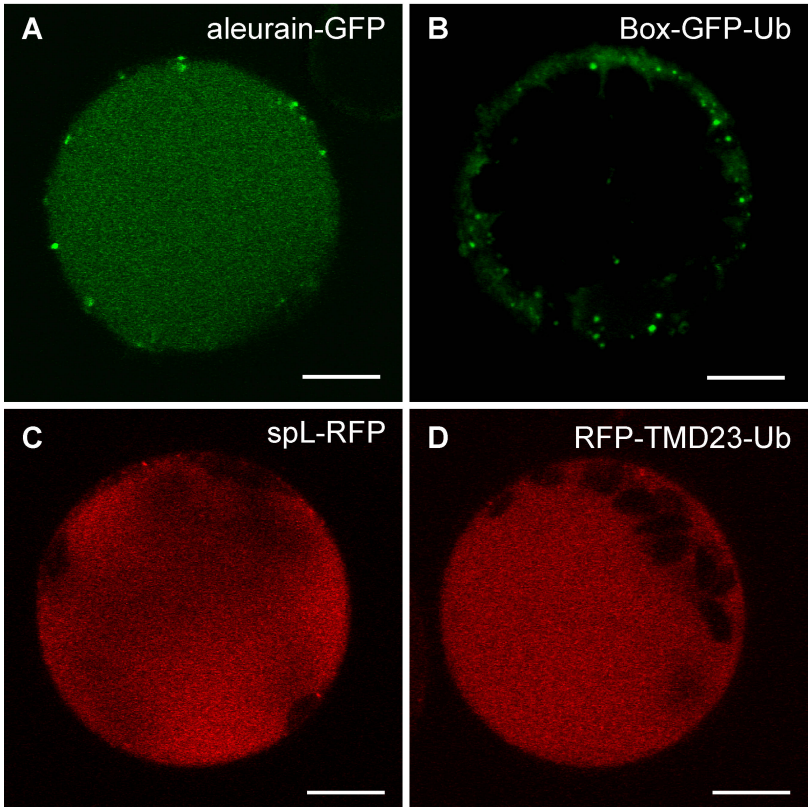

Additional file 3. Comparison of the ubiquitin-modified reporters and soluble vacuolar cargo. Tobacco mesophyll protoplasts were transfected with plasmids encoding for fluorescent markers/ reporters as indicated below. Fluorescent proteins were expressed for 24 h prior to CLSM analysis. Scale bars = 5 µm. Aleurain-GFP is delivered to the lumen of the vacuole (**A**), whereas Box-GFP-Ub reveals punctuate signals in the cortical cytoplasm (**B**). spL-RFP (the linker peptide from proricin fused to RFP, (**C**)) and RFP-TMD23-Ub (**D**) give the same expression pattern being localized to the vacuolar lumen.

Additional file 4

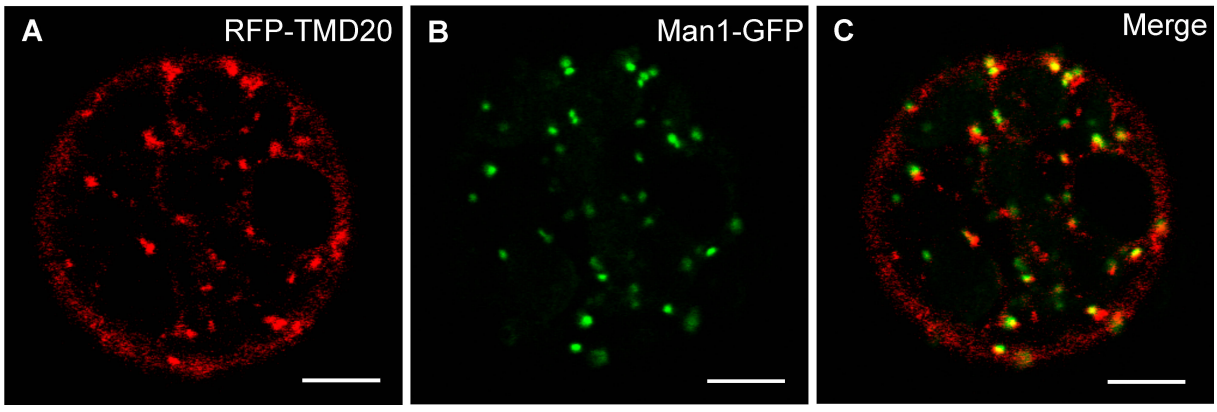

Additional file 4. Analysis of Golgi markers and modified derivatives. Tobacco mesophyll protoplasts were transfected with plasmids encoding for fluorescent markers/reporters as indicated below. Fluorescent proteins were expressed for 24 h prior to CLSM analysis. Scale bars = 5 µm. **A-C**: Coexpression of RFP-TMD20 with the Golgi marker Man1-GFP, demonstrating colocalization of both molecules.

Additional file 5. Table S1. Primers used for cloning.

Oligonucleotide	Sequence (5' – 3' direction)	Template	Recipient vector
Box-GFP-Ub (pDS10):			
Box_*Nco*I_*Cla*I_sense	CATGGCAGTGAAACAAAAGGAGAAGAAGAAGAAGCAGAAGCCTCGAAGCGGATGTCTCTCAAACATTCTGTGTGGGAAGAATGGAT	Complementary to oligo 2)	pAmy-HDEL
Box_*Nco*I_*Cla*I_antisense	CGATCCATTCTTCCCACACAGAATGTTTGAGAGACATCCGCTTCGAGGCTTCTGCTTCTTCTTCTTCCTTTTGTTTCACTGC	Complementary to oligo 1)	pAmy-HDEL
GFP_*Cla*I_sense	TAGTGGATCGATGGTGAGCAAGGGCGAGGA	pSN9	pAmy-HDEL
GFP_*Not*I_antisense	CCTATCGCGGCCGCCCTTGTACAGCTCGTCCATGC	pSN9	pAmy-HDEL
Ub_*Not*I_sens	AGTCTAGCGGCCGCATGCAAATCTTCGTGAAAAC	cDNA	pAmy-HDEL
Ub_*Xba*I_antisense	CTAGTCTAGATTATCCACCACGAAGACGGA	cDNA	pAmy-HDEL
Box-GFP-UbΔGG (pDS21):			
Box_*Nco*I_sense	CGAGCTCCATGGCAGTGAAACAAAAGG	pDS10	pAmy-HDEL
UbΔGG_*Bam*HI_antisense	CTCTAGTGGATCCTCAACGAAGACGGAGGACGAGAT	pDS10	pAmy-HDEL
Box-GFP (pDS9):			
Box_*Nco*I_sense	CGAGCTCCATGGCAGTGAAACAAAAGG	pDS10	pAmy-HDEL
GFP_*Bam*HI_antisense	TCGCGGGATCCTTACTTGTACAGCTC	pDS10	pAmy-HDEL
GFP-Ub (pFK17):			
GFP_*Cla*I_sense	TAGTGCATCGATGGTGAGCAAGGGCGAGG	pDS10	pPP11
Ub_*Bam*HI_antisense	AGTCGCGGATCCTTAACCACCTCTTAAACGG	pDS10	pPP11
RFP-TMD20 (pFK23):			
SP_*Cla*I_sense	AGTCTAATCGATGAGGCTTTGTAAATTCACAGCTC	TM20	pPP11
TMD_*Bam*HI_antisense	AGTCTAGGATCCTTAAGATCTCTTCCTGCCGACGA	TM20	pPP11
RFP-TMD20-Ub (pFK24):			
Ub_*Bgl*II_sense	AGTCTGAGATCTATGCAAATCTTCGTGAAAAC	pDS10	pFK23
Ub_*Bam*HI_antisense	AGTCTAGGATCCTTATCCACCACGAAGACGGA	pDS10	pFK23
RFP-TMD20-UbΔGG (pFK25):			
Ub_*Bgl*II_sense	AGTCTGAGATCTATGCAAATCTTCGTGAAAAC	pDS10	pFK23
UbΔGG_*Bam*HI_antisense	AGTCTAGGATCCTCAACGAAGACGGAGGACGAGAT	pDS10	pFK23
RFP-TMD23 (pFK12):			
SP_*Cla*I_sense	AGTCTAATCGATGAGGCTTTGTAAATTCACAGCTC	TM23	pPP11
TMD_*Bam*HI_antisense	AGTCTAGGATCCTTAAGATCTCTTCCTGCCGACGA	TM23	pPP11

RFP-TMD23-Ub (pFK13):

Ub_*Bgl*II_sense	AGTCTGAGATCTATGCAAATCTTCGTGAAAAC	pDS10	pFK12
Ub_*Bam*HI_antisense	AGTCTAGGATCCTTATCCACCACGAAGACGGA	pDS10	pFK12

RFP-TMD23-UbΔGG (pFK19):

Ub_*Bgl*II_sense	AGTCTGAGATCTATGCAAATCTTCGTGAAAAC	pDS10	pFK12
UbΔGG_*Bam*HI_antisense	AGTCTAGGATCCTCAACGAAGACGGAGGACGAGAT	pDS10	pFK12

RFP-Hub1 (pFK26):

mRFP_*Nhe*I_sense	AGTCTAGCTAGCATGGCCTCCTCCGAGGACG	pFK13	pGD5
mRFP_*Nco*I_antisense	AGTCTACCATGGCTCCAGTACTGTGGC	pFK13	pGD5
CHub_*Nco*I_sense	AAGCATCCATGGGATTCAAGAAGTTTAACTTAAA	cDNA	pGD5
CHub_*Bam*HI_antisense	TTCCCAGGATCCTTAGTAGCCGCCCATCGGTG	cDNA	pGD5

Modifications in pGreenII, generating plasmid pCN1

(1) Point mutation in the nos-Kan selection cassette to remove intrinsic *Nhe*I site:

nos_Prom_M_sense	AAGAAATATTTGCTATCTGATAGTGACCTTA	pGreenII 0029
nos_Prom_M_antisense	TAAGGTCACTATCAGATAGCAAATATTTCTT	pGreenII 0029

(2) Deletion of the multiple cloning site:

pGIIBB_*Hind*III_sense	CGCCACAAGCTTGGAGCTCCAGCTTTTG	pGreenII 0029, modified in (1)
pGIIBB_*Eco*RI_antisense	GGTACGGAATTCGCCCTATAGT	pGreenII 0029, modified in (1)

9.3 Vacuolar sorting receptors transport ligands from the ER and the Golgi to the TGN/EE

Fabian Künzl, Simone Früholz, Florian Fäßler, Beibei Li, and Peter Pimpl

(Submitted manuscript)

Vacuolar sorting receptors transport ligands from the ER and the Golgi to the TGN/EE

Fabian Künzl, Simone Früholz, Florian Fäßler, Beibei Li and Peter Pimpl*

Center for Plant Molecular Biology (ZMBP), University of Tübingen, Germany

* **Corresponding author:**
Peter Pimpl, ZMBP, University of Tübingen, Auf der Morgenstelle 32, D-72076 Tübingen
Tel: +49-7071-2978889
Fax: +49-7071-295797
e-mail: peter.pimpl@zmbp.uni-tuebingen.de

Running title: Compartment-specific analysis of VSR-ligand interaction

Abstract

Sorting of soluble vacuolar proteins is of vital importance for plant cells and requires that vacuolar sorting receptors (VSRs) bind and release their cargo ligands. However, it is controversial, where in the endomembrane system these interactions occur. Here, we present an *in vivo* analysis of VSR-ligand interactions for all compartments of the vacuolar transport route. For this, we have developed compartment-specific VSR sensors and performed FRET-FLIM analysis to monitor for ligand binding. We show that VSRs bind ligands in the ER and in the Golgi, but not in the *trans*-Golgi network/early endosome (TGN/EE) nor in multivesicular late endosomes (MVBs/LEs). This implies that *post*-TGN/EE trafficking of ligands towards the vacuole is VSR-independent. We verify this by demonstrating that also non-VSR-ligands are delivered to the vacuole from the TGN/EE after endocytic uptake. Thus, we postulate that vacuolar sorting receptors transport ligands from the ER and the Golgi to the TGN/EE, followed by a VSR-independent default flow onwards to the vacuole.

Introduction

Soluble vacuolar proteins and their corresponding vacuolar sorting receptors (VSRs) were identified in plants more than twenty years ago[1-4]. However, the mechanism of VSR-mediated sorting as implemented in the plant endomembrane system[5] is still not yet understood. Vacuolar sorting signals of soluble plant proteins are encoded by short peptide motifs within the primary amino acid sequence[1-3]. The first VSR was isolated from detergent-solubilised Golgi and clathrin-coated vesicle (CCV) fractions at neutral pH using synthetic peptides containing sorting signals[5]. VSRs are type I transmembrane proteins encoded by a gene family unique to plants[6-8]. They bind ligands via a structured N-terminal luminal binding domain (LBD) consisting of a protease associated domain, a central domain and three epidermal growth factor repeats[9, 10]. VSRs also carry sorting signals for their own transport in the cytosolic C-terminus[11-13]. Based on assumed similarities to the lysosomal sorting machinery in mammals concerning receptor localisation and pH dependency of ligand binding, it was proposed almost twenty years ago that VSR-mediated sorting in plants occurs via CCV-facilitated transport from the *trans*-Golgi to a prevacuolar compartment, where ligands dissociate due to the lower pH.

In the intervening years, major discoveries have challenged this model: the *trans*-Golgi network (TGN) in plants was identified as the early endosome (EE)[14, 15] that is distinct from the Golgi stack[16]. This hybrid structure (TGN/EE) has now been shown to be the most acidic compartment *en route* to the vacuole[17-19]. The TGN/EE harbours the retromer complex necessary for recycling of the VSRs[20, 21]. Most important, however, was the demonstration that the TGN/EE is the source for the biogenesis of the prevacuolar compartment, the multivesicular late endosome (MVB/LE), which confers transport by fusion with the vacuole[22]. These recent findings still await integration into the proposed concept of VSR-mediated sorting. In order to determine the compartments that constitute the framework for the bi-directional receptor transport, it is of paramount importance to firstly identify the locations at which VSRs bind or release their ligands.

To this end, we have developed genetically encoded VSR sensors that allow for non-invasive compartment-specific detection of VSR-ligand interactions *in vivo*. Hereto, we assembled VSR sensors from a soluble LBD and compartment-specific green fluorescent protein (GFP)-containing membrane markers via a GFP-binding V_HH domain of a heavy-chain antibody from *Camelidae* sp., termed nanobody[23]. We

monitored for VSR-ligand interaction using red fluorescent protein (RFP) ligands in a comprehensive approach, combining localisation analysis with Förster resonance energy transfer-fluorescence lifetime imaging microscopy (FRET-FLIM). With this novel strategy, we were able to show that VSRs bind ligands only in the ER and in the Golgi stack, but not in *post*-Golgi compartments such as the TGN/EE or the MVB/LE. This suggests that *post*-TGN/EE trafficking of soluble proteins towards the vacuole is independent of VSR-ligand interactions. Confirmation of this conclusion was provided by identifying the vacuole as being the default location for soluble proteins of the endocytic route that merges with the biosynthetic vacuolar route at the TGN/EE. Consequently, we postulate a two-stage process for vacuolar transport of soluble proteins. Firstly, VSRs confer the transport of ligands to the TGN/EE, followed by a VSR-independent default flow onwards to the vacuole via budding of MVBs/LEs and their fusion with the vacuole.

RESULTS

Compartment-specific targeting via nanobody-mediated protein assembly

The challenge in using genetically encoded reporters for non-invasive compartment-specific analysis *in vivo* is to achieve their precise targeting[24]. This is particularly true for the analysis of the Golgi stack, the TGN/EE and the MVB/LE, since sorting signals specific for these compartments are largely unknown. A common targeting strategy is the use of translational fusions between reporter domains and membrane marker proteins. This strategy is however subject to topology restrictions of the fusion partners. In this regard, the N-terminal LBD of the type I VSRs can only be fused to type I membrane marker proteins[25], which are known only for the ER and MVB/LE but neither for the Golgi stack nor the TGN/EE. To overcome these constraints, we have developed a targeting strategy based on nanobody-mediated protein assembly. To demonstrate successful targeting, we have generated a construct consisting of a fluorescent LBD fused to an anti-GFP nanobody (Nb)[26] as a soluble VSR (LBD-RFP-Nb) that can be used in combination with epitope (GFP)-tagged membrane marker proteins to assemble compartment-specific VSR sensors *in vivo* (Fig. 1a). To rule out that the soluble VSR bears intrinsic sorting signals that compromise targeting, we first analysed its transport properties (Fig. 1b-d). Fluorescence signals of the LBD-RFP-Nb are largely absent in cells but appear only when secretion out of the ER is prevented by Sec12 overproduction[27]. To test for nanobody-mediated protein

assembly in all compartments *en route* to the vacuole, we have expressed the soluble VSR with membrane anchors for the ER, the Golgi, the TGN/EE and the MVB/LE (Fig. 1e-i). In all cases, strong red fluorescence signals from the LBD-RFP-Nb become detectable and colocalised precisely with the respective anchor due to nanobody-epitope interaction at the inner leaflet of the compartmental membrane. This is most evident for the colocalising signals at the ring-shaped periphery of the Golgi[28] (Fig. 1f) and at the ring-like MVB/LE structures after treatment with the drug wortmannin (WM)[29] (Fig. 1i).

The nanobody-epitope interaction persisted in all compartments tested, irrespective of their individual biochemical properties. This is even true for the vacuole. Here, the interaction is visualised by the emergence of vacuolar signals from the MVB/LE anchor GFP-BP80. In this case, the nanobody stabilises the GFP core, a vacuolar degradation product of the proteolytically cleaved GFP-domain of the anchor, which otherwise would escape detection (Supplementary Fig. 1).

Assembled VSR sensors possess ligand-binding competence

We have generated a soluble LBD-Nb fusion protein for coexpression with the GFP-based membrane anchors. Due to the nanobody-epitope interaction, both molecules constitute a green fluorescent membrane protein, employed as a compartment-specific VSR sensor. Usage of these sensors together with the RFP-tagged ligand Aleu-RFP allows to test for receptor-ligand interactions via ligand localisation and FRET-FLIM as an intensity-independent approach to detect FRET[30]. In these experiments, binding of Aleu-RFP to the LBD triggers close proximity of both fluorophores and thus FRET becomes possible. In this situation, excited-stage energy from the donor GFP upstream of the LBD is transferred to the acceptor RFP of the ligand, thereby reducing the fluorescence lifetime of GFP[30]. Consequently, lack of ligand binding does not alter the fluorescence lifetime (Fig. 2a).

During the course of VSR-mediated sorting, ligand binding is reversible. Therefore, we expected to identify compartments *en route* to the vacuole that either support or restrict ligand binding. To rule out that the experiments were compromised by differences in the ligand-binding competence of the LBD-Nb in the context of different membrane anchors, we first confirmed the ligand-binding capability of all VSR sensors *in vitro* (Fig 2b). For this, we assembled the sensors in the ER, the Golgi, the TGN/EE and the MVB/LE (Supplementary Fig. 2) and immunoprecipitated them by

using GFP antibodies in bead-binding assays. For direct comparison of their ligand-binding capabilities, we incubated the bead-bound VSR sensors with the ligand Aleu-RFP[31] at binding conditions[4]. In all cases, Aleu-RFP was coprecipitated while secretory Sec-RFP in control experiments was not. This demonstrates that all VSR sensors possess ligand-binding competence.

VSR-ligand interaction occurs in the ER but not in the MVB/LE

We have recently shown that placement of LBDs in the lumen of the ER triggers accumulation of ligands, suggesting VSR-ligand binding[25]. Consistently, assembly of VSR sensors in the ER also retains the ligand Aleu-RFP, preventing its delivery to the vacuole (Fig. 3a,b). To test whether this accumulation is indeed due to VSR-ligand interaction, we have performed FRET-FLIM. The analysis revealed a significant reduction of the GFP lifetime within the VSR sensor in the presence of the ligand, as readout for the occurring VSR-ligand interaction. Fluorescence lifetime was not influenced in control experiments either by the non-ligand Sec-RFP or in the absence of the LBD (Fig. 3c and Supplementary Fig. 3a). This demonstrates that the accumulation of ligands in the ER is due to interaction with the VSR sensors and thus identifies the ER as a compartment that promotes VSR-ligand binding.

Receptor-mediated transport of ligands is completed by their release. With the MVB/LE being the last morphologically characterised compartment *en route* to the vacuole, ligands should be released from their receptors at the latest in this compartment. At steady-state conditions, Aleu-RFP localises to the MVB/LE in addition to the vacuole, which is not altered by the LBD-Nb after sensor assembly (Fig. 3d,e). Therefore, it is difficult to judge VSR-ligand interactions in this compartment solely by localisation. FRET-FLIM analysis however revealed that these colocalising ligands do not reduce the fluorescence lifetime of the VSR sensor (Fig. 3f and Supplementary Fig. 3b). Reduction of lifetime can only be triggered in control experiments by the direct attachment of RFP via the nanobody (LBD-RFP-Nb, compare to Fig. 1h). This demonstrates that the VSR sensors do not bind ligands in this compartment. To extend the analysis, we applied the drug wortmannin (WM) which induces enlargement of MVBs/LEs by homotypic fusion[29]. The resulting ring-like structures now reveal a differential distribution of fluorescence, with signals from the VSR sensor being present at the limiting membrane while signals from Aleu-RFP locate to the compartmental lumen (Fig 3g). This also suggests that ligands do not

bind to VSRs in this transit compartment towards the vacuole, since this would indeed require colocalisation (compare to Fig. 1i). Together, these data demonstrate that ligands do indeed interact with the VSR sensors in the ER and that they do not interact in the MVB/LE. These findings furthermore reveal that only a combination of localisation analysis and FRET-FLIM allows assessing whether a given compartment supports or restricts VSR-ligand binding.

VSR-ligand interaction occurs in the Golgi but not in the TGN/EE

Having identified the ER as a compartment that supports ligand binding and the MVB/LE as compartment that does not, we next tested the Golgi and the TGN/EE for possible VSR-ligand interactions. The Golgi marker Man1-GFP never colocalises with Aleu-RFP, whose punctate signals represent MVBs/LEs (Fig. 4a, compare to Fig. 3d,g). Assembly of VSR sensors in the Golgi however causes colocalisation of Aleu-RFP with all GFP-labelled VSR sensors (Fig. 4b). These colocalising signals appear in addition to the RFP signals from punctate MVBs/LEs and the vacuole. The redistribution of Aleu-RFP to the Golgi can be emphasised by the employment of transport competitors for the endogenous VSRs[32], which reduce vacuolar delivery. The competitor HA-BP80, a HA-epitope-tagged LBD-deletion mutant of BP80, reduces RFP signals in the MVB/LE and in the vacuole, but does not alter the Golgi-colocalisation of the VSR sensors with Aleu-RFP (Fig. 4c). The colocalising signals at the inner leaflet of the Golgi membrane are similar to the signals previously seen for the LBD-RFP-Nb targeted to this compartment (compare to Fig. 1f). This suggests an interaction between the sensors and ligands. FRET-FLIM analysis revealed that the ligand Aleu-RFP significantly reduces the fluorescence lifetime of the VSR sensor (Fig. 4d and Supplementary Fig. 4a). This reduction depends on the presence of the LBD, demonstrating that the Golgi-localisation of Aleu-RFP is caused by interaction with the VSR sensor.

The situation in the TGN/EE yields another picture. Here, assembly of VSR sensors does not cause colocalisation of the ligand Aleu-RFP (Fig. 5a-c), questioning the occurrence of VSR-ligand interactions in this compartment. FRET-FLIM analysis of the TGN/EE-localising VSR sensor revealed that Aleu-RFP did not influence the fluorescence lifetime of the sensor, a situation identical to control experiments where the non-ligand Sec-RFP was used instead (Fig. 5d, Supplementary Fig. 4b). FLIM data of the assembled VSR sensors in different compartments revealed different

lifetimes, which are longest in the ER and shortest in the TGN/EE. Fluorescence lifetime depends on the pH[33] and therefore reflects the relative compartmental pH, which is the highest in the ER (pH 7.1-7.5) and the lowest in the TGN/EE (6.3-5.6)[17-19] To demonstrate that protein-protein interactions can shorten the lifetime even in the TGN, we attached the red fluorescent LBD (LBD-RFP-Nb) via nanobody-epitope interaction to the membrane anchor SYP61-GFP. This control confirmed the assembly of VSR sensors in the TGN/EE as illustrated in Fig. 1g and proves that the principle of FRET-FLIM interaction analysis is also applicable to this compartment (Fig. 5d).

Together, these data favour the idea that VSRs and ligands do not interact in the TGN/EE. Consequently, it is tempting to speculate that the VSRs in this compartment have already released their ligands. This however would imply that these VSRs did bind ligands upstream of the TGN/EE. To verify this hypothesis, we blocked the arrival of the TGN/EE-targeted VSR sensor with the drug brefeldin A (BFA), causing retention of sensors and ligands in the ER (Fig. 5e). BFA-induced ER localisation causes a drastic increase of the fluorescence lifetime of SYP61-GFP-based sensors, with values being identical to those of ER-targeted GFP-CNX-based sensors (compare to Fig. 3c). Under these conditions, coexpressed Aleu-RFP strongly reduced the fluorescence lifetime of the SYP61-GFP-based sensor, thus demonstrating ligand binding. This does not occur in the presence of Sec-RFP (Fig. 5f, Supplementary Fig. 4b). The capability of the TGN/EE-targeted VSR sensor to bind ligands in the ER was furthermore confirmed by coimmunoprecipitation experiments (Fig. 5g). Here, only BFA-triggered ER-localisation of the VSR sensor resulted in coimmunoprecipitation of the ligand Aleu-RFP, which does not occur if the sensor localises to the TGN/EE. (Fig. 5g, compare to Fig.3a-c). Altogether, our data demonstrate that VSRs bind their ligands very early in the secretory pathway and release ligands upon arrival in the TGN/EE.

VSRs do not mediate *post*-TGN/EE transport of soluble proteins to the vacuole

The compartment-specific analysis identified the ER and the Golgi as compartments that promote VSR-ligand binding while the TGN/EE and the MVB/LE restrict this interaction. Consequently, this suggests that VSRs do not contribute to the *post*-TGN/EE transport of soluble proteins towards the vacuole. Receptor-independent

transport from the TGN/EE implies that this route does not require sorting signals and is thus the default route for all soluble proteins.

To test for this hypothesis, we have developed a strategy to analyse *post*-TGN/EE transport of soluble proteins lacking vacuolar sorting signals. Since these signals are required for the VSR-mediated sorting to the TGN/EE via the biosynthetic pathway, we took advantage of the early endosomal properties of the TGN/EE and targeted soluble proteins to the TGN/EE via the endocytic route. For these experiments, we used protoplast-secreted triple (3x) RFP from the culture medium of 3xRFP-secreting cells as a fluorescent reporter protein for endocytic uptake. The use of a reporter that was secreted by protoplasts ensures that this reporter does neither carry cryptic intrinsic vacuolar sorting signals nor signs of damage that could possibly trigger vacuolar degradation via mechanisms of quality control later on [34, 35].

Incubation of cells expressing cytosolic GFP (Cyt-GFP) with the protoplast-secreted 3xRFP results in vacuolar delivery of this reporter (Fig. 6a). Consequently, the endocytosed reporter is recovered as soluble protein from cellular extracts and does not cofractionate with membranes (Fig 6b). To prove that the reporter reaches the vacuole via the TGN/EE and the MVB/LE, we have used the protoplast-secreted anti-GFP nanobody fusion 3xRFP-Nb, which is also delivered to the vacuole in endocytic uptake assays (Fig. 6c). This time however, we used cells expressing GFP-membrane anchors either at the cell surface (SYP132-GFP), the TGN/EE (SYP61-GFP) or the MVB/LE (GFP-BP80). In all cases, the reporter 3xRFP-Nb colocalised with the respective membrane anchor due to nanobody-mediated assembly (Fig. 6d-f), demonstrating its transport via the endocytic route. Together, this shows that soluble proteins reach the vacuole from the TGN/EE independent of sorting receptors, defining the vacuole as being the default location of *post*-TGN/EE transport of soluble proteins.

Discussion

We have developed novel VSR sensors for analysis of VSR-ligand interactions. These sensors assemble by a nanobody-triggered interaction from a soluble LBD-nanobody fusion protein with an epitope-tagged compartment-specific membrane anchor. This allows for the first time the direct linkage of the type I LBD with type-II membrane anchors for the Golgi and the TGN/EE, thus enabling the use of the very same sensing protein at different locations, rather than employing VSR trafficking

mutants that exhibit altered distributions [13, 18]. We demonstrate that VSR-ligand interactions occur in the ER and in the Golgi, but do not occur in the TGN/EE nor in the MVB/LE (Fig. 6g). Our data demonstrating ligand binding in the ER and in the Golgi are in agreement with previous observations showing that LBDs, when fused to the ER retrieval signal HDEL[32, 36] or to the ER-membrane protein calnexin[25], cause the accumulation soluble vacuolar proteins. Moreover, VSRs have been isolated from solubilised Golgi fractions with immobilised sorting signals at neutral pH[4] which is also found in these compartments[17, 18].

Release of ligands was suggested to occur at low pH[4] and in combination with the initial localisation of VSRs at the Golgi and at prevacuoles it was suggested that the VSR transports the ligands between these compartments[7]. Since then, localisation analysis was refined and VSRs were found in *trans*-Golgi cisternae[37, 38], the TGN/EE[20, 39], the MVB/LE[20, 29, 40] and even the PM[13, 41], implying that location alone is insufficient to judge the ligand-binding status of the VSR[5].

Our data show ligand binding of the SYP61-GFP-based sensor *in vitro* and *in vivo*. This however strictly depends on its intracellular localisation, with demonstrated binding in the ER but the complete lack thereof in the TGN/EE, suggesting that ligands have been released. Recently, the pH values of intracellular compartments have become available[17-19], identifying the TGN/EE with pH values ranging from 6.3 - 5.5 as being the most acidic compartment of the vacuolar route and the MVB/LE possessing either similar[17] or slightly more alkaline pH[18]. Another key factor modulating VSR-ligand interaction is calcium[42], possibly due to conformational changes induced by Ca^{2+}-binding to an EGF repeat within the LBD[9, 42]. Ca^{2+} facilitates ligand binding and prevents release, even at a pH of 4[42], showing that Ca^{2+} supports ligand binding at unfavourable pH[5]. Experimental data on compartmental Ca^{2+} concentrations are scarce. The presence of Ca^{2+} pumps in the ER and the tonoplast suggests that concentrations are the highest there, with an estimate from 50 µM to 5 mM[43], falling off to the nanomolar range in compartments en route to the vacuole like the Golgi [44]. Together, this suggests that VSR-mediated sorting depends on an intricate interplay between pH, Ca^{2+} and possibly other factors that differ between the compartments in order to trigger ligand binding and release.

Release of ligands in the TGN implies that further anterograde transport to the vacuole is independent of VSRs. This is in full agreement with the TGN-localisation of the VSR-recycling retromer complex[20, 21] and the observation that MVBs/LEs

originate at the TGN/EE[22] and fuse with the vacuole. This scenario does not necessitate VSRs for the ligands to be exported from the TGN/EE. Consequently, all soluble proteins would share the fate of passive vacuolar delivery via the MVB/LE. Indeed, our endocytic uptake assays with secreted non-ligand proteins revealed vacuolar delivery, which occurred via the TGN/EE and the MVB/LE, thus confirming the operation of such a passive vacuolar delivery. Together with previously reported findings that polystyrene beads also reach the vacuole via the endocytic route [45], it seems justified to postulate that the vacuole is the default location for soluble proteins of the endocytic route, which consequently does not require a receptor-mediated transport step between the TGN/EE and the MVB/LE for vacuolar delivery.

METHODS

Plant materials and growth conditions. Tobacco plants (*Nicotiana tabacum* L. cv. Petit Havana SR1) were grown under sterile conditions on Murashige and Skoog (MS) medium supplemented with 2% (w/v) sucrose in a controlled room at 22 °C and long-day illumination (16 h light).

Drugs and cellular treatments. The following drugs were used: wortmannin (WM) from Calbiochem (30 µM from a 20 mM DMSO stock solution), latrunculin B (LatB) from Sigma-Aldrich (4 µM from a 4 mM DMSO stock solution) and brefeldin A (BFA) from Life Technologies (50 µM from a 50 mM EtOH:DMSO 1:1 stock solution). WM was applied 1 h prior to CLSM. LatB was applied to reduce Golgi and TGN/EE movement 1 h prior to FRET-FLIM. Cells were supplemented with BFA directly after transfection and incubated overnight.

Plasmid constructs. Established plasmids were used encoding for markers or effectors as indicated: Cyt-GFP, ERD2-CFP [46], Man1-RFP [47] and Sec12 [48]. All DNA manipulations were performed according to established procedures using *Escherichia coli* strain MC1061 [49] for plasmid amplifications. Coding sequences were amplified by PCR or subcloned from established plasmids as indicated below. Recipient vectors were either pUC-based [48] or pGreenII binary plasmids [35], both driven by the 35S promoter of cauliflower mosaic virus. New strategic restriction sites were introduced if necessary. Sites and primers used for cloning of all constructs are listed in Supplementary Table 1. The anti-GFP nanobody (Nb) coding sequence was

generated by reverse translation of the corresponding amino acid sequence [26] into genetic code optimised for *Arabidopsis thaliana*-specific codon usage (EMBOSS Backtranseq, www.ebi.ac.uk). The nucleotide sequence was chemically synthesised to include N-terminal HA and C-terminal 6x His tags, a stop codon and flanking *Kpn*I and *BamH*I restriction sites (GeneArt Gene Synthesis). Based on this sequence, the following C-terminal fusions were generated: LBD-RFP-Nb was assembled by ligation of the N-terminal luminal binding domain (LBD) from AtVSR4 (GenBank accession NM_127036), monomeric RFP [35] and the Nb sequence. The derivatives LBD-Nb, ΔLBD-Nb and Cyt-RFP-Nb were generated by deletions of the RFP and/or the LBD from LBD-RFP-Nb. For compartment-specific anchoring of the Nb fusions, established compartmental markers were used, in which fluorophores had been uniformly replaced by enhanced GFP (EGFP, GenBank accession BAQ19368) to warrant comparable fluorescence lifetimes. These markers have been described previously: GFP-CNX [32], Man1-GFP [47] and GFP-BP80 [32]. SYP61-GFP and SYP132-GFP derived from YFP-SYP61 [20] and RFP-SYP132 [50], respectively, which were converted to C-terminal fusions to expose the EGFP either in the TGN/EE lumen (SYP61-GFP) or on the extracytosolic side of the plasma membrane (SYP132-GFP). Soluble fluorescent reporters used in this study were based on monomeric RFP [35] and are as follows: Sec-RFP and Cyt-RFP were amplified to either contain or lack the N-terminal signal peptide of sweet potato sporamin [32]. Aleu-RFP was generated by exchanging fluorophores in the vacuolar ligand Aleu-GFP [31]. The reporters 3xRFP and 3xRFP-Nb were cloned for endocytic uptake experiments. They were designed to have the N-terminal signal peptide of Sec-RFP (see above) in order to be secreted into the culture medium for isolation. The effector molecule HA-BP80 was constructed by replacing EGFP in GFP-BP80 (see above) for a HA tag. Fluorophores of some established compartmental markers had to be exchanged for colocalisation studies: GFP-CNX [32] was converted to RFP-CNX, YFP-SYP61 [20] was converted to GFP-SYP61 and RFP-SYP61, and GFP-BP80 [32] was converted to RFP-BP80. Correct localisation of all newly generated marker/reporter fluorophore fusions was confirmed by coexpression with the original markers.

Isolation of protoplasts and gene expression. Tobacco mesophyll protoplasts were isolated from leaves of 6- to 8-week-old plants and transfected via electroporation as described previously [51] using a square wave pulse generator EPI

2500 (Dr. L. Fischer, Heidelberg, www.electroporation.eu). Unless otherwise stated, 10-50 ng/µL plasmid DNA were used for transfection and protoplasts were incubated for 18 to 24 h at 25 °C in the dark.

Biosynthesis of fluorescent reporters for endocytic uptake.
The reporters 3xRFP and 3xRFP-Nb were synthesised as secretory proteins by transient gene expression in protoplasts. After expression, the reporter-containing culture medium was harvested. To obtain reporter solutions, devoid of synthesising cells, the medium was sonicated and cleared by centrifugation. For endocytic uptake, populations of protoplasts expressing GFP markers were supplemented with the cleared reporter-containing culture medium after their transfection and incubated for 24 h. This strategy warrants that detected intracellular RFP fluorescence can only result from endocytic uptake but is not due to contamination with the synthesising cell population.

Confocal microscopy. Imaging was performed with a Leica TCS SP8 confocal laser scanning microscope equipped with a x63 (1.2 NA) water immersion objective. The following fluorophores were excited (ex) and emission (em) was detected by line switching in the sequential mode using HyD detectors: CFP (ex: 458 nm, em: 464-525 nm), GFP (ex: 488 nm, em: 496-525 nm), and RFP (ex: 561 nm, em: 569-636 nm). Pinholes were adjusted to 1 Airy unit for each wavelength. *Post*-acquisition image processing was performed using Adobe Photoshop CS3 (v10.0.1) and CorelDraw X6 (v16.0.0.707).

Statistical analysis of CLSM localisation data. The PSC colocalisation plug-in [52] for ImageJ (v1.41o) was used to calculate the linear Pearson's correlation coefficient (r_p) and the nonlinear Spearman's rank correlation coefficient (r_s) of red and green fluorescent signals. Both tests produce values in the range of -1 (negative correlation) to +1 (positive correlation), with 0 indicating no discernible correlation. Masking of regions of interest was performed with the ImageJ brush tool as described [52]. The threshold level, under which pixels were treated as background noise, was set to 10. For statistics, correlation coefficients of 10 individually analysed cells per experiment were considered and are given as mean values with standard

errors of the mean. Statistical significance was calculated using ANOVA, followed by Tukey's HSD test.

Fluorescence lifetime imaging microscopy (FLIM). Data acquisition was performed with a Leica TCS SP8 combined with a PicoHarp 300 TCSPC module and a PDL 808 Sepia multichannel picosecond pulsed diode laser driver (PicoQuant). For GFP excitation, a 470-nm laser (LDH-P-C-470B) was used at a pulse frequency of 40 MHz and emission was recorded at 496-525 nm by time-correlated single photon counting (TCSPC). Data analysis was performed with PicoQuant's SymPhoTime software (v5.3.2.2) according to the manufacturer's instructions. To calculate fluorescence lifetimes, TCSPC histograms were reconvoluted with an instrumental response function (IRF) and fitted against a bi-exponential decay function. All fluorescence signals of compartmental markers were specifically selected with the software's region of interest (ROI) selection tools to avoid potential miscalculations caused by background noise. In case of GFP-BP80, vacuolar background fluorescence, as seen in addition to punctate endosomal signals, was excluded from lifetime calculations. All selected signals of a cell were recorded and calculated as mean fluorescence lifetime. Per experimental condition, 12-20 cells were independently analysed, thus representing a total of more than 200 individual Golgi stacks (Man1-GFP), TGNs/EEs (SYP61-GFP) or MVBs/LEs (GFP-BP80). For statistics, calculated fluorescent lifetimes of all cells were averaged. Error bars indicate standard errors of the mean. Statistical significance was calculated using ANOVA, followed by Tukey's HSD test.

Protein extraction. Unless otherwise indicated, cell suspensions were diluted 5-fold with 250 mM NaCl and centrifuged for 5 min at 80 g to sediment the protoplasts. After removal of the supernatant, cells were resuspended and sonicated in a 10-fold lower volume as the initial cell suspension using extraction buffer (100 mM Tris, pH 7.8, 200 mM NaCl, 1 mM EDTA, 2 % (v/v) β-mercaptoethanol and 0.2 % (v/v) Triton X-100). Extracts were cleared by centrifugation for 15 min at 4 °C. If culture medium was to be analysed, cell suspensions were centrifuged for 5 min at 80 g causing flotation of the protoplasts, and a fraction of the underlying cleared culture medium was removed with a syringe by puncturing the test tube. Proteins of the culture medium were precipitated with aqueous ammonium sulphate (60% final

concentration) in the presence of 100 µg BSA as a carrier and concentrated 10-fold in extraction buffer. After removing culture medium, test tubes were resealed and the remaining cells were sedimented and processed as described above. All protein samples were finally mixed with an equal volume of 2x Xtreme loading dye [34] and incubated for 5 min at 95 °C before SDS-PAGE.

Coimmunoprecipitation. Cells were resuspended in an equal volume of non-denaturing 2x binding buffer (40 mM HEPES, 300 mM NaCl, 2 mM $CaCl_2$, 2 mM $MgCl_2$, pH 7.1) and homogenised by sonication. Protein extracts were cleared by centrifugation for 15 min at 4 °C and incubated with anti-GFP-bound Dynabeads Protein A (10001D, Life Technologies) overnight at 4 °C. Beads were washed three times with binding buffer and finally boiled in a mix of equal volumes extraction buffer (see above) and 2x Xtreme loading dye [34] to elute immunoprecipitated proteins for SDS-PAGE.

Ligand-LBD *in vitro* binding assay. VSR sensors were assembled *in vivo* by coexpression of the LBD-Nb and either of the four compartmental anchors (GFP-CNX, Man1-GFP, SYP61-GFP and GFP-BP80). Cells were harvested and resuspended in binding buffer as mentioned above. Extracts were cleared by centrifugation and VSR sensors were coupled to anti-GFP-bound Dynabeads Protein A for 2 h at 4 °C. Beads were washed three times with binding buffer. In parallel, the ligand Aleu-RFP was extracted in binding buffer from cells overproducing Sec12, which inhibits ER export and thus ensures high yields of the unprocessed Aleu-RFP transit form. The Aleu-RFP extract was equally distributed to the four bead-coupled VSR sensors and these were incubated overnight at 4 °C. As negative control, a Sec-RFP extract was generated as mentioned above and was added to an additional sample of coimmunoprecipitated sensors. Beads were washed and processed for SDS-PAGE as mentioned above.

Cellular fractionation. Cell suspensions were split into equal parts and both were sedimented in 250 mM NaCl. One aliquot was used as total (T) and resuspended in a fourfold volume of extraction buffer (see above), sonicated and cleared by centrifugation for 15 min at 4 °C. The supernatant was mixed with an equal volume of 2x Xtreme loading dye [34] and boiled for 5 min at 95 °C prior to SDS-PAGE. The

second aliquot was used for cellular fractionation by osmotic shock. Cells were resuspended in a fourfold volume of Tris buffer (50 mM Tris pH 8.0, 1 mM EDTA) and centrifuged for 15 min at 42,000 g. After centrifugation, the supernatant (S) was removed and mixed with an equal volume of 2x Xtreme loading dye. The membrane pellet (P) was resuspended in extraction buffer (see above) using the same volume as the supernatant and the suspension was sonicated and cleared by centrifugation for 15 min at 4 °C. Both fractions were mixed with an equal volume of 2x Xtreme loading dye and boiled for 5 min at 95 °C before SDS-PAGE.

Western blotting and antibodies. All proteins were separated by denaturing SDS-PAGE and transferred to nitrocellulose membranes. Membranes were blocked in 5 % (w/v) BSA in TBS + 0.05 % (v/v) Tween 20 (TBS-T), washed in TBS-T and incubated with primary antibodies diluted in 1 % (w/v) BSA + 0.02 % (w/v) sodium azide in TBS overnight at 4 °C. After washing in TBS-T, membranes were incubated with HRP-conjugated secondary antibodies diluted in blocking buffer and immunodetection was performed using enhanced chemiluminescence. Antibodies used for immunodetection include: mouse monoclonal anti-GFP (Roche 11814460001, clones 7.1 and 13.1; 1:1,000), rat monoclonal anti-RFP (ChromoTek, clone 5F8; 1:1,000) and rat monoclonal anti-HA-Peroxidase (Roche 12013819001, clone BMG-3F10; 1:2,500). For immunoprecipitations, a rabbit polyclonal GFP antibody (Life Technologies A6455) was used to saturate Protein A Dynabeads prior to precipitation of the target antigen.

Acknowledgments

We thank Sébastien Peter (Institute of Physical and Theoretical Chemistry, University of Tübingen) for technical support and helpful discussions on FRET-FLIM. The financial support of the Deutsche Forschungsgemeinschaft (PI 769/1-2 and the Collaborative Research Centre SFB 1101 “Molecular Encoding of Specificity in Plant Processes”) is gratefully acknowledged.

Author Contributions

F.K., F.F., S.F and P.P. designed and analysed the experiments. F.K., S.F. and B.L. performed experiments. F.K. and P.P. wrote the manuscript.

Figure Legends and Tables

Figure 1 Compartment-specific targeting of luminal ligand-binding domains (LBDs) in the plant endomembrane system via nanobody-epitope interactions. (**a**) Schematic representation of the assembly of VSR sensors via the anti-GFP nanobody (Nb). The soluble LBD-RFP-Nb and GFP (epitope)-tagged membrane anchors interact in the compartmental lumen. Assembly occurs irrespective of type I or type II topology of the anchor. (**b**) Immunoblot showing the secretion of the soluble LBD-RFP-Nb. Tobacco mesophyll protoplasts expressing LBD-RFP-Nb, either in the absence (-) or presence (+) of ER-export-inhibiting Sec12 overproduction, were analysed 24 h after transfection. Cells (C) were separated from the culture medium (M) and proteins were extracted independently. Immunoblots were probed with α-HA antibodies (detecting LBD-RFP-Nb) and α-GFP antibodies (detecting ERD2-CFP). Mock-transfected cells served as negative control (co) to illustrate antibody specificity. The coexpressed Golgi marker ERD2-CFP was used as a loading control. Relative molecular masses of detected proteins are as follows: LBD-RFP-Nb, 103K; ERD2-CFP, 52K. (**c**,**d**) Representative CLSM analysis of cells described in **b**. (**c**) Fluorescence signals of secreted LBD-RFP-Nb are largely absent from cells. The Golgi marker ERD2-CFP serves as an internal transfection control. (**d**) Signals of the LBD-RFP-Nb emerge in the ER upon inhibition of ER export by Sec12 overproduction, which also causes coaccumulation of the Golgi marker ERD2-CFP. (**e**-**i**) CLSM analysis of protoplasts assembling VSR sensors within the compartments of the vacuolar pathway. Cells were transfected with plasmids encoding for the LBD-RFP-Nb and either of the GFP-tagged membrane anchors as indicated: (**e**) colocalisation with GFP-CNX (type I) in the ER, (**f**) colocalisation with Man1-GFP (type II) in the Golgi, (**g**) colocalisation with SYP61-GFP (type II) in the TGN/EE, (**h)** colocalisation with GFP-BP80 (type I) in the MVB/LE and the vacuole, and (**i**) colocalisation with GFP-BP80 in ring-like MVB/LE structures after wortmannin (WM) treatment (arrowheads). Inlays: magnified sections in **c**,**f**-**i** and cortical sections in **d**,**e**. Scale bars: 5 µm and 2.5 µm (inlays).

Figure 2 Assembled VSR sensors are ligand-binding competent. (**a**) Schematic representation of the strategy to test for VSR-ligand interactions in specific compartments. A GFP-tagged membrane anchor and the soluble LBD-Nb assemble to reconstitute a fluorescent VSR sensor. Coexpression with the red fluorescent

ligand Aleu-RFP allows for sensing of receptor-ligand interaction via FRET-FLIM. Binding of the ligand triggers close proximity of the fluorophores and thus FRET. This shortens the fluorescence lifetime of the GFP, identifying compartments that promote ligand binding. In compartments that do not provide ligand-binding conditions, Aleu-RFP does not trigger FRET. (**b**) Immunoblot showing ligand-binding capability of all VSR sensors *in vitro*. Protoplasts were transfected with plasmids encoding for the soluble LBD-Nb and either of the indicated membrane anchors: GFP-CNX, Man1-GFP, SYP61-GFP and GFP-BP80. After 24 h of expression, proteins were extracted and VSR sensors were immunoprecipitated with anti-GFP beads (IP: α-GFP) and incubated with Aleu-RFP *in vitro.* Afterwards, beads were recovered and subjected to SDS-PAGE. Immunoblots (IB) were probed with antibodies for detection of membrane anchors (α-GFP), the LBD-Nb (α-HA) and Aleu-RFP (α-RFP). In all cases, coimmunoprecipitated ligands are detectable while in control experiments, the non-ligand Sec-RFP is absent from the precipitate. Relative molecular masses of labelled proteins are as follows: LBD-Nb, 77K; GFP-CNX, 38K; Man1-GFP, 92K; SYP61-GFP, 55K; GFP-BP80, 38K; Aleu-RFP, 30K; Sec-RFP, 28K.

Figure 3 Analysis of VSR-ligand interaction in compartments that promote or restrict ligand binding. (**a**) CLSM image of a protoplast expressing the ER marker GFP-CNX and the soluble reporter Aleu-RFP, which is efficiently transported into the vacuole. (**b**) Protoplast coexpressing the LBD-Nb to assemble VSR sensors in the ER retain Aleu-RFP. Inlays in **a**,**b**: cortical section. (**c**) FRET-FLIM analysis identifies the ER as compartment favouring ligand binding. Binding of Aleu-RFP causes FRET, significantly decreasing fluorescence lifetime of the GFP within the VSR sensor. This does not occur in the presence of the non-ligand Sec-RFP or the absence of the LBD (ΔLBD-Nb) as binding partner. FLIM data are presented as mean ± s.e.m. fluorescence lifetime (n = 12 measurements). Statistical significance was calculated using ANOVA, followed by Tukey's HSD test (*** $P < 0.001$ compared to every other experimental group; NS, not significant). Right: representative FLIM image combining fluorescence intensity and lifetime (colour-coded) of ER-localised VSR sensors in a cortical section. (**d**) Protoplast expressing the MVB/LE marker GFP-BP80 and the soluble vacuolar reporter Aleu-RFP. Aleu-RFP colocalises in the MVB/LE, the transit compartment of the vacuolar route. (**e**) Coexpression of the LBD-Nb to assemble VSR sensors in the MVB/LE does not influence the distribution of Aleu-RFP. Inlays in

d,**e**: magnified section. (**f**) FRET-FLIM analysis of MVB/LE-localised VSR sensors identifies the MVB/LE as a compartment that does not support ligand binding. Fluorescence lifetime of the sensor is not affected by Aleu-RFP or the non-ligand Sec-RFP. FRET-triggered reduction of fluorescence lifetime was confirmed to occur in this compartment by targeting the red fluorescent LBD-RFP-Nb (see Fig. 1) to the membrane anchor in the MVB/LE. FLIM data are presented as mean ± s.e.m. fluorescence lifetime (*n* = 17 measurements). Statistical significance was calculated as in **c**. Right: representative FLIM image combining fluorescence intensity and lifetime (colour-coded) of the MVB/LE-localised VSR sensors. (**g**) Wortmannin-induced ring-like MVB/LE structures show differential distribution between the membrane marker GFP-BP80 and soluble Aleu-RFP (left panel). Coexpression of the LBD-Nb (right panel) does not change this distribution. Scale bars: 5 µm and 2.5 µm (inlays).

Figure 4 The Golgi provides ligand-binding conditions for VSRs. (**a**) CLSM analysis of protoplasts expressing the Golgi marker Man1-GFP and the soluble vacuolar reporter Aleu-RFP. Punctate signals do not colocalise. (**b**) Coexpression of the LBD-Nb to assemble VSR sensors in the Golgi leads to retention of Aleu-RFP (arrowheads). (**c**) Retention in the Golgi is highlighted by coexpression of the VSR-transport competitor HA-BP80, eliminating Aleu-RFP signals from MVBs/LEs and the vacuole. Inlays in **a**-**c**: magnified section. (**d**) FRET-FLIM analysis identifies the Golgi as compartment favouring ligand binding. Binding of Aleu-RFP causes FRET, significantly decreasing fluorescence lifetime of the GFP within the VSR sensor. This does not occur in the absence of the LBD (ΔLBD-Nb) as binding partner. FLIM data are presented as mean ± s.e.m. fluorescence lifetime (*n* = 12 measurements). Statistical significance was calculated using ANOVA, followed by Tukey's HSD test (*** $P < 0.001$ compared to every other experimental group; NS, not significant). Right: representative FLIM image combining fluorescence intensity and lifetime (colour-coded) of Golgi-localised VSR sensors in a cortical section. Scale bars: 5 µm and 2.5 µm (inlays).

Figure 5 The TGN/EE does not provide ligand-binding conditions for VSRs. (**a**) CLSM analysis of protoplasts coexpressing the TGN/EE marker SYP61-GFP and the vacuolar reporter Aleu-RFP. Punctate signals do not colocalise. (**b**) Assembled VSR

sensors (+LBD-Nb) in the TGN/EE do not influence ligand distribution. Inlays in **a**,**b**: magnified section. (**c**) Pearson's (r_P) and Spearman's (r_S) correlation (PSC) coefficients calculated for punctate signals of SYP61-GFP and Aleu-RFP from cells in **a**,**b**. Coexpression of SYP61-GFP and LBD-RFP-Nb as positive control for colocalisation (see Fig. 1g). Coefficients are presented as mean ± s.e.m (n = 10 individual cells). Statistical significance was calculated using ANOVA, followed by Tukey's HSD test (*** P < 0.001; NS, not significant). (**d**) FRET-FLIM analysis identifying the TGN/EE as non-binding compartment. Fluorescence lifetime of TGN/EE-localised sensors is unaffected by Aleu-RFP or Sec-RFP (non-ligand). FRET-triggered reduction of fluorescence lifetime occurs if red fluorescent LBD-RFP-Nb (see Fig. 1g) is coexpressed. FLIM data are presented as mean ± s.e.m. fluorescence lifetime (n = 17 measurements). Statistical significance was calculated as in **c**. Right: FLIM image combining fluorescence intensity and lifetime (colour-coded) of TGN/EE-localised VSR sensors. (**e**) Cells from **b** were treated with brefeldin A (BFA) to cause ER-export inhibition. Inlay: cortical section. (**f**) FRET-FLIM measurements of SYP61-GFP-based sensors in the absence (-) or presence (+) of BFA. Fluorescence lifetime of ER-localised SYP61-GFP increases to the value of the ER marker GFP-CNX (see Fig. 3c). ER-localised LBD-Nb interacts with Aleu-RFP causing FRET and thus decreases fluorescence lifetime, in contrast to non-binding Sec-RFP (mean ± s.e.m.; n = 20 measurements). Statistical significance was calculated as in **d**. Right: FLIM image of ER-localising SYP61-GFP after BFA treatment. Scale bars: 5 µm and 2.5 µm (inlays). (**g**) Immunoblot showing ligand-binding capability of SYP61-GFP-based sensors. Protoplasts expressing indicated proteins ± BFA were lysed and proteins were immunoprecipitated with anti-GFP beads. Immunoprecipitates (IP: α-GFP) were subjected to SDS-PAGE and immunoblotted (IB) with α-GFP, α-HA (detecting LBD-Nb) and α-RFP. Samples are shown as total (T) and immunoprecipitate (IP). SYP61-GFP-based sensors bind Aleu-RFP only if localised to the ER (+BFA, black arrowhead), but not in the TGN/EE (-BFA, white arrowhead).

Figure 6 Vacuolar delivery of endocytosed soluble proteins does not depend on sorting signals. (**a**) Protoplasts expressing Cyt-GFP were supplemented with protoplast-secreted 3xRFP and incubated 24 h before CLSM analysis. 3xRFP is endocytosed and delivered to the vacuole. (**b**) Immunoblot of cellular extracts after

endocytic uptake of 3xRFP. Cells were osmotically shocked and total protein extracts (T) were separated into membrane (M) and soluble (S) fractions. After SDS-PAGE, immunoblots were probed with α-RFP identifying 3xRFP as soluble protein (left). Right: Cells expressing the plasma membrane marker RFP-TMD23 were used as fractionation control. (**c**) Cells expressing Cyt-GFP were supplemented with the nanobody-tagged reporter 3xRFP-Nb showing vacuolar delivery (compare to **a**). (**d**-**f**) Vacuolar delivery of the endocytosed reporter 3xRFP-Nb occurs via the TGN/EE and the MVB/LE. (**d**) Incubation of cells coexpressing the GFP epitope at the cell surface (SYP132-GFP) with 3xRFP-Nb trap the reporter and prevent its vacuolar delivery (compare to **c**). (**e**) Incubation of cells expressing SYP61-GFP with 3xRFP-Nb traps the endocytosed reporter in the TGN/EE. (**f**) Incubation of cells expressing GFP-BP80 with 3xRFP-Nb traps the endocytosed reporter in the MVB/LE. Inlays in **e**,**f**: magnified section. Scale bars: 5 µm and 2.5 µm (inlays). (**g**) Concept of sorting and transport of soluble proteins to the vacuole. The ER and the Golgi provide binding conditions (green) for VSR-ligand interaction, while the *post*-Golgi compartments TGN/EE and MVB/LE do not (red). This suggests that VSR-mediated transport of soluble vacuolar proteins ends in the TGN/EE by their release from the receptor. Further transport from the TGN/EE towards the vacuole does not involve VSRs but occurs via budding of MVBs/LEs and their ultimate fusion with the tonoplast, instead. Consequently, vacuolar sorting signals of soluble proteins in the TGN/EE are of no further use for onward transport. This is supported by the observation that endocytosed soluble proteins lacking vacuolar sorting information reach the vacuole via the TGN/EE and the MVB/LE. This identifies the vacuole as the default location for soluble proteins of the endocytic pathway.

Supplementary Figure 1 The anti-GFP nanobody stabilises the vacuolar GFP core of GFP-BP80. Protoplasts were transfected with plasmids encoding for the indicated proteins and incubated 24 h before analysis. (**a**) The MVB/LE marker GFP-BP80 colocalises with LBD-RFP-Nb in the vacuole additionally to the MVB/LE. (**b**) Vacuolar signals of GFP-BP80 are not detectable in the absence of the nanobody. (**c**) Immunoblot demonstrating the nanobody-mediated accumulation of the vacuolar GFP core. Cells were cotransfected with a constant amount of GFP-BP80 and raising concentrations of LBD-RFP-Nb as indicated. Proteins were extracted and subjected to SDS-PAGE. Immunoblots were probed with α-GFP and α-HA (detecting LBD-RFP-

Nb). In contrast to the full-length transit form, the vacuolar GFP-core accumulates dependent on the expression level of the nanobody. Mock transfected cells served as negative control (co) to illustrate antibody specificity. Asterisk: DNA concentration of LBD-RFP-Nb as used in **a** and in all other experiments of this study. Relative molecular masses: transit form of GFP-BP80, 38K; vacuolar GFP core, ≈25K; LBD-RFP-Nb, 103K. Scale bars: 5 µm.

Supplementary Figure 2 The assembly of VSR sensors does not influence the localisation of the membrane anchors. Protoplasts were transfected with plasmids encoding for the indicated proteins and incubated 24 h before CLSM analysis. (**a**-**d**) Sensors were assembled from LBD-Nb and the GFP-tagged membrane anchors and localisation was compared to RFP-tagged derivatives of the respective compartmental marker. (**a**) Colocalisation with RFP-CNX in the ER, (**b**) colocalisation with Man1-RFP in the Golgi, (**c**) colocalisation with RFP-SYP61 in the TGN/EE and (**d**) colocalisation with RFP-BP80 in the MVB/LE. Inlays in **a**-**d**: magnified section. Scale bars: 5 µm and 2.5 µm (inlays). (**e**) Pearson's (r_P) and Spearman's (r_S) correlation (PSC) coefficients calculated for green and red signals as shown in **a**-**d** demonstrating colocalisation. Coefficients are presented as mean ± s.e.m (n = 10 individual cells). Statistical significance was calculated using ANOVA, followed by Tukey's HSD test (*** $P < 0.001$).

Supplementary Figure 3 Representative CLSM images of cells analysed by FRET-FLIM to asses VSR-ligand binding in the ER and the MVB/LE. (**a**) FLIM data for the ER. The diagram shows the fluorescence lifetimes from Figure 3c. The different experimental groups are represented by Latin numbers (I-V). A representative image is given for each group ensuring expression of tested fluorescent pairs. (**b**) FLIM data for the MVB/LE. The diagram shows the fluorescence lifetimes from Figure 3f. The different experimental groups are represented by Latin numbers (I-IV). A representative image is given for each group ensuring expression of tested fluorescent pairs. Scale bars: 5 µm.

Supplementary Figure 4 Representative CLSM images of cells analysed by FRET-FLIM to asses VSR-ligand binding in the Golgi and the TGN/EE. (**a**) FLIM data for the Golgi. The diagram shows the fluorescence lifetimes from Figure 4d. The different

experimental groups are represented by Latin numbers (I-IV). A representative image is given for each group ensuring expression of tested fluorescent pairs. (**b**) FLIM data for the TGN/EE. The diagram shows the fluorescence lifetimes from Figure 5d,f (± BFA) in direct comparison. The different experimental groups are represented by Latin numbers (I-IV). A representative image is given for each group ensuring expression of tested fluorescent pairs. Scale bars: 5 µm.

Supplementary Table 1

	Primers	Sequence (5'-3' direction)	Template	Recipient Vector
LBD-RFP-Nb (pBL14)	LBD_*Nhe*I_S	AGCTGAGCTAGCATGAA GCAGCTTCTATGTTA	pJLH21[32]	pCN1 [35]; modified to contain following strategic restriction sites: P35S-*Nhe*I-CDS-*Bam*HI-T3nos
	LBD_*Sal*I_AS	GCTGATGTCGACGCAAG TGTCATGGTCTCTCA		
	mRFP_*Sal*I_S	TGCCGGGTCGACATGGC CTCCTCCGAGGACGT	pFK12 [35]	
	mRFP_*Kpn*I_AS	TCCTTAGGTACCTGCTCC AGTGCTGTGGCGGC		
	PLUS: anti-GFP nanobody (*Kpn*I/*Bam*HI); chemically synthesised			
LBD-Nb (pFF29)	LBD_*Nhe*I_S	AGCTGAGCTAGCATGAA GCAGCTTCTATGTTA	pJLH21 [32]	pBL14 (see above); cut *Kpn*I/*Nhe*I
	LBD_*Kpn*I_AS	CGTATTGGTACCGCAAGT GTCATGGTCTCTCA		
ΔLBD-Nb (pFK120)	Nb_*Nhe*I_S	AGTCTAGCTAGCGCCATG TATCCTTATGATGTTCC	pBL14 (see above)	RFP-TMD23 in pCN1 [35]; cut *Bam*HI/*Nhe*I to keep the N-terminal signal peptide of RFP-TMD23
	Nb_*Bam*HI_AS	TGCTTCGGATCCCTAATG AT		
Cyt-RFP-Nb (pFF31)	mRFP_*Cla*I_S	AGTCTAATCGATGGCCTC CTCCGAGGACGT	pBL14 (see above)	RFP-TMD23 in pCN1 [35]; cut *Bam*HI/*Cla*I
	Nb_*Bam*HI_AS	TGCTTCGGATCCCTAATG AT		
GFP-CNX (pFF4)	EGFP_*Nhe*I_S	GCATGAGCTAGCGCCAT GGTGAGCAAGGGCGAGG	pJB13 [51]	pFK120 (see above); cut *Bam*HI/*Nhe*I
	EGFP_*Not*I_AS	AGTCTAGCGGCCGCCCT TGTACAGCTCGTCCATGC		
	CNX-TMD_*Not*I_S	GATCCGGCGGCCGCGAA CTGATTGAGAAAGCCGA	pSLH6 [32]	
	CNX-CT_*Bam*HI_AS	TGCTTCGGATCCTCTAGA GC		
GFP-BP80 (pFF3)	BP80a-TMD_*Not*I_S	AGTCTAGCGGCCGCATC AGTAAGACGGGTTCACA	pLL38 [32]	pFF4 (see above); cut *Bam*HI/*Not*I
	BP80a-CT_*Bam*HI_AS	TGCTTCGGATCCCTTAGG CA		
ManI-GFP (pFF6)	ManI_*Nhe*I_S	GCATGAGCTAGCATGGC GAGAGGGAGCAGATC	pBP30 [47]	pBL14 (see above); cut *Bam*HI/*Nhe*I
	ManI_*Not*I_AS	AGTCTAGCGGCCGCCAC TAGTTCTAGAAAAAGGT		
	EGFP_*Not*I_S	AGTCTAGCGGCCGCATG GTGAGCAAGGGCGAGGA	pJB13 [51]	

	EGFP_*Bam*HI_AS	AGCTGAGGATCCTTACTT GTACAGCTCGTCCA		
SYP61-GFP (pFF25)	SYP61_*Nhe*I_S	AGTCTAGCTAGCATGTCT TCAGCTCAAGATCC	pDS13 [20]	pFF6 (see above); cut *Not*I/*Nhe*I
	SYP61_*Not*I_AS	GCTGTAGCGGCCGCCGG TCAAGAAGACAAGAACGA		
SYP132-GFP (FF13)	SYP132_*Nhe*I_S	AGTCTAGCTAGCATGAAC GATCTTCTGAAGGG	RFP-SYP132 [50]	pFF6 (see above); cut *Not*I/*Nhe*I
	SYP132_*Not*I_AS	GATCCGGCGGCCGCCAG CACTCTTGTTTTTCCAAG		
Cyt-RFP (pFK98)	mRFP_*Nhe*I_S	AGTCTAGCTAGCATGGCC TCCTCCGAGGACG	pFK12 [35]	pGD5 [20]; cut *Bam*HI/*Nhe*I
	mRFP_*Bam*HI_AS	AGTCTAGGATCCTTATGC TCCAGTACTGTGGCGGC		
Sec-RFP (pFF14)	SP_*Xho*I_*Sal*I_S	TCGAGATGAAAGCCTTCA CACTCGCTCTCTTCTTAG CTCTTTCCCTCTATCTCC TGCCCAATCCAGCCATGA CG	Complementary oligonucleotides to assemble the coding sequence of the GFP-spo N-terminal signal peptide [32]	pCN1 [35]; modified to contain following strategic restriction sites: P35S-*Xho*I-CDS-*Spe*I-T3nos
	SP_*Sal*I_*Xho*I_AS	TCGACGTCATGGCTGGAT TGGGCAGGAGATAGAGG GAAAGAGCTAAGAAGAG AGCGAGTGTGAAGGCTTT CATC		
	mRFP_*Sal*I_S	CTCTATGTCGACTATGGC CTCCTCCGAGGACGT	pFK12 [35]	
	mRFP_*Spe*I_AS	AGTCTAACTAGTTTATGC TCCAGTACTGTGGCGGC		
Aleu-RFP (pFF15)	Aleu_*Xho*I_S	AGTCTACTCGAGATGTCT CGTCTGTCACTCCT	aleu-GFP [31]	pFF14 (see above); cut *Spe*I/XhoI
	Aleu_*Nhe*I_AS	CATTGCGCTAGCGCTTTC CA		
	mRFP_*Nhe*I_S	CTTTCTGCTAGCGCCATG GC	pFK12 [35]	
	mRFP_*Spe*I_AS	AGTCTAACTAGTTTATGC TCCAGTACTGTGGCGGC		
3xRFP (pSF70)	mRFP_*Sal*I_S	TGCCGGGTCGACGATGG CCTCCTCCGAGGACGT	pFK12 [35]	pFF14 (see above); cut *Spe*I/*Sal*I to keep the N-terminal signal peptide of pFF14
	mRFP_*Nde*I_AS	TTCGGACATATGTGCTCC AGTACTGTGGCGGC		
	mRFP_*Nde*I_S	AGTCTACATATGGCCTCC TCCGAGGACG	pFK12 [53]	
	mRFP_*Nhe*I_AS	AGTCTAGCTAGCTGCTCC AGTACTGTGGC		
	mRFP_*Nhe*I_S	GTTGACTGCTAGCGCCAT GGCCTCCTC	pFK12 [35]	
	mRFP_*Spe*I_AS	CTGCAACTAGTTTATGCT CCAGTACTGTGGCGGC		
3xRFP-Nb (pSF71)	mRFP_*Nhe*I_S	AGTCTAGCTAGCATGGCC TCCTCCGAGGACG	pFK12 [35]	pSF70 (see above); cut *Hind*III/*Nhe*I
	mRFP_*Kpn*I_AS	TCCTTAGGTACCTGCTCC AGTGCTGTGGCGGC		
	PLUS: nanobody-T3nos (*Kpn*I/*Hind*III), subcloned from pBL14 (see above)			
RFP-CNX (pLBY13)	CNX-TMD_*Sal*I_S	AGTCTAGTCGACGGAACT GATTGAGAAAGCCGAG	pSLH6 [32]	RFP-TMD23 in pCN1 [35]; cut *Bam*HI/*Sal*I
	CNX-CT_*Bam*HI_AS	AGTCTAGGATCCCTAATT		

		ATCACGTCTCGGTT		
GFP-SYP61 (pFK94)	EGFP_*Nco*I_S	AGTCTACCATGGTGAGCA AGGGCGAGG	pJB13 [51]	pDS13 [20]; cut *Cla*I/*Nco*I
	EGFP_*Cla*I_AS	AGTCTAATCGATGCTCCA CCCTTGTACAGCTCGTCC ATGC		
RFP-SYP61 (pML4)	mRFP_*Nhe*I_S	AGTCTAGCTAGCATGGCC TCCTCCGAGGACG	pBP30 [47]	pGD5 [20]; cut *Bam*HI/*Nhe*I
	mRFP_*Cla*I_AS	GCTGTAATCGATGCGGC GCCGGTGGAGTGGCGGC		
	PLUS: SYP61 (*Cla*I/*Bam*HI), subcloned from pDS13 [20]			
RFP-BP80 (pFK121)	BP80a-SP_*Nhe*I_S	TCCTTAGCTAGCATGAAG CAGCTTCTGTGTTA	pJLH21 [32]	pGD5 [20]; cut *Bam*HI/*Nhe*I
	BP80a-SP_*Not*I_AS	AGTCTAGCGGCCGCGAG CCTCGCTAAAAGGGGAA		
	mRFP_*Not*I_S	AGTCTAGCGGCCGCATG GCCTCCTCCGAGGACGT	pBP30 [47]	
	mRFP_*Sal*I_AS	AGTCTAGTCGACCGGCG CCGGTGGAGTGGCGGC		
	BP80a-TMD_*Sal*I_S	GCTGATGTCGACTTTCAC AAGTGAAATCAGCG	pLL38 [32]	
	BP80a-CT_*Bam*HI_AS	TGCTTCGGATCCCTTAGG CA		
HA-BP80 (pFK119)	SP_*Cla*I_S	CTCTATATCGATGAGGCT TT	pFK120 (see above)	pFF3 (see above); cut *Not*I/*Cla*I
	HA_*Not*I_AS	AGTCTAGCGGCCGCCAG CATAATCAGGAACATCA		

References

1. Wilkins, T.A., Bednarek, S.Y. & Raikhel, N.V. Role of propeptide glycan in post-translational processing and transport of barley lectin to vacuoles in transgenic tobacco. *Plant Cell* **2**, 301-313 (1990).
2. Holwerda, B.C., Padgett, H.S. & Rogers, J.C. Proaleurain vacuolar targeting is mediated by short contiguous peptide interactions. *Plant Cell* **4**, 307-318 (1992).
3. Bednarek, S.Y., Wilkins, T.A., Dombrowski, J.E. & Raikhel, N.V. A carboxyl-terminal propeptide is necessary for proper sorting of barley lectin to vacuoles of tobacco. *Plant Cell* **2**, 1145-1155 (1990).
4. Kirsch, T., Paris, N., Butler, J.M., Beevers, L. & Rogers, J.C. Purification and initial characterization of a potential plant vacuolar targeting receptor. *Proc. Natl. Acad. Sci. USA* **91**, 3403-3407 (1994).
5. Robinson, D.G. & Pimpl, P. Receptor-mediated transport of vacuolar proteins: a critical analysis and a new model. *Protoplasma* **251**, 247-264 (2014).
6. Ahmed, S.U., Bar-Peled, M. & Raikhel, N.V. Cloning and subcellular location of an Arabidopsis receptor-like protein that shares common features with protein-sorting receptors of eukaryotic cells. *Plant Physiol.* **114**, 325-336 (1997).
7. Paris, N. *et al.* Molecular cloning and further characterization of a probable plant vacuolar sorting receptor. *Plant Physiol.* **115**, 29-39 (1997).
8. De Marcos Lousa, C., Gershlick, D.C. & Denecke, J. Mechanisms and concepts paving the way towards a complete transport cycle of plant vacuolar sorting receptors. *Plant Cell* **24**, 1714-1732 (2012).

9. Cao, X., Rogers, S.W., Butler, J., Beevers, L. & Rogers, J.C. Structural requirements for ligand binding by a probable plant vacuolar sorting receptor. *Plant Cell* **12**, 493-506 (2000).
10. Luo, F. *et al.* How vacuolar sorting receptor proteins interact with their cargo proteins: crystal structures of apo and cargo-bound forms of the protease-associated domain from an Arabidopsis vacuolar sorting receptor. *Plant Cell* **26**, 3693-3708 (2014).
11. daSilva, L.L., Foresti, O. & Denecke, J. Targeting of the plant vacuolar sorting receptor BP80 is dependent on multiple sorting signals in the cytosolic tail. *Plant Cell* **18**, 1477-1497 (2006).
12. Kim, H. *et al.* Homomeric interaction of AtVSR1 is essential for its function as a vacuolar sorting receptor. *Plant Physiol.* **154**, 134-148 (2010).
13. Saint-Jean, B., Seveno-Carpentier, E., Alcon, C., Neuhaus, J.M. & Paris, N. The cytosolic tail dipeptide Ile-Met of the pea receptor BP80 is required for recycling from the prevacuole and for endocytosis. *Plant Cell* **22**, 2825-2837 (2010).
14. Dettmer, J., Hong-Hermesdorf, A., Stierhof, Y.D. & Schumacher, K. Vacuolar H+-ATPase activity is required for endocytic and secretory trafficking in Arabidopsis. *Plant Cell* **18**, 715-730 (2006).
15. Lam, S.K. *et al.* BFA-induced compartments from the Golgi apparatus and trans-Golgi network/early endosome are distinct in plant cells. *Plant J.* **60**, 865-881 (2009).
16. Foresti, O. & Denecke, J. Intermediate organelles of the plant secretory pathway: identity and function. *Traffic* **9**, 1599-1612 (2008).
17. Shen, J. *et al.* Organelle pH in the *Arabidopsis* Endomembrane System. *Mol Plant* **6**, 1419-1437 (2013).
18. Martiniere, A. *et al.* In Vivo Intracellular pH Measurements in Tobacco and Arabidopsis Reveal an Unexpected pH Gradient in the Endomembrane System. *Plant Cell* **25**, 4028-4043 (2013).
19. Luo, Y. *et al.* V-ATPase activity in the TGN/EE is required for exocytosis and recycling in Arabidopsis. *Nature Plants* **1**, 15094 (2015).
20. Niemes, S. *et al.* Retromer recycles vacuolar sorting receptors from the trans-Golgi network. *Plant J.* **61**, 107-121 (2010).
21. Stierhof, Y.D., Viotti, C., Scheuring, D., Sturm, S. & Robinson, D.G. Sorting nexins 1 and 2a locate mainly to the TGN. *Protoplasma* **250**, 235-240 (2013).
22. Scheuring, D. *et al.* Multivesicular bodies mature from the trans-Golgi network/early endosome in Arabidopsis. *Plant Cell* **23**, 3463-3481 (2011).
23. Rothbauer, U. *et al.* Targeting and tracing antigens in live cells with fluorescent nanobodies. *Nature methods* **3**, 887-889 (2006).
24. Martiniere, A., Desbrosses, G., Sentenac, H. & Paris, N. Development and properties of genetically encoded pH sensors in plants. *Frontiers in plant science* **4**, 523 (2013).
25. Niemes, S. *et al.* Sorting of plant vacuolar proteins is initiated in the ER. *Plant J.* **62**, 601-614 (2010).
26. Kubala, M.H., Kovtun, O., Alexandrov, K. & Collins, B.M. Structural and thermodynamic analysis of the GFP:GFP-nanobody complex. *Protein Sci.* **19**, 2389-2401 (2010).
27. Nishikawa, S., Hirata, A. & Nakano, A. Inhibition of endoplasmic reticulum (ER)-to-Golgi transport induces relocalization of binding protein (BiP) within the ER to form the BiP bodies. *Mol. Biol. Cell* **5**, 1129-1143 (1994).

28. Ritzenthaler, C. *et al.* Reevaluation of the effects of brefeldin A on plant cells using tobacco Bright Yellow 2 cells expressing Golgi-targeted green fluorescent protein and COPI antisera. *Plant Cell* **14**, 237-261 (2002).
29. Tse, Y.C. *et al.* Identification of multivesicular bodies as prevacuolar compartments in Nicotiana tabacum BY-2 cells. *Plant Cell* **16**, 672-693 (2004).
30. Bucherl, C.A., Bader, A., Westphal, A.H., Laptenok, S.P. & Borst, J.W. FRET-FLIM applications in plant systems. *Protoplasma* **251**, 383-394 (2014).
31. Humair, D., Hernandez Felipe, D., Neuhaus, J.M. & Paris, N. Demonstration in yeast of the function of BP-80, a putative plant vacuolar sorting receptor. *Plant Cell* **13**, 781-792 (2001).
32. daSilva, L.L. *et al.* Receptor salvage from the prevacuolar compartment is essential for efficient vacuolar protein targeting. *Plant Cell* **17**, 132-148 (2005).
33. Schmitt, F.J. *et al.* eGFP-pHsens as a highly sensitive fluorophore for cellular pH determination by fluorescence lifetime imaging microscopy (FLIM). *Biochim. Biophys. Acta* **1837**, 1581-1593 (2014).
34. Pimpl, P. *et al.* Golgi-mediated vacuolar sorting of the endoplasmic reticulum chaperone BiP may play an active role in quality control within the secretory pathway. *Plant Cell* **18**, 198-211 (2006).
35. Scheuring, D. *et al.* Ubiquitin initiates sorting of Golgi and plasma membrane proteins into the vacuolar degradation pathway. *BMC plant biology* **12**, 164-180 (2012).
36. Watanabe, E. *et al.* An ER-Localized Form of PV72, a Seed-Specific Vacuolar Sorting Receptor, Interferes the Transport of an NPIR-Containing Proteinase in Arabidopsis Leaves. *Plant Cell Physiol.* **45**, 9-17 (2004).
37. Hinz, G., Hillmer, S., Baumer, M. & Hohl, I. Vacuolar storage proteins and the putative vacuolar sorting receptor BP- 80 exit the golgi apparatus of developing pea cotyledons in different transport vesicles. *Plant Cell* **11**, 1509-1524 (1999).
38. Hillmer, S., Movafeghi, A., Robinson, D.G. & Hinz, G. Vacuolar storage proteins are sorted in the cis-cisternae of the pea cotyledon Golgi apparatus. *J. Cell Biol.* **152**, 41-50 (2001).
39. Hinz, G., Colanesi, S., Hillmer, S., Rogers, J.C. & Robinson, D.G. Localization of vacuolar transport receptors and cargo proteins in the Golgi apparatus of developing Arabidopsis embryos. *Traffic* **8**, 1452-1464 (2007).
40. Viotti, C. *et al.* Endocytic and Secretory Traffic in Arabidopsis Merge in the Trans-Golgi Network/Early Endosome, an Independent and Highly Dynamic Organelle. *Plant Cell* **22**, 1344-1357 (2010).
41. Wang, H., Zhuang, X., Hillmer, S., Robinson, D.G. & Jiang, L. Vacuolar Sorting Receptor (VSR) Proteins Reach the Plasma Membrane in Germinating Pollen Tubes. *Mol Plant* **4**, 845-853 (2011).
42. Watanabe, E., Shimada, T., Kuroyanagi, M., Nishimura, M. & Hara-Nishimura, I. Calcium-mediated association of a putative vacuolar sorting receptor PV72 with a propeptide of 2S albumin. *J. Biol. Chem.* **277**, 8708-8715 (2002).
43. Stael, S. *et al.* Plant organellar calcium signalling: an emerging field. *J Exp Bot* **63**, 1525-1542 (2012).
44. Ordenes, V.R. *et al.* In vivo analysis of the calcium signature in the plant Golgi apparatus reveals unique dynamics. *Cell Calcium* **52**, 397-404 (2012).
45. Etxeberria, E., Gonzalez, P., Baroja-Fernandez, E. & Romero, J.P. Fluid phase endocytic uptake of artificial nano-spheres and fluorescent quantum dots by sycamore cultured cells: evidence for the distribution of solutes to different intracellular compartments. *Plant Signal Behav* **1**, 196-200 (2006).

46. Brandizzi, F., Snapp, E.L., Roberts, A.G., Lippincott-Schwartz, J. & Hawes, C. Membrane protein transport between the endoplasmic reticulum and the Golgi in tobacco leaves is energy dependent but cytoskeleton independent: evidence from selective photobleaching. *Plant Cell* **14**, 1293-1309 (2002).
47. Nebenfuhr, A. *et al.* Stop-and-go movements of plant Golgi stacks are mediated by the acto-myosin system. *Plant Physiol.* **121**, 1127-1142 (1999).
48. Phillipson, B.A. *et al.* Secretory bulk flow of soluble proteins is efficient and COPII dependent. *Plant Cell* **13**, 2005-2020 (2001).
49. Casadaban, M.J. & Cohen, S.N. Analysis of gene control signals by DNA fusion and cloning in Escherichia coli. *J. Mol. Biol.* **138**, 179-207 (1980).
50. Reichardt, I. *et al.* Mechanisms of functional specificity among plasma-membrane syntaxins in Arabidopsis. *Traffic* **12**, 1269-1280 (2011).
51. Bubeck, J. *et al.* The syntaxins SYP31 and SYP81 control ER-Golgi trafficking in the plant secretory pathway. *Traffic* **9**, 1629-1652 (2008).
52. French, A.P., Mills, S., Swarup, R., Bennett, M.J. & Pridmore, T.P. Colocalization of fluorescent markers in confocal microscope images of plant cells. *Nat Protoc* **3**, 619-628 (2008).
53. Robinson, D.G. *et al.* Trying to make sense of retromer. *Trends Plant Sci.* **17**, 431-439 (2012).

PimpI, Figure 1

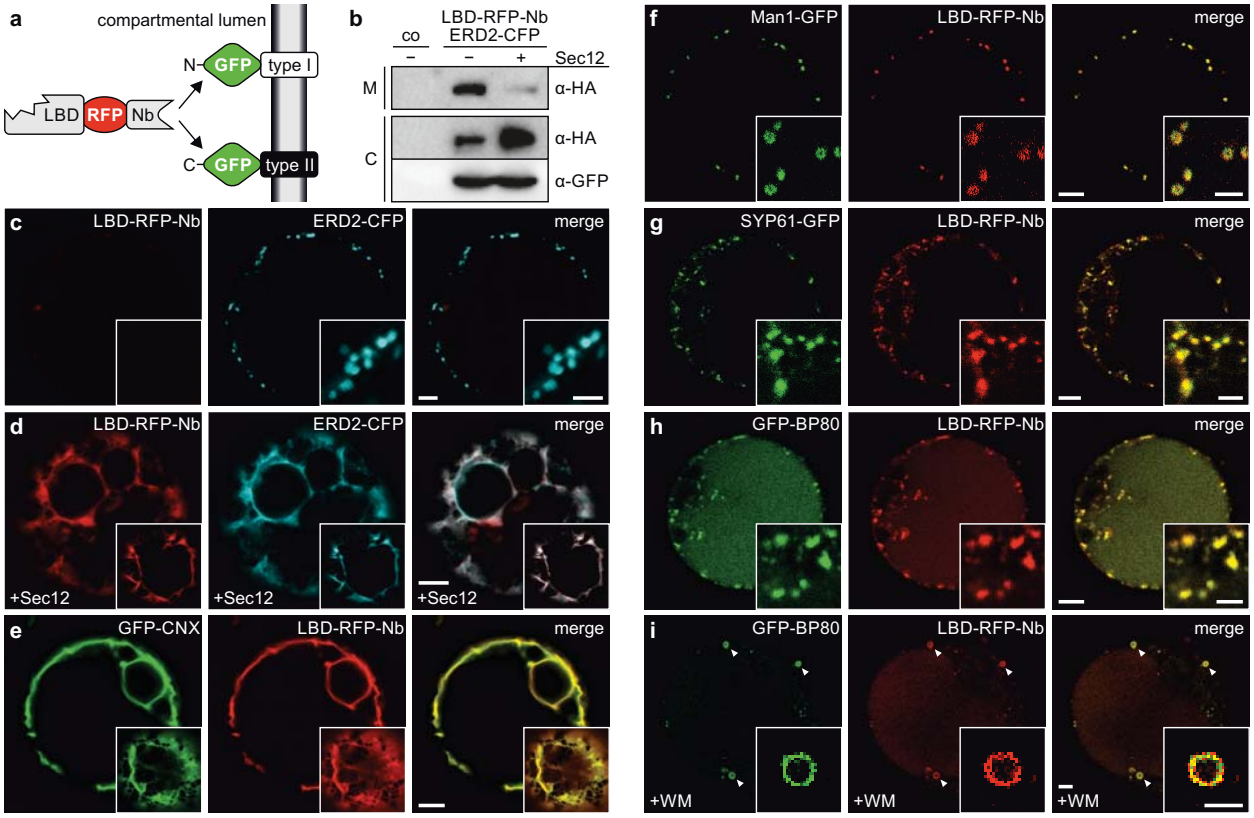

Figure 1 Compartment-specific targeting of luminal ligand-binding domains (LBDs) in the plant endomembrane system via nanobody-epitope interactions. (**a**) Schematic representation of the assembly of VSR sensors via the anti-GFP nanobody (Nb). The soluble LBD-RFP-Nb and GFP (epitope)-tagged membrane anchors interact in the compartmental lumen. Assembly occurs irrespective of type I or type II topology of the anchor. (**b**) Immunoblot showing the secretion of the soluble LBD-RFP-Nb. Tobacco mesophyll protoplasts expressing LBD-RFP-Nb, either in the absence (-) or presence (+) of ER-export-inhibiting Sec12 overproduction, were analysed 24 h after transfection. Cells (C) were separated from the culture medium (M) and proteins were extracted independently. Immunoblots were probed with α-HA antibodies (detecting LBD-RFP-Nb) and α-GFP antibodies (detecting ERD2-CFP). Mock-transfected cells served as negative control (co) to illustrate antibody specificity. The coexpressed Golgi marker ERD2-CFP was used as a loading control. Relative molecular masses of detected proteins are as follows: LBD-RFP-Nb, 103K; ERD2-CFP, 52K. (**c**,**d**) Representative CLSM analysis of cells described in **b**. (**c**) Fluorescence signals of secreted LBD-RFP-Nb are largely absent from cells. The Golgi marker ERD2-CFP serves as an internal transfection control. (**d**) Signals of the LBD-RFP-Nb emerge in the ER upon inhibition of ER export by Sec12 overproduction, which also causes coaccumulation of the Golgi marker ERD2-CFP. (**e-i**) CLSM analysis of protoplasts assembling VSR sensors within the compartments of the vacuolar pathway. Cells were transfected with plasmids encoding for the LBD-RFP-Nb and either of the GFP-tagged membrane anchors as indicated: (**e**) colocalisation with GFP-CNX (type I) in the ER, (**f**) colocalisation with Man1-GFP (type II) in the Golgi, (**g**) colocalisation with SYP61-GFP (type II) in the TGN/EE, (**h**) colocalisation with GFP-BP80 (type I) in the MVB/LE and the vacuole, and (**i**) colocalisation with GFP-BP80 in ring-like MVB/LE structures after wortmannin (WM) treatment (arrowheads). Inlays: magnified sections in **c**,**f-i** and cortical sections in **d**,**e**. Scale bars: 5 µm and 2.5 µm (inlays).

PimpI, Figure 2

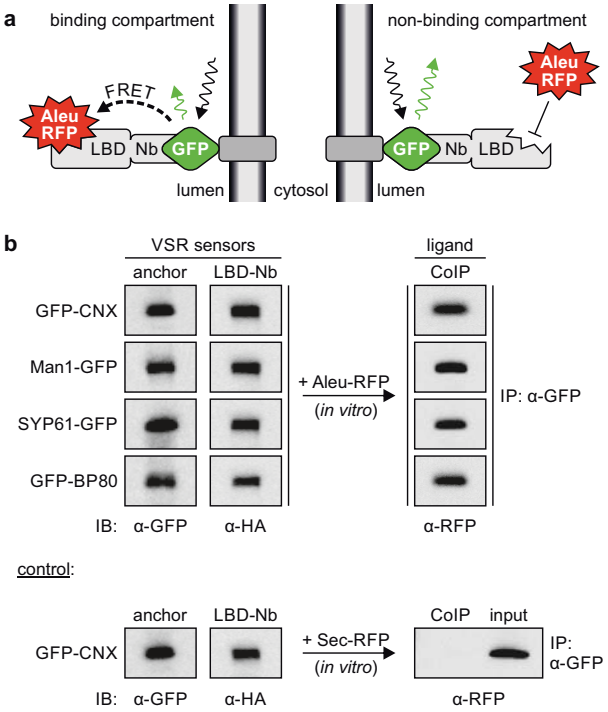

Figure 2 Assembled VSR sensors are ligand-binding competent. (**a**) Schematic representation of the strategy to test for VSR-ligand interactions in specific compartments. A GFP-tagged membrane anchor and the soluble LBD-Nb assemble to reconstitute a fluorescent VSR sensor. Coexpression with the red fluorescent ligand Aleu-RFP allows for sensing of receptor-ligand interaction via FRET-FLIM. Binding of the ligand triggers close proximity of the fluorophores and thus FRET. This shortens the fluorescence lifetime of the GFP, identifying compartments that promote ligand binding. In compartments that do not provide ligand-binding conditions, Aleu-RFP does not trigger FRET. (**b**) Immunoblot showing ligand-binding capability of all VSR sensors *in vitro*. Protoplasts were transfected with plasmids encoding for the soluble LBD-Nb and either of the indicated membrane anchors: GFP-CNX, Man1-GFP, SYP61-GFP and GFP-BP80. After 24 h of expression, proteins were extracted and VSR sensors were immunoprecipitated with anti-GFP beads (IP: α-GFP) and incubated with Aleu-RFP *in vitro*. Afterwards, beads were recovered and subjected to SDS-PAGE. Immunoblots (IB) were probed with antibodies for detection of membrane anchors (α-GFP), the LBD-Nb (α-HA) and Aleu-RFP (α-RFP). In all cases, coimmunoprecipitated ligands are detectable while in control experiments, the non-ligand Sec-RFP is absent from the precipitate. Relative molecular masses of labelled proteins are as follows: LBD-Nb, 77K; GFP-CNX, 38K; Man1-GFP, 92K; SYP61-GFP, 55K; GFP-BP80, 38K; Aleu-RFP, 30K; Sec-RFP, 28K.

PimpI, Figure 3

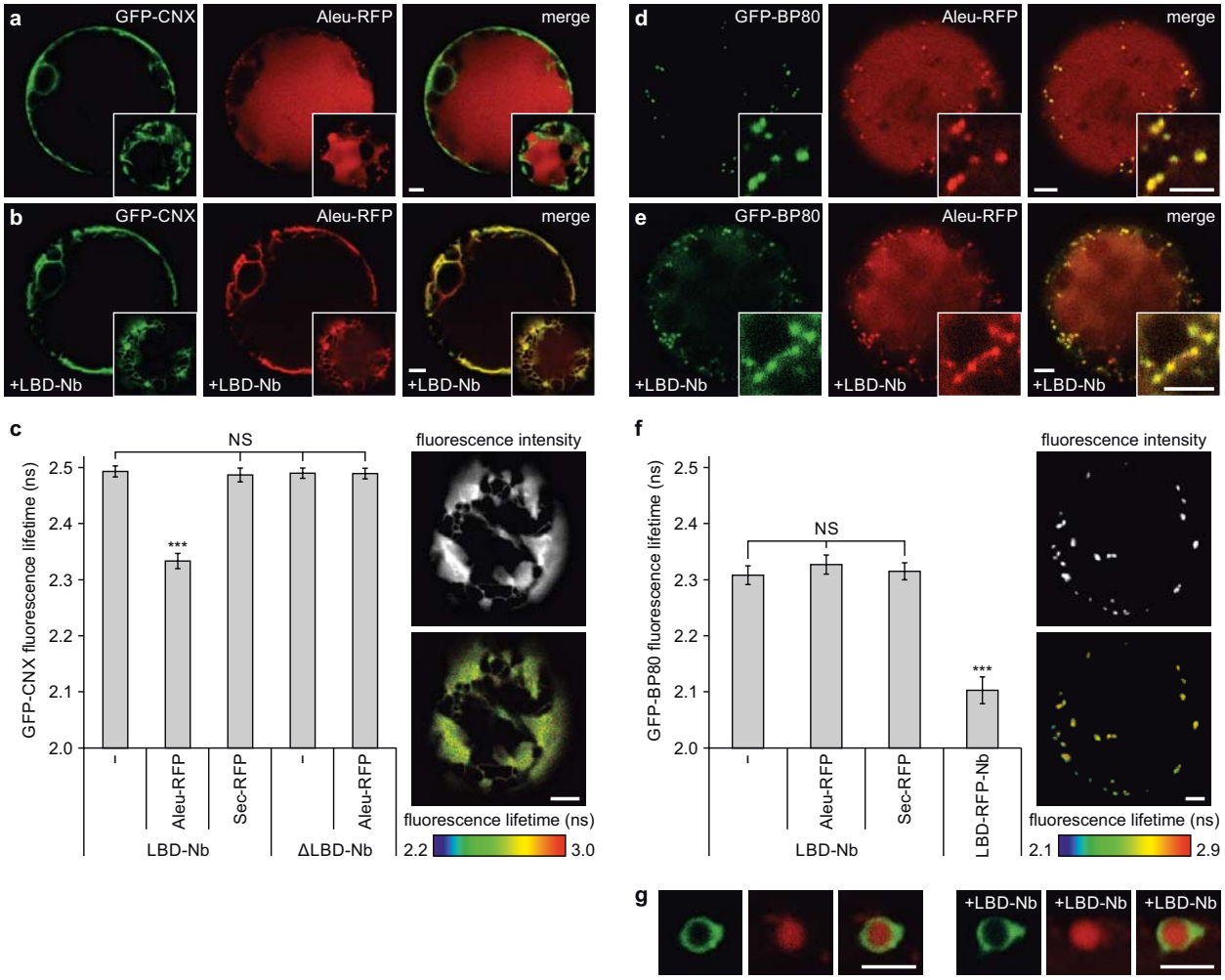

Figure 3 Analysis of VSR-ligand interaction in compartments that promote or restrict ligand binding. (**a**) CLSM image of a protoplast expressing the ER marker GFP-CNX and the soluble reporter Aleu-RFP, which is efficiently transported into the vacuole. (**b**) Protoplast coexpressing the LBD-Nb to assemble VSR sensors in the ER retain Aleu-RFP. Inlays in **a**,**b**: cortical section. (**c**) FRET-FLIM analysis identifies the ER as compartment favouring ligand binding. Binding of Aleu-RFP causes FRET, significantly decreasing fluorescence lifetime of the GFP within the VSR sensor. This does not occur in the presence of the non-ligand Sec-RFP or the absence of the LBD (ΔLBD-Nb) as binding partner. FLIM data are presented as mean ± s.e.m. fluorescence lifetime (n = 12 measurements). Statistical significance was calculated using ANOVA, followed by Tukey's HSD test (*** $P < 0.001$ compared to every other experimental group; NS, not significant). Right: representative FLIM image combining fluorescence intensity and lifetime (colour-coded) of ER-localised VSR sensors in a cortical section. (**d**) Protoplast expressing the MVB/LE marker GFP-BP80 and the soluble vacuolar reporter Aleu-RFP. Aleu-RFP colocalises in the MVB/LE, the transit compartment of the vacuolar route. (**e**) Coexpression of the LBD-Nb to assemble VSR sensors in the MVB/LE does not influence the distribution of Aleu-RFP. Inlays in **d**,**e**: magnified section. (**f**) FRET-FLIM analysis of MVB/LE-localised VSR sensors identifies the MVB/LE as a compartment that does not support ligand binding. Fluorescence lifetime of the sensor is not affected by Aleu-RFP or the non-ligand Sec-RFP. FRET-triggered reduction of fluorescence lifetime was confirmed to occur in this compartment by targeting the red fluorescent LBD-RFP-Nb (see Fig. 1) to the membrane anchor in the MVB/LE. FLIM data are presented as mean ± s.e.m. fluorescence lifetime (n = 17 measurements). Statistical significance was calculated as in **c**. Right: representative FLIM image combining fluorescence intensity and lifetime (colour-coded) of the MVB/LE-localised VSR sensors. (**g**) Wortmannin-induced ring-like MVB/LE structures show differential distribution between the membrane marker GFP-BP80 and soluble Aleu-RFP (left panel). Coexpression of the LBD-Nb (right panel) does not change this distribution. Scale bars: 5 µm and 2.5 µm (inlays).

PimpI, Figure 4

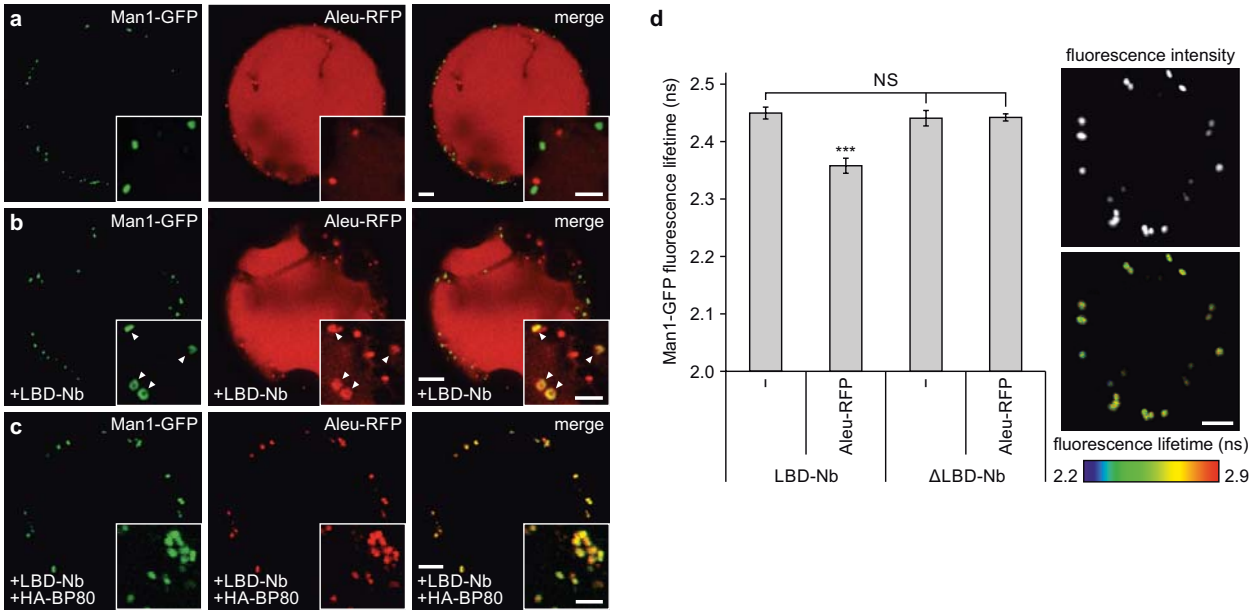

Figure 4 The Golgi provides ligand-binding conditions for VSRs. (**a**) CLSM analysis of protoplasts expressing the Golgi marker Man1-GFP and the soluble vacuolar reporter Aleu-RFP. Punctate signals do not colocalise. (**b**) Coexpression of the LBD-Nb to assemble VSR sensors in the Golgi leads to retention of Aleu-RFP (arrowheads). (**c**) Retention in the Golgi is highlighted by coexpression of the VSR-transport competitor HA-BP80, eliminating Aleu-RFP signals from MVBs/LEs and the vacuole. Inlays in **a**-**c**: magnified section. (**d**) FRET-FLIM analysis identifies the Golgi as compartment favouring ligand binding. Binding of Aleu-RFP causes FRET, significantly decreasing fluorescence lifetime of the GFP within the VSR sensor. This does not occur in the absence of the LBD (ΔLBD-Nb) as binding partner. FLIM data are presented as mean ± s.e.m. fluorescence lifetime (n = 12 measurements). Statistical significance was calculated using ANOVA, followed by Tukey's HSD test (*** $P < 0.001$ compared to every other experimental group; NS, not significant). Right: representative FLIM image combining fluorescence intensity and lifetime (colour-coded) of Golgi-localised VSR sensors in a cortical section. Scale bars: 5 µm and 2.5 µm (inlays).

PimpI, Figure 5

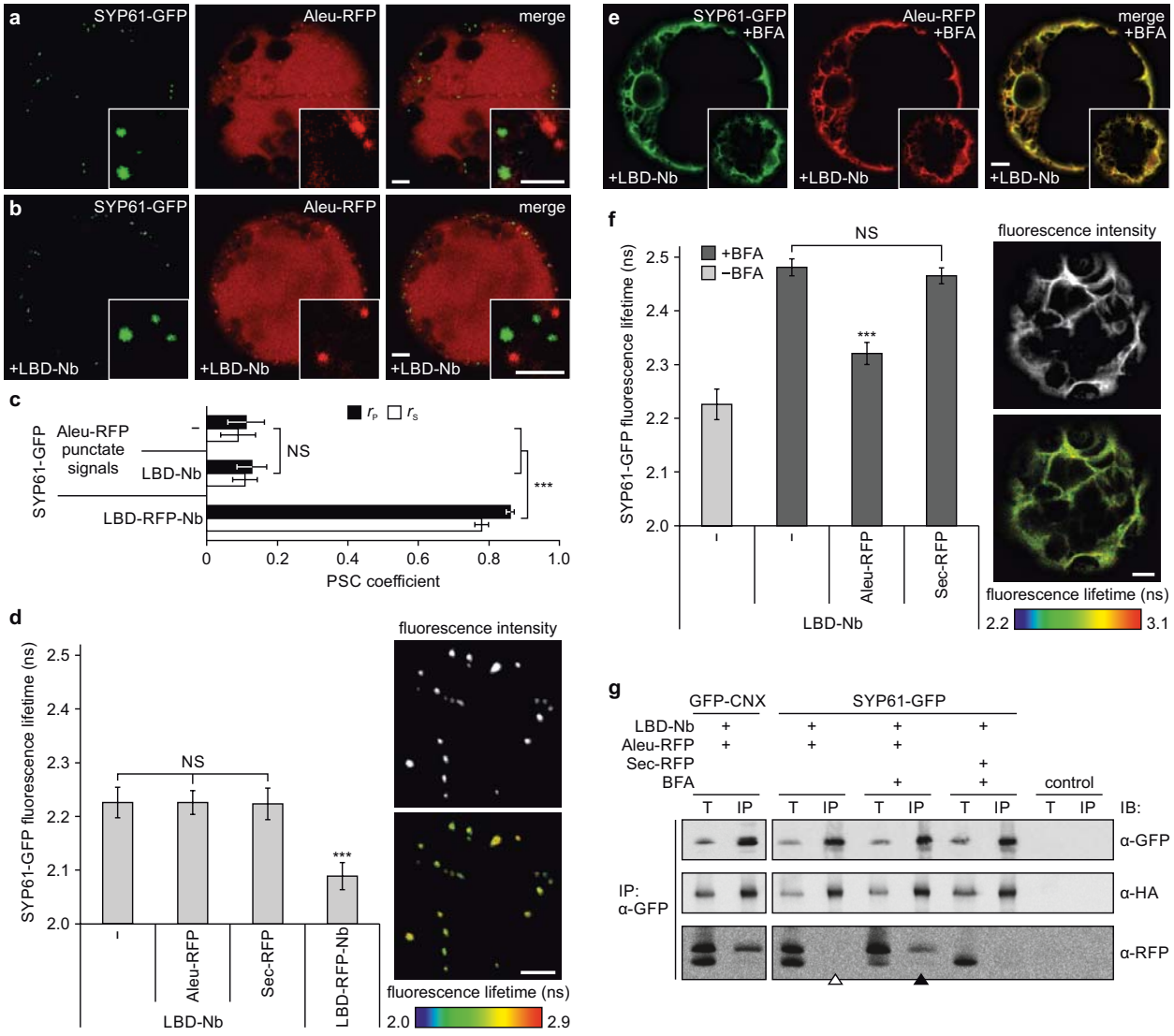

Figure 5 The TGN/EE does not provide ligand-binding conditions for VSRs. (**a**) CLSM analysis of protoplasts coexpressing the TGN/EE marker SYP61-GFP and the vacuolar reporter Aleu-RFP. Punctate signals do not colocalise. (**b**) Assembled VSR sensors (+LBD-Nb) in the TGN/EE do not influence ligand distribution. Inlays in **a**,**b**: magnified section. (**c**) Pearson's (r_P) and Spearman's (r_S) correlation (PSC) coefficients calculated for punctate signals of SYP61-GFP and Aleu-RFP from cells in **a**,**b**. Coexpression of SYP61-GFP and LBD-RFP-Nb as positive control for colocalisation (see Fig. 1g). Coefficients are presented as mean ± s.e.m (n = 10 individual cells). Statistical significance was calculated using ANOVA, followed by Tukey's HSD test (*** P < 0.001; NS, not significant). (**d**) FRET-FLIM analysis identifying the TGN/EE as non-binding compartment. Fluorescence lifetime of TGN/EE-localised sensors is unaffected by Aleu-RFP or Sec-RFP (non-ligand). FRET-triggered reduction of fluorescence lifetime occurs if red fluorescent LBD-RFP-Nb (see Fig. 1g) is coexpressed. FLIM data are presented as mean ± s.e.m. fluorescence lifetime (n = 17 measurements). Statistical significance was calculated as in **c**. Right: FLIM image combining fluorescence intensity and lifetime (colour-coded) of TGN/EE-localised VSR sensors. (**e**) Cells from **b** were treated with brefeldin A (BFA) to cause ER-export inhibition. Inlay: cortical section. (**f**) FRET-FLIM measurements of SYP61-GFP-based sensors in the absence (-) or presence (+) of BFA. Fluorescence lifetime of ER-localised SYP61-GFP increases to the value of the ER marker GFP-CNX (see Fig. 3c). ER-localised LBD-Nb interacts with Aleu-RFP causing FRET and thus decreases fluorescence lifetime, in contrast to non-binding Sec-RFP (mean ± s.e.m.; n = 20 measurements). Statistical significance was calculated as in **d**. Right: FLIM image of ER-localising SYP61-GFP after BFA treatment. Scale bars: 5 µm and 2.5 µm (inlays). (**g**) Immunoblot showing ligand-binding capability of SYP61-GFP-based sensors. Protoplasts expressing indicated proteins ± BFA were lysed and proteins were immunoprecipitated with anti-GFP beads. Immunoprecipitates (IP: α-GFP) were subjected to SDS-PAGE and immunoblotted (IB) with α-GFP, α-HA (detecting LBD-Nb) and α-RFP. Samples are shown as total (T) and immunoprecipitate (IP). SYP61-GFP-based sensors bind Aleu-RFP only if localised to the ER (+BFA, black arrowhead), but not in the TGN/EE (-BFA, white arrowhead).

PimpI, Figure 6

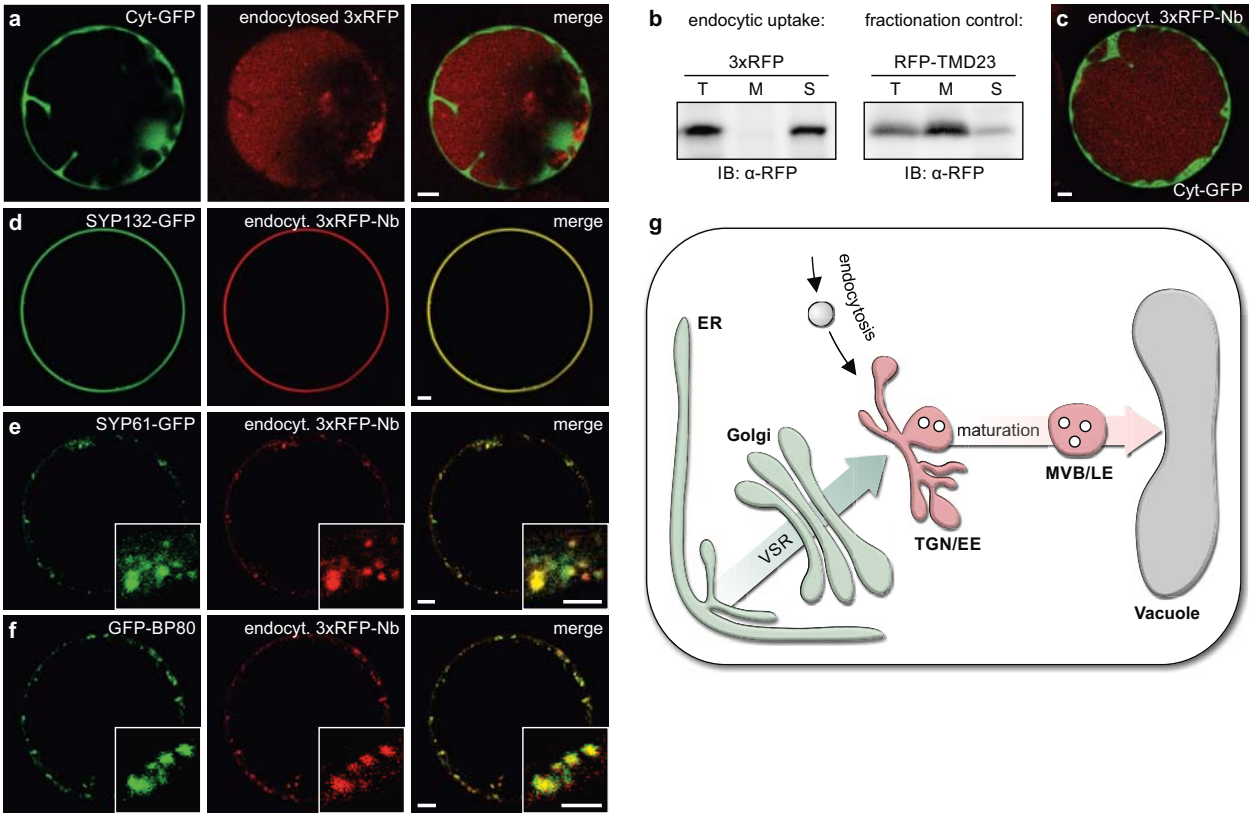

Figure 6 Vacuolar delivery of endocytosed soluble proteins does not depend on sorting signals. (**a**) Protoplasts expressing Cyt-GFP were supplemented with protoplast-secreted 3xRFP and incubated 24 h before CLSM analysis. 3xRFP is endocytosed and delivered to the vacuole. (**b**) Immunoblot of cellular extracts after endocytic uptake of 3xRFP. Cells were osmotically shocked and total protein extracts (T) were separated into membrane (M) and soluble (S) fractions. After SDS-PAGE, immunoblots were probed with α-RFP identifying 3xRFP as soluble protein (left). Right: Cells expressing the plasma membrane marker RFP-TMD23 were used as fractionation control. (**c**) Cells expressing Cyt-GFP were supplemented with the nanobody-tagged reporter 3xRFP-Nb showing vacuolar delivery (compare to **a**). (**d**-**f**) Vacuolar delivery of the endocytosed reporter 3xRFP-Nb occurs via the TGN/EE and the MVB/LE. (**d**) Incubation of cells coexpressing the GFP epitope at the cell surface (SYP132-GFP) with 3xRFP-Nb trap the reporter and prevent its vacuolar delivery (compare to **c**). (**e**) Incubation of cells expressing SYP61-GFP with 3xRFP-Nb traps the endocytosed reporter in the TGN/EE. (**f**) Incubation of cells expressing GFP-BP80 with 3xRFP-Nb traps the endocytosed reporter in the MVB/LE. Inlays in **e**,**f**: magnified section. Scale bars: 5 µm and 2.5 µm (inlays). (**g**) Concept of sorting and transport of soluble proteins to the vacuole. The ER and the Golgi provide binding conditions (green) for VSR-ligand interaction, while the *post*-Golgi compartments TGN/EE and MVB/LE do not (red). This suggests that VSR-mediated transport of soluble vacuolar proteins ends in the TGN/EE by their release from the receptor. Further transport from the TGN/EE towards the vacuole does not involve VSRs but occurs via budding of MVBs/LEs and their ultimate fusion with the tonoplast, instead. Consequently, vacuolar sorting signals of soluble proteins in the TGN/EE are of no further use for onward transport. This is supported by the observation that endocytosed soluble proteins lacking vacuolar sorting information reach the vacuole via the TGN/EE and the MVB/LE. This identifies the vacuole as the default location for soluble proteins of the endocytic pathway.

PimpI, Supplementary Figure 1

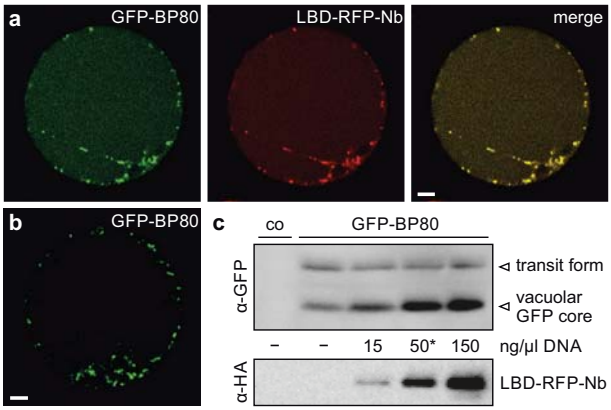

Supplementary Figure 1 The anti-GFP nanobody stabilises the vacuolar GFP core of GFP-BP80. Protoplasts were transfected with plasmids encoding for the indicated proteins and incubated 24 h before analysis. (**a**) The MVB/LE marker GFP-BP80 colocalises with LBD-RFP-Nb in the vacuole additionally to the MVB/LE. (**b**) Vacuolar signals of GFP-BP80 are not detectable in the absence of the nanobody. (**c**) Immunoblot demonstrating the nanobody-mediated accumulation of the vacuolar GFP core. Cells were cotransfected with a constant amount of GFP-BP80 and raising concentrations of LBD-RFP-Nb as indicated. Proteins were extracted and subjected to SDS-PAGE. Immunoblots were probed with α-GFP and α-HA (detecting LBD-RFP-Nb). In contrast to the full-length transit form, the vacuolar GFP-core accumulates dependent on the expression level of the nanobody. Mock transfected cells served as negative control (co) to illustrate antibody specificity. Asterisk: DNA concentration of LBD-RFP-Nb as used in **a** and in all other experiments of this study. Relative molecular masses: transit form of GFP-BP80, 38K; vacuolar GFP core, ≈25K; LBD-RFP-Nb, 103K. Scale bars: 5 µm.

PimpI, Supplementary Figure 2

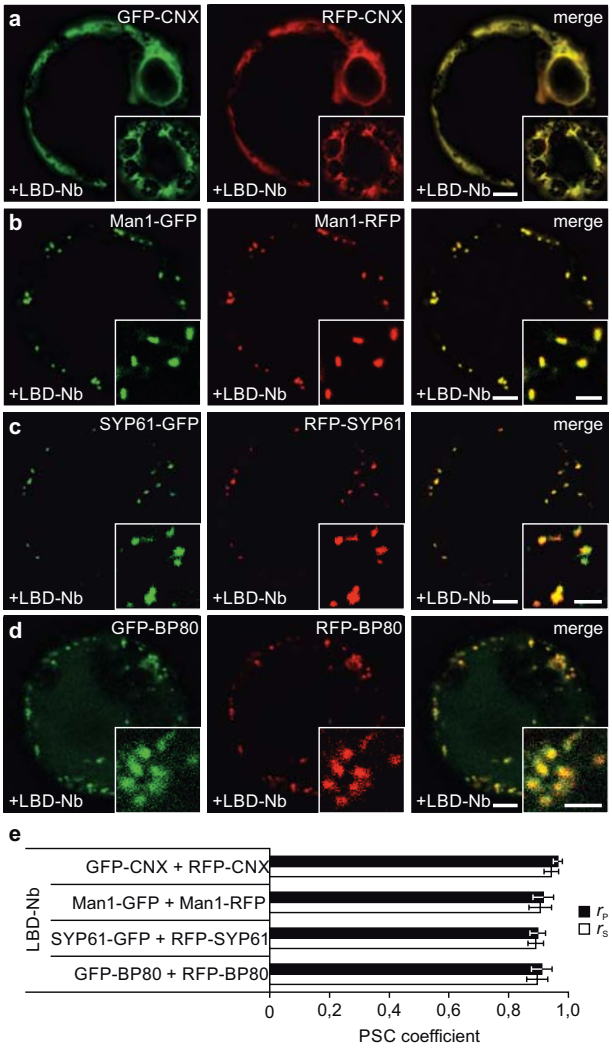

Supplementary Figure 2 The assembly of VSR sensors does not influence the localisation of the membrane anchors. Protoplasts were transfected with plasmids encoding for the indicated proteins and incubated 24 h before CLSM analysis. (**a**-**d**) Sensors were assembled from LBD-Nb and the GFP-tagged membrane anchors and localisation was compared to RFP-tagged derivatives of the respective compartmental marker. (**a**) Colocalisation with RFP-CNX in the ER, (**b**) colocalisation with Man1-RFP in the Golgi, (**c**) colocalisation with RFP-SYP61 in the TGN/EE and (**d**) colocalisation with RFP-BP80 in the MVB/LE. Inlays in **a**-**d**: magnified section. Scale bars: 5 µm and 2.5 µm (inlays). (**e**) Pearson's (r_P) and Spearman's (r_S) correlation (PSC) coefficients calculated for green and red signals as shown in **a**-**d** demonstrating colocalisation. Coefficients are presented as mean ± s.e.m (n = 10 individual cells). Statistical significance was calculated using ANOVA, followed by Tukey's HSD test (*** P < 0.001).

PimpI, Supplementary Figure 3

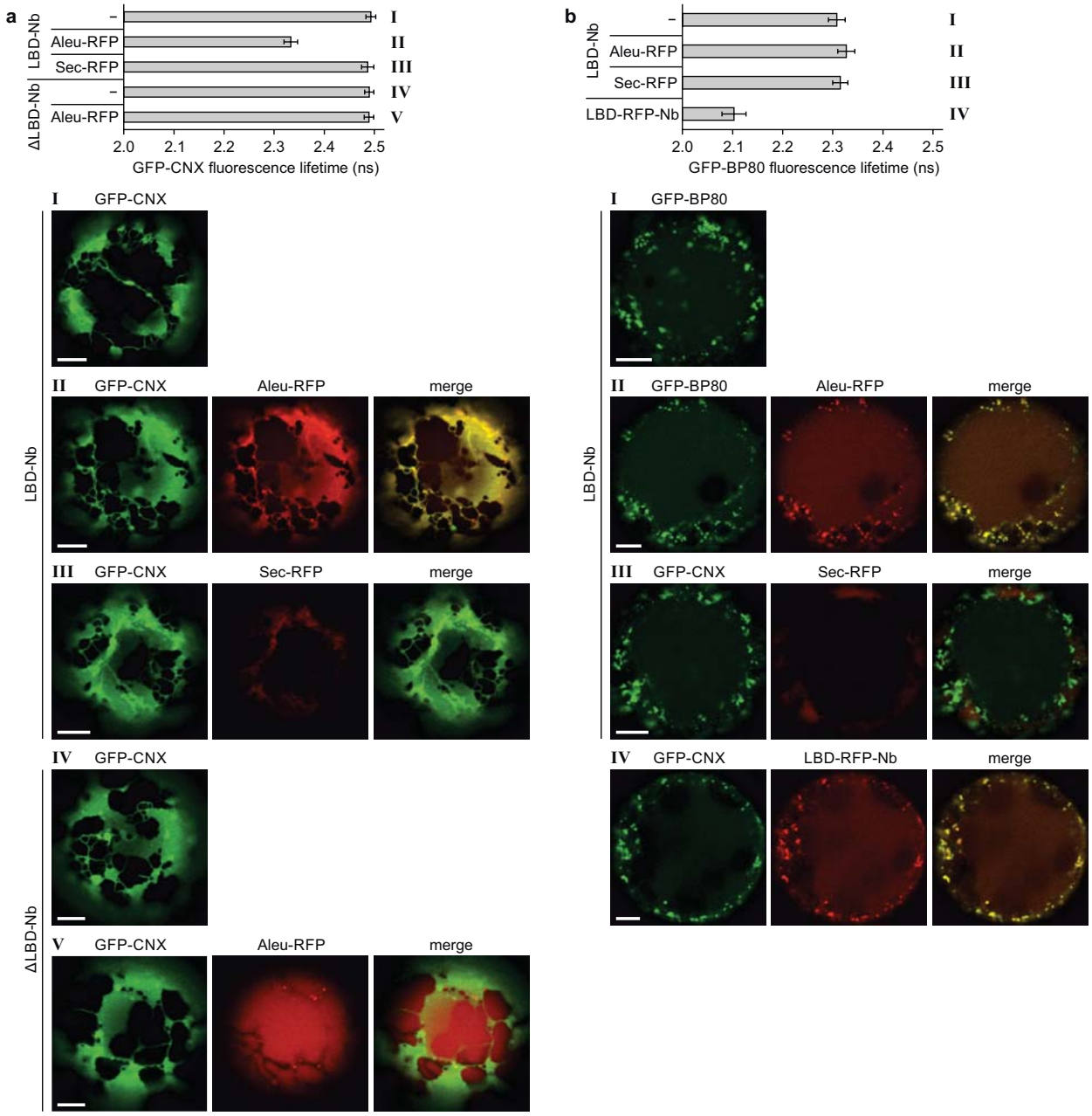

Supplementary Figure 3 Representative CLSM images of cells analysed by FRET-FLIM to asses VSR-ligand binding in the ER and the MVB/LE. (**a**) FLIM data for the ER. The diagram shows the fluorescence lifetimes from Figure 3c. The different experimental groups are represented by Latin numbers (I-V). A representative image is given for each group ensuring expression of tested fluorescent pairs. (**b**) FLIM data for the MVB/LE. The diagram shows the fluorescence lifetimes from Figure 3f. The different experimental groups are represented by Latin numbers (I-IV). A representative image is given for each group ensuring expression of tested fluorescent pairs. Scale bars: 5 µm.

PimpI, Supplementary Figure 4

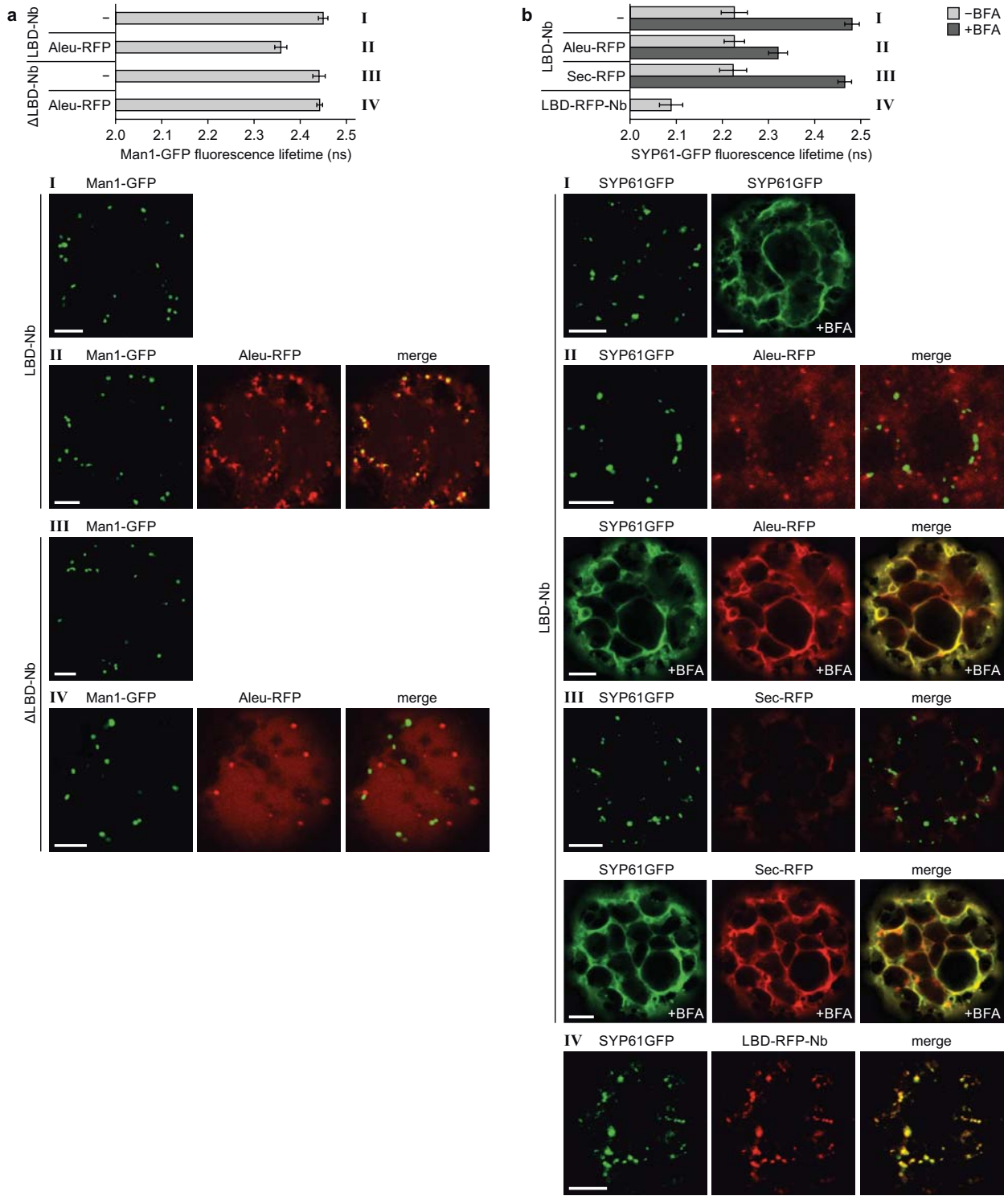

Supplementary Figure 4 Representative CLSM images of cells analysed by FRET-FLIM to asses VSR-ligand binding in the Golgi and the TGN/EE. (**a**) FLIM data for the Golgi. The diagram shows the fluorescence lifetimes from Figure 4d. The different experimental groups are represented by Latin numbers (I-IV). A representative image is given for each group ensuring expression of tested fluorescent pairs. (**b**) FLIM data for the TGN/EE. The diagram shows the fluorescence lifetimes from Figure 5d,f (± BFA) in direct comparison. The different experimental groups are represented by Latin numbers (I-IV). A representative image is given for each group ensuring expression of tested fluorescent pairs. Scale bars: 5 µm.